Distributed Quasi-Orthogonal Space-Time Coding in Wireless Cooperative Relay Networks

Matthew Hayes

School of Electronic, Electrical and Systems Engineering

Loughborough University

Submitted in partial fulfilment of the requirements of the award of

Doctor of Philosophy

I would like to dedicate this thesis to my loving wife Fiona Hayes.

Acknowledgements

Firstly, I would like to express my appreciation to both of my supervisors Prof. Jonathon Chambers and Prof. Malcolm Macleod for their expertise, guidance and continued support without which I would have never reached this point. I was told before I started my Ph.D. that the relationship between a supervisor and student is special and although the journey has been challenging; I do very much appreciate their patience and help.

I would particularly like to show my appreciation to my former colleagues at QinetiQ who helped me begin this journey. Without the help and encouragement of Nick Frall, Dr. Nigel Davies, Prof. Paul Cannon and Prof. John McWhirter I do not believe I would have ever started down this path.

I would also like to acknowledge the financial support of both QinetiQ and the EPSRC through the industrial sponsorship program. Without this contribution it would have been almost impossible for me to undertake a Ph.D. at the point I did in my career.

Although most of the duration of my studies were undertaken remotely I wish to thank all the members of the Advanced Signal Processing Group, Loughborough University, for creating a welcoming and friendly environment when I visited.

At this point I would like to show special appreciation to my loving parents for all their unconditional support. I owe you so much for your help and encouragement in the challenges I have faced. The scarifies you have made helped me get to where I am today.

Last but definitely not least, without the loving support of Fiona, my wife, from when I started the Ph.D. until the end I would not have come this far. You have supported me in my weakest moments and believed in me when I did not believe in myself. Over the last five years you have made so many sacrifices for my goals I don't think I will ever be able to make it up to you. I look forward to spending the rest of our lives together and living our dreams. Yes Naomi, Daddy can do "story-time" every night now!

Abstract

Cooperative diversity provides a new paradigm in robust wireless relay networks that leverages Space-Time (ST) processing techniques to combat the effects of fading. Distributing the encoding over multiple relays that potentially observe uncorrelated channels to a destination terminal has demonstrated promising results in extending range, data-rates and transmit power utilization. Specifically, Space Time Block Codes (STBCs) based on orthogonal designs have proven extremely popular at exploiting spatial diversity through simple distributed processing without channel knowledge at the relaying terminals. This thesis aims at extending further the extensive design and analysis in relay networks based on orthogonal designs in the context of Quasi-Orthogonal Space Time Block Codes (QOSTBCs).

The characterization of Quasi-Orthogonal MIMO channels for cooperative networks is performed under Ergodic and Non-Ergodic channel conditions. Specific to cooperative diversity, the sub-channels are assumed to observe different shadowing conditions as opposed to the traditional co-located communication system. Under Ergodic channel assumptions novel closed-form solutions for cooperative channel capacity under the constraint of distributed-QOSTBC processing are presented. This analysis is extended to yield closed-form approximate expressions and their utility is verified through simulations. The effective use of partial feedback to orthogonalize the QOSTBC is examined and significant gains under specific channel conditions are demonstrated.

Distributed systems cooperating over the network introduce challenges in synchronization. Without extensive network management

it is difficult to synchronize all the nodes participating in the relaying between source and destination terminals. Based on QOSTBC techniques simple encoding strategies are introduced that provide comparable throughput to schemes under synchronous conditions with negligible overhead in processing throughout the protocol. Both mutli-carrier and single-carrier schemes are developed to enable the flexibility to limit Peak-to-Average-Power-Ratio (PAPR) and reduce the Radio Frequency (RF) requirements of the relaying terminals.

The insights gained in asynchronous design in flat-fading cooperative channels are then extended to broadband networks over frequency-selective channels where the novel application of QOSTBCs are used in distributed-Space-Time-Frequency (STF) coding. Specifically, coding schemes are presented that extract both spatial and mutli-path diversity offered by the cooperative Multiple-Input Multiple-Output (MIMO) channel. To provide maximum flexibility the proposed schemes are adapted to facilitate both Decode-and-Forward (DF) and Amplify-and-Forward (AF) relaying. In-depth Pairwise-Error-Probability (PEP) analysis provides distinct design specifications which tailor the distributed-STF code to maximize the diversity and coding gain offered under the DF and AF protocols.

Numerical simulation are used extensively to confirm the validity of the proposed cooperative schemes. The analytical and numerical results demonstrate the effective use of QOSTBC over orthogonal techniques in a wide range of channel conditions.

Statement Of Originality

The novelty of Chapter 3 is in the derivation of closed-form expressions for the characterization of Quasi-Orthogonal Rayleigh flat-fading MIMO channels with partial feedback under ergodic and non-ergodic channel conditions. Chapter 3 presented novel closed-form expressions for the MIMO capacity of flat-fading Rayleigh distributed cooperative channels under the constraint of distributed-QOSTBC. For the first time closed-form expressions were derived to evaluate the effects of quantization of the feedback phase rotators on the degradation of the achievable channel capacity. Following on in a similar manner, Chapter 3 extended the analysis of QOSTBC for the case of non-ergodic channels. Whilst exact closed-form expression of the outage-probability for a given SNR and communications rate proved elusive: tight approximations verified using numerical simulations were derived using the Mellin transform for flat-fading Rayleigh cooperative channels.

The contribution of Chapter 4 is the development of robust single- and multi-carrier Distributed Quasi-Orthogonal Space-Time Block Codes for use in Rayleigh flat-fading cooperative networks under Decoding-Forward (DF) and Amplify-Forward (AF) relaying protocols. Asynchronous distributed-QOSTBC schemes were developed that utilize both single- and multi-carrier transmission for flat-fading 2-stage cooperative relay netorks. Both single- and multi-carrier block based transmission demonstrated decoding complexity comparable to synchronous symbol based implementations. As was the case with the characterization of the cooperative quasi-orthogonal channel in Chapter 3; feedback was introduced to orthogonalize the channel. Several

time- and frequency-domain processing techniques to apply the required phase rotation at the r-MT to orthogonalize the MIMO channel were illustrated.

The contribution of Chapter 5 is the analysis and design of robust multi-carrier Distributed Space-Time-Frequency codes based on Quasi-Orthogonal Space-Time component coding for use in broadband cooperative networks under Decoding-Forward and Amplify-Forward relaying protocols. Pairwise-Error-Probability analysis was performed under the assumption of DF and AF protocols to determine available multi-path and spatial diversity and coding gains from a frequency-selective 2-stage cooperative netork. A full-distributed asynchronous cooperative-STF coding scheme was developed that leverages QOSTBC as the ST-component code for deployment under both the DF and AF protocols. Numerical analysis demonstrated the utility of QOSTBC enabled cooperative-STF coding as a robust solution with and without limited feedback available.

The novelty of the work is supported by the following publications:

1. M.Hayes, S.K.Kassim, J.A.Chambers, M.D.Macleod, 'Exploitation of Quasi-Orthogonal Space Time Block Codes in Virtual Antenna Arrays: Part I - Theoretical Capacity and throughput Gains', in Proc. IEEE Vehicular Technology Conference, Singapore, Apr. 2008.
2. S.K.Kassim, M.Hayes, N.M.Eltayeb, J.A.Chambers 'Exploitation of Quasi-Orthogonal Space Time Block Codes in Virtual Antenna Arrays: Part II Monte Carlo-Based throughput Evaluation', in Proc. IEEE Vehicular Technology Conference, Singapore, Apr. 2008.
3. M.Hayes, J.A.Chambers, M.D.Macleod, 'A simple quasi-orthogonal space-time scheme for use in asynchronous virtual antenna array enabled cooperative networks', in EUSIPCO 2008, Lausanne, Switzerland.

4. M.Hayes, J.A.Chambers, M.D.Macleod, 'A Simple Alamouti Single-Carrier Space-Time Relaying Scheme for use in Asynchronous Wireless Relay Networks', in IMA Dec 2008, Cirencester, UK.
5. M.Hayes, J.A.Chambers, M.D.Macleod, 'A single-carrier quasi-orthogonal transmission scheme for asynchronous cooperative relay networks', in EUSIPCO 2009, Glasgow, UK.
6. M.Hayes, J.A.Chambers, M.D.Macleod, 'A high-rate quasi-orthogonal enabled transmission scheme for broadband asynchronous cooperative relay networks', in IET Proc. Communications, in preparation for submission.

Contents

List of Figures

List of Acronyms

AF	Amplify-and-Forward
AOA	Angle Of Arrival
ARQ	Automatic-Repeat-Request
ASPG	Advanced Signal Processing Group
AWGN	Additive White Gaussian Noise
BER	Bit Error Rate
BLAST	Bell Laboratories Layered Space-Time
BS	Base Station
CDD	Cyclic Delay Diversity
CDMA	Code Division Multiple Access
CF	Compress-and-Forward
CIR	Channel-Impulse-Response
CL-QOSTBC	Closed-Loop Quasi-Orthogonal Space Time Block Code
COD	Complex Orthogonal Design
CP	Cyclic Prefix
CRC	Cyclic Redundancy Check
CSI	Channel State Information
d-MT	destination-Mobile Terminal
DDF	Dynamic Decode-and-Forward
DF	Decode-and-Forward
DFE	Decision Feedback equalizer

DFT	Discrete Fourier Transform
DLC-STC	Distributed Linear Convolutive Space-Time Code
DTFT	Discrete Time Fourier Transform
D-STBC	Distributed-STBC
EOSTBC	Extended-OSTBC
FD	Fractional Delay
FDMA	Frequency Division Multiple Access
FEC	Forward Error Correction
FER	Frame Error Rate
FFT	Fast Fourier Transform
FIR	Finite Impulse Response
FSK	Frequency Shift Keying
GCOD	Generalized Complex Orthogonal Design
GF	Galois Field
GSTF	Grouped-STF
GUI	Graphical User Interface
IBI	Inter-Block-Interference
IDFT	Inverse Discrete Fourier Transform
IDTFT	Inverse Discrete Time Fourier Transform
IFFT	Inverse Fast Fourier Transform
IIR	Infinite Impulse Response
i.i.d.	independent identically distributed

ISI	Inter-Symbol-Interference
LCFC	Linear Complex Field Code
LoS	Line-Of-Sight
LRA	Lattice Reduction Algorithm
LTE	Long Term Evolution
LTI	Linear-Time-Invariant
MAC	Medium Access Control
MGF	Moment Generating Function
MIMO	Multiple-Input Multiple-Output
MIMO-OFDM	Multiple-Input Multiple-Output Orthogonal Frequency Division Multiplexing
MISO	Multiple-Input Single-Output
ML	Maximum Likelihood
MLSE	Maximum Likelihood Sequence Estimation
MMSE	Minimum Mean Square Error
MRC	Maximal Ratio Combining
MSE	Mean Square Error
MSSNR	Maximium Shortening Signal-to-Noise-Ratio
MT	Mobile Terminal
MU-MIMO	Multi-User MIMO
MUI	Multi-User Interference
NAF	Nonorthogonal Amplify-and-Forward

OF	Observe-and-Forward
OFDM	Orthogonal Frequency Division Multiplexing
O-MIMO	Orthogonal-MIMO
OSTBC	Orthogonal Space Time Block Code
PAM	Phase Amplitude Modulation
PAPR	Peak-to-Average-Power-Ratio
PDA	Probabilistic Data Association Algorithm
pdf	probability density function
PDP	Power Delay Profile
PEP	Pairwise-Error-Probability
PIC	Parallel Interference Cancellation
pmf	probability mass function
PSK	Phase Shift Keying
QAM	Quadrature Amplitude Modulation
QoS	Quality-of-Service
QOSTBC	Quasi-Orthogonal Space Time Block Code
QPSK	Quadrature Phase Shift Keying
RF	Radio Frequency
RMS	Root Mean Square
r-MT	relaying-Mobile Terminal
SC	Single Carrier
SCPQ	Sub-Carrier Phase Quantization

SCQLPI	Sub-Carrier Quantized Linear Phase Interpolation
SDA	Sphere Decoding Algorithm
SDP	Semi-Definite Programming
s-MT	source-Mobile Terminal
SER	Symbol Error Rate
SF	Space-Frequency
SIMO	Single-Input-Multiple-Output
SINR	Signal-to-Interference-plus-Noise Ratio
SISO	Single-Input-Single-Output
SLC	Square-Law Combining
SNR	Signal-to-Noise Ratio
ST	Space-Time
STF	Space-Time-Frequency
STBC	Space Time Block Code
STC	Space-Time-Coding
ST-LCFC	Space-Time LCFC
STTC	Space-Time Trellis Code
SU-MIMO	Single-User MIMO
SVD	Singular Value Decomposition
t-MRC	transmit-Maximal Ratio Combining
TAST	Threaded Algebraic Space-Time
TDMA	Time Division Multiple Access

VAA	Virtual Antenna Array
WLAN	Wireless Local-Area-Network
ZF	Zero-Forcing
ZMCSCG	Zero Mean Circularly Symmetric Complex Gaussian

List of Notation

∂	Partial differentiation
A^H	Hermitian transpose of A
$a \otimes b$	Convolution of a and b
$\otimes$	Kronecker product
$\delta(\cdot)$	Dirac delta function
$r(\cdot)$	Rank of an matrix argument
$\|\cdot\|_F$	Frobenius norm
$\|\cdot\|_2$	Euclidean norm
$argmax$	Maximum among arguments
det	Determinant
$\|\cdot\|$	Determinant
$\|\cdot\|$	Cardinality of a set
$\|\cdot\|$	Absolute value
$\zeta(\cdot)$	Time reversal
$E_x\{\cdot\}$	Expectation with respect to x
$\langle\cdot\rangle_N$	Modulo-N operation
$\dagger$	Pseudo-inverse operator
$vect(\cdot)$	Vectorizes a matrix argument
$\Re\{\cdot\}$	Returns real component of the argument
$\angle$	Returns angle of the argument
lim	Limit
min	Minimum of argument
$diag$	Diagonal matrix from vector argument
Pr	Probability
sup	Supremum of argument
inf	Infimum of argument
Tr	Trace of Matrix
$2F1$	Gauss Hypergeometric function
$M\{\cdot\}$	*Mellin* transform
$f_X(x)$	Probability density function
$(\cdot)!$	Factorial

List of Notation

$\begin{pmatrix} N \\ k \end{pmatrix}$	Permutation operator
F_1	Appell Hypergeometric function
$\Gamma(x)$	Complete Gamma function
$\gamma(a, x)$	Lower Incomplete Gamma function
$\hat{C}_\zeta(a)$	Capacity Integral
$\mathcal{L}_k$	Laguerre polynomial of order k
W	Wishart matrix
xFy	Generalised Hypergeometric function
$\mathbb{C}$	Complex numbers set
$\mathbb{N}$	Natural numbers set
$\mathcal{N}$	Gaussian distribution
$\mathcal{N}_\mathbb{C}$	Complex Gaussian distribution
$\mathcal{U}$	Uniform distribution
α	QOSTBC interference term
α	MRC complex weight parameters
β	Fractional transmission power
ϵ_ϕ	QOSTBC phase quantization error
η	QOSTBC effective gain term
γ	QOSTBC gain term
$\bar{\gamma}$	Average sub-channel gain
γ_{MRC}	Instantaneous SNR for MRC scheme
$\bar{\gamma}_{MRC}$	Average SNR for MRC scheme
γ_{t-MRC}	Instantaneous SNR for transmit-MRC scheme
$\bar{\gamma}_{t-MRC}$	Average SNR for transmit-MRC scheme
$\bar{\gamma}_{Alamouti}$	Average SNR for Alamouti-STBC scheme
λ	Eigenvalue
λ	Instantaneous channel power
λ	Wave-Length
ω	Frequency-mapping vector
σ^2	Variance
τ	Number of transmit antennas
τ	Time lag
ψ	QOSTBC phase angle rotation

List of Notation

ϕ	QOSTBC phase angle rotation
ρ	Linear SNR
τ_{max}	Maximum delay spread
$\phi_\lambda(s)$	Moment Generating Function
$\mathcal{X}$	Chi-square distribution
θ_{RMS}	Root-mean square AOA spread
θ	Angular spread
θ_i	LCFC i^{th} matrix row
Θ	Normalised throughput
$\mathbf{\Theta}_{LCF}$	LCFC constellation pre-coder matrix
$\Lambda(r,t)$	Approximate MIMO Gain
ϕ	Communication rate
d	Distance
d	Diversity gain
d_{min}	Minimum Euclidean distance between constellation points
e	Natural constant
f	Radio frequency
f_D	Maximum doppler frequency
h	Complex channel coefficient
k	Number of transmitted symbols
k	Sampling index
k	Discrete sub-carrier index
m	min(t, r)
m	Time slots in a data block
n	Complex baseband noise
n	max(t, r)
p	Sub-carrier index
I_s	Number of information symbols
s	Transmitted symbol
t	Continuous time
u	Total number of MIMO sub-channels
x	Coded symbol
y	Received signal
z	Arbitrary complex number

z	Processed received signal
$\mathbf{A}$	QOSTBC coupling matrix
A_s	Finite symbol alphabet
$\mathbf{B}$	QOSTBC coupling matrix
B_c	Coherence bandwidth
C	Capacity
D_c	Coherence distance
D	Destination node
E	Energy
Eb	Bit energy
Es	Symbol energy
$H(\cdot)$	Entropy
$I(x, y)$	Mutual information
J	Cost function
K	Number of relaying stages
$K_\beta(\cdot)$	Modified Bessel function of the second kind
L	Channel length in sampling periods
L	Laplace transform
$K_{i,j}$	Expansion coefficient
$K_{n,m}$	Normalization factor
M	Modulation order
N	Noise power
$\bar{N}_e$	Number of nearest neighbors
N_0	Noise power spectral density
O	Number of modulation orders
$P_{out}(\cdot)$	Outage probability
P_s	Source transmit power
P_r	Relay transmit power
R	STBC rate
R_j	Relay node j
$\mathbb{S}_g$	Sub-carrier index mapping
S	Source node
S	Signal power
$S()$	QOSTBC formulation matrix

List of Notation

T	Time duration
T_c	Coherence time
T_M	Delay spread
W	Bandwidth
$\mathbf{w}$	Beamforming weight vector
$\mathbf{G}_{v,d}$	Codeword diversity gain metric
$\mathbf{G}_{v,c}$	Codeword coding gain metric
$\mathbf{G}$	Givens matrix
$\mathbf{G}$	Givens matrix
$\mathbf{G}$	STBC generator matrix
$\mathbf{H}$	Channel matrix
$\mathbf{H}_{eff}$	Effective channel matrix
$\mathbf{I}_r$	Identity matrix of size r $\times$ r
$\mathbf{S}$	Alamouti STBC generator matrix
N_t	Number of transmit antenna elements
N_r	Number of receiver antenna elements
μ	Transmit antenna index
ν	Receiver antenna index
$\delta(\cdot)$	Delta function
τ	Time delay
α	Instantaneous channel coefficient
$L_{\mu\nu}$	Sub-channel order
S	Source node reference
R_μ	Relay node reference
D_ν	Destination terminal antenna reference
$\sigma^2_{\mu\nu}$	Channel power denoted by sub-channel index
$E\{\cdot\}$	Expectation operand
T_s	Sampling period
L_ν	Sum of sub-channel order to specified receive antenna
$\mathbf{x}^\mu_n(p)$	Space-Time-Frequency codeword
N_x	Codeword time-slots
N_c	Number of sub-carriers
N_p	Cyclic-prefix length
N_s	Number of symbols

List of Notation

J	Frame length
$\mathbf{F}_N$	Unitary DFT matrix of dimension NxN
$\mathbf{F}_{pw}$	Pre-whitening matrix
H	Toeplitz structured convolutional channel matrix
$\mathbf{Q}$	Equalizer matrix
$\mathbf{R_{ss}}$	Symbol covariance matrix
$\mathbf{I_N}$	Identity matrix of dimension NxN
$\mathbf{T}_{cp}$	Cyclic prefix matrix operator
$\mathbf{U}$	Left singular vector
$\mathbf{V}$	Right singular vector
$\mathbf{\Omega}$	Frequency characterization matrix
$\mathbf{\Delta}$	Codeword difference matrix
$\mathbf{\Delta}_{LCF}$	LCFC difference matrix
$\mathbf{\Delta}$	QOSTBC coupling matrix
$\mathbf{A}_{14}$	QOSTBC sub-system coupling matrix
$\mathbf{A}_{23}$	QOSTBC sub-system coupling matrix
$\mathbf{\Delta}_{14}$	QOSTBC sub-system coupling matrix
$\mathbf{\Delta}_{23}$	QOSTBC sub-system coupling matrix
$\mathbf{\Lambda}_{14}$	QOSTBC sub-system eigenvalue matrix
$\mathbf{\Lambda}_{23}$	QOSTBC sub-system eigenvalue matrix
$\mathbf{\Sigma}$	Noise covariance matrix
$\mathbf{\Phi}$	QOSTBC phase rotation matrix
$\mathbf{\Phi}_g$	STF sub-carrier mapping matrix
$\mathbf{\Pi}$	Permutation matrix
$\mathbf{P}$	Time-reversal matrix
$\mathbf{R}$	Channel covariance matrix
$\mathbf{B}$	Channel whitening matrix
$\mathbf{\Psi}$	Codeword mapping function
$\mathbf{X}$	Codeword matrix
$\mathbf{E}$	Channel gain matrix

Chapter 1

Overview

1.1 Motivation

For over a decade traditional wireless networks, in the form of cellular networks, have provided end users with the ability to communicate on the move. These networks enabled information to be transferred from a source to destination terminal usually via controlling Base Stations (BSs) or access points. Terminals wishing to transmit and receive information usually do so over a single wireless point-to-point link with a controlling BS with data packets routed between BSs over a fixed wireline infrastructure.

In contrast to traditional wireless networks, Ad-Hoc networks do not utilize fixed network infrastructures; an attractive characteristic for applications deployed in settings where traditional infrastructure based networks are not feasible. Rather than utilizing a fixed infrastructure, nodes in Ad-Hoc networks self-organize through the use of decentralized routing and control algorithms which cooperate using peer-to-peer communication to enable information to be transmitted between source and destination nodes. Although this emerging technology has its origins in the military sphere, real commercial and civil applications are emerging; one of the most widespread examples of a one-hop Ad-Hoc network is the Bluetooth piconet[1].

The real challenges and opportunities of Ad-Hoc networks can only start to be realized when considering network topologies where multiple hops between network nodes are utilized to forward information between the sender and re-

cipient. Unlike point-to-point channels which have been widely researched and characterized [2], researchers are only just starting to evaluate the performance limits of wireless Ad-Hoc networks and realizable implementations.

The challenges faced by communication engineers when mitigating the effects of the wireless environment with respect to a single point-to-point link, such as path-loss and fading are however still pertinent to researchers today investigating Ad-Hoc networks. The traditional problems in wireless channels of shadowing and fading were usually unilaterally tackled within a single layer of a network, i.e. the physical layer. Today researchers still face the same challenges in distributed systems in the form of Ad-Hoc networks, but the arbitration between network layers appears to be diluting and creating a cross fertilization of ideas from the information theoretic community to signal processing and communication specialists. It is in these new approaches to solving old problems that *User Cooperation* has been established as a network solution to a typically physical layer problem.

1.2 User Cooperation

In practical wireless communication systems incorporating cellular handsets and wireless sensor nodes, it may not be practical or even feasible to employ multiple antenna elements on the host due to the physical size of a device and power constraints. To overcome these constraints researchers have been investigating *User Cooperation*, also referred to as *Cooperative Diversity*, inspired by the papers [3, 4], as a novel technique for extracting spatial diversity in situations where network nodes may only employ a single transceiver antenna element.

Essentially, *User Cooperation* is enabled by multiple signal copies originating from a source and overheard by other nodes due to omnidirectional mobile antennas. The additional signal copies effectively come at no additional cost in transmit power therefore taking advantage of the broadcast nature of wireless channels. By cooperating and forming clusters with partnering nodes which are closely located geographically, as illustrated in Figure 1.1, source and destination nodes can exploit the power of joint encoding and decoding. This form of cooperation is usually referred to in the literature as Virtual Antenna Arrays (VAAs) [5], due to the distributed nature of the array processing. The use of VAAs to im-

plement MIMO like transmitter and receiver arrays enables cooperative diversity strategies that can tap into the vast knowledge already available on Space-Time-Coding (STC)[6]. However, unlike STCs which are typically implemented on a single communications platform, *User Cooperation* is complicated further by the fact that the interuser channel is noisy and unreliable between distributed nodes.

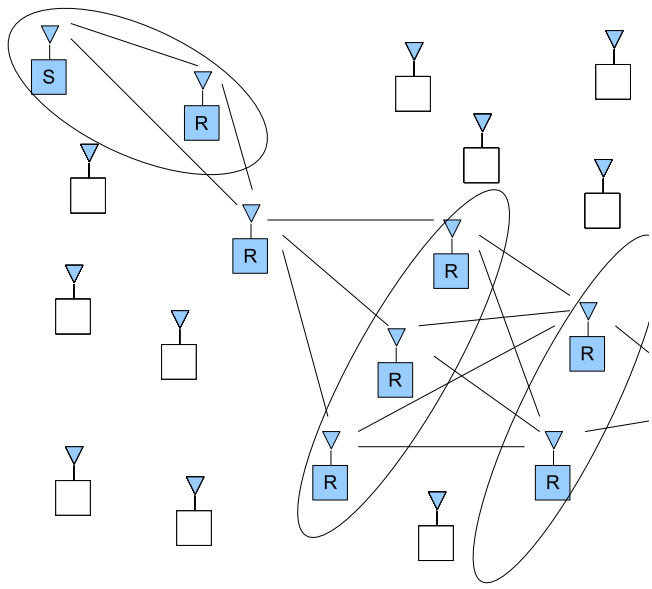

Figure 1.1: User Cooperation enabled Ad-Hoc Network

Early theoretical and practical results within the area of *User Cooperation* look promising with many interesting results neatly summarized in [7] for a variety of two-transmitter, two-receiver cooperative channels using DF[1], AF[2] and Compress-and-Forward (CF)[3] relaying schemes. Cooperative schemes have subse-

[1]DF: this scheme fully decodes the received signal ideally without error, then optionally processes the signal before relaying.

[2]AF: this scheme amplifies the signal without additional processing before relaying.

[3]CF: this scheme compresses the received signal within specified distortion limits before

quently demonstrated substantial benefits over non-cooperative systems in terms of a multitude of network performance metrics including; sum rate capacity improvements [3, 4, 8], resistance to fading in the form of increased spatial diversity [9, 10], increased network coverage [3, 4] and superior power saving performance [3, 4, 5].

Although Figure 1.1 demonstrates what may appear to be a simple relaying structure, there are significant research challenges still to be addressed in this topology. A select few of the challenges are addressed in this thesis; namely, increasing the robustness of the relaying stages to fading observed over the wireless relaying links and synchronization issues encountered with distributed systems. This thesis is primarily concerned with extending and realizing the potential of cooperative relay networks through the use of QOSTBCs which are shown to demonstrate high-diversity gains and low-complexity encoding and decoding in traditional point-to-point deployments [11, 12].

1.3 Outline of the Thesis

In Chapter 2, a review of the relevant literature as well as necessary background information will be given to provide a basis for the understanding of the theoretical concepts introduced later in this thesis . Initially an overview will be provided of the fundamental concepts of information theory in regard to Gaussian and fading channels. The categorization of channels into *ergodic* and *non-ergodic* based on statistical properties will be explored and associated concepts such as channel capacity as well as throughput will be discussed and used as a basis for the characterization of distributed-MIMO channels in Chapter 3. For completeness these ideas are briefly extended to analyze deterministic and non-deterministic traditional MIMO channels where the antenna arrays are co-located. Later in Chapter 2 the classifications of communications channels will be defined under the umbrella terminology; time-selective, frequency-selective and spatial-selective. The understanding of the properties of channels with these characteristics will be fundamental in the design of distributed coding schemes for wireless relay networks. Specifically of interest early on in the thesis presentation is the idea of spatial-

relaying.

selectivity and the ensuing diversity gain offered by channels with this characteristic. These concepts are fundamental in the ideas and analysis discussed in Chapters 3 & 4. As a prelude to the novel coding designs documented in this thesis the ideas of diversity are introduced through a review of the literature behind some of the main contributions in this interesting and actively researched area. Some of the coding examples illustrated form directly the foundations which are extended to the interesting area of distributed coding for co-operative wireless relay networks in this thesis.

Chapter 3 provides the fundamental analysis and characterization of flat-fading Quasi-Orthogonal MIMO channels for exploitation in co-operative wireless relay networks. Although incapable of achieving the channel capacity as eluded to by Shannon in his breakthrough memo [13]; the same analytical techniques used to derive the capacity of communications channels can be utilized under the constraints of specified coding schemes to provide insight into their achievable capacity and throughput. Using the framework illustrated in Chapter 2 the performance of Quasi-Orthogonal MIMO channels can be measured in *ergodic* and *non-ergodic* scenarios. This analysis provides valuable insight and guidance into the deployment of QOSTBCs under such channel conditions and direct comparisons, both analytically and numerically, are made against their orthogonal counterparts. Fundamentally, the chapter investigates the subtle but substantial differences that are inherent between traditional Quasi-Orthogonal MIMO channels and those observed in distributed implementations where distinct differences in shadowing and path-loss are observed between sub-channels[1]. This contribution leads to closed form analytical expressions that define both the capacity and throughput of QOSTBC in cooperative wireless relay networks. The contribution is extended by applying partial-Channel State Information (CSI) at the transmitter to orthogonalize the effective[2] MIMO channel which demonstrates significant gains for some channel classifications.

Chapter 4 builds upon the theoretical ideas developed in Chapter 3 to consider ST code designs for asynchronous distributed-QOSTBC in flat-fading co-

[1]Sub-channels are defined as the channels observed between individual transmit/receiver antenna pairings.

[2]Effective channel: defines an equivalent channel model after pre-ccoding at the transmit and/or receiver.

operative wireless relay networks. Although the problems of channel correlation associated with co-located antenna arrays are known to degrade the capacity and diversity gains of more traditional communication systems these are mitigated in distributed implementations; however the added complexity of synchronization both in time and frequency is introduced between all the participating communication terminals. Chapter 4 proposes a novel asynchronous distributed-QOSTBC that overcomes the problem of temporal synchronization. As a prelude to the presentation of the coding scheme a simple network architecture is introduced which leverages a virtual array of relay nodes. Initially, a multi-carrier scheme is developed to showcase the simplicity of the novel distributed-QOSTBC and demonstrate several receiver structures. It is well known that multi-carrier enabled communications systems suffer from high PAPR which imposes significant cost and complexities in the RF design of the power amplifier at the source and relaying terminals. In some deployments this may become a limiting constraint so the fundamental ideas introduced using multi-carrier transmission are extended to a single-carrier scheme which is known to constrain the PAPR. Finally, full-rate full-diversity asynchronous distributed-QOSTBC is demonstrated through the use of a low-rate feedback channel and efficient processing at the relay nodes.

Chapter 5 extends the asynchronous multi-carrier distributed-QOSTBC developed for flat-fading channels to channels that display multi-path characteristics. Fundamentally, the network architecture between Chapter 4 is reused in Chapter 5 enabling many of the coding insights gained from the previous chapter to be leveraged and recycled. However, multi-path channels introduce additional diversity which can be harnessed assuming proper design of the pre-coder. The proposed asynchronous broadband designs adopt a two-stage scheme that distributes the pre-coding between both the source and relaying terminals. Through minimal knowledge of the distributed-MIMO channel the source node implements an efficient pre-coding strategy that extracts the multi-path diversity at the destination mobile terminal. The basic processing developed in the previous chapter is then implemented at the relaying terminals to extract the spatial diversity offered by the distributed-MIMO channel. At the receiver Maximum Likelihood (ML) combining followed by an efficient decoding process renders the proposed scheme suitable for use in high data rate networks. Finally, the scheme is exploited in a point-to-point as well as a relaying architecture under both DF and AF protocols.

Optimum performance is demonstrated under the design metrics specified using PEP analysis.

This thesis is concluded with a summarizing chapter that discusses the contributions made and opportunities for further research.

Chapter 2

Literature Review and Background

2.1 Channel Capacity Basics

2.1.1 Gaussian Channels

The Gaussian channel model has its origin in many practical channels for example satellite communications where the additive noise in such channels can be approximated as the cumulative effect of a large number of independent noise sources; therefore by virtue of the central limit theorem the Gaussian assumption is valid for multiple communications scenarios. A simple expression for the channel is given by,

$$Y = X + Z \tag{2.1}$$

where the random variables X, Y and Z are associated with the transmitted, received and noise signals respectively. Shannon introduced the maximum mutual information between the transmitted and received signals as the channel capacity,

$$C = \sup_{f_X(x)} I(X;Y) \tag{2.2}$$

where $\sup\{\cdot\}$ denotes the supremum. The mutual information is based on the principle of entropy $H(\cdot)$, which for a particular continuous random variable x with associated probability density function (pdf) $f_X(x)$ is defined as,

$$H(X) := -\int f_X(x) log_2(f_X(x)) dx \tag{2.3}$$

Based on the definition of entropy (2.3) the channel capacity can be evaluated by expanding (2.2),

$$I(X;Y) = H(Y) - H(Z) \tag{2.4}$$

for which $H(Y)$ and $H(Z)$ define the entropy of the source signal and the noise entropy respectively. It is interesting to observe the scenario when $H(Y) = H(Z)$, then zero mutual information is conveyed by the channel and a receiver is unable to determine which realization of x was transmitted. In the absence of noise, i.e. $H(Z) = 0$, then it is possible to detect the realization x based on the observation y without error. In addition, with no further conditions the channel capacity maybe considered infinite assuming X can undertake any arbitrary real value and no errors are introduced by the channel. By imposing a limitation on the input signal in the form of a power constraint, Shannon demonstrated [13, Theorem 16] that the normal distribution maximizes the entropy of a random variable for a given variance. Therefore to maximize (2.2) it is assumed X follows a Gaussian distribution, i.e. $x \sim N(0, \sigma_X^2)$, with entropy,

$$H(X) = \frac{1}{2} log_2\, 2\pi e \sigma_X^2. \tag{2.5}$$

Assuming X and Z are independent and Z follows a Gaussian distribution, $z \sim N(0, \sigma_Z^2)$, then an upper bound on the mutual information can be derived,

$$\begin{aligned} I(X;Y) &\leq \frac{1}{2} log_2\, 2\pi e(\sigma_Z^2 + \sigma_X^2) - \frac{1}{2} log_2\, 2\pi e \sigma_Z^2 && (2.6) \\ &= \frac{1}{2} log_2\, (1 + \sigma_X^2/\sigma_Z^2). && (2.7) \end{aligned}$$

Shannon then linked the mutual information bound (2.6) to channel capacity using the Nyquist rate which determines that approximately $2WT$ symbols maybe transmitted on a band-limited channel with bandwidth W over a time duration T. Since the capacity per channel use is governed by (2.6) the capacity of a bandlimted channel over duration T is given by,

$$C := WTlog_2\left(1+\sigma_X^2/\sigma_Z^2\right) \qquad [bits] \tag{2.8}$$

Assuming that each codeword, where we refer to the ensemble of codewords as a code-book, is infinite in length then the normalized channel capacity defined in $[bits/s/Hz]$ simplifies to,

$$\begin{aligned} C &:= \lim_{T\to\infty} \frac{WTlog_2\left(1+\sigma_X^2/\sigma_Z^2\right)}{WT} && (2.9)\\ &= log_2\left(1+\sigma_X^2/\sigma_Z^2\right) \qquad [bits/s/Hz] && (2.10) \end{aligned}$$

Shannon subsequently proved that error free transmission cannot be guaranteed when signaling above the capacity of a given channel.

2.1.2 Ergodic and Non-Ergodic Fading

Wireless channels where the transmitted signal experiences multi-path propagation can generally be characterized by large, medium and small-scale fading [14]. Large scale fading can be considered a deterministic effect attributed to path-loss and reflections from the Earth's surface. Shadowing, a medium scale effect, occurs in the presence of large reflecting or diffraction objects which are located at a large distance relative to the motion of a communications terminal. It is assumed that in low-mobility scenarios the effects of large and medium scale fading can be incorporated into a single parameter γ and assumed to be deterministic. Small-scale fading can create dramatic fluctuations in the received signal power when a mobile terminal is moved over a relatively small distance comparable to the carrier wavelength. This stochastic effect, represented by λ, is manifest in the temporal and spatial dimensions and is generally categorized into slow or fast fading and frequency- or flat-selective fading. In this section the analysis focuses on the achievable capacity and throughput of flat-fading channels.

The channel is referred to as *ergodic* if λ varies over the transmitted codeword so that over an infinite length codeword the ensemble of λs are realized according to a given distribution. For *ergodic* channels with deterministic shadowing effects the capacity is evaluated as,

$$C = \int_0^\infty \log_2\left(1+\gamma\lambda\rho\right) f_\lambda(\lambda)d\lambda \tag{2.11}$$

In scenarios when the channel realizations are fixed for the duration of the codeword then it is assumed that λ is drawn at random from the ensemble defined by the pdf $f_\lambda(\lambda)$. These channel characteristics are referred to as *non-ergodic*. Therefore using the definition for the channel capacity of deterministic channels,

$$C = \log_2 (1 + \gamma\lambda\rho) \tag{2.12}$$

there is a non-zero probability that such a channel cannot not support error free transmission at a specific rate ϕ. This probability is referred to as the *outage probability* and is calculated as,

$$Pr(C < \phi) = \int_0^{\hat{\lambda}} f_\lambda(\lambda) d\lambda \tag{2.13}$$

where (2.12) is rearranged,

$$\hat{\lambda} = \frac{2^\phi - 1}{\gamma\rho} \tag{2.14}$$

to determine the necessary realization of λ to guarantee error-free transmission for a given transmission rate.

2.2 Capacity of MIMO channels

In this section the fundamental capacity limit of a MIMO wireless channel that can support error-free transmission will be considered. Several different cases of MIMO channels are reviewed: CSI known and unknown at the transmitter, together with deterministic and random fading channels. The fundamental limit on the spectral efficiency of MIMO communication discussed here will provide a benchmark upon which to compare the various proposed coding schemes later in the thesis.

2.2.1 System Model

Consider a generic MIMO channel $\mathbf{H}$ with N_t transmit antennas and N_r receive antennas,

$$\mathbf{H} = \begin{bmatrix} h_{1,1} & h_{1,2} & \dots & h_{1,N_t} \\ h_{2,1} & h_{2,2} & \dots & h_{2,N_t} \\ \vdots & \vdots & \vdots & \vdots \\ h_{N_r,1} & h_{N_r,2} & \dots & h_{N_r,N_t} \end{bmatrix} \tag{2.15}$$

where the channel between the ith, $i \in \{1, \dots, N_t\}$, transmit antenna and the jth, $j \in \{1, \dots, N_r\}$, receive antenna is denoted by $h_{i,j}$. Equating $N_t = 1$ or $N_r = 1$ reduces the MIMO channel to either Single-Input-Multiple-Output (SIMO) or Multiple-Input Single-Output (MISO) channels which are noted as particular sub-sets of the MIMO case. From this channel representation a typical MIMO transceiver model can be expressed using the input-output relationship,

$$\mathbf{y} = \mathbf{H}\mathbf{s} + \mathbf{n} \tag{2.16}$$

where $\mathbf{y} \in \mathbb{C}^{N_r \times 1}$ is the observed signal vector at the receiver array, $\mathbf{s} \in \mathbb{C}^{N_t \times 1}$ is the transmitted codeword and $\mathbf{y} \in \mathbb{C}^{N_r \times 1}$ is the Zero Mean Circularly Symmetric Complex Gaussian (ZMCSCG) noise with covariance matrix $E\{\mathbf{n}\mathbf{n}^H\} = N_0 \mathbf{I}_{N_r}$. Assuming S defines the total transmit energy, then the covariance matrix $\mathbf{R_{ss}} = E\{\mathbf{s}\mathbf{s}^H\}$ must satisfy $Tr\{\mathbf{R_{ss}}\} \leq S$.

2.2.2 Deterministic MIMO Channel

In the following it is assumed that the MIMO channel $\mathbf{H}$ is deterministic and known without error at the receiver. In this scenario the capacity of the MIMO channel has been defined by taking the supremum [15],

$$C = \sup_{F_{\mathbf{s}}(\mathbf{s})} \{I(\mathbf{s}; \mathbf{y})\} \tag{2.17}$$

where it can be shown [15],

$$I(\mathbf{s}; \mathbf{y}) = H(\mathbf{y}) - H(\mathbf{n}) \tag{2.18}$$

Therefore the problem of maximizing the mutual information $I(\mathbf{s}; \mathbf{y})$ reduces to maximizing the observation entropy $H(\mathbf{y})$. In [16] it was shown that the

differential entropy $H(\mathbf{y})$ is maximized when $\mathbf{y}$ assumes a ZMCSCG distribution, which links into the analysis performed by Shannon for Single-Input-Single-Output (SISO) channels. The differential entropies shown in (2.18) are given by,

$$H(\mathbf{y}) = \log_2 \det(\pi e \mathbf{R}_{yy}) \tag{2.19}$$

$$H(\mathbf{n}) = \log_2 \det(\pi e N_0 \mathbf{I}_r) \tag{2.20}$$

where the covariance matrix of $\mathbf{y}$, $\mathbf{R}_{yy} = E\{\mathbf{y}\mathbf{y}^H\}$, satisfies,

$$\mathbf{R}_{yy} = \mathbf{H}\mathbf{R}_{ss}\mathbf{H}^H + N_0 \mathbf{I}_{N_r} \tag{2.21}$$

assuming $\mathbf{R}_{ss} = E\{\mathbf{s}\mathbf{s}^H\}$ is the covariance matrix of $\mathbf{s}$ in addition to the noise and data sources being independent $E\{\mathbf{s}^H\mathbf{n}\} = 0$. Then substituting (2.18)-(2.20) into (2.17) results in the MIMO capacity expression [15],

$$C = \arg \max_{Tr(\mathbf{R}_{ss} \leq S)} \log_2 \det \left(\mathbf{I}_{N_r} + \frac{1}{N_0} \mathbf{H}\mathbf{R}_{ss}\mathbf{H}^H \right) \tag{2.22}$$

Channel Unknown Assuming the MIMO CSI is unknown to the transmitter then no statistical advantage in pre-coding is available thus reducing (2.22) to,

$$C = \log_2 \det \left(\mathbf{I}_{N_r} + \frac{S}{N_0} \mathbf{H}\mathbf{H}^H \right) \tag{2.23}$$

where $\mathbf{R}_{ss} = S.\mathbf{I}_{N_t}$ and S denotes the transmit power. Expression (2.23) is not the Shannon channel capacity since there exist capacity achieving source covariance matrices $\mathbf{R}_{ss}$ that outperform the capacity achieved without CSI at the transmitter.

Channel known at the transmitter When the CSI is available at the transmitter $\mathbf{R}_{ss}$ can be designed to achieve the channel capacity. To simplify the design the channel is firstly decomposed into a set of orthogonal SISO channels using the Singular Value Decomposition (SVD) and determinant properties,

$$\log_2 \det \left(\mathbf{I}_{N_r} + \frac{1}{N_0} \mathbf{H}\mathbf{R}_{ss}\mathbf{H}^H \right) = \sum_{i=1}^{N_r} \log_2 \left(1 + \frac{\lambda_i}{N_0} \gamma_i \right) \tag{2.24}$$

where $\mathbf{U}^H\mathbf{HV} = diag\{\sqrt{\lambda_1}, \ldots, \sqrt{\lambda_{N_r}}\}$ and γ_i is the power allocated to the ith sub-channel (singular value). The optimisation problem (2.22) can now be expressed as,

$$\max. \quad \sum_{i=1}^{N_r} \log_2 \left(1 + \frac{\lambda_i}{N_0}\gamma_i\right) \tag{2.25}$$

$$s.t. \quad \sum_{i=1}^{N_r} \gamma_i \leq S \tag{2.26}$$

The optimization problem can therefore be solved iteratively using the celebrated *water-pouring* algorithm [17, 15, 18, 19] or convex optimization techniques [20].

2.2.3 Frequency-Flat Ergodic Fading MIMO Channel

The ergodic channel capacity is the ensemble average of the error-free transmission rate over the distribution of channel realizations $\mathbf{H}$ utilizing a capacity maximizing codebook covariance matrix $\mathbf{R}_{ss}$. The *ergodic* channel capacity when each individual sub-channel of the MIMO channel $\mathbf{H}$ experiences uncorrelated Raleigh fading has been derived by Telatar [15]. The derivation itself is rather involved so the examination is restricted to the important results for brevity.

Telatar demonstrated that a ZMCSCG codebook was the optimal strategy to maximize the ergodic channel capacity,

$$I(\mathbf{s};\mathbf{y}) = E_H\{\log_2 \det\left(\mathbf{I}_{N_r} + \mathbf{HR}_{ss}\mathbf{H}^H\right)\} \tag{2.27}$$

Since $\mathbf{R}_{ss}$ is positive definite, then eigenvalue decomposition yields $\mathbf{R}_{ss} = \mathbf{U}_{ss}\mathbf{D}_{ss}\mathbf{U}_{ss}^H$ where $\mathbf{U}_{ss}$ is a unitary matrix and $\mathbf{D}_{ss}$ is a diagonal matrix. Therefore the search for the optimal covariance matrix can be restricted to a non-negative diagonal matrix $\mathbf{D}_{ss}$,

$$I(\mathbf{s};\mathbf{y}) = E_H\{\log_2 \det\left(\mathbf{I}_{N_r} + (\mathbf{HU}_{ss})\mathbf{D}_{ss}(\mathbf{HU}_{ss})^H\right)\} \tag{2.28}$$

noting that the distribution of $\mathbf{HU}_{ss}$ is the same as that of $\mathbf{H}$. Telatar then demonstrates that $\mathbf{D}_{ss}$ must be of the form $a\mathbf{I}$ which subject to the transmit power constraintm yields the channel capacity when $a = S/N_t$,

$$C = E_H\left\{\log_2 \det\left(\mathbf{I}_{N_r} + \frac{S}{N_t}\mathbf{H}\mathbf{H}^H\right)\right\} \tag{2.29}$$

$$= E_H\left\{\log_2 \det\left(\mathbf{I}_{N_t} + \frac{S}{N_t}\mathbf{H}^H\mathbf{H}\right)\right\} \tag{2.30}$$

To evaluate the expectation the matrix $\mathcal{W}$ is introduced such that,

$$\mathcal{W} = \begin{cases} \mathbf{H}\mathbf{H}^H, & N_r < N_t \\ \mathbf{H}^H\mathbf{H}, & N_r \geq N_t \end{cases} \tag{2.31}$$

where $\mathcal{W}$ is referred to as an $m \times m$ *Wishart* matrix with the parameters $n := max\{N_r, N_t\}$ and $m := min\{N_r, N_t\}$. The capacity expressions (2.29)-(2.30) can now be reformulated in terms of the eigenvalues $\lambda_1, \ldots, \lambda_m$ of $\mathcal{W}$,

$$C = E_\lambda\left\{\sum_{i=1}^{m} \log_2\left(1 + \frac{S}{N_t}\lambda_i\right)\right\} \tag{2.32}$$

where the joint pdf of the order eigenvalues of a *Wishart* matrix is known to be [21],

$$f_\lambda(\lambda) := K_{m,n}^{-1} \prod_i \lambda_i^{n-m} e^{-\lambda_i} \prod_{i<j} (\lambda_i - \lambda_j)^2 \tag{2.33}$$

and $K_{m,n}$ is a normalizing factor. Telatar conjectures that the channel capacity only depends on the distribution of one of the eigenvalues,

$$E_\lambda\left\{\sum_{i=1}^{m} \log_2\left(1 + \frac{S}{N_t}\lambda_i\right)\right\} = \sum_{i=1}^{m} E_{\lambda_i}\left\{\log_2\left(1 + \frac{S}{N_t}\lambda_i\right)\right\} \tag{2.34}$$

$$= mE_{\lambda_1}\left\{\log_2\left(1 + \frac{S}{N_t}\lambda_1\right)\right\} \tag{2.35}$$

Thereby yielding the landmark MIMO capacity theorem derived by Telatar [15],

$$C = m\int_0^\infty \log_2\left(1 + \frac{S}{N_t}\lambda_1\right) f_{\lambda_1}(\lambda_1) d\lambda_1 \tag{2.36}$$

where the marginal pdf for λ_1 is given by [15],

$$f_{\lambda_1}(\lambda_1) := \frac{1}{m}\sum_{k=0}^{m-1}\frac{k!}{(k+n-m)!}[\mathcal{L}_k^{n-m}(\lambda_1)]^2\lambda_1^{(n-m)}e^{\lambda_1} \tag{2.37}$$

and $\mathcal{L}_k^{n-m}(\lambda_1)$ is the Laguerre polynomial of order k. Associated closed form and iterative solutions for the MIMO capacity integral (2.36) are derived in [5].

SIMO channel capacity Consider then a SIMO channel $\mathbf{H}\mathbf{H}^H = \|\mathbf{h}\|_F^2$ with N_r receive antennas ($N_t = 1$). The SIMO channel exhibits a single spatial data pipe $\lambda_1 = \|\mathbf{h}\|_F^2$ rendering the parameters $m = N_r$ and $n = N_t$, therefore reducing (2.36) to,

$$C_{SIMO} = \frac{1}{\Gamma(N_r)}\int_0^\infty \log_2(1+S\lambda_1).\lambda_1^{(N_r-1)}e^{\lambda_1}d\lambda_1 \tag{2.38}$$

where $\Gamma(\cdot)$ defines the *Gamma* function and the associated pdf is a central chi-square distribution with $2N_r$ degrees of freedom. Note that channel knowledge at the transmitter provides no additional improvement in achievable channel capacity.

MISO channel capacity Alternatively, a MISO channel $\mathbf{H}^H\mathbf{H} = \|\mathbf{h}\|_F^2$ with N_t transmit antennas ($N_r = 1$). The MISO channel exhibits similar characteristics to the SIMO channel, i.e. a single spatial data pipe $\lambda_1 = \|\mathbf{h}\|_F^2$, yielding,

$$C_{MISO} = \frac{1}{\Gamma(N_t)}\int_0^\infty \log_2\left(1+\frac{S}{N_t}\lambda_1\right).\lambda_1^{(N_t-1)}e^{\lambda_1}d\lambda_1 \tag{2.39}$$

Here it is assumed that CSI is unavailable at the transmitter and in conjunction with the MIMO case we assume $\mathbf{R}_{ss} = S/N_t.\mathbf{I}_{N_t}$. Clearly, without CSI, $C_{MISO} < C_{SIMO}$, by observing the $1/N_t$ factor in (2.40) and that logarithmic functions are monotonically increasing. If for every channel realization the transmitter has knowledge of the CSI then a beam-forming approach may be used to transmit through λ_1,

$$C_{MISO} = \frac{1}{\Gamma(N_t)}\int_0^\infty \log_2(1+S\lambda_1).\lambda_1^{(N_t-1)}e^{\lambda_1}d\lambda_1 \tag{2.40}$$

Therefore MISO with transmit CSI achieves SIMO capacity with the same $\|\mathbf{h}\|^2$.

2.2.4 Non-Ergodic MIMO Channel

In the case of non-ergodic MIMO channels the *Shannon* [13] channel capacity is zero since there is a non-zero probability that the fixed channel realization cannot support error-free transmission at a predetermined rate. As stated previously in Section 2.1.2; a more meaningful metric for the analysis of such channels would be the achievable tradeoff *rate* for a given *outage probability* and vice versa. An interesting open problem is to determine the optimal code-book for any given rate R and SNR ρ that minimizes the total probability $P_{out}(R, S)$ that a channel realization $\mathbf{H}$ does not support the desired rate R,

$$P_{out}(R, S) = \inf_{Q \succeq 0, Tr(Q) \leq S} \left\{ Pr\left(\mathbf{I}_{N_r} + \mathbf{HQH}^H < R \right) \right\} \tag{2.41}$$

where $\inf\{\cdot\}$ denotes the infimum. Telatar conjectures that the $\mathbf{Q}$ which minimizes the outage probability (2.41) utilizes only a subset of the available transmit antennas and has the form,

$$\mathbf{Q} = \frac{S}{\tau} \begin{bmatrix} \mathbf{I}_\tau & \mathbf{0}_{N_t-\tau} \\ \mathbf{0}_{N_t-\tau} & \mathbf{0}_{N_t-\tau} \end{bmatrix} \tag{2.42}$$

where τ defines the size of the subset of transmit antennas selected Adopting this coding strategy by substituting (2.42) into (2.41) and performing eigenvalue decomposition yields the *outage probability*,

$$P_{out}(R, S) = Pr\left(\sum_{i=1}^{\tilde{m}} \log_2 \left(1 + \frac{S}{\tau} \lambda_i \right) < R \right) \tag{2.43}$$

where $\tilde{m} = \min\{\tau, N_r\}$. Clearly, if all the eigenvalues $\lambda_1, \cdots, \lambda_{\tilde{m}}$ are independent the evaluation of (2.43) requires an $\tilde{m}$-fold convolution of the pdf $\log_2\left(1 + \frac{S}{\tau}\lambda_i\right)$ according to the unordered distribution $f_{\lambda_1}(\lambda_1)$ (2.37). The evaluation of the *outage probability* is greatly simplified in the SIMO or MISO case which is considered next.

SIMO Outage Probability As stated in [15, Example 6], the outage probability is minimized for any given rate and SNR region for $\mathbf{S} = S$, yielding,

$$P_{out}(R, S) = \gamma\left(N_r, (2^R - 1)/\rho\right) / \Gamma(N_r) \tag{2.44}$$

where $\gamma(\cdot)$ denotes the incomplete Gamma function defined as $\gamma(a,x) := \int_0^x u^{(a-1)}e^{-u}du$. As in the case of *ergodic* channels, CSI at the transmitter does not improve the link performance.

SIMO Outage Probability Using Telatar's conjecture (2.42), transmitting equally over τ antennas out of the N_t available the outage probability of the MISO case is expressed as [15, Example 7],

$$P_{out}(R,S) = \gamma\left(N_t, N_t(2^R-1)/\rho\right)/\Gamma(N_t) \tag{2.45}$$

Telatar's conjecture in this case is substantiated by the observation that in the low rate region a higher τ, i.e. using more of the available transmit antennas, reduces the likelihood that the channel cannot support the rate. However, in the high rate low reliability region it is acknowledged that reducing τ and transmitting over fewer antennas with more power yields a reduction in outage probability.

2.3 Channel Characteristics and Classification

Unlike simple *Gaussian* channels that are only impaired by Additive White Gaussian Noise (AWGN) at the receiver, other wireless channels suffer additionally from random fluctuations in the received signal level across space, time and/or frequency. This effect is referred to in the literature [14, 6] as channel fading and can be classified into two main categories. Each is briefly summarized below:

- *slow fading* - caused by a large reflecting object or diffraction effects which are geographically distant from the receiver. These fading factors only induce small perturbations in the signal strength when the distance travelled by the receiver is small compared to the propagation distance from the objects concerned.

- *fast fading* - caused by reflectors close to the receiving terminal and the movement of the receiver with respect to these objects. Each reflector effectively creates a copy of the transmitted signal, which introduces a *multipath* effect. Each path differs in length and introduces phase perturbations in the transmitted signal, therefore multiple copies of the receive signal superimpose in either a constructive or destructive manner.

The main method to stabilize a wireless channel exhibiting fading is to introduce diversity, especially if the channel is experiencing fast fading. Diversity introduces multiple copies of the information bearing signal over ideally independent realizations of the fading channel. In the literature each copy is referred to as a *diversity branch*. It can be proven that increasing the number of diversity branches sharply reduces the probability that all branches will be in fade and therefore stabilizes the wireless link in the limiting case to that of an equivalent Gaussian channel [6].

A communication system can only extract diversity that is intrinsically available in a channel. The diversity available in a wireless channel can be simply categorized as follows:

- *Temporal Diversity* - redundancy is introduced in the time domain through the use of temporal interleaving and channel coding. To ensure the transmitted signal experiences independent fading, replicas should be spaced at intervals no less than the *coherence time* of the channel (Section 2.3.1).

- *Frequency Diversity* - the information bearing signal is transmitted to the receiver using multiple carrier frequencies. Selecting carriers that are spaced greater than the *coherence bandwidth* (Section 2.3.2) in the frequency domain ensures that the transmitted signal undergoes independent fading.

- *Spatial Diversity* - using multiple transmit and/or receive antennas at the source and destination terminals ensures that replicas of the signal are available at the receiver. To maximize diversity gain antenna elements should be separated by a distance greater than the *coherence distance* (Section 2.3.3) so that correlation in received signal copies are minimized and the fading channels are independent.

Temporal or frequency diversity traditionally have additional cost factors associated with introducing redundancy, in the form of additional channel utilization and bandwidth consumption. The wireless medium is a scarce resource, therefore the majority of this thesis shall focus primarily on spatial diversity techniques, limiting the costs to additional complexity of the transceiver design.

2.3.1 Time Selective

Time-selective channels show fast-fading characteristics as a result of self interference from local reflectors. This type of selectivity assumes that the multiple paths displayed in the channel are observed at the same instance in time and the channel has no memory. Wireless channels are extremely complicated three-dimensional systems, therefore engineers have devised statistical models [14] to simplify the analysis. For small-scale fast fading effects without a Line-Of-Sight (LoS) component the random channel gains can be modelled fairly accurately by the Rayleigh distribution [14], where each channel realization $h(t)$ models the impulse response at continuous time t and follows the distribution,

Channels classified as time-selective, can be modeled using a Rayleigh distributed complex gain term $h(t)$ (2.46), for the impulse response at time t.

$$h \sim \mathcal{N}_{\mathbb{C}}(0, 1) \tag{2.46}$$

The input-output relationship of a time-selective SISO channel is shown as,

$$y(t) = h(t)\ s(t) \tag{2.47}$$

Modern communication signal processing techniques are typically implemented in the discrete-time domain, therefore the equivalent sampled signal model of (2.47) can be expressed as,

$$y[k] = h[k]\ s[k] \tag{2.48}$$

where k represents the sampling index with normalized unity sampling period. This simple SISO signal model can be extended for MIMO type channels,

$$\mathbf{y}[k] = \mathbf{H}[k]\ \mathbf{s}[k] \tag{2.49}$$

where $\mathbf{y}[k]$ is the received signal vector of dimension $N_r \times 1$ ignoring the effects of additive noise at the receiver, $\mathbf{s}[k]$ is the transmit signal vector of dimension $N_t \times 1$ and $\mathbf{H}[k]$ represents the matrix form of a channel with dimension $N_r \times N_t$. Each element $\mathbf{H}_{i,j}[k]$ represents the sampled impulse response sequence of the SISO channel between transmit antenna j and receive antenna i, the MIMO channel is represented in matrix form as,

$$\mathbf{H}[k] = \begin{bmatrix} h_{1,1}[k] & h_{1,2}[k] & \cdots & h_{1,N_t}[k] \\ h_{2,1}[k] & h_{2,2}[k] & \cdots & h_{2,N_t}[k] \\ \vdots & \vdots & \ddots & \vdots \\ h_{N_r,1}[k] & h_{N_r,2}[k] & \cdots & h_{N_r,N_t}[k] \end{bmatrix} \tag{2.50}$$

By definition a time-selective channel implies that the channel is more favorable at some moments in time than others. In real channels with mobile terminals and/or mobile objects that cause scattering effects, the fading process will introduce Doppler spread of $2f_D$, where f_D is defined as the maximum Doppler frequency. The time period over which the channel remains strongly correlated can be defined by (2.51) and is referred to as *coherence time* [14].

$$T_c \approx \frac{1}{2f_D} \tag{2.51}$$

To extract maximum diversity, replicas of the transmitted signal should ideally observe i.i.d. instances of the channel from the distribution (2.46). Although temporal spacing at greater than the *coherence time* does not imply the channel realizations will be i.i.d., it does provide useful guidance for mitigating temporal fading.

2.3.2 Frequency Selective

Frequency-selective channels introduce a delay spread T_M caused by the received signal propagating through multi-paths of different lengths. Constructive and destructive interference is a function of received signal wavelength therefore the channel responds as a filter in the frequency domain. The input-output relationship of a time-varying frequency-selective SISO channel in the continuous time domain can be represented as,

$$y(t) = h(t, \tau) \otimes s(t) \tag{2.52}$$

where $\otimes$ represents the convolution operator. For analysis in the discrete-time domain the channel can be simplified and converted to an equivalent time-invariant sample signal model,

$$y[k] = \sum_{l=0}^{L-1} h[k-l]\ s[l] \tag{2.53}$$

where L denotes the length of the channel in sampling periods (usually sampled at the baud rate). For frequency-selective time invariant channels $h[l]$ can be modeled using ZMCSCG variables distribution according to (2.46). A power delay profile may be applied to model the attenuation of paths with longer delays. A MIMO sample channel model is easily derived by expressing the multiple SISO channels (2.53) between the ith receive and j^{th} transmit antenna, shown in matrix notation as,

$$\mathbf{y}[k] = \begin{bmatrix} \mathbf{h}_{1,1} & \cdots & \mathbf{h}_{1,N_t} \\ \vdots & \ddots & \vdots \\ \mathbf{h}_{N_r,1} & \cdots & \mathbf{h}_{N_r,N_t} \end{bmatrix} \begin{bmatrix} \mathbf{s}_1[k] \\ \vdots \\ \mathbf{s}_{N_t}[k] \end{bmatrix} \tag{2.54}$$

where,

$$\mathbf{h}_{i,j} = [h_{i,j}[L-1]\ \cdots\ h_{i,j}[0]] \tag{2.55}$$

and,

$$\mathbf{s}_j[k] = \begin{bmatrix} s_j[k-L+1] \\ \vdots \\ s_j[k] \end{bmatrix} \tag{2.56}$$

To extract diversity from a frequency-selective channel one needs to determine the *coherence bandwidth* B_c, the bandwidth over which the channel fading remains strongly correlated. *Coherence bandwidth* can be expressed as a function of the multipath delay spread T_M[14],

$$B_c \approx \frac{1}{T_M} \tag{2.57}$$

To maximize diversity in real channels it should be ensured that the frequency spacing of any information bearing sub-carriers is ideally greater than the *coherence bandwidth.*

2.3.3 Spatially Selective

Channels where the received signal amplitude is dependent on the location of the antenna can be described as *spatially selective*. The cause of this spatially selective fading, is the *angular spread* or spread in Angle Of Arrival (AOA) of the multipath signal components at the receive antenna array.

The *coherence distance* D_c of the channel characterizes the spatial selective fading process, and defines a separation distance for which the normalized autocorrelation coefficient falls to 0.7. The relationship between the *angular spread* θ and *coherence distance* D_c is clearly shown as [6, Eq.2.16],

$$D_c \approx \frac{1}{\theta_{RMS}} \tag{2.58}$$

where θ_{RMS} defines the Root Mean Square (RMS) angular spread. To maximize diversity the aim should be to achieve uncorrelated fading across the diversity branches and therefore an appropriate rule of thumb should be to position antenna elements at a minimum spatial separation defined by D_c.

2.4 Techniques for Extracting Diversity Gain in Fading Environments

Several techniques are reviewed to demonstrate how diversity gains can be leveraged to increase the robustness when operating in the classifications of fading-channels presented in the previous section. Codes and techniques that extract diversity from the channel both at the transmit and receiver side will be presented. In the case of receiver-side processing it will be assumed that CSI is available as a byproduct of the channel estimation process used in the operation of the decoder. At the transmit side the qualification of CSI cannot always be assumed and may be dependent upon the availability of a feedback channel and how static the fading processes is to evaluate the information content from the feedback channel. In scenarios where it is prohibitive to use feedback or the channel cannot be estimated at the transmitter techniques are presented that extract the full-diversity gain available from a spatially-selective channel in the absence of CSI. These techniques will form a foundation for the novel processing techniques

developed in this thesis for application in cooperative wireless relay networks.

2.4.1 Diversity at the Receiver

To extract receive antenna diversity, multiple receiving antennas are used to form an array. If the antennas are spaced at a distance greater than the *coherence distance* (approx several radio wavelengths) then each copy of the broadcast transmitted signal can be assumed to be uncorrelated or essentially independent from a fading perspective. The independent copies from the receive antennas can then be *combined* using linear processing (or non-linear Square-Law Combining (SLC)) to improve receiver performance. Four such combining techniques are summarized below:

1. *Square-Law Combining* - a non-coherent form of combining that does not require CSI, however this technique is only applicable to particular modulation techniques such as FSK.

2. *Selection Combining* - selects the antenna from the receive array with the highest SNR output signal.

3. *Equal-Gain Combining* - multiplies the received signal from each antenna with a constant magnitude complex weighting parameter α that corrects for the phase introduced by the channel.

4. *Maximal Ratio Combining (MRC)* - uses a similar approach to equal-gain combining, however the weighting parameter α is assumed to be the complex conjugate of the estimated channel gain. This technique is optimal amongst all linear diversity techniques therefore further analysis is outlined below.

Consider a communication system with a single transmit antenna and a receive antenna array (SIMO) for the purpose of illustrating receive antenna diversity in the form of MRC. Also assuming the channel is i.i.d. Rayleigh distributed (2.46) and flat fading, therefore omitting the sample index k, the channel vector $\mathbf{h}$ can be expressed as,

$$\mathbf{h} := [h_1 \; h_2 \; \cdots \; h_{N_r}]^T \tag{2.59}$$

where N_r denotes the number of receive antenna elements. The received signal including noise perturbations can therefore be expressed in vector form as,

$$\mathbf{y} = \mathbf{h}s + \mathbf{n} \tag{2.60}$$

where s denotes the transmitted signal from a finite constellation with average energy E_s and $\mathbf{n}$ denotes AWGN at each receiver branch with covariance matrix $E\{\mathbf{n}\mathbf{n}^H\} = N_0\mathbf{I}_{N_r}$ denoted by the power spectral density N_0. Assuming perfect CSI at the receiver, *MRC* can be performed,

$$z = \|\mathbf{h}\|^2 s + \mathbf{h}^H\mathbf{n} \tag{2.61}$$

where z is the combined output of the receiver and $\|\mathbf{h}\|^2 = \mathbf{h}^H\mathbf{h}$, i.e. the squared Euclidean norm. In the same way that *matched filter* techniques provide optimal reciever performance for AWGN channels using temporal processing [2], MRC optimizes SNR by matching the channel in the spatial domain, where the instantaneous SNR γ_{mrc} at the receiver is given by,

$$\gamma_{mrc} = \frac{E_s}{N_0}\sum_{j=1}^{N_{N_r}} |h_j|^2 \tag{2.62}$$

Assuming i.i.d. Rayleigh faded complex channel gains with unity variance, then the expected SNR can be expressed as,

$$\bar{\gamma}_{mrc} = \frac{E_s}{N_0}\sum_{j=1}^{N_r} E\{|h_j|^2\} \tag{2.63}$$

$$= N_r.\frac{E_s}{N_0} \tag{2.64}$$

Clearly, (2.64) shows that the receive antenna array provides a gain in the average SNR of the received signal, this gain is referred to as *array gain*, and is shown to be proportional to the number of receive antennas N_r. Using MRC and assuming ML detection at the receiver the average probability of error in the high SNR scenario was shown to be upper bounded by [6],

$$\bar{P}_e \leq \bar{N}_e \left(\frac{E_s\, d_{min}^2}{4\, N_0}\right)^{-N_r} \tag{2.65}$$

where $\bar{N}_e$ and d_{min} are the number of nearest neighbours and minimum distance of an underlying scalar constellation $\mathbb{S}$. The diversity order of the system is clearly represented in (2.65) as the exponent and is shown to be equal to the number of adequately spaced antenna elements at the receiver. To summarize, benefits of diversity at the receiver are clearly illustrated through increasing the number of receive antennas as presented in Figure 2.1.

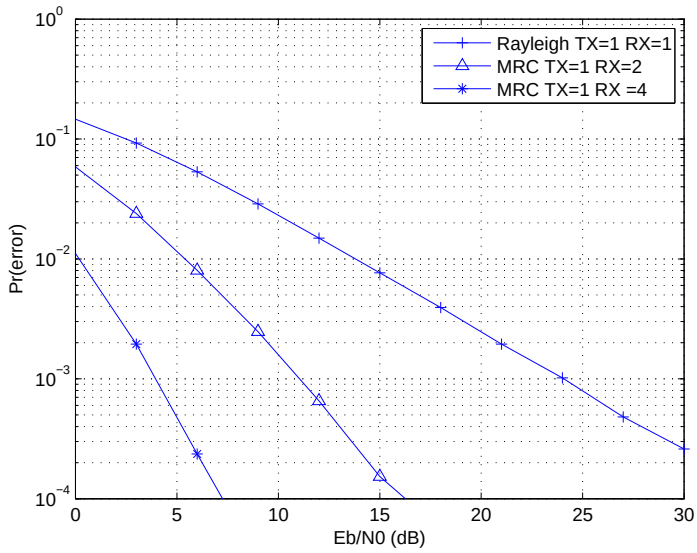

Figure 2.1: BER performance of an MRC scheme in Rayleigh flat-fading channels

2.4.2 Exploiting CSI for Transmit Diversity Gain

In the same way multiple receive antennas can be utilized to extract diversity from a channel, there are algorithms to achieve transmit antenna diversity. Considering a MISO channel with N_t transmit antennas and one receive antenna, using the same assumptions that formulated (2.59), the channel can be expressed as,

$$\mathbf{h} = [h_1 \; h_2 \; \cdots \; h_{N_t}] \tag{2.66}$$

Pre-processing the transmitted signal with a weighting vector $\mathbf{w}$ produces a received signal y expressed as,

$$y = \sqrt{\frac{1}{N_t}}\mathbf{h}\mathbf{w}s + n \tag{2.67}$$

where s is the symbol from a finite constellation with constant energy E_s and n is ZMCSCG noise at the receiver with variance N_0. With full CSI available at the transmitter the problem is remarkably similar to the MRC case (Section (2.4.1)) and is referred to in the literature as transmit-Maximal Ratio Combining (t-MRC) [22]. Thus it can be shown that the weight vector that maximizes SNR is given by,

$$\mathbf{w} = \sqrt{N_t}\frac{\mathbf{h}^H}{\|\mathbf{h}\|} \tag{2.68}$$

the scalar normalizing coefficient $\sqrt{N_t}/\|\mathbf{h}\|$ ensures that the transmit energy is constrained to E_s. The instantaneous SNR at the receiver can then be calculated as,

$$\gamma_{t-mrc} = \frac{E_s}{N_0}\sum_{i=1}^{N_t}|h_i|^2 \tag{2.69}$$

Assuming i.i.d. Rayleigh faded complex channel gains with unity variance, then the expected SNR can be expressed as,

$$\bar{\gamma}_{t-mrc} = \frac{E_s}{N_0}\sum_{i=1}^{N_t}E\{|h_i|^2\} \tag{2.70}$$

$$= N_t.\frac{E_s}{N_0} \tag{2.71}$$

This result (2.71) clearly shows that t-MRC offers increased SNR performance at the receiver through pre-processing at the transmitter in the form of *array gain* which is proportional to the number of transmit antenna elements N_t.

Adopting a similar approach used to analyze the MRC scheme the average probability of error for t-MRC, assuming ML detection at the receiver and a high SNR regime, can be upper bounded by [6],

$$\bar{P}_e \leq \bar{N}_e\left(\frac{E_s\ d_{min}^2}{4\ N_0}\right)^{-N_t} \tag{2.72}$$

when $\bar{N}_e$ and d_{min} are the number of nearest neighbours and minimum distance of an underlying scalar constellation respectively. Consistent with MRC at the receiver, t-MRC also extracts a diversity order equal to the number of antennas t in the transmit antenna array, which is clearly illustrated in the exponent of (2.72). For completeness the Bit Error Rate (BER) performance of t-MRC is included in Figure 2.2 where the similarity to MRC Figure 2.1 is demonstrated.

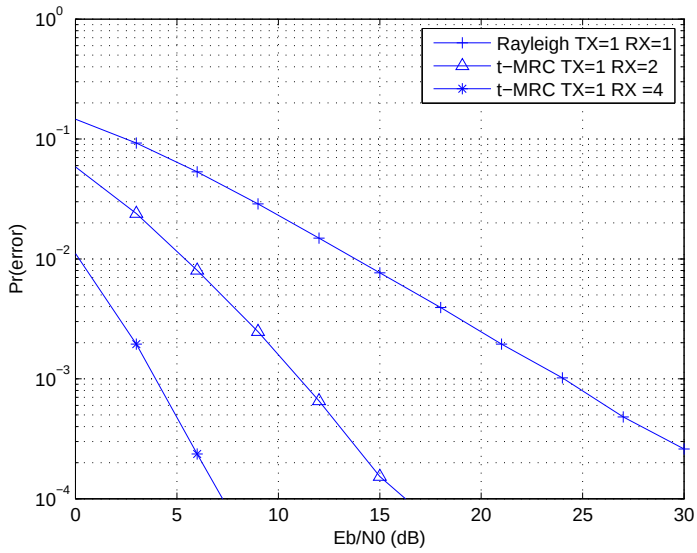

Figure 2.2: BER performance of t-MRC in Rayleigh flat-fading channels

Although this technique extracts full diversity gain from the channel, as well as array gain, there is still the additional problem of estimating the CSI. Usually this is achieved by channel estimation at the receiver employing feedback to the transmit side, which requires a strong stationarity assumption on the channel. The next section introduces a transmit diversity technique which extracts full diversity from the channels without the additional complications of feedback.

2.4.3 Transmit Diversity In the Absence of CSI

2.4.3.1 Orthogonal Space-Time Block Codes

Considering a MISO channel with two transmit antennas and a single receive antenna, expressed as,

$$\mathbf{h} = [h_1 \; h_2] \tag{2.73}$$

where h_i is again denoted by ZMCSCG random variables with unity variance. There exist techniques that extract full diversity without CSI at the transmitter. A simple method to extract full diversity, but not the most spectrally efficient, would be to use a simple repetition based STBC,

$$\mathbf{G} = \begin{bmatrix} s_1 & 0 \\ 0 & s_1 \end{bmatrix} \tag{2.74}$$

where the transmission matrix $\mathbf{G}(z_1, \cdots, z_k)$ is formulated by the number of transmitted symbols N_x, i.e. $N_x = 1$ in the above example (2.74), the number of transmit antennas N_t (columns) and time slots in a data block N_s (rows).

Alamouti Coding Alamouti [23] devised the first *full-rate* Orthogonal Space Time Block Code (OSTBC),

$$\mathbf{S} = \begin{bmatrix} s_1 & s_2 \\ -s_2^* & s_1^* \end{bmatrix} \tag{2.75}$$

In the case of *Alamouti* coding the set of complex symbols $\{s_i\}_{i=1}^2$ is linearly mapped to form a transmission matrix (2.75) with dimension $N_s = N_t = 2$, where N_t and N_s denote the spatial and temporal dimension size respectively. In the first time-slot k simultaneous transmission occurs with the symbol s_1 transmitted from the first transmit antenna and s_2 transmitted from the second antenna. In the proceeding time-slot $k+1$, $-s_2^*$ is transmitted from the first antenna and simultaneously s_1^* from the second antenna. From (2.75) it is obvious that the *code-rate*, defined by the ratio N_x/N_s, is unity (one data symbol per time-slot). For a simple system with a single receive antenna the following input-output relationship is observed,

$$\begin{bmatrix} r_k \\ r_{k+1} \end{bmatrix} = \begin{bmatrix} s_1 & s_2 \\ -s_2^* & s_1^* \end{bmatrix} \begin{bmatrix} h_1 \\ h_2 \end{bmatrix} + \begin{bmatrix} n_k \\ n_{k+1} \end{bmatrix} \tag{2.76}$$

$$\mathbf{r} = \mathbf{S}\mathbf{h} + \mathbf{n} \tag{2.77}$$

where n_k denotes the additive ZMCSCG noise component incident at the receiver and r_k denotes the noisy copy of the transmitted signal at time-slot k. Conjugating the second row of (2.76) allows for an equivalent system representation that formulates the system of equations using an *effective* channel matrix,

$$\begin{bmatrix} r_k \\ r_{k+1}^* \end{bmatrix} = \begin{bmatrix} h_1 & h_2 \\ h_2^* & -h_1^* \end{bmatrix} \begin{bmatrix} s_1 \\ s_2 \end{bmatrix} + \begin{bmatrix} n_k \\ n_{k+1}^* \end{bmatrix} \tag{2.78}$$

$$\mathbf{r}' = \mathbf{H}_{eff}\mathbf{s} + \mathbf{n}' \tag{2.79}$$

Without loss of generality we can translate (2.79) to new co-ordinates using the unitary matrix $\mathbf{H}_{eff}^H/\sqrt{|h_1|^2 + |h_2|^2}$,

$$\frac{\mathbf{H}_{eff}^H\mathbf{r}'}{\sqrt{|h_1|^2 + |h_2|^2}} = \frac{\mathbf{H}_{eff}^H\mathbf{H}_{eff}}{\sqrt{|h_1|^2 + |h_2|^2}}\mathbf{s} + \frac{\mathbf{H}_{eff}^H}{\sqrt{|h_1|^2 + |h_2|^2}}\mathbf{n}' \tag{2.80}$$

$$\mathbf{r}'' = \sqrt{|h_1|^2 + |h_2|^2}\mathbf{I}_2\ \mathbf{s} + \mathbf{n}'' \tag{2.81}$$

where we have used the substitution $\mathbf{H}_{eff}^H\mathbf{H}_{eff} = (|h_1|^2 + |h_2|^2)\mathbf{I}_2$ in (2.80) to derive (2.81). In addition it is worth highlighting that the statistics of the noise term $\mathbf{n}''$ are $N(0, N_0\mathbf{I}_2)$ and are equivalent to the underlying noise $\mathbf{n}$ incident at the receiver. As a result of the unitary matched filtering operation the noise remains spectrally white. Maximum Likelihood (ML) symbol-by-symbol estimation can now be performed using the decoupled observation by performing a search over the finite alphabet A_s the transmitted symbols were generated from,

$$\hat{s}_k = \arg\min_{\forall \hat{s}_k \in A_s} \left(r_k'' - \sqrt{|h_1|^2 + |h_2|^2}\hat{s}_k \right) \tag{2.82}$$

In the absence of CSI at the transmitter it has been shown [6] that distributing equally available transmit power over all transmitting antenna is the optimal strategy from a capacity achieving perspective, therefore yielding an average SNR at the receiver,

$$\bar{\gamma}_{Alamouti} = \frac{E_s}{2.\,N_0}\sum_{k=1}^{2} E\{|h_k|^2\} \tag{2.83}$$

$$= \frac{E_s}{N_0} \tag{2.84}$$

Equation (2.84) demonstrates a penalty in not utilizing the available *array gain* of approximately 3dB (i.e. $1/N_t$) against the averaged-SNR of the transmit diversity scheme (2.71).
Using a similar analytical approach to the previous section the average probability of error for the transmit scheme (2.75) was shown [6] to be proportional to (2.72) when $N_t = 2$, i.e. full order diversity.
The design of the transmission matrix can be classified into two categories:

- Complex Orthogonal Design (COD) - which must satisfy the condition of complex orthogonality in both the spatial and temporal sense,

$$\mathbf{G}\mathbf{G}^H = \mathbf{G}^H\mathbf{G} = \left(\sum_{i=1}^{k} |z_i|^2\right)\mathbf{I}, \qquad z_i \forall C \tag{2.85}$$

- Generalized Complex Orthogonal Design (GCOD) - the spatial orthogonality constraint is relaxed,

$$\mathbf{G}\mathbf{G}^H \neq \mathbf{G}^H\mathbf{G} = \left(\sum_{i=1}^{k} |z_i|^2\right)\mathbf{I}, \qquad z_i \forall C \tag{2.86}$$

In [24] it was proved that the only *full-rate* (rate of unity) OSTBCs must satisfy (2.85) and only exist for $N_t = 2$. Satisfying only (2.86) permits OSTBCs to be designed for $N_t = 3, 4$, however the *code-rate* performance is reduced to *half-rate* for a constant power envelope. Sporadic OSTBCs, defined in [24], can achieve a *3/4-rate* therefore increasing the bandwidth efficiency. However, this may increase the linearity required of RF power amplifiers because of increased transmit power fluctuations.
Generally, there are three properties that all OSTBCs possess which makes for an extremely powerful STC technique, namely:

1. Simple linear processing of the encoded symbols to generate the transmit OSTBC as shown in (2.75).

2. Full spatial diversity extracted from a MIMO channel without the transmitter having any knowledge of CSI, i.e. feedback unnecessary so long as the channel remains static over block transmission. In [25] a criterion for

the construction of space-time codewords to achieve full spatial diversity was set out and referred to as the *rank criterion*.

3. Simple linear processing at the receiver can generate a ML estimate of the transmitted symbol sequence, due to the orthogonalization of the MIMO channel [23].

Additionally STBC can be extended to MIMO channels as was shown in [23]. In MIMO channels however, only array gain at the receive side can be leveraged as shown in Figure 2.3. Note, MRC techniques have been included for comparison to demonstrate the effects of unutilized array gain at the transmit side. As demonstrated in Figure 2.3, without knowledge of the CSI at the transmitter, STBC cannot leverage the array gain available at the transmit-side resulting in an 3dB SNR to meet the BER of an equivalent order MRC scheme. However the gradient of the plots demonstrates that diversity gain is extracted where available from the channel.

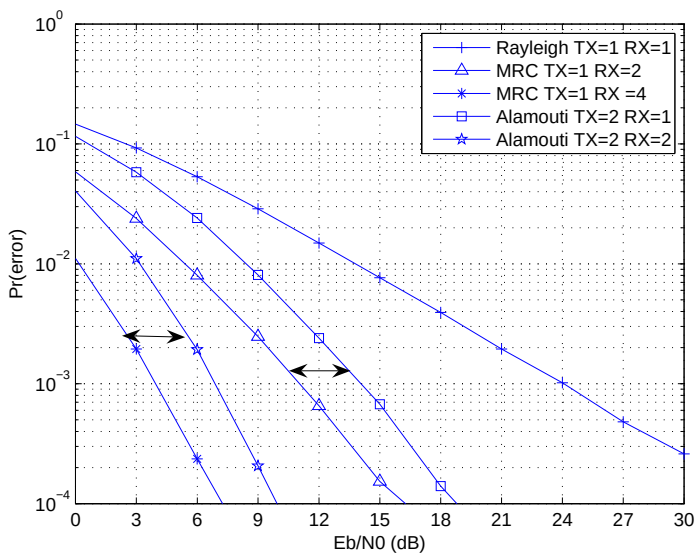

Figure 2.3: BER performance of Alamouti STBC scheme in Rayleigh flat-fading channels

2.4.3.2 Quasi-Orthogonal STBCs

Quasi-Orthogonal Space Time Block Codes (QOSTBCs) have many of the attractive properties of orthodox OSTBCs, such as; full-rate transmission[1], simple linear processing at the transmitter and low complexity ML decoding at the receiver side. Initially, both Papadias [12] and Jafarkhani [11] proposed an extension to the *Alamouti* scheme for four transmit antennas by relaxing the orthogonality constraint. Illustrated below are coding examples of QOSTBCs,

$$\mathbf{S} = \begin{bmatrix} s_1 & s_2 & s_3 & s_4 \\ s_2^* & -s_1^* & s_4^* & -s_3^* \\ s_3 & -s_4 & -s_1 & s_2 \\ s_4^* & s_3^* & -s_2^* & -s_1^* \end{bmatrix} \tag{2.87}$$

$$\mathbf{S} = \begin{bmatrix} s_1 & s_2 & s_3 & s_4 \\ -s_2^* & s_1^* & -s_4^* & s_3^* \\ -s_3^* & -s_4^* & s_1^* & s_2^* \\ s_4 & -s_3 & s_2 & -s_1 \end{bmatrix} \tag{2.88}$$

where (2.87) refers to the Papadias implementation and (2.88) refers to the Jafarkhani derivative. Clearly, QOSTBCs exhibit a code-rate of unity, i.e. four complex data symbols are transmitted over four time-slots. It can be shown that although the codes (2.87) and (2.88) vary in the implementation, the properties of both codes are identical therefore this thesis proceeds without prejudice on the basis of the Jafarkhani scheme (2.88).

For the purposes of brevity the input-output system representation is omitted and instead focus on the effective system representation where it should be noted that the observed symbols at the second and third time-slots have been conjugated to represent the system with an effective MIMO ST channel matrices,

$$\begin{bmatrix} r_k \\ r_{k+1}^* \\ r_{k+2}^* \\ r_{k+3} \end{bmatrix} = \begin{bmatrix} h_1 & h_2 & h_3 & h_4 \\ h_2^* & -h_1^* & h_4^* & -h_3^* \\ h_3^* & h_4^* & -h_1^* & -h_2^* \\ h_4 & -h_3 & -h_2 & h_1 \end{bmatrix} \begin{bmatrix} s_1 \\ s_2 \\ s_3 \\ s_4 \end{bmatrix} + \begin{bmatrix} n_k \\ n_{k+1}^* \\ n_{k+2}^* \\ n_{k+3} \end{bmatrix} \tag{2.89}$$

$$\mathbf{r}' = \mathbf{H}_{eff}\mathbf{s} + \mathbf{n}' \tag{2.90}$$

[1]Note: Only feasible for the two-transmitter *Alamouti* coding when restricted to OSTBCs

Performing spatial matched filtering with $\mathbf{H}_{eff}^H$ renders a sparse system representation,

$$\mathbf{H}_{eff}^H \mathbf{r}' = \mathbf{H}_{eff}^H \mathbf{H}_{eff} \mathbf{s} + \mathbf{H}_{eff}^H \mathbf{n}' \tag{2.91}$$

$$\mathbf{r}'' = \mathbf{\Delta}\ \mathbf{s} + \mathbf{n}'' \tag{2.92}$$

Note: After matched filtering is applied the noise observed at the receiver is colored according to $\mathbf{n}'' \sim \mathcal{N}_{\mathbb{C}}(0, N_0 \mathbf{\Delta})$. What makes QOSTBCs so interesting is the sparsity pattern of the matrix Δ,

$$\mathbf{\Delta} = \begin{bmatrix} \gamma & 0 & 0 & \alpha \\ 0 & \gamma & -\alpha & 0 \\ 0 & -\alpha & \gamma & 0 \\ \alpha & 0 & 0 & \gamma \end{bmatrix} \tag{2.93}$$

where,

$$\gamma = \sum_{i=1}^{4} |h_i|^2 \tag{2.94}$$

$$\alpha = 2.\Re\{h_1 h_4^* - h_2 h_3^*\} \tag{2.95}$$

The operator $\Re\{\cdot\}$ returns the real component of the argument. In (2.93) the loss of orthogonality is clearly demonstrated by the presence of α terms in the off diagonal, which generate interference between the coupled symbol pairs $\{x_1, x_4\}$ and $\{x_2, x_3\}$. Later in this section a simple phase rotation at a subset of transmit antennas based on CSI will demonstrate interference nulling (i.e. $\alpha = 0$) and provide equivalence in *diversity gain* to that of higher order ($N_t = 4$) OSTBCs. Observing (2.93) it is possible to decouple the system representation into two parts, for simplicity the ensuing presentation shall only consider the pair $\{s_1, s_4\}$ however it is possible to deduce the pair $\{s_2, s_3\}$ from the following steps,

$$\begin{bmatrix} \mathbf{r}_1'' \\ \mathbf{r}_4'' \end{bmatrix} = \begin{bmatrix} \gamma & \alpha \\ \alpha & \gamma \end{bmatrix} \begin{bmatrix} s_1 \\ s_4 \end{bmatrix} + \begin{bmatrix} n_1'' \\ n_4'' \end{bmatrix} \tag{2.96}$$

$$\mathbf{r}_{14}'' = \mathbf{\Delta}_{14}\ \mathbf{s}_{14} + \mathbf{n}_{14}'' \tag{2.97}$$

Interestingly, $\mathbf{\Delta}_{14}$ can be decomposed into the following matrix multiplication $\mathbf{H}_{14}^H\mathbf{H}_{14}$ where $\mathbf{H}_{14}$ is constructed from the columns of (2.89) associated with $\{s_1, s_4\}$,

$$\mathbf{H}_{14} = \begin{bmatrix} h_1 & h_4 \\ h_2^* & -h_3^* \\ h_3^* & -h_2^* \\ h_4 & h_1 \end{bmatrix} \tag{2.98}$$

The equivalent sub-system (2.97) is still a MIMO representation although the dimensions of the coupling matrix no longer reflect that of space and time. When eigenvalue decomposition is performed on $\mathbf{\Delta}_{14}$, i.e. $\mathbf{\Delta}_{14} = \mathbf{V}\mathbf{\Lambda}_{14}\mathbf{V}^H$, it is straightforward to verify that the unitary eigenvector matrix $\mathbf{V}$ is,

$$\mathbf{V} = \frac{1}{\sqrt{2}} \begin{bmatrix} 1 & 1 \\ 1 & -1 \end{bmatrix} \tag{2.99}$$

The important concept to note is that unlike uncoded MIMO systems, QOSTBCs condition the effective channel matrix so that the eigenvectors are constant and independent of the underlying channel realizations. The eigenvalues can be shown to be,

$$\mathbf{\Lambda}_{14} = \begin{bmatrix} \gamma + \alpha & 0 \\ 0 & \gamma - \alpha \end{bmatrix} \tag{2.100}$$

$$\mathbf{\Lambda}_{23} = \begin{bmatrix} \gamma - \alpha & 0 \\ 0 & \gamma + \alpha \end{bmatrix} \tag{2.101}$$

.

If the assumption about no CSI at the transmitter is relaxed then it has been shown [26] that it is possible to cancel the interference arising due to the presence of the α term in (2.93) through the use of phase rotations at a subset of transmitter elements. To illustrate this concept the phase rotation is introduced as a matrix operation $\mathbf{\Phi} = diag(e^{j(\theta_1)}, \ldots, e^{j(\theta_4)})$ where the set $\{e^{j(\theta_1)}, \ldots, e^{j(\theta_4)}\}$ denotes the phase rotations applied across the four transmit antennas. This basic linear transform generates a new set of effective channel coefficients according to,

$$\tilde{\mathbf{h}} = \mathbf{\Phi}\mathbf{h} \tag{2.102}$$

Including the effects of the phase rotations the new transformed decoupling term α' can be expressed as,

$$\begin{aligned} \alpha' &= 2\Re\{\varrho e^{j(\psi)} - \vartheta e^{j(\phi)}\} && (2.103) \\ &= 2\left(|\varrho|\cos(\psi + \angle\varrho) - |\vartheta|\cos(\phi + \angle\vartheta)\right) && (2.104) \end{aligned}$$

where Euler's formula is employed in the second line and for simplicity in notation $\varrho = h_1 h_4^*$, $\vartheta = h_2 h_3^*$, $\psi = \theta_1 - \theta_4$ and $\phi = \theta_2 - \theta_3$. Note that the transformation does not affect the received path gain γ (2.94),

$$\begin{aligned} \gamma' &= \sum_{i=1}^{4} |\tilde{h}_i|^2 && (2.105) \\ &= \sum_{i=1}^{4} |h_i|^2 && (2.106) \\ &= \gamma && (2.107) \end{aligned}$$

It can be shown by evaluating the following equality,

$$|\varrho|\cos(\psi + \angle\varrho) = |\vartheta|\cos(\phi + \angle\vartheta) \tag{2.108}$$

that there are an infinite number of solutions to ψ and ϕ that obtain the desired $\alpha' = 0$. However, the original problem can be reformulated to reduce the solution space to two by casting the problem as,

$$\phi = \frac{\pi}{2} - \angle\vartheta \tag{2.109}$$

and correspondingly ψ. Observing either (2.108) or (2.109) it was shown that by selecting an arbitrary θ_1 and θ_2 to satisfy $\alpha' = 0$, the phases of the signals at the third and fourth antennas are rotated by $\theta_3 = \theta_2 - \psi$ and $\theta_4 = \theta_1 - \phi$, respectively. Setting either $\theta_1 = \theta_2 = 0$ or $\theta_4 = \theta_3 = 0$ demonstrates that phase rotations need only apply to two, i.e. $\{\theta_4, \theta_3\}$ or $\{\theta_1, \theta_2\}$, out of the four transmit antennas.

In the preceding analysis infinite precision in the phase rotation was assumed. However, in a practical implementation a more accurate assumption would be a band-limited feedback channel between transmitter and receiver which results

in a quantized implementation. If it is assumed that only K bits are used to quantize then the permissible set can be computed as $\{\{\tilde{\psi}, \tilde{\phi}\} \in \Omega\{\frac{2\pi k}{2^{(K-1)}}\}, k = 0, 1, \ldots, 2^{(K-1)} - 1\}$, where α' is minimized according to [26],

$$\{\tilde{\psi}, \tilde{\phi}\} = \arg \min_{\{\tilde{\psi}, \tilde{\phi}\} \in \Sigma} \left(|\varrho e^{j(\tilde{\psi})} - \vartheta e^{j(\tilde{\phi})}|^2 \right) \tag{2.110}$$

Various tradeoffs in error performance, bandwidth efficiency and decoding complexity are offered by OSTBCs and QOSTBCs. However, the design flexibility is limited partly because the designs involve difference matrices between all possible distinct ST code matrices. A different class of ST codes, namely Linear Complex Field Codes (LCFCs), are intrinsically more flexible in their design because of the systematically constructed code matrices. These are introduced in the next section.

2.4.3.3 ST Linear Complex Field Codes

What are now termed LCFC were first studied for use in SISO flat-fading channel using lattice codes that rotate Quadrature Amplitude Modulation (QAM) or Phase Amplitude Modulation (PAM) constellations to increase what was then termed *signal diversity* [27, 28, 29, 30]. Independently, Giannakis et al. were investigating (non-) redundant linear pre-coders using (square) tall *Vandermonde* matrix to increase what was then termed *symbol detectability* of block transmissions over SISO, MIMO and Multi-User MIMO (MU-MIMO) irrespective of the channel zero conditions and underlying constellation [31, 32, 33, 34]. The link came when it was established [35] that *Vandermonde* matrices can be used to implement lattice codes and complement Galois Field (GF) codes; therefore enabling maximum diversity and coding gains in flat-fading, frequency-selective and time-selective SISO channels [36, 37, 35]. For MIMO flat-fading channels Space-Time LCFC (ST-LCFC) were researched independently by [38, 39] for one symbol per channel use and any transmit antenna configuration.

Designing Linear Precoding Matrices In ST-LCFC the symbol re-mapping is assumed to be a linear mapping corresponding to,

$$\mathbf{x}_{LCF} = \mathbf{\Theta}_{LCF}\mathbf{s} \tag{2.111}$$

where the pre-coded symbol vectors $\mathbf{x}_{LCF} \in \mathbb{C}^{N_t \times 1}$ are related to the input symbol vectors $\mathbf{s} \in \mathbb{C}^{N_s \times 1}$ via a linear pre-coding matrix $\mathbf{\Theta}_{LCF} \in \mathbb{C}^{N_t \times N_t}$ assuming N_t and N_s denote the number of transmit antennas and time-slots used respectively. Constraining $N_t = N_s$ equates to a code design of one symbol per channel use. To understand the code properties $\mathbf{X}_{LCF}(\mathbf{s})$ is introduced according to,

$$\mathbf{X}_{LCF}(\mathbf{s}) = diag(\theta_1^T\mathbf{s}, \theta_2^T\mathbf{s}, \ldots, \theta_{N_t}^T\mathbf{s}) \tag{2.112}$$

with $\theta_i^T\mathbf{s}$ denoting the ith row of $\mathbf{\Theta}_{LCF}$. The design of the LCFC pre-coder can now be explored to maximize both diversity and coding gains. A difference matrix formulated from two distinct information blocks $\mathbf{s} \neq \mathbf{s}'$ is illustrated,

$$\mathbf{\Delta}_{LCF} = [\mathbf{X}_{LCF}(\mathbf{s}) - \mathbf{X}_{LCF}(\mathbf{s}')][\mathbf{X}_{LCF}(\mathbf{s}) - \mathbf{X}_{LCF}(\mathbf{s}')]^H \tag{2.113}$$

as a basis for evaluating the diversity and coding gain. Recalling (2.112), (2.113) can now be expressed as a diagonal matrix,

$$\mathbf{\Delta}_{LCF} = \begin{bmatrix} |\theta_1^T(\mathbf{s}-\mathbf{s}')|^2 & 0 & 0 & 0 \\ 0 & |\theta_2^T(\mathbf{s}-\mathbf{s}')|^2 & 0 & 0 \\ \vdots & \vdots & \ddots & \vdots \\ 0 & \cdots & \cdots & |\theta_{N_t}^T(\mathbf{s}-\mathbf{s}')|^2 \end{bmatrix} \tag{2.114}$$

The design for LCFCs can now be summarized with the following criteria [40]:

$$|\theta_i^T(\mathbf{s}-\mathbf{s}')| \neq 0, \quad \forall i \in [1, N_t], \quad \forall \mathbf{s} \neq \mathbf{s}' \in \mathbb{S}^{N_t \times 1} \tag{2.115}$$

to achieve maximum available spatial diversity and [40],

$$d_{min}^2 = \min_{\forall \mathbf{s} \neq \mathbf{s}' \in \mathbb{S}^{N_t \times 1}} \prod_{i=1}^{N_t} |\theta_i^T(\mathbf{s}-\mathbf{s}')|^2 \tag{2.116}$$

to achieve maximal coding gain with the LCFC design constraints which generally depend on the underlying constellation $\mathbb{S}$. Note that once the maximal coding gain is achieved then the diversity gain will be achieved by default.

Logically, the maximum coding gain can then be expressed as [40],

$$d_{min}^2 \leq \prod_{i=1}^{N_t} |\theta_i^T(\mathbf{s}-\mathbf{s}')|^2 \leq \Delta_{min}^{2N_t} \prod_{i=1}^{N_t} |\theta_{ip}|^2 \tag{2.117}$$

where Δ_{min} is the minimum distance among constellation points $\in \mathbb{S}$ and p denotes the column position of the different symbols in $\mathbf{s}-\mathbf{s}'$. Using the arithmetic-geometric inequality yields [40],

$$d_{min}^2 \leq \Delta_{min}^{2N_t} \left(\frac{\sum_{i=1}^{N_t} |\theta_{ip}|^2}{N_t} \right)^{N_t} \leq \left(\frac{\Delta_{min}^2}{N_t} \right)^{N_t} \tag{2.118}$$

an upper bound on the coding independent of the linear pre-coding matrix $\mathbf{\Theta}_{LCF}$ assuming the power constraint $\sum_{i=1}^{N_t} |\theta_{ip}|^2 = 1$ [40]. Briefly the construction of LCFCs using parameterization and algebraic tools is discussed next.

Construction based on parameterization Constraining the LCFC design to that of unitary matrices ensures that the Euclidean distance amongst N_t dimensional constellation points is preserved: a useful property when the wireless channel varies between AWGN and Rayleigh fading channels. Fortunately there always exists at least one unitary pre-coder [39] that satisfies (2.117) for a finite constellation $\mathbb{S}$ therefore achieving the maximum possible diversity gain of order $N_t N_r$ in a flat-fading MIMO channel. To reduce the non-linear optimization over N_t^2 complex entries; the search space is reduced by expressing $\mathbf{\Theta}_{LCF}$ as a product of Givens matrices $\mathbf{G}$[41],

$$\mathbf{\Theta}_{LCF} = \prod_{p=1}^{N_t-1} \prod_{q=p+1}^{N_t} \mathbf{G}_{pq}(\psi_{pq}, \phi_{pq}) \tag{2.119}$$

where the $N_t(N_t-1)/2$ parameters ψ_{pq} and ϕ_{pq} take values over $[-\pi, \pi]$. The Givens matrices $\mathbf{G}$ elements are defined as an identity matrix with the following elements replaced for a given p and q index: $\mathbf{G}_{pp} = \cos(\psi_{pp})$, $\mathbf{G}_{qq} = \cos(\psi_{qq})$, $\mathbf{G}_{pq} = e^{-j\phi_{pq}} \sin(\psi_{pq})$ and $\mathbf{G}_{qp} = -e^{j\phi_{qp}} \sin(\psi_{qp})$, which in the N_t case results in,

$$\mathbf{\Theta}_{LCF} = \begin{bmatrix} \cos(\psi) & e^{-j\phi} \sin(\psi) \\ -e^{j\phi_{qp}} \sin(\psi) & \cos(\psi) \end{bmatrix} \tag{2.120}$$

An exhaustive search over small N_t and $\mathbb{S}$ becomes feasible as is the case with the example when $N_t = 3$ and Quadrature Phase Shift Keying (QPSK) is employed [40],

$$\mathbf{\Theta}_{LCF} = \begin{bmatrix} 0.687 & 0.513 - 0.113j & -0.428 + 0.264j \\ -0.358 - 0.308j & 0.696 - 0.172j & -.0.11 - 0.513j \\ 0.190 + 0.520j & 0.243 - 0.389j & 0.687 \end{bmatrix} \tag{2.121}$$

Introduced next are construction methods suitable for large N_t and $\mathbb{S}$.

Construction based on algebraic tools Two algebraic construction methods proposed in [39] are presented which yield closed-form pre-coders with near-optimal coding gains. The mathematical derivation in this specific algebraic construction of LCFC is left to the excellent presentation in [39], only a basic overview is offered within the scope of this thesis.

1. LCF-A: This encoder constructs $\mathbf{\Theta}_{LCF}$ according to,

$$\mathbf{\Theta}_{LCF} = \frac{1}{\lambda} \begin{bmatrix} 1 & \alpha_1 & \cdots & \alpha_1^{N_t-1} \\ 1 & \alpha_2 & \cdots & \alpha_2^{N_t-1} \\ \vdots & \vdots & & \vdots \\ 1 & \alpha_{N_t} & \cdots & \alpha_{N_t}^{N_t-1} \end{bmatrix} \tag{2.122}$$

where $\{\alpha_k\}_{k=1}^{N_t}$ are the roots of $m_{\alpha,\mathbb{Q}(j)(x)}$ [1]. The design parameters for the set of transmit antenna orders $N_t = \{2, 3, \ldots, 6\}$ is clearly stated in [39, Table 3.3] with example ST-LCFC designs for $N_t = 2, 4$ illustrated respectively as,

$$\mathbf{\Theta}_{LCF} = \frac{1}{\sqrt{2}} \begin{bmatrix} 1 & e^{\frac{-j5\pi}{4}} \\ 1 & e^{\frac{-j\pi}{4}} \end{bmatrix} \tag{2.123}$$

$$\mathbf{\Theta}_{LCF} = \frac{1}{2} \begin{bmatrix} 1 & e^{\frac{-j\pi}{8}} & e^{\frac{-j2\pi}{8}} & e^{\frac{-j3\pi}{8}} \\ 1 & e^{\frac{-j5\pi}{8}} & e^{\frac{-j10\pi}{8}} & e^{\frac{-j15\pi}{8}} \\ 1 & e^{\frac{-j9\pi}{8}} & e^{\frac{-j18\pi}{8}} & e^{\frac{-j27\pi}{8}} \\ 1 & e^{\frac{-j13\pi}{8}} & e^{\frac{-j26\pi}{8}} & e^{\frac{-j39\pi}{8}} \end{bmatrix} \tag{2.124}$$

[1] According to [39]: $m_{\alpha,\mathbb{Q}(j)(x)}$ is the minimum polynomial of α over $\mathbb{Q}(j)$ by choosing α as an integer over $\mathbb{Z}[j]$ such that $deg(m_{\alpha,\mathbb{Q}(j)(x)}) = N_t$ where $\mathbb{Q}(j)$ is the smallest subfield containing both $\mathbb{Q}(j)$ and j.

2. LCF-B: Constructs a unitary pre-coder for any N_t according to,

$$\mathbf{\Theta}_{LCF} = \mathbf{F}_N^H diag\left(1, \alpha, \ldots, \alpha^{N_t-1}\right) \tag{2.125}$$

The choice of α is clearly defined in [39] and when N_t is a power of 2 leads to,

$$\alpha = e^{\frac{j\pi}{2N_t}} \tag{2.126}$$

In the case when N_t is not a power of 2 an heuristic rule is presented in [39]. An example ST-LCFC designs using the algebraic technique *LCF-B* for $N_t = 2$ is,

$$\mathbf{\Theta}_{LCF} = \frac{1}{\sqrt{2}} \begin{bmatrix} 1 & e^{\frac{-j\pi}{4}} \\ 1 & -e^{\frac{-j\pi}{4}} \end{bmatrix} \tag{2.127}$$

The construction of ST-LCFCs is established on the premise of ML decoding at the receiver. Observing the input-output relationship,

$$\mathbf{y} = \mathbf{H}\mathbf{\Theta}_{LCF}\mathbf{s} + \mathbf{n} \tag{2.128}$$

then ML decoding involves a search over $|\mathbb{S}|^{N_t}$ possible vectors[1] to evaluate,

$$\hat{\mathbf{s}} = \min_{\hat{\mathbf{s}} \in \mathbb{S}} |\mathbf{y} - \mathbf{\Theta}_{LCF}\hat{\mathbf{s}}|_2^2 \tag{2.129}$$

In a practical implementation this may prove computationally prohibitive; therefore [40] suggests using the Sphere Decoding Algorithm (SDA) which can decode $\mathbf{s}$ with ML or near-ML performance which is polynomial in N_t. However in a range of practical settings the average decoding complexity generally is cubic [40].

2.5 Equalization

The observed signal at the receiver $\mathbf{y}$ is generally a non-deterministic function of the data symbols $\mathbf{s}$ that has been corrupted by noise and perturbations introduced

[1] $|\cdot|$ denotes that cardinality of the set.

when passed through the physical channel. Therefore channel equalization is necessitated to invert these effects by combating fading and interference from symbols other than those of interest at a particular decoding stage by the receiver. Equalization techniques have been widely studied after Lucky's pioneering paper [42] and can be generally categorized into serial or block based. Serial equalizers generally are computationally simpler with the tradeoff that channel invertibility is not always guaranteed. By contrast, block equalizers do guarantee invertibility and better performance at the cost of increased complexity [34]. A thorough review of this broad area in telecommunications is beyond the scope of this thesis, therefore only techniques that are used directly in the development of new schemes in the ensuing chapters are explored.

2.5.1 Transmitter Equalization

Channel equalization techniques are generally thought of as processing implemented at the receiver side to combat the effects of the physical channel. Channel equalization can also be performed at the transmitter, also referred to as pre-equalization, to remove interference caused by the channel. This pre-processing generally requires knowledge of the CSI at the transmitter which imposes some limitations on the temporal coherence time in the case of feedback from the receiver, or invariance properties of the channel so the estimate from the reverse channel can be applied to the forward channel. Assuming CSI is available at the transmitter pre-equalization can aid in avoiding noise enhancement if the channel is ill-conditioned.

A combination of pre- and post-equalization techniques have been popularized in the now mature field of MIMO communications; with a pertinent example illustrated in the execution of a SVD of the MIMO channel to yield associated eigenvectors to create orthogonal parallel spatial data pipes between the transmitter and receiver [6]. An example of a balanced equalization technique with no requirement of CSI knowledge at the transmitter is Orthogonal Frequency Division Multiplexing (OFDM). This balanced equalization technique relies on the insertion of a CP to convert the linear convolution of the Channel-Impulse-Response (CIR) with the transmitted signal into that of a circular convolution. Channel independent processing at the transmitter in the form

of a Discrete Fourier Transform (DFT) transform and associated Inverse Discrete Fourier Transform (IDFT) at the receiver is known to diagonalize a channel represented with a circulant matrix. This particular form of balanced equalization has gained wide attraction due to the efficient implementation of the DFT and IDFT with the much celebrated Fast Fourier Transform (FFT).

2.5.2 Zero Forcing Equalization

The Zero-Forcing (ZF) equalizer operates on the observed signal to perfectly recover the input signal and eliminate Inter-Symbol-Interference (ISI) altogether [2] in the absence of noise. Although ISI is eliminated the primary disadvantage of the ZF is the possibility of noise enhancement in ill-conditioned channels which degrades the performance of the receiver.

The basic functionality of an N_r sample block-based ZF equalizer is illustrated with the example of a MIMO system in which the observation $\mathbf{y} \in \mathbb{C}^{N_r \times 1}$ is expressed as,

$$\mathbf{y} = \mathbf{H}\mathbf{s} + \mathbf{n} \tag{2.130}$$

where $\mathbf{H} \in \mathbb{C}^{N_r \times N_t}$, $\mathbf{s} \in \mathbb{C}^{N_t \times 1}$ and $\mathbf{n} \in \mathbb{C}^{N_r \times 1}$ denote the channel matrix the symbol vector and noise vector respectively. The ZF solution $\mathbf{Q}_{ZF}$ that perfectly recovers the symbol vector in the absence of noise satisfies the following criterion,

$$\mathbf{Q}_{ZF}\mathbf{H} = \mathbf{I}_N \tag{2.131}$$

Assuming that the noise is i.i.d. white noise the ZF solution reduces to,

$$\mathbf{Q}_{ZF} = \left(\mathbf{H}^H\mathbf{H}\right)^{-1}\mathbf{H}^H \tag{2.132}$$

which is the Moore Penrose pseudo matrix inverse projecting the observed vector $\mathbf{y}$ onto the signal subspace.

2.5.3 MMSE Equalization

In scenarios where the channel matrix is ill-conditioned there is the possibility of noise enhancement when executing a ZF equalizer at the receiver which will significantly degrade the decoding performance of the receiver. Another linear

equalizer design, namely Minimum Mean Square Error (MMSE) equalization, retains many of the advantages characteristics of the ZF equalizer, such as low computational complexity, whilst accounting for the noise distortion observed at the receiver.

To compare with the ZF, the basic functionality of an N_r sample block-based MMSE equalizer is illustrated using the MIMO communication system model presented in (2.130). Assuming MMSE equalization is performed using the following matrix operand $\mathbf{Q}_{MMSE}$, the observed signal post equalization can be described by,

$$\hat{\mathbf{s}} = \mathbf{Q}_{MMSE}\mathbf{y} \tag{2.133}$$

Instead of minimizing the peak distortion, as was the criterion of the cost function in ZF equalization, the MMSE equalization objective is to minimize the Mean Square Error (MSE) defined as,

$$J := E\{|\epsilon|^2\} = E\{|\hat{\mathbf{s}} - \mathbf{s}|^2\} \tag{2.134}$$

where $E\{\cdot\}$ denotes the statistical expectation operator. According to the orthogonality principle that dictates the equalization error is uncorrelated with the data used [43], $E\{\epsilon\mathbf{s}^H\} = \mathbf{0}$, the MSE is directly achieved when,

$$\mathbf{Q}_{MMSE} = \mathbf{R}_{ss}\mathbf{H}^H \left(\mathbf{H}^H\mathbf{R}_{ss}\mathbf{H} + \mathbf{R}_{nn}\right)^{-1} \tag{2.135}$$

where $\mathbf{R}_{ss} := E\{\mathbf{s}\mathbf{s}^H\}$ and $\mathbf{R}_{nn} := E\{\mathbf{n}\mathbf{n}^H\}$ denote the autocorrelation matrices of the data and noise respectively.

2.6 Summary

The objective of this work is to derive novel ST coding techniques for use in cooperative wireless relay networks. In order to fully contribute in this area it is important to understand some of the more established ST coding techniques that are applied to tradition transceivers that operate a co-located antenna array. This chapter has reviewed some of the fundamentals of the field of information theory in the context of SISO in addition to MIMO systems and derivatives thereof. This will prove a significant foundation in quantifying the channel capacity and

achievable throughput of cooperative channels of candidate ST coding designs. The review extended to the characterization of communications channels with respect to the selectivity of the channel. This basis will provide valuable insights into the design of the ST codeword and the mechanism of diversity offered by the channel which can be exploited to create robust combinations in wireless fading environments. Next a review of diversity techniques was undertaken to exploit the diversity offered by the various channel classifications already introduced. Specifically, two methodologies were reviewed; transmit antenna diversity and receive antenna diversity. Many of the schemes discussed in this review will form the basis of more complicated novel coding schemes developed in this thesis to provide solutions to problems particularly encountered in cooperative systems. Finally, for completeness a brief review of equalization techniques is presented for use in the decoding of schemes presented in this thesis.

Chapter 3

Characterization of Quasi-Orthogonal MIMO Channels for Cooperative Networks

3.1 Introduction

In the context of communication systems the maximum error-free transmission rate that a given channel can support is referred to as the channel capacity. Channel capacity and the problem of data compression are two of the most pertinent questions in communication theory and some of the solutions lie in the vast field of information theory.

Previous to the publication of Shannon's monogram on "A mathematical Theory of Communication" in 1948 [13], it was hypothosised that increasing the transmission rate of information over a communications channel increased the probability of error without any consideration of the noise statistics. Shannon astounded the communication theory community by proving that the channel capacity can be determined with knowledge only of the given input distribution, noise distribution, SNR and bandwidth. Whilst demonstrating achievable channel capacity design rules, he presented only the design of an infinite complexity transceiver which for all practical purposes proved to be computationally infea-

sible.

Many of the traditional Forward Error Correction (FEC) schemes have incrementally brought the goal of achieving the predicted Shannon channel capacity closer to realization. However, it was the innovative use of iterative decoding and the exchange of extrinsic soft information that has enabled Turbo codes described originally by Benedetto *et al.* [44] to operate close to the Shannon limit. Turbo codes compare favorably with traditional FEC schemes through only incurring modest computational costs when comparing encoding and decoding procedures [14].

With the introduction of Turbo codes and the assumption that it was impossible to communicate error-free beyond the Shannon capacity the research area was considered partially closed in the information theoretic community. However, in a rich scattering environment the additional independent degrees of freedom offered by the spatial dimension offers further capacity gains. This was brought to the attention of the research community by the landmark contributions of *Foschini & Gans* [45, 46] and *Telatar* [15] which provided both practical implementations such as the Bell Laboratories Layered Space-Time (BLAST) methodology and a mathematical foundation for characterizing MIMO systems in fading channels. This work inspired *Tarokh* to publish [25] detailed design metrics to derive coding schemes that achieve the capacity bounds offered by MIMO channels.

In the same period *Alamouti* proposed a simple transmit diversity scheme for two transmit antennas [23] that achieves a comparable channel capacity to a t-MRC scheme [22] of the same order in the absence of CSI at the transmitter[1]. This opened up the field of OSTBCs which leverage diversity gains offered by a channel without the expense of exponentially increasing processing costs at the receiver for ML decoding. Tarokh et al. [24] later extended the work of Alamouti to prove the existence of real and complex orthogonal coding designs for an arbitrary number of transmit antennas. However, the existence of spectrally efficient full-rate[2] complex designs was proven [24] to extend only to the original *Alamouti* [23] scheme limited to two antennas at the transmitter side. To utilize

[1]Array gain cannot be leveraged at the transmitter due to absence of CSI; therefore typically a 3 dB difference in BER performance is observed.

[2]Full-rate coding in the context of ST-codeword design is defined as the ratio of symbols transmitted to the time-slots used to transmit the symbols when the ratio is unity.

more antennas at the transmitter and increase the degrees of freedom offered by the MISO/MIMO channel *Jafarkhani* [11] and *Papadias* et al. [12] independently proposed a novel Quasi-Orthogonal Space Time Block Code (QOSTBC) scheme which operates at the full-rate and therefore provides greater spectral efficiency than OSTBCs at higher transmit array sizes. However, the loss of orthogonality of this new approach resulted in implications for increased decoding complexity and a loss of achievable diversity gain. Consequently, *Papadias* [47] proposed a constellation specific phase rotation scheme that yields full diversity. Unfortunately, the constellation specific basis of the *Papadias* approach renders mathematical analysis of the achievable capacity in the Shannon sense intractable. Ingeniously, a method achieving full-diversity irrespective of the underlying code-book design was proposed by Toker [26]. The freedom from specific implementation choices enables mathematical tractability to evaluate the capacity limits of QOSTBCs in a multitude of channel settings.

It is this background in addition to the work of Laneman [10] which demonstrates the utility of OSTBCs for exploiting diversity in wireless cooperative networks that forms the inspiration of this chapter. A short overview of the chapter is offered for perusal. Firstly, it is assumed that the reader is familiar with the content in Section 2.1 where basic notions of channel capacity were introduced to provide a foundation and context to the ensuing analysis. Later in Section 2.1 the classifications of fading-channels as ergodic and non-ergodic were also reviewed to characterize the performance of coding schemes in different communications scenarios. Secondly, in Section 3.2 of this chapter the distributed implementations of OSTBCs are reviewed to provide a foundation to compare the performance of QOSTBCs in ergodic and non-ergodic flat MIMO Rayleigh fading channels. Examining ergodic channels, novel closed-form expressions are developed to evaluate the normalized capacity within a range of distributed shadowing scenarios. The extension to non-ergodic channels yields approximations that tightly bound the outage probability within a multitude of communications scenarios. The analysis in both ergodic and non-ergodic channels is extended to allow for partial-CSI at the transmitter to be utilized to orthogonalize the channel using a technique developed by Toker [26]. The novel investigation of the capacity and outage probability of QOSTBCs in distributed wireless relay networks provides both an interesting theoretic basis for the design and implementation in the following

chapters, along with guidelines for effective deployment in physical systems utilizing the rich uncorrelated scattering environment that distributed MIMO channels offer.

3.2 Capacity and Outage Probability analysis of Orthogonal and Quasi Orthogonal-MIMO channels

Shannon channel capacity derives the maximum mutual information a channel can support between a source and sink using an optimal coding strategy. Deriving the required pdf for closed-form expressions of MIMO channel capacity with arbitrary statistics can prove challenging; fortunately, the expressions are generally simplified when adopting Complex Orthogonal Designs (CODs).

It is possible to analyze the achievable channel capacity with constraints on the code-book design. Laneman et al. [10] introduced the idea of STBCs in a distributed implementation as a simple and spectrally efficient method for extracting transmit cooperative diversity without channel knowledge at the transmitter. In constraining the coding scheme to a class of CODs [24], OSTBCs inherently orthogonalize the MIMO channel reducing the analysis to that of a series of SISO channels which is henceforth referred to as the Orthogonal-MIMO (O-MIMO) channel. This greatly simplifies the analysis as demonstrated below. Limiting the class of design to orthogonal codes does impose a significant cost in spectral efficiency when attempting to utilize more than two transmit antennas. A class of QOSTBC which enables full-rate transmission with four transmit antennas, therefore increasing the achievable spatial diversity available from the channel, is fully characterized for the first time in a cooperative deployment where variations in sub-channel shadowing are observed.

3.2.1 System Model

Observing the communication chain depicted in Figure 3.1 it is assumed that an information source followed by the appropriate channel encoder sends space-time encoded symbols over a MIMO channel. The reverse operations of space-time

decoding and channel decoding are performed at the receiver and decoded data is transported to an information sink. The objective of the distributed space-time block encoder is to improve the performance of the channel encoder by extracting the available transmit diversity using ST codewords that are spatially encoded across the distributed transmit antennas.

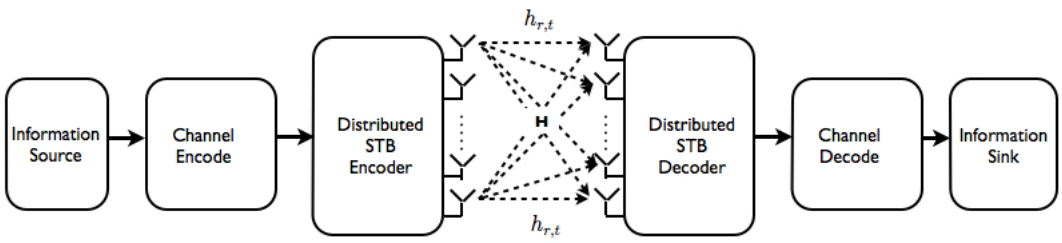

Figure 3.1: Schematic of a baseband distributed ST-coding transceiver

The theory of linear Orthogonal and QOSTBCs is a mature area of research and the reader is referred to the excellent texts [14, 6] for in-depth analysis of code construction for flat-fading channels which is beyond the scope of this section. To facilitate general understanding of the later material presented the key ideas are summarized. A mapping function takes an incoming binary data stream $\{b_k\}$, $b_k = \pm 1$, and generates a sequence of (complex) symbols $\mathbf{x}$ according to some predetermined code-book design. The symbol squence is then parsed into blocks $x_1, x_2, \ldots, x_s$ whose length s is determined by the block encoder used. The space-time block encoder then linearly maps each symbol block onto a transmis-

sion matrix $\mathbf{S}$ of size $N_s \times N_t$ where N_s and N_t are the temporal and spatial dimensions respectively. To preserve orthogonality in the code construction the rate of transmission $R := N_x/N_s$, defined as the ratio of number of symbols per codeword N_x to number of time-slots used to transmit the codeword N_s, may have to be sacrificed. In [24] it was proved that the Alamouti-scheme is the only full-rate COD which is defined with the following property,

$$\mathbf{S}\mathbf{S}^H = \mathbf{S}^H\mathbf{S} \propto \left(\sum_{i=1}^{s} |x_i|^2\right)\mathbf{I}_s, \qquad x_i \in \mathbb{C}. \tag{3.1}$$

Relaxing the transmission rate below unity yields a set of codeword designs referred to as GCOD[24];

$$\mathbf{S}\mathbf{S}^H \neq \mathbf{S}^H\mathbf{S} \propto \left(\sum_{i=1}^{s} |x_i|^2\right)\mathbf{I}_s, \qquad x_i \in \mathbb{C}. \tag{3.2}$$

yielding half-rate $R = 1/2$ codes for any number of transmit antennas and so called sporadic codes yielding $R = 3/4$ specifically for $N_t = \{3, 4\}$ transmit antenna configurations.

To form the basis of the ensuing analysis, Figure 3.2 illustrates three generalized scenarios for deployment of VAAs. The traditional communication system scenario assumes co-located transmit and receiver arrays as illustrated in Figure 3.2a. In this configuration sub-channels $h_{i,j}$ defined as the channel gain between the ith transmit antenna and j^{th} receive antenna experience the same expected gain $\bar{\gamma}$ attributed to shadowing or path-loss over all transceiver pairings, $i \in \{1, \ldots, N_t\}$ and $j \in \{1, \ldots, N_r\}$. Making the extension to the fully distributed case with only one antenna per node, Figure 3.2b, illustrates the case when individual $h_{i,j}$ are parameterized with a unique expected sub-channel gain, $\{\bar{\gamma}_1, \ldots, \bar{\gamma}_u\}$, which is different from that observed by the other transceiver pairs. To encapsulate other scenarios with hybrid configurations the case of generic channel gains incorporates nodes with co-located antenna arrays cooperating with other distributed nodes, illustrated by Figure 3.2c. This category then allows for analysis of nodes with multiple co-located antennas that observe the same shadowing and path-loss parameters in specific sub-channels cooperating with other distributed nodes to jointly decode data.

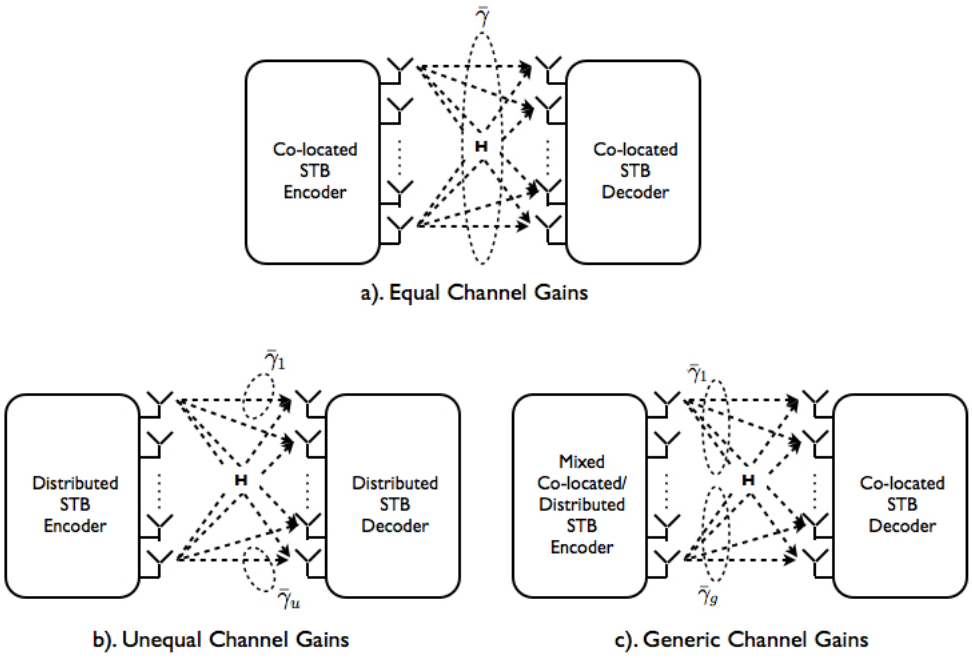

Figure 3.2: Example baseband scenarios for distributed ST-coding schemes with various shadowing models

3.2.2 Ergodic Flat-Fading Channel

Assuming CSI is unutilized or unavailable at the transmitter the maximum capacity of a deterministic MIMO channel $\mathbf{H}$ is achieved by allocating equal power across the transmit antennas [15],

$$C = log_2 \det\left(\mathbf{I} + \frac{\rho}{N_t}\mathbf{H}\mathbf{H}^H\right), \qquad [bits/s/Hz] \tag{3.3}$$

where ρ denotes the linear SNR and $\det(\cdot)$ denotes the determinant of the matrix. Using the idea of a deterministic effective channel matrix $\mathbf{H}_{eff}$, introduced in Section 2.4.3, the achievable capacity of a STBC enabled system can be expressed as [48, 5],

$$C = \frac{R}{N_s} \log_2 \det \left(\mathbf{I} + \frac{\rho}{RN_t} \mathbf{H}_{eff} \mathbf{H}_{eff}^H \right), \qquad [bits/s/Hz] \tag{3.4}$$

For purely static channels that are known to the system designer before deployment, (3.4) accurately expresses the channel capacity.

3.2.2.1 O-MIMO Channel

From an information theoretic perspective OSTBCs result in a sub-optimal implementation at the expense of increased diversity gains, where the normalized capacity [bits/s/Hz] for a deterministic channel $\mathbf{H}$ is expressed as [6],

$$C = R \log_2 \left(1 + \frac{\rho}{RN_t} \|\mathbf{H}\|_F^2 \right), \qquad [bits/s/Hz] \tag{3.5}$$

where $\| \cdot \|_F^2$ denotes the Frobenius norm of a matrix. To simplify the ensuing analysis the following notation is adopted,

$$\mathbf{h} := vec(\mathbf{H}) \tag{3.6}$$

$$u := N_t \cdot N_r \tag{3.7}$$

$$\gamma := \mathbf{h}^H \mathbf{h} \tag{3.8}$$

$$\gamma_i := h_i h_i^* \tag{3.9}$$

$$\bar{\gamma}_i := E\{\gamma_i\} \tag{3.10}$$

where $vec(\cdot)$ vectorizes a matrix argument so that $\mathbf{h} \in \mathbb{C}^{N_t N_r \times 1}$. MIMO channels are often not deterministic and are instead usually represented as a stochastic process with an associated pdf. Unlike the case of MIMO channels the associated pdf for sub-channel gains in O-MIMO channels is readily derived from the underlying SISO channel statistics through the use of a u-fold convolution [5],

$$f_\gamma(\gamma) = f_{\gamma_1}(\gamma_1) \otimes f_{\gamma_2}(\gamma_2) \otimes \cdots \otimes f_{\gamma_u}(\gamma_u) \tag{3.11}$$

where $f_{\gamma_i}(\gamma_i), \forall i \in \{1, 2, \ldots, u\}$ and $f_\gamma(\gamma)$ represents the pdfs for sub-channel gains and convoluted pdf respectively. Assuming that the entries of $\mathbf{H}$ are i.i.d. Rayleigh faded, corresponding to ZMCSCG random variables of variance $\bar{\gamma}_i/2$ per

dimension, then the pdf of individual SISO sub-channel gains can be expressed as,

$$f_{\gamma_i}(\gamma_i) = \begin{cases} \frac{1}{\bar{\gamma}_i}\, e^{-\gamma_i/\bar{\gamma}_i} & (\gamma_i \geq 0) \\ 0 & otherwise. \end{cases} \tag{3.12}$$

The evaluation of (3.11) can be simplified by taking the *Laplace transform* to represent the pdf using the Moment Generating Function (MGF);

$$\phi_{\gamma_i}(s) := \int_0^\infty f_{\gamma_i}(\gamma_i)\, e^{s\gamma_i} d\gamma_i \tag{3.13}$$

$$= \frac{1}{(1-\bar{\gamma}_i s)} \tag{3.14}$$

then multiplying in the *s-domain* yields the MGF for the sub-channel gain as shown below,

$$\phi_\gamma(s) = \prod_{i=1}^{u} \phi_{\gamma_i}(s) \tag{3.15}$$

The pdf for the O-MIMO sub-channel gain can be expressed using standard inverse Laplace transforms [49],

$$\frac{1}{(1-xs)^n} \overset{L^{-1}}{\Rightarrow} \frac{1}{\Gamma(n)} \frac{t^{n-1}}{x^n}\, e^{-\frac{t}{x}} \tag{3.16}$$

where $\Gamma(\cdot)$ denotes the Gamma function. As stated in Section 2.1.2 a channel can be described as *ergodic* if for every channel use the random channel power gains, represented by γ, are independently realized and all the moments are the same from codeword to codeword. Selecting an asymptotically optimal codebook based on a Gaussian distribution [13] the capacity of an *ergodic* channel approaches the Shannon capacity [13]. The normalized *ergodic* capacity of an O-MIMO channel is shown below, approximation

$$C = E_\gamma \left\{ R \log_2 \left(1 + \frac{1}{R} \frac{\gamma}{N_t} \rho \right) \right\} \tag{3.17}$$

$$= R \int_o^\infty \log_2 \left(1 + \frac{1}{R} \frac{\gamma}{N_t} \rho \right) f_\gamma(\gamma) d\lambda \tag{3.18}$$

It has been shown [5] that (3.18) can be evaluated in closed form for the capacity of an O-MIMO channel for a specific pdf of the random channel gain γ. In the ensuing sections the discussion on channel capacity with *equal* and *unequal* sub-channel gains is illustrated further.

Equal Channel Gains In environments where cooperating Mobile Terminals (MTs) are closely spaced, as illustrated previously in Figure 3.2a, the shadowing effects experienced across multiple sub-channels can be approximated by $\bar{\gamma}_1 = \cdots = \bar{\gamma}_u$. This approximation simplifies the derivation of $f_\gamma(\gamma)$ by adopting a similar analysis as illustrated in the derivations (3.11-3.16) to yield [5],

$$f_\gamma(\gamma) = \frac{1}{\Gamma(u)} \frac{\gamma^{u-1}}{\bar{\gamma}^u} \, e^{-\gamma/\bar{\gamma}}, \qquad \bar{\gamma} = \bar{\gamma}_i, \quad i \, \forall\{1, \ldots, u\} \tag{3.19}$$

a central chi-squared distribution with $2u$ degrees of freedom and a mean $\bar{\gamma}u$. Substituting (3.19) into the capacity expression (3.18) yields the maximum channel capacity for an *ergodic* O-MIMO channel with equal sub-channel gains,

$$C = R. \, E_\gamma \left\{ \log_2 \left(1 + \frac{\hat{\gamma}}{R} \frac{\bar{\gamma}}{N_t} \frac{S}{N} \right) \right\} \tag{3.20}$$

$$= \frac{R}{\Gamma(u)} \, \hat{C}_{u-1}(\frac{1}{R} \frac{\bar{\gamma}}{N_t} \frac{S}{N}) \tag{3.21}$$

where the change of variable $\hat{\gamma} = \gamma/\bar{\gamma}$ is used to simplify the integral,

$$\hat{C}_\zeta(a) := \int_0^\infty \log_2(1 + a\hat{\gamma}) \, \hat{\gamma}^\zeta \, e^{-\hat{\gamma}} d\hat{\gamma} \tag{3.22}$$

An iterative solution of (3.22) can be found in [5, Eq.2.45] and because of the frequency of use (3.22) is henceforth referred to as the *Capacity Integral* [5].

Unequal and Generic Channel Gains As illustrated by the scenario depicted in Figure 3.2b; sub-channels may experience unequal shadowing effects as a direct consequence of the spatial distribution of participating relay nodes resulting in $\bar{\gamma}_1 \neq \cdots \neq \bar{\gamma}_u$. To allow the use of standard Laplace transforms the MGF is derived through a partial fraction expansion instead of the simple product shown in (3.19) [5],

$$\phi_\gamma(s) = \sum_{i=1}^{u} K_i \phi_{\gamma_i}(s) \tag{3.23}$$

whereby solving a set of linear simultaneous equations the constants K_i are resolved,

$$K_i = \prod_{i'=1, i' \neq i}^{u} \frac{\bar{\gamma}_i}{\bar{\gamma}_i - \bar{\gamma}_{i'}} \tag{3.24}$$

From expressions (3.14), (3.16), (3.22) and (3.23) the closed form expression for the capacity of an O-MIMO channel with unequal sub-channels was shown to be [5],

$$C = R \sum_{i=1}^{u} K_i \, \hat{C}_0 (\frac{1}{R} \frac{\bar{\gamma}_i}{N_t} \frac{S}{N}) \tag{3.25}$$

Generalizing to the case where some sub-channel gains are repeated, the distinct gains are denoted by $\hat{\gamma}_{i \in (1,g)}$ with each being repeated $\nu_{i \in (1,g)}$ times yielding an MGF for λ equal to,

$$\phi_\gamma(s) = \prod_{i=1}^{g} \phi_{\hat{\gamma}_i(s)} = \frac{1}{(1 - s\bar{\gamma}_1)^{\nu_1}} \cdot \frac{1}{(1 - s\bar{\gamma}_2)^{\nu_2}} \cdots \frac{1}{(1 - s\bar{\gamma}_g)^{\nu_g}} \tag{3.26}$$

where the groups of sub-channels sum to the total number of sub-channels $\sum_{i=1}^{g} \nu_i = u$. The partial fraction expansion of (3.26) is expressed as,

$$\phi_\gamma(s) = \sum_{i=1}^{g} \sum_{j=1}^{\nu_g} K_{i,j} \phi^j_{\hat{\gamma}_i}(s) \tag{3.27}$$

where $K_{i,j}$ is derived by Dohler in [5, Appendix 2.7]. The capacity expression for generic channels is therefore expressed as [5, Eq. 2.83],

$$C = R \sum_{i=1}^{g} \sum_{j=1}^{g} \frac{K_{i,j}}{\Gamma(j)} . \hat{C}_{j-1} \left(\frac{1}{R} \frac{\bar{\gamma}_i}{N_t} \frac{S}{N} \right) \tag{3.28}$$

As illustrated through the previous derivations the characterization of O-MIMO channels when deploying OSTBC is simplified by the intrinsic orthogonalization of the MIMO channel. To maintain this property for higher transmit array sizes, as stated previously in the chapter, there is a loss in spectral efficiency. Analyzed

next is a coding methodology that trades off orthogonality against spectral efficiency; the set of codes are referred to as Quasi-Orthogonal Space Time Block Codes (QOSTBCs).

3.2.2.2 Quasi O-MIMO Channel

As previously demonstrated OSTBCs decouple the MIMO channel into a set of parallel SISO channels with channel statistics that are favorable in comparison with the fading-channel process encountered without coding. The channel capacity offered by employing an OSTBC at the transmitter can then be analyzed as an effective SISO channel with modified channel statistics. This simplification is not possible when employing QOSTBCs where the equivalent channel shall still be considered MIMO albeit with reduced dimensionality.

Unlike the case of the MIMO channel without any coordinated coding the eigenvectors of the QOSTBC effective channel are constant and do not depend on the actual channel realizations as reviewed in Section 2.4.3.2. Recall from the review of QOSTBCs in Section 2.4.3.2 that the effective channel after employing a QOSTBC at the transmitter and ST combining of the observed signal at the receiver has been shown (2.93) to be,

$$\mathbf{\Delta} = \begin{bmatrix} \gamma & 0 & 0 & \alpha \\ 0 & \gamma & -\alpha & 0 \\ 0 & -\alpha & \gamma & 0 \\ \alpha & 0 & 0 & \gamma \end{bmatrix} \tag{3.29}$$

where $\mathbf{\Delta} := \mathbf{H}_{eff}\mathbf{H}_{eff}^{H}$ assuming,

$$\mathbf{H}_{eff} = \begin{bmatrix} h_1 & h_2 & h_3 & h_4 \\ h_2^* & -h_1^* & h_4^* & -h_3^* \\ h_3^* & h_4^* & -h_1^* & -h_2^* \\ h_4 & -h_3 & -h_2 & h_1 \end{bmatrix} \tag{3.30}$$

and β and α are denoted by (2.94) and (2.95) respectively. Performing eigenvalue decomposition on (3.29) the associated eigenvalue and eigenvector matrices are extracted,

$$\mathbf{\Lambda} = \begin{bmatrix} \gamma+\alpha & 0 & 0 & 0 \\ 0 & \gamma-\alpha & 0 & 0 \\ 0 & 0 & \gamma-\alpha & 0 \\ 0 & 0 & 0 & \gamma+\alpha \end{bmatrix} \tag{3.31}$$

$$\mathbf{U} = (\mathbf{I}_2 \otimes \mathbf{V})\mathbf{\Pi} \tag{3.32}$$

where $\otimes$ denotes the Kronecker product, $\mathbf{V}$ is expressed in (2.99) and the permutation matrix $\mathbf{\Pi}$ specifically tailored for *Jafarkhani* QOSTBC [11] takes the form,

$$\mathbf{\Pi} = \begin{bmatrix} 1 & 0 & 0 & 0 \\ 0 & 0 & 0 & 1 \\ 0 & 1 & 0 & 0 \\ 0 & 0 & 1 & 0 \end{bmatrix}. \tag{3.33}$$

Applying the matched filter described in (2.92) for QOSTBC colours the noise $\mathcal{N}(0, N_0\mathbf{\Delta})$; therefore it is desirable to perform pre-whitening to formulate the capacity expression in the generic form previously expressed (3.4) for the capacity analysis of STBCs. With knowledge of the eigenvalue (3.31) and eigenvector (3.32) matrices it is possible to compute the pre-whitening spatial-temporal filter as $\mathbf{F}_{pw} = \mathbf{\Lambda}^{-1/2}\mathbf{V}^H$. Performing a pre-whitening operation at the front-end of a receiver is well known [50] to be an information preserving operation and therefore does not affect the capacity analysis. Therefore, for a determininistic effective channel $\mathbf{H}_{eff}$ the normalized achievable capacity of a system utilizing a QOSTBC is expressed as,

$$\begin{aligned} C &= \frac{R}{N_s}\log_2\det\left(\mathbf{F}_{pw}\left(\mathbf{\Delta} + \frac{\rho}{RN_t}\mathbf{\Delta}\mathbf{\Delta}^H\right)\mathbf{F}_{pw}^H\right) && (3.34) \\ &= \frac{R}{N_s}\log_2\det\left(\mathbf{I} + \frac{\rho}{RN_t}\mathbf{\Lambda}\right) && (3.35) \\ &= \frac{R}{N_s}\sum_{k=1}^{4}\log_2\left(1 + \frac{\rho}{RN_t}\lambda_k\right) && (3.36) \end{aligned}$$

where λ_k denotes the kth eigenvalue of $\mathbf{\Delta}$ corresponding to $\mathbf{\Lambda}_k$. To evaluate the channel capacity for non-deterministic channels the eigenvalue pdf needs to be de-

rived. Observing that eigenvalues and the sub-channel coefficients corresponding to the jth receive antenna $\mathbf{h}_j := [\mathbf{H}_{j,1}, \mathbf{H}_{j,2}, \ldots, \mathbf{H}_{j,N_t}]$ are associated according to,

$$\lambda_k = \mathbf{h}_j^H \mathbf{S}(k,j)\mathbf{h}_j \tag{3.37}$$

where $\mathbf{S}(k,j)$ is uniquely specified for distributed-QOSTBCs as,

$$\mathbf{S}(k,j) = \begin{cases} \mathbf{A}+\mathbf{B}, & k = \{1,4\} \\ \mathbf{A}-\mathbf{B}, & k = \{2,3\} \end{cases} \tag{3.38}$$

and,

$$\mathbf{A} = \begin{bmatrix} \bar{\gamma}_{1,j} & 0 & 0 & 0 \\ 0 & \bar{\gamma}_{2,j} & 0 & 0 \\ 0 & 0 & \bar{\gamma}_{3,j} & 0 \\ 0 & 0 & 0 & \bar{\gamma}_{4,j} \end{bmatrix} \tag{3.39}$$

$$\mathbf{B} = \begin{bmatrix} 0 & 0 & 0 & \sqrt{\bar{\gamma}_{1,j}}\sqrt{\bar{\gamma}_{4,j}} \\ 0 & 0 & -\sqrt{\bar{\gamma}_{2,j}}\sqrt{\bar{\gamma}_{3,j}} & 0 \\ 0 & -\sqrt{\bar{\gamma}_{2,j}}\sqrt{\bar{\gamma}_{3,j}} & 0 & 0 \\ \sqrt{\bar{\gamma}_{1,j}}\sqrt{\bar{\gamma}_{4,j}} & 0 & 0 & 0 \end{bmatrix} \tag{3.40}$$

where the expected sub-channel gain of the physical channel between the ith transmit antenna and j^{th} receive antenna is denoted by $\bar{\gamma}_{i,j} = E\{h_{i,j}h_{i,j}^*\}$. The extension to a full MIMO system with multiple receivers corresponds to,

$$\lambda_k = \mathbf{h}^H \mathbf{S}(k)\mathbf{h} \tag{3.41}$$

where,

$$\mathbf{S}(k) = \begin{bmatrix} \mathbf{S}(k,1) & & & \\ & \mathbf{S}(k,2) & & \\ & & \ddots & \\ & & & \mathbf{S}(k,N_r) \end{bmatrix} \tag{3.42}$$

Interestingly, the matrix group $\{\mathbf{S}(1,j)\ldots\mathbf{S}(4,j)\}$ represents a *conjugate* class of *similar* matrices which perform the same linear transformation under different basis and therefore shares the same eigenvalue properties.

Recalling from previous sections that to derive the channel capacity for random channel gains, the channel capacity should be averaged over the stochastic fading process, for QOSTBCs (3.36) extends to,

$$E_{\lambda_i}\left\{\frac{R}{N_s}\sum_{i=1}^{4}\log_2\left(1+\frac{\rho}{RN_t}\lambda_i\right)\right\} = \frac{R}{N_s}\sum_{i=1}^{4}E_{\lambda_i}\left\{\log_2\left(1+\frac{\rho}{RN_t}\lambda_i\right)\right\} \quad (3.43)$$

$$= R.E_{\lambda_1}\left\{\log_2\left(1+\frac{\rho}{Rt}\lambda_1\right)\right\} \quad (3.44)$$

Since the members of the matrix group $\{\mathbf{S}(1,j)\ldots\mathbf{S}(4,j)\}$ share eigenvalue properties and $\mathbf{h}$ is a ZMCSCG vector with unit variance under any basis transformation; only the expectation over a single eigenvector λ_1 needs to be evaluated. This property will be used extensively in the forthcoming capacity analysis of distributed-QOSTBC under equal and unequal shadowing conditions.

Equal Channel Gains For comparison with OSTBCs, QOSTBCs are analyzed in environments where the MTs experience equivalent shadowing across sub-channels, i.e. $\bar{\gamma} = \bar{\gamma}_i, \forall i \in \{1,\ldots,u\}$. Assuming a change of basis $\mathbf{u}_k = \mathbf{U}_{S(k)}\mathbf{h}$,where the distribution of $\mathbf{u}_k$ is the same as $\mathbf{h}$, the equivalence in shadowing reduces (3.41) to,

$$\lambda_k = \mathbf{u}_k^H \mathbf{\Lambda}_{S(k)}\mathbf{u}_k \quad (3.45)$$

assuming $\mathbf{U}_{S(k)}$ and $\mathbf{\Lambda}_{S(k)}$ denote the eigenvector and eigenvalue matrix of $\mathbf{S}(k)$ respectively where the eigenvalue pair evaluates to $2\bar{\gamma}$. Therefore, repeating the analysis in [51] for the derivation of the characteristic function of Hermitian quadratic forms in complex normal variables it can be shown that the MGF for λ_k is,

$$\phi_{\lambda_k} = \frac{1}{(1-2\bar{\gamma}s)^{2N_r}} \quad (3.46)$$

which is the MGF of the sum of squares of $2r$ independent complex normally distributed random variables. As for OSTBCs standard Laplace transforms [49] enable the simple inverse Laplace transform of (3.46). Therefore the eigenvalue pdf can be expressed as,

$$f_{\lambda_k}(\lambda_k) = \frac{1}{\Gamma(2N_r)} \frac{\lambda_k^{(2N_r-1)}}{(2\bar{\gamma})^{2N_r}} e^{-\lambda_k/2\bar{\gamma}} \tag{3.47}$$

which is described as a central chi-squared distribution with $4N_r$ degrees of freedom and a mean of $2\bar{\gamma}N_r$. With reference to (3.43) and exploiting the change of variable $\hat{\lambda}_k = \lambda_k/2\bar{\gamma}$ the capacity of the QOSTBC channel can be expressed in closed form as,

$$C = \frac{1}{N_s\Gamma(2N_r)} \sum_{k=1}^{4} \int_0^{\infty} \log_2\left(1 + \hat{\lambda}_k \rho \frac{2\bar{\gamma}}{N_t}\right) \hat{\lambda}_k^{(2N_r-1)} e^{-\hat{\lambda}_k} d\hat{\lambda}_k \tag{3.48}$$

$$= \frac{1}{\Gamma(2N_r)} \hat{C}_{(2N_r-1)}\left(\rho \frac{2\bar{\gamma}}{N_t}\right) \tag{3.49}$$

where in the second line the equivalence of the eigenvalue pdfs (3.47) has been exploited to simplify the expression by evaluating the expectation for only one of the eigenvalues. For equivalent sub-channel shadowing $\bar{\gamma}$ it maybe noted that the QOSTBC (3.49) with four transmit antennas ($N_t = 4$) yields the same channel capacity as the *Alamouti* scheme (3.21).

Unequal Channel Gains In the case when the sub-channel gains are unequal, $\bar{\gamma}_1 \neq \cdots \neq \bar{\gamma}_u$, the capacity of the distributed-QOSTBCs is derived. Without loss of generality the generic eigenvalue matrix $\mathbf{\Lambda_{S(k,j)}} = \mathbf{U}_{S(k,j)}\mathbf{S}(k,j)\mathbf{U}_{S(k,j)}^H$ becomes,

$$\mathbf{\Lambda_{S(k,j)}} = \begin{bmatrix} \eta_{1,j} & 0 & 0 & 0 \\ 0 & \eta_{2,j} & 0 & 0 \\ 0 & 0 & 0 & 0 \\ 0 & 0 & 0 & 0 \end{bmatrix} \qquad \forall j \in (1,r), k \in (1,4) \tag{3.50}$$

with associated non-zero eigenvalues henceforth referred to as the expected *virtual sub-channel gains* and $\mathbf{U}_{S(k,j)}$ denoting the eigenvector matrix. Adopting the new notation it is now possible to express λ_k as,

$$\lambda_k = \sum_{j=1}^{N_r} \mathbf{u}_{j,k}^H \mathbf{\Lambda_{S(k,j)}} \mathbf{u}_{j,k} \tag{3.51}$$

where the linear transform of the channel vector $\mathbf{u}_{j,k} = \mathbf{U}_{j,k}\mathbf{h}_j$ has the same distribution as $\mathbf{h}_j$. Proceeding on the basis of the analysis performed for O-MIMO with un-equal channel gains (3.23) the MGF of λ_k can then be expressed as,

$$\phi_{\lambda_k}(s) = \prod_{j=1}^{N_r}\prod_{i=1}^{2}\frac{1}{(1-\eta_{i,j}s)} \tag{3.52}$$

Assuming $\eta_{1,1} \neq, \ldots, \neq \eta_{2,N_r}$ then resolving (3.52) into its constituent partial fractions results in,

$$\phi_{\lambda_k}(s) = \sum_{j=1}^{N_r}\sum_{i=1}^{2}\frac{K_{i,j}}{(1-\eta_{i,j}s)} \tag{3.53}$$

where,

$$K_{i,j} = \prod_{i'=1,i'\neq i}^{2}\prod_{j'=1,j'\neq j}^{N_r}\frac{\eta_{i,j}}{\eta_{i,j}-\eta_{i',j'}} \tag{3.54}$$

The linearity of the MGF enables the pdf to be expressed as,

$$f_{\lambda_k}(\lambda_k) = \sum_{j=1}^{N_r}\sum_{i=1}^{2}K_{i,j}\frac{1}{\eta_{i,j}}e^{-\frac{\lambda_k}{\eta_{i,j}}} \tag{3.55}$$

Evaluating (3.21) using the pdf (3.55) results in the channel capacity for QOSTBCs with unequal channel gains,

$$C = \frac{1}{N_s\Gamma(2)}\sum_{j=1}^{N_r}\sum_{i=1}^{2}\sum_{k=1}^{4}\int_0^\infty \log_2\left(1+\hat{\lambda}_k\rho\frac{\eta_{i,j}}{N_t}\right)e^{-\hat{\lambda}_k}d\hat{\lambda}_k \tag{3.56}$$

$$= \frac{1}{\Gamma(2)}\sum_{j=1}^{N_r}\sum_{i=1}^{2}K_{i,j}.\hat{C}_0\left(\rho\frac{\eta_{i,j}}{N_t}\right) \tag{3.57}$$

where the equivalence of pdfs (3.53) for the eigenvalues $\lambda_1, \ldots, \lambda_4$ reduces the capacity expression (3.56) to a single integrand as shown in (3.57).

It is feasible that some of the virtual sub-channel gains denoted by $\eta_{i,j}$ may be repeated, therefore this case is further analyzed. It is assumed that there are $g < 2N_r$ distinct virtual sub-channel gains denoted as $\hat{\eta}_{i\in(1,g)}$ where each distinct

gain is repeated $\nu_{i\in(1,g)}$ times. The case for generic virtual sub-channel gains is similarly obtained from that of the OSTBC case by substituting $\hat{\eta}_{i\in(1,g)}$ for $\hat{\gamma}_{i\in(1,g)}$ in (3.26) and following through the derivation (3.26)-(3.27) the pdf is given by,

$$f_{\lambda_k}(\lambda_k) = \sum_{i=1}^{g}\sum_{j=1}^{\nu_i} \frac{K_{i,j}}{\Gamma(j)}.\frac{\lambda_k^{j-1}}{(\hat{\eta}_i)^j} e^{-\lambda_k/\hat{\eta}_i} \tag{3.58}$$

to yield the generic QOSTBC capacity expression,

$$C = R\sum_{i=1}^{g}\sum_{j=1}^{\nu_i} \frac{K_{i,j}}{\Gamma(j)}.\hat{C}_{j-1}\left(\frac{\rho}{R}\frac{\hat{\eta}_i}{N_t}\right) \tag{3.59}$$

Partial Transmit CSI In [26] Toker demonstrated that full CSI at the transmitter with simple phase rotations can orthogonalize the effective channel (3.29) by rendering $\alpha = 0$[1]. These concepts were developed upon by the realization of a finite rate constraint on the feedback channel between the receiver and transmitter, therefore necessitating some form of quantization. Toker's work [26] proposed a quantization approach which searches over a permissible set of phase rotations to determine the minimum α' as shown in (2.110) which is repeated here for clarity,

$$\{\tilde{\psi}, \tilde{\phi}\} = \arg \min_{\{\tilde{\psi},\tilde{\phi}\}\in\Omega} (\alpha') \tag{3.60}$$

where $\alpha' = |h_1 h_4^* e^{j(\tilde{\psi})} - h_2 h_3^* e^{j(\tilde{\phi})}|^2$, i.e. the original α term with phase rotations applied at the transmitter, and $\{\{\psi_q, \phi_q\} \in \Omega\{\frac{2\pi k}{2^{(K-1)}}\}, k = 0, 1, \ldots, 2^{(K-1)} - 1\}$ denotes the finite set of phasors with K defining the number of bits used to encode the quantized phase.

To enable a sufficient characterization of the channel capacity for QOSTBC with partial knowledge of CSI Toker's implementation [26] is modified so that a single phasor is calculated for rotation over two transmit antennas. To facilitate the analysis ζ is defined as,

$$\zeta = h_1 h_4^* - h_2 h_3^* \tag{3.61}$$

[1] A detailed review can be found in Section 2.4.2

therefore from (2.95) it is observed that $\alpha = 2\Re\{\zeta\}$. With the same phase rotation ϕ' applied at antennas one and two then ζ is modified to,

$$\zeta' = h_1 h_4^* e^{j(\phi')} - h_2 h_3^* e^{j(\phi')} \tag{3.62}$$

in this case α can be rewritten as,

$$\begin{aligned} \alpha'' &= 2\Re\{\zeta'\} && (3.63)\\ &= 2\Re\{|\zeta| e^{j(\phi'+\angle\zeta)}\} && (3.64)\\ &= 2(|\zeta|\cos(\phi'+\angle\zeta)) && (3.65) \end{aligned}$$

The coupling term α'' is equal to zero when,

$$\phi' = \frac{\pi}{2} - \angle\zeta \tag{3.66}$$

It is assumed that the phase rotation ψ' is calculated with infinite precision according to (3.66), then mapped by way of a quantizer operation $\mathcal{Q}(\cdot)$ onto the finite set $\{\{\phi'_q\} \in \Omega\{\frac{2\pi k}{2^{(K-1)}}\}, k = 0, 1, \ldots, 2^{(K-1)} - 1\}$. In order to minimize the quantization error, $\mathcal{Q}(\cdot)$ performs a rounding operation as defined,

$$\phi'_q = \arg\min_{\phi'_q \in \Omega}(|\epsilon_\phi|) \tag{3.67}$$

where ϵ_ϕ defines the quantization error,

$$\epsilon_\phi = \phi' - \phi'_q. \tag{3.68}$$

Comparing (3.60) with (3.67), (3.67) results in a single quantization error parameter that is uniformly distributed $\epsilon_\phi \sim \mathcal{U}(-\frac{\pi}{2^{(K-1)}}, \frac{\pi}{2^{(K-1)}})$, which enables greater mathematical tractability to the ensuing analysis. Whilst infinite precision in ϕ' results in no intereference, $\alpha'' = 0$ as is shown by substituting (3.66) into (3.65), quantization results in residual interference in the form,

$$\begin{aligned} \alpha'' &\leq 2|\zeta|\cos(\phi'_q + \angle\zeta) && (3.69)\\ &= 2|\zeta|\sin(-\epsilon_\phi) && (3.70)\\ &= \alpha''_q && (3.71) \end{aligned}$$

where the second line is derived using the substitutions (3.68) and (3.66) in addition to leveraging simple trigonometric identities. Clearly, (3.71) demonstrates that for any particular channel realization resulting in ζ the residual interference α_q'' is proportional to the absolute quantization error $|\epsilon_\phi|$. To provide a simple but useful upper bound on the absolute residual interference, an interference maximizing probability mass function (pmf) is adopted for ϵ_ϕ,

$$pmf_{\hat{\epsilon}_\phi}(\hat{\epsilon}_\phi) = \delta\left(\frac{\pi}{2^{(K-1)}} - \hat{\epsilon}_\phi\right) \tag{3.72}$$

It can now be shown that QOSTBC with the proposed quantization scheme yields an effective channel,

$$\mathbf{\Delta}' = \begin{bmatrix} \beta & 0 & 0 & \alpha_q'' \\ 0 & \beta & -\alpha_q'' & 0 \\ 0 & -\alpha_q'' & \beta & 0 \\ \alpha_q'' & 0 & 0 & \beta \end{bmatrix} \tag{3.73}$$

where α_q'' is substituted for α in (3.29). The eigenvector matrix of (3.73) is equivalent to that of (3.29), i.e. $\mathbf{V}$ (3.32), with the associated eigenvalue matrix,

$$\mathbf{\Lambda}_q = \begin{bmatrix} \gamma + \alpha_q'' & 0 & 0 & 0 \\ 0 & \gamma - \alpha_q'' & 0 & 0 \\ 0 & 0 & \gamma - \alpha_q'' & 0 \\ 0 & 0 & 0 & \gamma + \alpha_q'' \end{bmatrix} \tag{3.74}$$

From (3.74), λ_i is denoted as the ith eigenvalue of $\mathbf{\Lambda}_q$, i.e. $\lambda_i = [\mathbf{\Lambda}_q]_{i,i}$. With respect to the definitions of γ (2.94), α_q'' (3.71) and ζ (3.61), the eigenvalues for a fixed channel realization $\mathbf{h}$ can be expressed as,

$$\lambda_k = \mathbf{h}_j^H \tilde{\mathbf{S}}(k,j) \mathbf{\Gamma}^{\frac{1}{2}} \mathbf{h}_j \tag{3.75}$$

where (3.38) is adapted to express the effects of phase rotations at the transmitters and quantization errors,

$$\tilde{\mathbf{S}}(k,j) = \begin{cases} \mathbf{A} + \sin(-\epsilon_\phi)\mathbf{B}, & i = \{1,4\} \\ \mathbf{A} - \sin(-\epsilon_\phi)\mathbf{B}, & i = \{2,3\} \end{cases} \tag{3.76}$$

Therefore, (3.75) represents the deterministic eigenvalues. To evaluate the channel capacity under fading conditions maximal quantization error is assumed by

adopting the pmf for the quantization error (3.72). This generates a coupling matrix with maximal residual interference resulting from quantization error,

$$\breve{\mathbf{S}}(k,j) = \begin{cases} \mathbf{A} + \sin\left(\frac{\pi}{2^{(K-1)}}\right)\mathbf{B}, & i = \{1,4\} \\ \mathbf{A} - \sin\left(\frac{\pi}{2^{(K-1)}}\right)\mathbf{B}, & i = \{2,3\} \end{cases} \tag{3.77}$$

A lower-bound on the capacity for the case with partial-CSI available at the transmitter can now be similarly outlined as for the case of open-loop QOSTBC schemes and is therefore omitted here for brevity.

The capacity of QOSTBC in ergodic channels under various different networking scenarios is now explored through numerical simulation studies.

3.2.2.3 Simulations

Case Study 1: Figure 3.3 depicts the normalized capacity $[bits/s/Hz]$ against SNR $[dB]$ for a set of OSTBCs and QOSTBCs with varying degrees of partial CSI at the transmitter. The case study focuses on configurations with only one target receive antenna. Depicted are the following cases: (1) $N_t = 1$ Gaussian, (2) $N_t = 1$ SISO, (3) $N_t = 2$ Alamouti & $N_t = 4$ QOSTBC, (4) $N_t = 3$ OSTBC (3/4 Rate), (5) $N_t = 4$ OSTBC (3/4 Rate), (6) $N_t = 3$ OSTBC (Half-Rate), (7) $N_t = 4$ OSTBC (Half-Rate), (8) $N_t = 4$ QOSTBC ($\epsilon_\phi = 0$), (9) $N_t = 4$ QOSTBC ($\epsilon_\phi = \pi/4$), (10) $N_t = 4$ QOSTBC ($\epsilon_\phi = \pi/8$). Interestingly the capacity of the AWGN channel is not exceeded by any of the codes operating in a fading environment. It can be observed that both the *Alamouti* and open-loop QOSTBC achieve the same capacity of that of a $N_t = 2$ MISO channel with CSI at the transmitter. Furthermore only the Alamouti and QOSTBC derivatives outperform the SISO scheme due to the loss in transmission rate of COD schemes when there are more than two transmit antennas. Therefore when operating close to the capacity limit it is suboptimal to deploy OSTBC schemes with more than two transmit antenna. When operating a QOSTBC with infinite precision feedback according to Toker's proposed scheme the channel capacity of a $N_t = 4$ MISO channel with CSI at the transmitter is achieved. It is interesting to note that no discernible difference can be observed between QOSTBCs operating in the infinite precision and quantized scenario with 3-bit precision ($\epsilon_{phi} = \pi/8$).

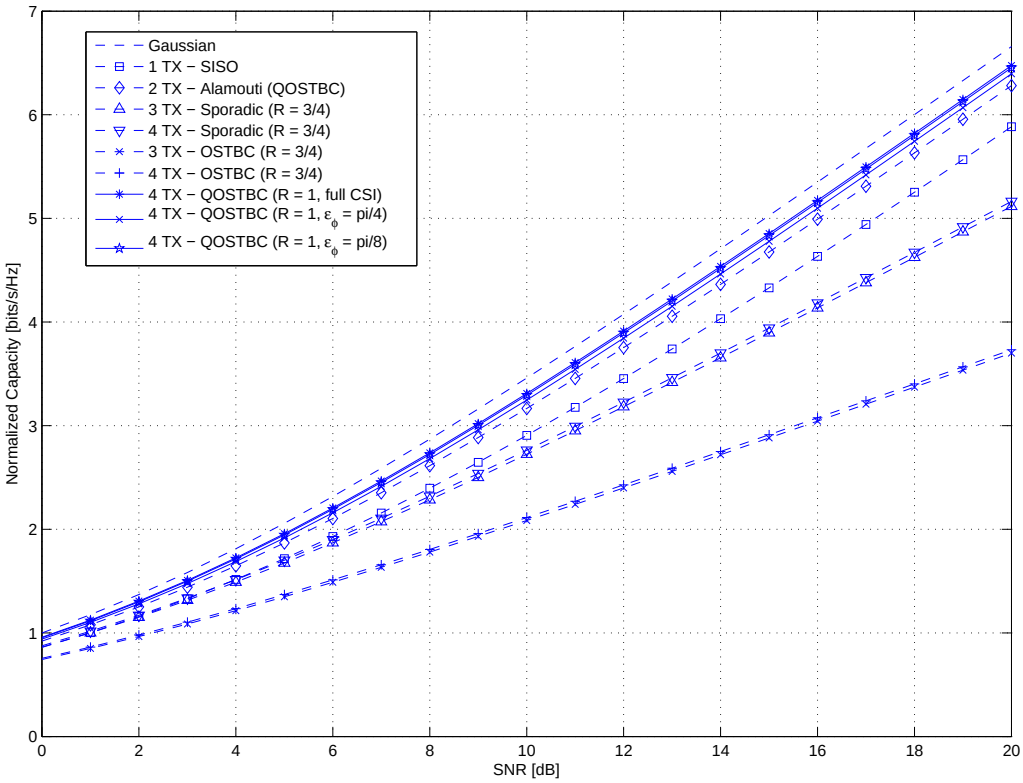

Figure 3.3: Normalized Capacity vs SNR for various OSTBCs & QOSTBCs; $N_r = 1$

Case Study 2: Figure 3.4 depicts the normalized capacity $[bits/s/Hz]$ against SNR $[dB]$ for a set of OSTBCs and QOSTBCs and varies from Figure 3.3 with the utilization of two receive antennas, i.e. $N_r = 2$. Again it is observed that none of the proposed coding schemes attains the channel capacity of the Gaussian case. However comparing Figure 3.4 with Figure 3.3 the relative capacity gap between the Gaussian channel and all the full-rate schemes is reduced. In addition the capacity of reduced rate CODs yields virtually identical results with $N_t = 3$ and $N_t = 4$ when like-for-like transmission rate comparisons are made, demonstrating the dominant effect of the number of receive antennas over that of transmitters. This corroborates the findings in the analysis on MISO and SIMO channels; where the former without CSI yields relatively flat improvement in performance against an increase in the number of transmit antennas whereas the latter yields a logarithmic increase against the number of receive antennas due to CSI availability to leverage receiver array gain. For clarity the results for QOSTBCs with partial CSI have been emitted as a result of the convergence between the performance of the Alamouti & open-loop QOSTBC scheme against that of the QOSTBC which adopts Toker's scheme with infinite precision. As stated in [5] the capacity gap between the *Alamouti* OSTBC and the equivalent Gaussian channel will reduce proportionally for a given number of receive antennas. Since the performance of these codes is limited by the equivalent Gaussian channel the capacity gains for adopting Toker's scheme will also be reduced proportionally.

Case Study 3: Figure 3.5 depicts the normalized capacity $[bits/s/Hz]$ against the normalized shadowing $\bar{\gamma}_1$ in the first link for a distributed Alamouti scheme or the joint shadowing $\bar{\gamma}_{1,4} := \bar{\gamma}_1 + \bar{\gamma}_4$ ($\bar{\gamma}_1 = \bar{\gamma}_4$) observed at transmitter pairs for the QOSTBC based scheme operating at an SNR of 10dB. For comparison the capacity of a SISO implementation experiencing the same shadowing effects as the space-time sub-channels is included where the mirror SISO channel observes $\bar{\gamma}_2 = 2 - \bar{\gamma}_1$ ($\bar{\gamma}_{2,3} = 2 - \bar{\gamma}_{1,4}$). Notably the distributed Alamouti & open-loop QOSTBC schemes outperform the strongest link over the range $0.8 < \gamma_1 < 1.2$. However, this range is extended to $0.7 < \gamma_1 < 1.3$ in the QOSTBC case when Toker's scheme is adopted with just two quantization bits ($\epsilon_\phi = \pi/4$). Furthermore, when extending the number of quantization bits to three ($\epsilon_\phi = \pi/8$) the distributed performance becomes indistinguishable from that of a scheme adopting infinite

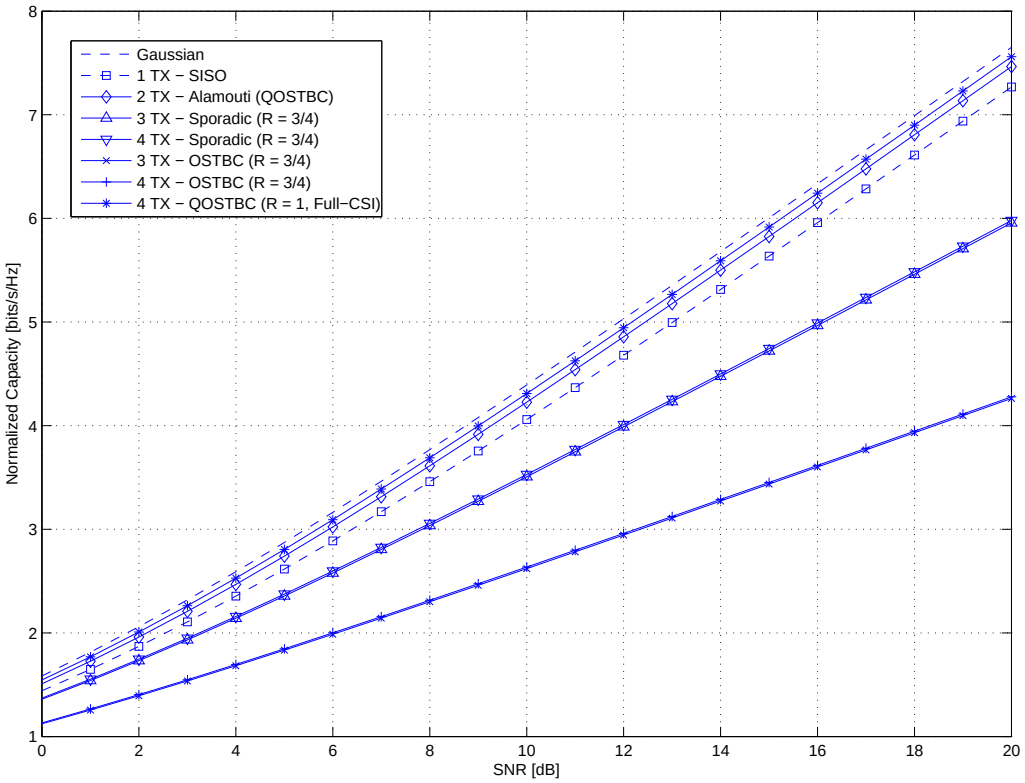

Figure 3.4: Normalized Capacity vs SNR for various OSTBCs & QOSTBCs; $N_r = 2$

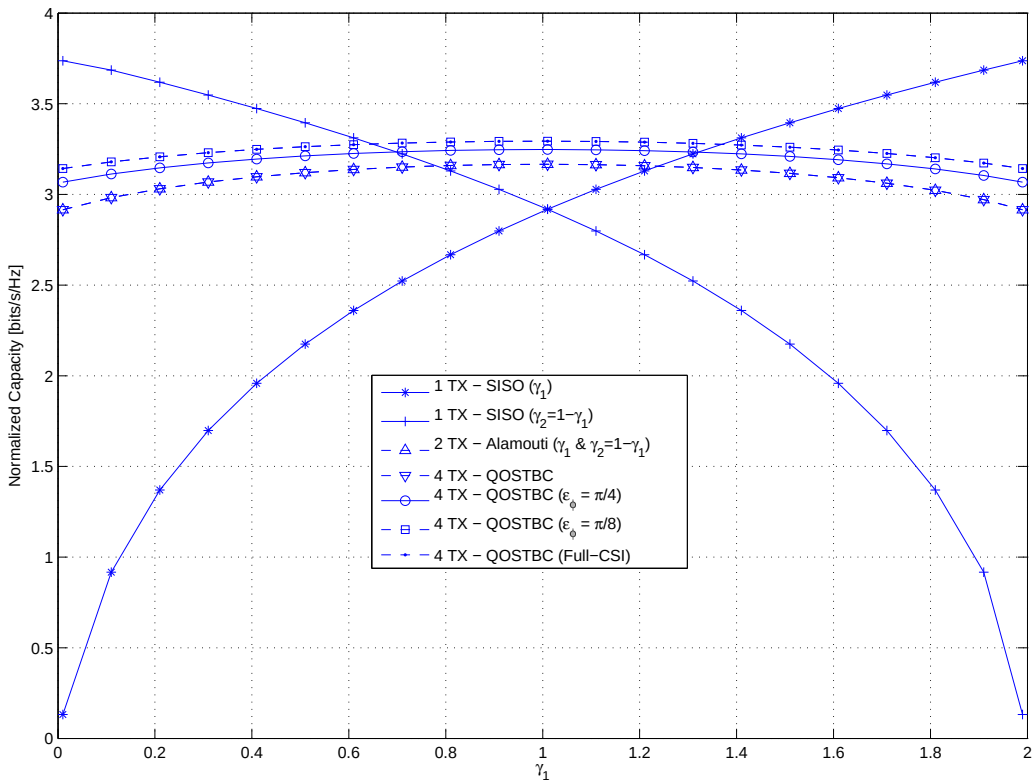

Figure 3.5: Normalized Capacity vs normalized power $\bar{\gamma}_1$ in the first link for the distributed Alamouti scheme or the symmetric link pair $\bar{\gamma}_{1,4}$ in the QOSTBC scheme; $SNR = 10dB$ and $\bar{\gamma}_2 = 2 - \bar{\gamma}_1$ or $\bar{\gamma}_{2,3} = 2 - \bar{\gamma}_{1,4}$

precision. This illustrates that the capacities of the Alamouti and QOSTBC distributed schemes are robust against the shadowing effects of the underlying individual links and provides an endorsement of their use as compared to SISO alternatives.

Case Study 4: Figure 3.6 is equivalent to Figure 3.5 with the only difference that the QOSTBC sub-systems experience the same shadowing variations $\bar{\gamma}_1 + \bar{\gamma}_4 = \bar{\gamma}_2 + \bar{\gamma}_3$ where the constraints $\bar{\gamma}_1 + \bar{\gamma}_4 = 2$ and $\bar{\gamma}_2 + \bar{\gamma}_3 = 2$ hold. The normalized power variations of the Alamouti and SISO schemes remain the same as Figure 3.5. The distributed QOSTBC variants however observe a shadowing

relationship this time according to $\bar{\gamma}_{3,4} = 2 - \bar{\gamma}_{1,2}$. Primarily, the capacity of the distributed open-loop QOSTBC scheme shows no variation due to the balancing of the effective shadowing $\bar{\gamma}_1 + \bar{\gamma}_4 = \bar{\gamma}_2 + \bar{\gamma}_3 = 2$ even in the extreme case when some of the links experience severe shadowing conditions. This observation gives guidance to the deployment of distributed QOSTBCs and suggests that the spatial branches 1 & 4 or 2 & 3 of the Jafarkhani QOSTBC variant should not be implemented on co-located systems or cooperating terminals experiencing similar shadowing conditions. In addition it maybe observed under extreme mismatches in fading $(\bar{\gamma_1} < 0.1) \cup (\bar{\gamma_1} > 0.9)$ that the capacity benefits of Toker's scheme are marginal in the case when interfering spatial branches of the codeword experience significant shadowing differences relative to each other. In either scenario shown in Figure 3.5 and Figure 3.6 deployment of a distributed QOSTBC is shown to provide a robust communications link equal or superior to that of Alamouti coding with or without feedback and when the channel conditions are unknown a priori.

Case Study 5: Figure 3.7 depicts the normalized capacity $[bits/s/Hz]$ against SNR $[dB]$ for the distributed Alamouti scheme with unequal sub-channel gains and a configuration of only one target receive antenna. Assuming equal channel coefficients the expectation of the equivalent SISO channel used in the previous analysis would yield t; and has direct relationship with the Frobenius norm which for the Alamouti case assuming normalized channels is $\|\mathbf{h}\|_F^2 = 2$ [5]. For comparision with a SISO implementation the coefficients are constrained such that $\bar{\gamma}_1 + \bar{\gamma}_2 \equiv 2$ and the shadowing ratio $\bar{\gamma}_1 : \bar{\gamma}_2 = 2 : 1$. Alternatively, the scenario of utilizing a SISO scheme over the strongest $\bar{\gamma}_1 = 4/3$ and weakest $\bar{\gamma}_2 = 2/3$ is illustrated to enable the assessment of the utility of distributed Alamouti coding over a straightforward SISO implementation. The distributed Alamouti scheme provides a robust performance to attenuation in either link with only negligible performance loss against a SISO implementation where all the transmit power is directed over the strongest link. Furthermore, significant loss in capacity is observed in the SISO case in comparison to the Alamouti scheme where severe shadowing is experienced. Again this demonstrated the utilization of distributed space-time coding in a network scenario which may experience significant levels of attenuation due to shadowing.

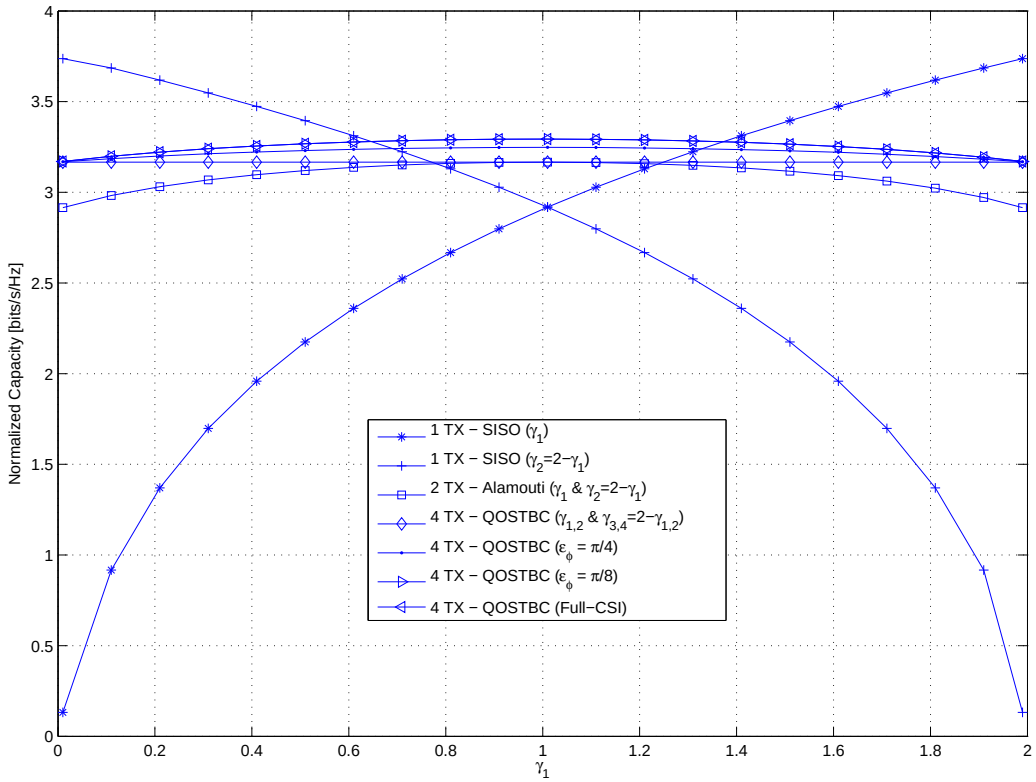

Figure 3.6: Normalized Capacity vs normalized power $\bar{\gamma}_1$ in the first link for the distributed Alamouti scheme or the asymmetric link pair $\bar{\gamma}_{1,2}$ in the QOSTBC scheme; $SNR = 10dB$ and $\bar{\gamma}_2 = 2 - \bar{\gamma}_1$ or $\bar{\gamma}_{3,4} = 2 - \bar{\gamma}_{1,2}$

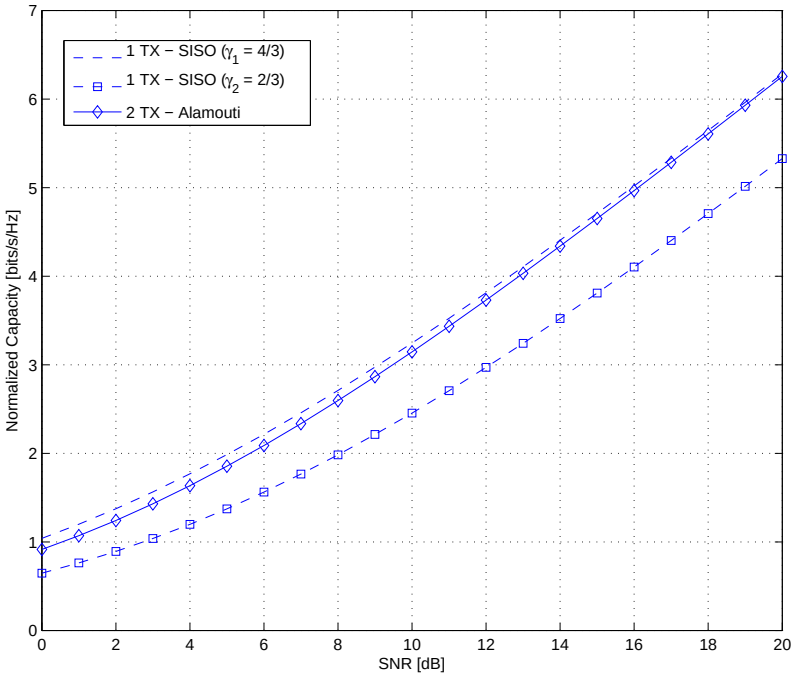

Figure 3.7: Normalized Capacity vs SNR for distributed Alamouti scheme; $r = 1$, $\bar{\gamma}_1 + \bar{\gamma}_2 \equiv 2$, $\bar{\gamma}_1 : \bar{\gamma}_2 = 2 : 1$

Case Study 6: Figure 3.8 depicts the normalized capacity $[bits/s/Hz]$ against SNR $[dB]$ for the distributed sporadic 3TX 3/4-rate OSTBC with unequal sub-channel gains and a configuration of only one target receive antenna. Again the channel coefficients are normalized according to $\bar{\gamma}_1 + \bar{\gamma}_2 + \bar{\gamma}_3 \equiv 3$ with the given ratio $\bar{\gamma}_1 : \bar{\gamma}_2 : \bar{\gamma}_3 = 4 : 2 : 1$ for comparative purposes against the SISO equivalent scheme of varying channel strengths. The distributed sporadic code offers some robustness against shadowing and performs favorably against the weaker channels in the low SNR region, i.e. $< 10dB$. However, the reduction in transmission rate over the full-rate SISO alternatives yields a reduced capacity slope and produces only superior capacity performance over the very weakest SISO scheme when evaluating in the high SNR region. As demonstrated in Figure 3.3 the case of half-rate codes yields an inferior performance to sporadic codes due to the rate penalty and thus have not been considered here for evaluation.

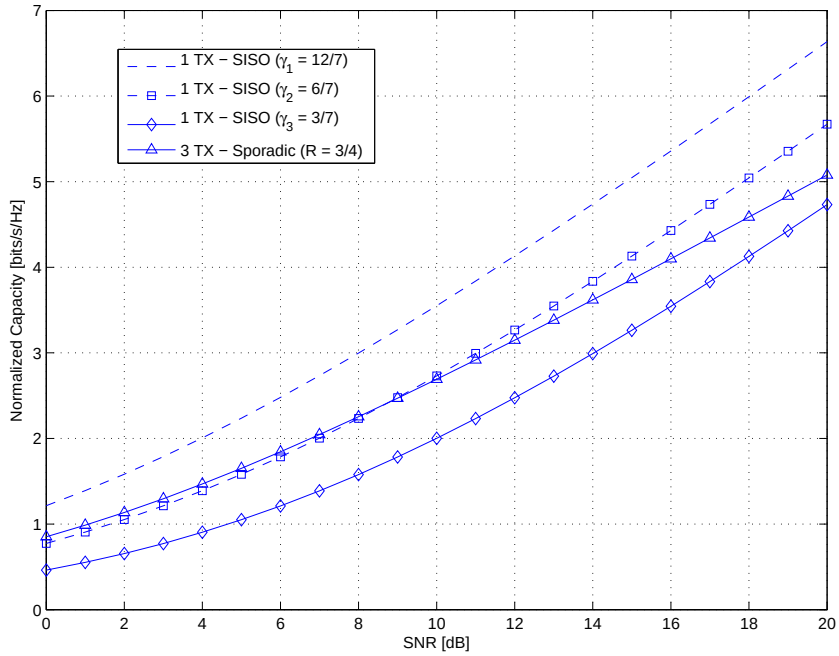

Figure 3.8: Normalized Capacity vs SNR for distributed 3Tx Sporadic (R = 3/4) scheme; $r = 1$, $\bar{\gamma}_1 + \bar{\gamma}_2 + \bar{\gamma}_3 \equiv 3$, $\bar{\gamma}_1 : \bar{\gamma}_2 : \bar{\gamma}_3 = 4 : 2 : 1$

Case Study 7: Figure 3.9 depicts the normalized capacity $[bits/s/Hz]$ against SNR $[dB]$ for the distributed sporadic 4TX 3/4-rate OSTBC and QOSTBC derivatives with unequal sub-channel gains and a configuration of only one target receive antenna. Again the channel coefficients are normalized according to $\sum_{i=1}^{4} \bar{\gamma}_i \equiv 4$ with the given ratio $\bar{\gamma}_1 : \bar{\gamma}_2 : \bar{\gamma}_3 : \bar{\gamma}_4 = 8 : 4 : 2 : 1$ for comparative purposes against SISO equivalent scheme of varying channel strengths. Again it is observed that with increasing SNR the performance advantage of the 4TX sporadic COD is reduced compared to the SISO schemes. In addition the sporadic code only outperforms the weakest SISO links over the SNR range evaluated. Conspicuously, the full-rate QOSTBC scheme outperforms all SISO schemes with the exception of the strongest link and provides a robust channel capacity even in extreme shadowing situations. Again when implementing Toker's scheme with only 3-bit quantization the scheme offers virtually the equivalent capacity gains as if operating with infinite precision. However, when introducing Toker's scheme

with quantized feedback Figure 3.9 demonstrates that benefits are marginal for unequal ergodic channels where the sub-channels are very unbalanced.

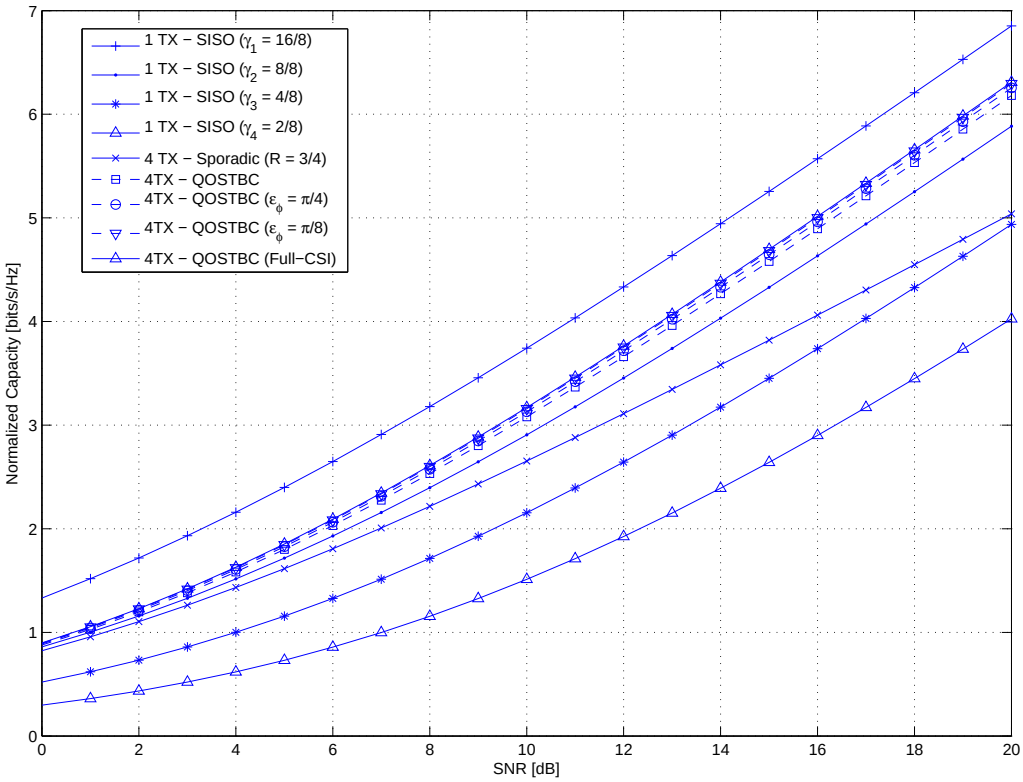

Figure 3.9: Normalized Capacity vs SNR for distributed 4Tx Sporadic (R = 3/4) scheme; $N_r = 1$, $\bar{\gamma}_1 + \bar{\gamma}_2 + \bar{\gamma}_3 + \bar{\gamma}_4 \equiv 4$, $\bar{\gamma}_1 : \bar{\gamma}_2 : \bar{\gamma}_3 : \bar{\gamma}_4 = 8 : 4 : 2 : 1$

3.2.3 Non-Ergodic Flat-Fading Channel

Previously the achievable channel capacity for distributed-STBCs deployed in ergodic channels was evaluated. In this section it is assumed that the channel realization is fixed at the start of the transmission and remains static for the length of the codeword. Therefore there is a finite probability that no matter how small the transmission rate is the channel cannot support error free transmission; this event is defined as the channel being in outage. A useful metric to evaluate the

performance of candidate coding schemes in this environment is the probability that the channel cannot support a given transmission rate, henceforth referred to as the outage probability.

Calculating the outage probability for O-MIMO channels in a distributed implementation with varying attenuation due to shadowing is simplified because OSTBCs are known to reduce MIMO channels to rank one SISO channels. For completeness the ensuing brief review summarizes closed-form expressions for the outage probability of the O-MIMO channel under various communications scenarios.

Deriving the outage probability for QOSTBCs in closed form is not as simple as the OSTBC case due to the residual MIMO structure of the effective channel observed after pre-processing at the transmitter and matched filtering at the receiver. However, as stated previously, QOSTBCs have the interesting property that the eigenvectors of the effective channel are independent of the channel realization therefore simplifying the ensuing analysis. The exact derivations of the outage probability proves difficult to achieve in closed form, however tight approximations are generated for a variety of communications scenarios where distributed QOSTBCs are employed.

3.2.3.1 O-MIMO Channel

Equal sub-channel gains Assuming that none of the sub-channel gains experience unequal shadowing or path-loss pertubations, i.e. $\gamma_1 =, \cdots, = \gamma_u$, and each sub-channel gain is independently modeled using ZMCSCG random variables with unity variance then the outage probability can be expressed as [5, Eq. 2.92],

$$P_{out}(\phi) = \frac{1}{\Gamma(u)} \int_0^{\hat{\lambda}} \lambda^{u-1}\, e^{-\lambda} d\lambda \tag{3.78}$$

$$= \frac{\gamma(u, \hat{\lambda})}{\Gamma(u)} \tag{3.79}$$

where $\gamma(\cdot\,,\cdot)$ denotes the *lower incomplete gamma function*, $\hat{\lambda}$ can be substituted for,

$$\hat{\lambda} = \frac{2^{\phi/R} - 1}{\frac{\bar{\gamma}}{R}\frac{\rho}{N_t}}. \tag{3.80}$$

Unequal sub-channel gains In the case of non-ergodic channels with unequal sub-channel gains caused by shadowing effect, i.e. $\gamma_1 \neq, \cdots, \neq \gamma_u$, a similar analytical approach can be assumed to that used in the ergodic case (see Section 3.2.2.1). Using a simple partial fraction expansion the outage probability can be calculated from the underlying sub-channel statistics [5, Eq. 2.93],

$$P_{out}(\phi) = \sum_{i=0}^{u} K_i \int_0^{\hat{\lambda}_i} f_{\lambda_i}(\lambda_i)\, d\lambda_i \tag{3.81}$$

$$= \sum_{i=0}^{u} K_i \left(1 - e^{-\hat{\lambda}_i}\right) \tag{3.82}$$

where $f_{\lambda_i}(\lambda_i)$ denotes the pdf and K_i is defined by (3.24) with the integral limit $\hat{\lambda}_i$ shown to be [5, Eq.2.93],

$$\hat{\lambda}_i = \frac{2^{\frac{\phi}{R}} - 1}{\frac{1}{R}\frac{\gamma_i}{t}\frac{S}{N}} \tag{3.83}$$

3.2.3.2 Quasi O-MIMO Channel

As previously expressed (3.35) the mutual information achieved using QOSTBC was shown to be [52],

$$I(s;y) = \frac{R}{N_s}\log_2 \det\left(\mathbf{I} + \frac{\rho}{RN_t}\mathbf{\Lambda}\right) \tag{3.84}$$

$$= \frac{R}{N_s}\log_2 \prod_{k=1}^{4}\left(1 + \frac{\rho}{RN_t}\lambda_k\right) \tag{3.85}$$

Noting the pairwise equivalence of eigenvalues $\lambda_1 \equiv \lambda_4$ and $\lambda_2 \equiv \lambda_3$ as observed from (3.35) for any channel realizations, then (3.85) can be expressed without loss of generality as,

$$I(s;y) = \frac{2R}{N_s}\log_2 \prod_{k=1}^{2}\left(1 + \frac{\rho}{RN_t}\lambda_k\right) \tag{3.86}$$

where the following derivations are equally applicable by substituting eigenvalues λ_3 & λ_4 for eigenvalues λ_1 & λ_2 respectively. Using the non-negative definiteness of the eigenvalues, (3.86) can be lower bounded as [52],

$$I(s;y) \geq \frac{2R}{N_s}\log_2\left(1+\left(\frac{\rho}{RN_t}\right)^2\lambda_1\lambda_2\right) \tag{3.87}$$

$$= I'(s;y) \tag{3.88}$$

which results in an upper bound on the outage probability by virtue of $Pr[I(s;y) < \phi] \leq Pr[I'(s;y) < \phi]$ for a given rate ϕ. The outage probability for any given channel statistics can by calculated by evaluating,

$$P_{out}(\phi) \leq \int_0^{\hat{\lambda}_{12}} f_{\lambda_{12}}(\lambda_{12})\, d\lambda_{12} \tag{3.89}$$

where $f_{\lambda_{12}}(\lambda_{12})$ is the pdf associated with the random variable $\lambda_{12} := \lambda_1\lambda_2$ and $\hat{\lambda_{12}}$ is defined as,

$$\hat{\lambda}_{12} = \frac{2^{\frac{N_s\phi}{2R}}-1}{\left(\frac{1}{R}\frac{1}{N_t}\rho\right)^2} \tag{3.90}$$

.

To simplify the derivation of $f_{\lambda_{12}}(\lambda_{12})$, the Mellin transform is used extensively for closed-form approximations of pdf of λ_{12} in distributed scenarios for equal and unequal sub-channel gains. The prior assumption of a product of i.i.d. variates when performing a Mellin transform is relaxed in the ensuing analysis since clearly $f_{\lambda_{12}}(\lambda_{12}) \neq f_{\lambda_1}(\lambda_1)f_{\lambda_2}(\lambda_2)$. However, the simulation results later presented verify the utility of the pdf derived under this assumption.

Equal sub-channel gains To determine a closed-form approximation to the outage probability it is desirable to find the pdf of the random variable $w = \lambda_1\lambda_2$; where the equal sub-channel case both λ_1 and λ_2 are Rayleigh variates with scale parameters equal to $\bar{\gamma}$ (3.47). It has been shown [53] that the Mellin transform provides an easier method for deriving the pdf of a product of two independent variates. The Mellin transform of the pdf of one of the eigenvalues (3.47) is expressed as,

$$\varphi_{\lambda_k} := \int_0^\infty \lambda_k^{s-1} f_{\lambda_k}(\lambda_k) d\lambda_k \tag{3.91}$$

which when evaluated by substituting (3.47) for $f_{\lambda_k}(\lambda_k)$ in (3.91) yields,

$$\varphi_{\lambda_k} = \frac{1}{(2\bar{\gamma})^{2N_r}\Gamma(2N_r)} \int_0^\infty \lambda_k^{2N_r+s-2} e^{-\lambda_k/2\bar{\gamma}} d\lambda_k \tag{3.92}$$

$$= \frac{(2\bar{\gamma})^{s-1}\Gamma(2N_r+s-1)}{\Gamma(2N_r)} \tag{3.93}$$

In [53] it is stated that Mellin transform of the pdf of the product of two independent random variables is the product of the Mellin transforms of the pdfs of the independent variables; therefore the Mellin transform of w is,

$$\varphi_w(s) = \frac{(2\bar{\gamma})^{2s-2}\Gamma(2N_r+s-1)^2}{\Gamma(2N_r)^2} \tag{3.94}$$

In order to find the pdf of w the inverse *Mellin* transform is evaluated using,

$$f_w(w) = \frac{1}{2\pi j} \int_{\sigma-j\infty}^{\sigma+j\infty} w^{-s} \varphi_w(s) ds \tag{3.95}$$

Making the change of variables $s'/2 = 2N_r + s - 1$ and substituting into (3.94) obtains,

$$f_w(w) = \frac{a_w}{2\pi j} \int_{\sigma-j\infty}^{\sigma+j\infty} (w^{\frac{1}{2}})^{-s'} (1/\bar{\gamma})^{-s'} 2^{s'-2} \Gamma\left(\frac{s'}{2}\right)^2 ds' \tag{3.96}$$

where the constant a_w is denoted by,

$$a_w = \frac{(w)^{(2N_r-1)}}{\Gamma(2N_r)^2 (2)^{4N_r-1} (\bar{\gamma})^{4N_r}} \tag{3.97}$$

The inversion integral (3.96) is of such form that direct use of inverse *Mellin* transforms [49, §17.43.32] can be utilized,

$$M^{-1}\left\{\alpha^{-s} 2^{s-2} \Gamma\left(\frac{1}{2}s - \frac{1}{2}\beta\right) \Gamma\left(\frac{1}{2}s + \frac{1}{2}\beta\right)\right\} = K_\beta(\alpha x) \tag{3.98}$$

where $M^{-1}\{\cdot\}$ denotes the inverse *Mellin* transform assuming $\Re\{s\} > |\Re\{\nu\}|$ and $K_\beta(\alpha x)$ is the modified *Bessel* function of the second kind. This leads to a closed form expression for the pdf,

$$f_w(w) = \frac{(w)^{(2N_r-1)}}{\Gamma(2N_r)^2(2)^{4N_r-1}(\bar{\gamma})^{4N_r}} K_0\left(\frac{\sqrt{w}}{\bar{\gamma}}\right) \tag{3.99}$$

The outage probability can then be evaluated by subsituting (3.99) into (3.89) and using the standard integral,

$$\int z^{\alpha-1}K_0(z)dz = \frac{z^\alpha}{\alpha}\left\{K_0(z)_1F_2\left(1;\frac{\alpha}{2}+1,\frac{\alpha}{2};\frac{z^2}{4}\right)+\frac{z}{\alpha}K_1(z)_1F_2\left(1;\frac{\alpha}{2}+1,\frac{\alpha}{2}+1;\frac{z^2}{4}\right)\right\} \tag{3.100}$$

where ${}_1F_2\left(a,b;c;x\right)$ is the generalised hypergeometric function with two parameters of type 1 and one parameter of type 2 [49][§9.14.1]; it is sometimes referred to as the Gauss hypergeometric function [49][§9.14.2]. After simple substitution $z = \sqrt{w}/\bar{\gamma}$ into (3.99) a closed-form expression that approximates the outage probability is derived in a form to exploit (3.100),

$$P_{out}\left(\phi\right) \approx \frac{1}{\Gamma(2N_r)^2\ 2^{4N_r-2}\ \bar{\gamma}^2}\int_0^{\tilde{R}} z^{4N_r-1}K_0(z)dz \tag{3.101}$$

where $\tilde{R} = \sqrt{\hat{\lambda}_{12}}/\bar{\gamma}$ and $\hat{\lambda}_{12}$ is shown in (3.90).

Unequal virtual sub-channel gains The linearity of the *Mellin* transform enables the pdf for unequal virtual sub-channel gains (3.55) to be transformed by the integral,

$$\varphi_{\lambda_k} = \sum_{j=1}^{N_r}\sum_{i=1}^{2}\frac{K_{i,j}}{\eta_{i,j}}\int_0^\infty \lambda_k^{s-1}e^{-\lambda_k/\eta_{i,j}}d\lambda_k \tag{3.102}$$

$$= \Gamma(s)\sum_{j=1}^{N_r}\sum_{i=1}^{2}K_{i,j}\eta_{i,j}^{s-1} \tag{3.103}$$

where the constant $K_{i,j}$ is defined by (3.54) and $\eta_{i,j}$ for $i \in \{1,2\}$ is previously defined in (3.50). The product of the *Mellin* transforms, $w = \lambda_1\lambda_2$, can now be expressed as,

$$\varphi_w = \varphi_{\lambda_1}\varphi_{\lambda_2} \tag{3.104}$$

$$= \Gamma(s)^2\sum_{j,n=1}^{N_r}\sum_{i,m=1}^{2}K_{i,j}K_{m,n}\left(\eta_{i,j}\eta_{m,n}\right)^{s-1} \tag{3.105}$$

A simple substitution $s'/2 = s$ and manipulations yields the inverse Mellin transform,

$$f_w = \sum_{j,n=1}^{N_r} \sum_{i,m=1}^{2} \frac{a_{i,j}^{m,n}}{2\pi j} \int_{\sigma-j\infty}^{\sigma+j\infty} \left(w^{\frac{1}{2}}\right)^{-s'} \left(\frac{2}{\sqrt{\eta_{i,j}\eta_{m,n}}}\right)^{-s'} (2)^{s'-2}\Gamma\left(\frac{s'}{2}\right)^2 ds' \quad (3.106)$$

where,

$$a_{i,j}^{m,n} = \frac{2K_{i,j}K_{m,n}}{\eta_{i,j}\eta_{m,n}} \quad (3.107)$$

which as previously shown can leverage the inverse transform (3.98) to yield the required distribution,

$$f_w = 2\sum_{j,n=1}^{N_r} \sum_{i,m=1}^{2} \frac{K_{i,j}K_{m,n}}{\eta_{i,j}\eta_{m,n}} K_0\left(\frac{2\sqrt{w}}{\sqrt{\eta_{i,j}\eta_{m,n}}}\right) \quad (3.108)$$

Again using a simple substitution $z = 2\sqrt{w}/\sqrt{\eta_{i,j}\eta_{m,n}}$ an approximation of the outage probability can be derived as,

$$P_{out}(\phi) \approx \sum_{j,n=1}^{N_r} \sum_{i,m=1}^{2} K_{i,j}K_{m,n} \int_0^{\tilde{R}_{i,j}^{n,m}} zK_0(z)dz \quad (3.109)$$

$$= -\sum_{j,n=1}^{N_r} \sum_{i,m=1}^{2} K_{i,j}K_{m,n}\tilde{R}_{i,j}^{n,m} K_1(\tilde{R}_{i,j}^{n,m}) \quad (3.110)$$

where $\tilde{R}_{i,j}^{n,m} = 2\sqrt{\hat{\lambda}_{12}}/\sqrt{\eta_{i,j}\eta_{m,n}}$.

Generic virtual sub-channel gains In this analysis the notation for generic gains when deploying QOSTBCs introduced in Section 3.2.2.1 is adopted and again it is assumed there exist $g < 2N_r$ distinct virtual sub-channel gains denoted by $\hat{\eta}_{i\in(1,g)}$ which are repeated $\nu_{i\in(1,g)}$ times. Therefore noting the pdf of λ_k as (3.58), the Mellin transform can be shown to be,

$$\varphi_{\lambda_k}(s) = \sum_{i=1}^{g} \sum_{j=1}^{\nu_i} K_{i,j}\hat{\eta}_i^{s-1} \frac{\Gamma(j+s-1)}{\Gamma(j)} \quad (3.111)$$

Therefore the Mellin transform for the product of uncorrelated eigenvalues is given by,

$$\varphi_w(s) = \sum_{i,m=1}^{g} \sum_{j=1}^{\nu_i} \sum_{n=1}^{\nu_m} K_{i,j} K_{m,n} (\hat{\eta}_i \hat{\eta}_m)^{s-1} \frac{\Gamma(j+s-1)\Gamma(n+s-1)}{\Gamma(j)\Gamma(n)} \tag{3.112}$$

Using the substitution, $s'/2 = s + |j-n|/2 + \min\{j,n\} - 1$ for the integral in each summand, with some manipulations yields the inverse Mellin integral,

$$f_w = \sum_{i,m=1}^{g} \sum_{j=1}^{\nu_i} \sum_{n=1}^{\nu_m} \frac{a_{i,j}^{m,n}}{2\pi j} \int_{\sigma-j\infty}^{\sigma+j\infty} \left(w^{\frac{1}{2}}\right)^{-s'} \left(\frac{2}{\sqrt{\hat{\eta}_i \hat{\eta}_m}}\right)^{-s'} (2)^{s'-2} \Gamma\left(\frac{s'}{2} - \frac{\beta_{j,n}}{2}\right) \Gamma\left(\frac{s'}{2} + \frac{\beta_{j,n}}{2}\right) ds' \tag{3.113}$$

where,

$$a_{i,j}^{m,n} = \frac{2w^{\left(\frac{\beta_{j,n}}{2} + \alpha_{j,n} - 1\right)} K_{i,j} K_{m,n}}{\Gamma(j)\Gamma(n) \left(\hat{\eta}_i \hat{\eta}_m\right)^{\frac{\beta_{j,n}}{2} + \alpha_{j,n}}} \tag{3.114}$$

assuming $\beta_{j,n} := |j-n|$ and $\alpha_{j,n} := \min\{j,n\}$. The integral can again be evaluated using (3.98) to yield the desired pdf,

$$f_w = \sum_{i,m=1}^{g} \sum_{j=1}^{\nu_i} \sum_{n=1}^{\nu_m} a_{i,j}^{m,n} K_{\beta_{j,n}} \left(\frac{2\sqrt{w}}{\sqrt{\hat{\eta}_i \hat{\eta}_m}}\right) \tag{3.115}$$

Replicating the step taken for unequal channel gains, the simple substitution $z = 2\sqrt{w}/\sqrt{\hat{\eta}_i \hat{\eta}_m}$ facilitates the derivation of a closed-form approximation on the outage probability,

$$P_{out}(\phi) \approx \sum_{i,m=1}^{g} \sum_{j=1}^{\nu_i} \sum_{n=1}^{\nu_m} \frac{K_{i,j} K_{m,n}}{(2)^{\beta_{j,n} + 2\alpha_{j,n} - 2} \Gamma(j)\Gamma(n)} \int_0^{\tilde{R}_{i,j}^{n,m}} z^{\beta_{j,n} + 2\alpha_{j,n} - 1} K_{\beta_{j,n}}(z)\, dz \tag{3.116}$$

where in the generic case $\tilde{R}_{i,j}^{n,m} = 2\sqrt{\hat{\lambda}_{12}}/\sqrt{\hat{\eta}_i \hat{\eta}_m}$. When evaluating (3.116) it is clear that (3.100) provides a solution to the integral when $\beta_{j,n} = 0$, i.e. $j = n$. Other solutions for particular realizations of $\beta_{j,n}$ and $\alpha_{j,n}$ are found in [49, §6.561.8], however a solution to the generic case has not to date been found in the literature.

The applicability of the proceeding analysis is substantiated in simulation studies presented at the end of this chapter. The interesting extension to the throughput performance of QOSTBCs in non-ergodic channels is briefly explored to show the results that partial-CSI knowledge at the transmitter can introduce.

Full-CSI at the receiver As previously demonstrated under certain constraints the outage probability for a distributed QOSTBC scheme can be closely approximated in closed form for a variety of distributed communications scenarios. Conspicuously, in the scenario where Toker's proposed scheme is adopted with infinite precision the upper-bound derived in [52, Eq.32] for the capacity of QOSTBCs is satisfied,

$$I = \frac{2R}{N_s}\log_2\prod_{k=1}^{2}\left(1+\frac{\rho}{RN_t}\lambda_k\right) \tag{3.117}$$

$$\leq \frac{2R}{N_s}\log_2\left(\frac{1}{2}\sum_{k=1}^{2}\left(1+\frac{\rho}{RN_t}\lambda_k\right)\right)^{\frac{1}{2}} \tag{3.118}$$

$$= log_2\left(1+\frac{\rho}{RN_t}\lambda_1\right) \tag{3.119}$$

where the geometric-arithmetic mean inequality is used in the second line and the upper bound is satisfied when $\lambda_1 = \lambda_2$ and $\lambda_k = \sum_{i=1}^{N_r}\sum_{j=1}^{N_t}|h_{i,j}|^2, \forall k$. The outage-probability for the infinite precision Toker scheme can then be calculated using the same methodology as OSTBCs which in the case of equal channel gains equates to (3.78) and for the unequal channel gains (3.81).

Interestingly, the following simulation studies demonstrate that in the case of coarse (3-bit) quantization the upper-bound (3.119) provides an accurate approximation under a variety of communications scenarios. This illustrates the maximum throughput achieving capabilities of Toker's scheme in the presence of a low-rate feedback channel.

3.2.3.3 Simulations

Case Study 8: Figure 3.10 depicts the outage probability $P_{out}(\phi)$ against a desired normalized transmission rate ϕ in $[bits/s/Hz]$ for a set of OSTBCs with

a single receive antenna. Depicted are the following cases: (1) $N_t = 1$ SISO, (2) $N_t = 2$ Alamouti & $N_t = 4$ QOSTBC, (3) $N_t = 3$ OSTBC (3/4 Rate), (4) $N_t = 4$ OSTBC (3/4 Rate), (5) $N_t = 3$ OSTBC (Half-Rate), (6) $N_t = 4$ OSTBC (Half-Rate). It can be observed that no single coding scheme is dominant over the transmission rate range observed. The Pareto-optimal frontier is attained by selecting the following rate dependent coding strategy; 4TX sporadic code (3/4 rate) code in the low-rate high-reliability region ($P_{out}(\phi) < 18\%$, $\phi < 2.2$), 2TX Alamouti code in the medium region ($18\% \geq P_{out}(\phi) < 70\%$, $2.2 \geq \phi < 3.8$ and the basic SISO scheme in the high-rate low-reliability region ($3.8 \geq P_{out}(\phi)$, $3.8 \geq \phi$). This supports Telatar's conjecture [15] that multiple antennas should be supported for low-rate high-reliabilty schemes when the channel conditions are favorable and in the high-rate low-reliabilty case a SISO scheme should be adopted.

Case Study 9: Figure 3.11 depicts the outage probability $P_{out}(\phi)$ against a desired normalized transmission rate ϕ in $[bits/s/Hz]$ for a set of OSTBCs and QOSTBCs with varying degrees of partial CSI at the transmitter and single receive antenna. Depicted are the following cases: (1) $N_t = 1$ SISO, (2) $N_t = 2$ Alamouti & $N_t = 4$ QOSTBC, (3) $N_t = 4$ OSTBC (3/4 Rate), (4) $N_t = 4$ QOSTBC Toker's scheme (Full-CSI), (5) $N_t = 4$ open-loop Jafarkhani QOSTBC, (6) $N_t = 4$ QOSTBC Toker's scheme (partial-CSI, quantization error $\pi/8$). With the availability of the aforementioned coding schemes the Pareto-optimal frontier is now attained by utilizing CSI at the transmitter according to the infinite-precision Toker scheme for QOSTBCs in the low-rate high-reliability region ($P_{out}(\phi) < 70\%$, $\phi < 3.75$) then switching to a SISO scheme in the high-rate low-reliability region ($70\% \leq P_{out}(\phi)$, $3.75 \leq \phi$). Furthermore, near-optimal coding is achieved in the high-reliability region using only partial CSI in the form of 3-bit quantization of the Toker scheme. In the absence of any CSI at the transmitter, numerical simulations still confirm the utility of QOSTBC in the high-reliability region ($P_{out}(\phi) < 40\%$) over OSTBCs therefore rendering the use of low-rate ($R < 1$) OSTBCs in the form of sporadic codes redundant.

Case Study 10: Depicted in Figure 3.12 is the outage probability $P_{out}(\phi)$ of various schemes against a given SNR $[dB]$ evaluated at $\phi = 2$ [bits/s/Hz]. Clearly,

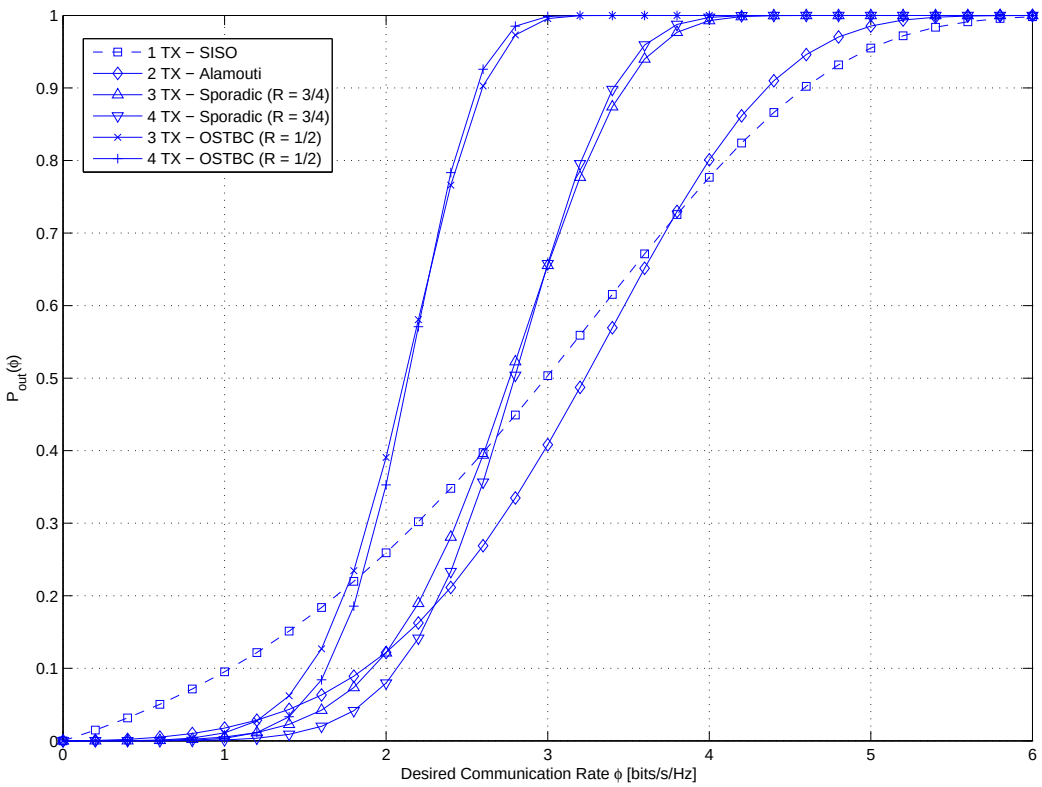

Figure 3.10: Outage Probability $P_{out}(\phi)$ vs transmission rate ϕ for various OST-BCs; $SNR = 10dB$, $N_r = 1$

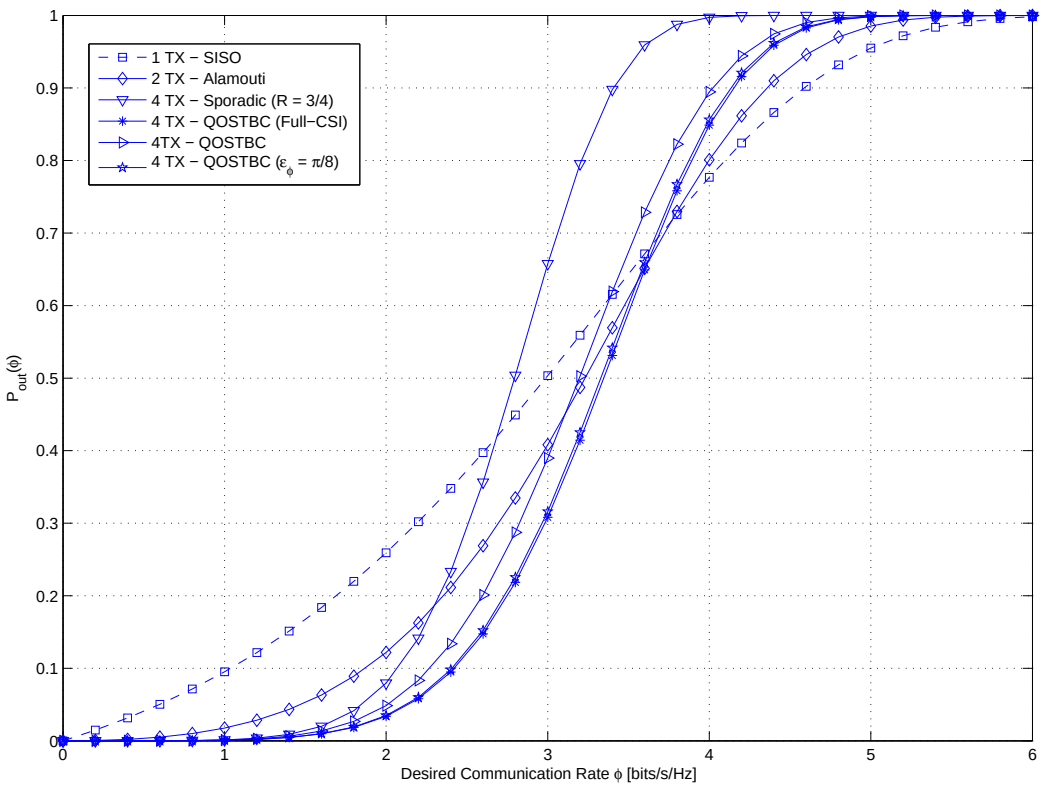

Figure 3.11: Outage Probability $P_{out}(\phi)$ vs transmission rate ϕ for various OST-BCs & QOSTBCs; $SNR = 10dB$, $N_r = 1$

Figure 3.12 illustrates the power saving potential of both OSTBCs and QOSTBCs when cooperation is leveraged to enable virtual MISO communications. Assuming a target outage probability of 10% the best OSTBC achieves the same performance as a SISO scheme with a SNR approximately 5dB lower translating to a 70% power saving. In addition QOSTBC achieves a further 0.75dB against the best OSTBC at $P_{out}(\phi) = 10\%$, achieving a power saving advantage of 15% over competitor OSTBCs. Furthermore, introducing partial-CSI at the transmitter through the Toker scheme increases the power saving advantage of the QOSTBC over the best OSTBC to 20% when operating at $P_{out}(\phi) = 10\%$ and $\phi = 2$ [bits/s/Hz]. In contrast to ergodic channels significant gains are made when employing more than two transmit antenna for OSTBCs. Again the dominance of QOSTBCs over OSTBCs is observed in Figure 3.12, however this time the benefits are more profound for non-ergodic channels than the previous results illustrated in the ergodic case.

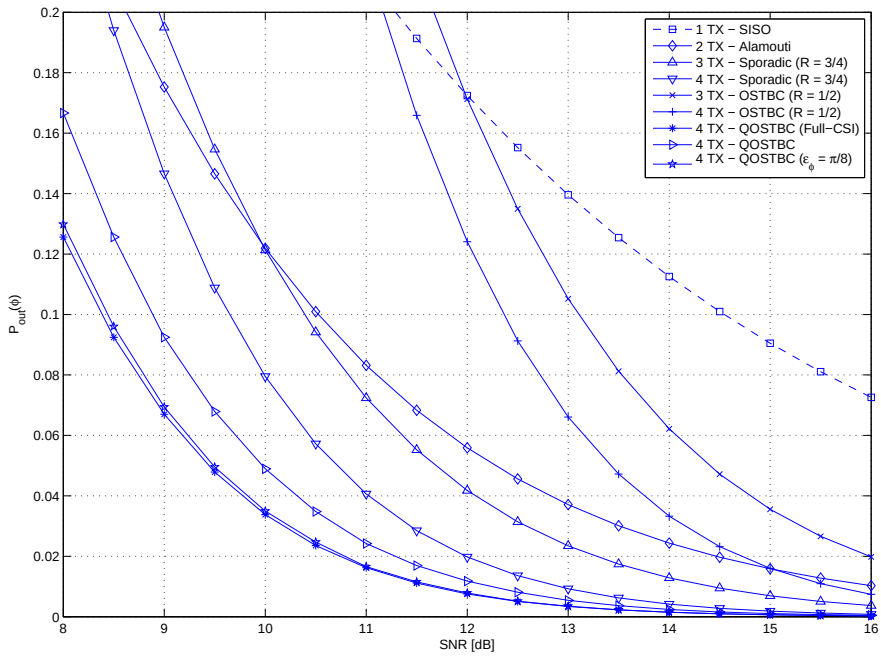

Figure 3.12: Outage Probability $P_{out}(\phi)$ vs SNR for various OSTBCs & QOSTBCs; $\phi = 2$ [bits/s/Hz], $N_r = 1$

Case Study 11: Depicted in Figure 3.13 is the outage probability $P_{out}(\phi)$ of various schemes against a given SNR $[dB]$ evaluated at $\phi = 4$ [bits/s/Hz]. The logarithmic scaling enables a forensic examination of competing schemes in the high-reliability region $P_{out}(\phi) \leq 10\%$, which was not possible using the linear scale in Figure 3.12. Immediately, it can be observed that the half-rate OSTBCs demonstrate inferior performance to all schemes and contrast in particular to their sporadic (3/4-rate) equivalents. The diversity gains are shown and demonstrate the utility of increasing the number of transmit antennas in high-SNR scenarios. Interestingly, Figure 3.13 as well as showing the dominance of QOSTBCs over the OSTBC counterparts, illustrates that it is possible to achieve full diversity for QOSTBCs as is shown in [47].

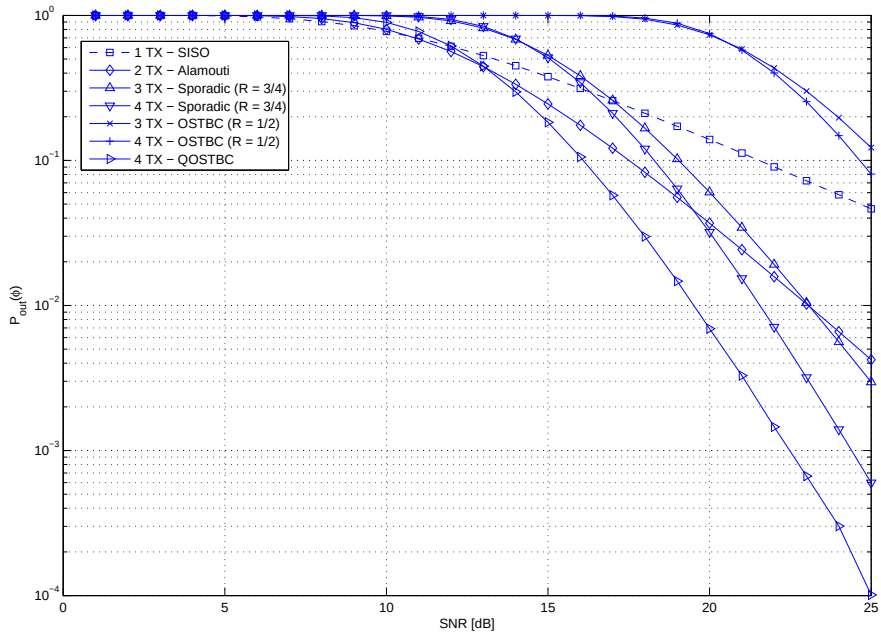

Figure 3.13: Outage Probability $P_{out}(\phi)$ vs SNR [dB] for various OSTBCs and QOSTBC schemes; $\phi = 4$ [bits/s/Hz], $N_r = 1$

Case Study 12: Depicted in Figure 3.14 is the outage probability $P_{out}(\phi)$ of various QOSTBCs evaluated over the SNR range 0-25 dB at a normalized transmission rate $\phi = 4$ [bits/s/Hz]. In this simulation study the upper bound for

the outage probability of QOSTBCs with equal channel coefficients is introduced and evaluated. Clearly, this bound provides a useful closed-form characterization of the open-loop QOSTBC scheme which tightens with an increasing number receive antennas. Conspicuously, the marginal effectiveness of implementing Toker's feedback scheme to orthogonalize the channel yields diminishing results, replicating observations in ergodic channels, when the receive array size is increased. However, Figure 3.14 clearly demonstrates the effectiveness of Toker's scheme under quantization with virtually no degradation in performance with only 3-bit ($\epsilon_\phi = \pi/8$) feedback.

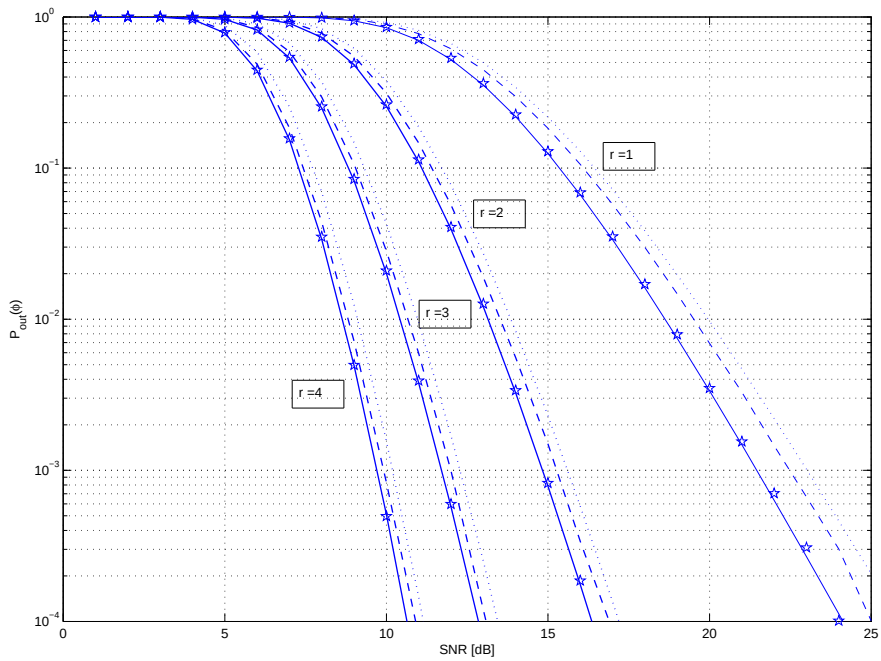

Figure 3.14: Outage Probability $P_{out}(\phi)$ vs transmission rate ϕ for various receive array sizes comparing QOSTBC (dashed lines), upper bound (dotted lines), full-CSI (solid lines), and quantized feedback (star marker); $\phi = 4$ [bits/s/Hz]

Case Study 13: Depicted in Figure 3.15 is the outage probability $P_{out}(\phi)$ versus the normalized power of the first link $\bar{\gamma}_1$ over various distributed schemes at a normalized transmission rate $\phi = 2$ [bits/s/Hz] and SNR of 15dB. The channel

powers of the remaining sub-channel vary inversely to the first link, reproducing a scenario where one sub-channel experiences severe shadowing. Therefore to maintain equivalence amongst schemes the constraint $\sum_{i=1}^{N_t} \bar{\gamma}_i = N_t$; which translates for the Alamouti code to $\bar{\gamma}_2 = 2 - \bar{\gamma}_1$, whereas for the sporadic 3/4-rate STBC with three transmit antennas it is satisfied by $\bar{\gamma}_2 = \bar{\gamma}_3 = (3 - \bar{\gamma}_1)2$ and for the remaining four transmit antennas it is satisfied by $\bar{\gamma}_2 = \bar{\gamma}_2 = \bar{\gamma}_3 = (4-\bar{\gamma}_1)3$. Clearly, Figure 3.15 demonstrates that a desired outage probability of $P_{out}(\phi) < 10\%$ is supported by all distributed STBCs whereas the SISO scheme only achieves this when the sub-channel gain is sufficiently high. It is also the case that increasing the number of antennas provides greater robustness in the form of reduced outage probability. Over the evaluated shadowing conditions the sporadic 3/4-rate STBC with four transmit antennas achieves an outage probability $P_{out}(\phi) < 1\%$. Furthermore significant outage performance increases can be observed when implementing QOSTBCs with varying degrees of quantization based on Toker's scheme [26]. It is worth noting that the performance benefits of using Toker's scheme in the distributed scenario are marginal compared to the open-loop equivalent scheme when the sub-channels experience more than marginal imbalancing. Finally, it is worth noting that with a relatively coarse 3-bit quantization Toker's scheme performs virtually identical to that where full-CSI is available at the transmitter.

Case Study 14: Depicted in Figure 3.16 is the outage probability $P_{out}(\phi)$ of various QOSTBCs evaluated over the SNR range 0-25 dB at a normalized transmission rate $\phi = 4$ [bits/s/Hz]. In this simulation study generic sub-channel gains are introduced to demonstrate the performance under a communications scenario with a co-located receiver array. When $N_r = 1$ the sub-channel gains are distributed according to $12/8 : 4/8 : 4/8 : 12/8 \equiv \bar{\gamma}_1 : \bar{\gamma}_2 : \bar{\gamma}_3 : \bar{\gamma}_4$ respectively. In this study it can be observed that $\bar{\gamma}_1 = \bar{\gamma}_4$ and $\bar{\gamma}_2 = \bar{\gamma}_3$ which maybe interpreted as a distributed implementation where the 1st-4th (2nd-3rd) branches of the QOSTBC are implemented at co-located transmitters experiencing equivalent shadowing perturbations. In the case $N_r = 2$ each sub-channel gain is again observed by the second receiver, therefore necessitating the need to analyze the channel using the methodology developed previously for generic sub-channel gains. As with Case Study 14, increasing the receiver array size tightens the gap

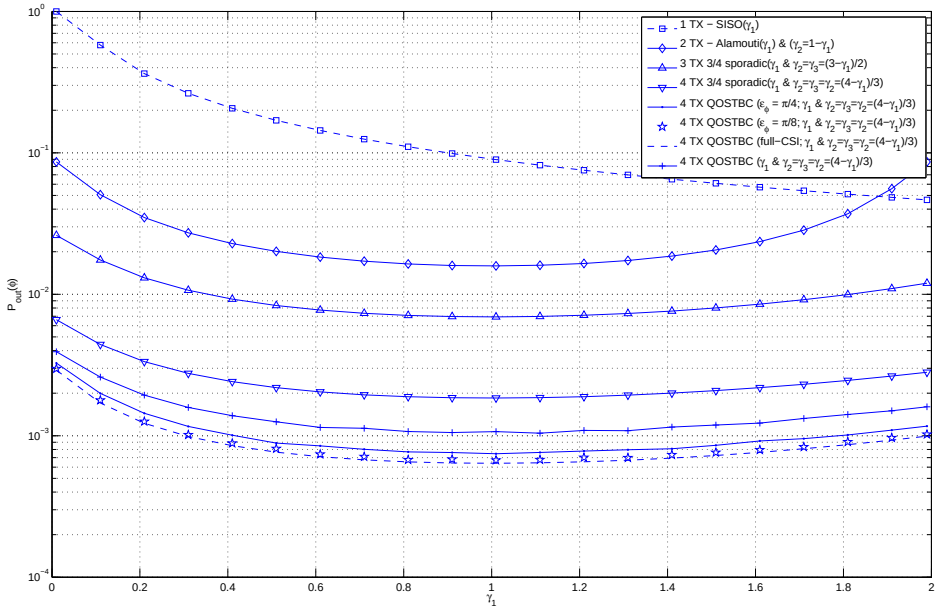

Figure 3.15: Outage Probability $P_{out}(\phi)$ versus the normalized power of the first link $\bar{\gamma}_1$ over various distributed schemes at a normalized transmission rate $\phi = 2$ [bits/s/Hz]; SNR of 15dB

between the upper and lower bounds, therefore providing diminishing returns when Toker's scheme is implemented with increasing receiver array size. Again employing only a very coarse quantization in Toker's scheme (3-bit, $\pi/8$) renders virtually identical performance to a lower-bound which assumes perfect CSI at the transmitter. In addition Figure 3.16 demonstrates the effectiveness of the derived upper-bound (3.116) on the outage performance of QOSTBCs in generic shadowing environments.

3.3 Conclusions

This chapter characterized cooperative MIMO channels that are encoded using both OSTBCs and QOSTBCs. The distributed transceiver pairs which denote a particular sub-channel may experience various shadowing and path-loss effects that are only observed in the case of cooperative networks. These have been

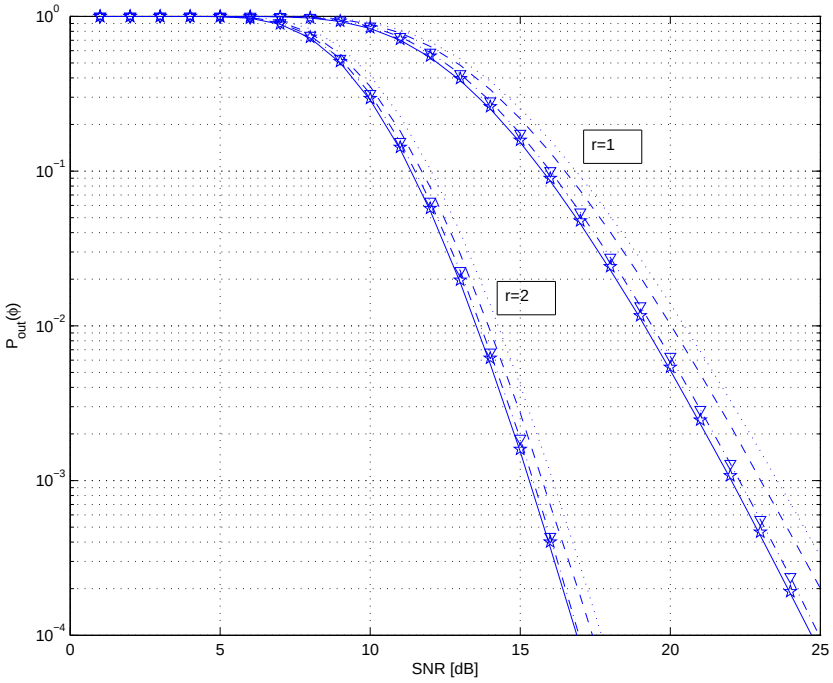

Figure 3.16: Outage Probability $P_{out}(\phi)$ vs SNR [dB] for various generic shadowing scenarios comparing QOSTBC (dashed lines), upper bound (dotted lines), full-CSI (solid lines), 2-bit quantized feedback (triangle marker with dot-dashed line) and 3-bit quantized feedback (star marker); $\phi = 4$ [bits/s/Hz]

categorized into equal, unequal and generic scenarios and analyzed in flat Rayleigh fading ergodic and non-ergodic MIMO channels. In this chapter the analysis and simulation studies demonstrated the superior channel capacity and outage-probability performance of QOSTBCs over traditional OSTBCs in a vast array of communications scenarios over the single-stage of a regenerative cooperative relay network.

In Section 3.2.1, the network architecture depicting a single-stage of a multi-stage wireless relay network was presented using a simple system model assuming distributed-Space Time Block Codes (STBCs) are deployed at the transmitter. It was assumed that each transmit antenna implements a pre-allocated spatial branch of the implemented space-time design and the analysis was limited to either OSTBCs or QOSTBCs. To highlight the differences between co-located

and distributed communications systems; three scenarios were highlighted and depicted in Figure 3.2. These scenarios formed the basis upon which OSTBCs and QOSTBCs could be categorized in both ergodic and non-ergodic deployments with cooperative wireless relay networks.

In Section 3.2.2 the case of communications in ergodic channels was explored. Firstly, traditional OSTBCs which are known to orthogonalize the MIMO channel (O-MIMO) were characterized in ergodic channels to formulate the theoretically achievable capacities in a number of communication scenarios. This review formed the foundation on which the candidacy of QOSTBC could be assessed against. Later, novel contributions were made in the characterization of the achievable capacities of distributed open-loop QOSTBCs where the sub-channels associated with transceiver pairs experience varying shadowing and path-loss perbutations. Simulation results verified that QOSTBCs with equal sub-channel gains achieve the capacity of full-rate Alamouti-style OSTBCs which are limited to only two transmit antennas. When the antenna order at the transmitter is increased beyond two QOSTBC demonstrated superior capacity for all SNRs, which is indicative of the reduced spectral efficiency of OSTBC in higher order antenna arrays. In unequal sub-channel gains environments typically encountered in systems where shadowing varies over the distributed antennas QOSTBC shows comparable robustness to Alamouti codes and exceed them under certain shadowing conditions. This work was then extended by allowing partial-CSI at the transmitter and utilizing the insights developed by Toker, the capacity of QOSTBCs using codebook independent phase-rotations at the transmitter were analyzed with varying degrees of quantization applied. It was demonstrated through simulation studies based on derived closed-form expressions that even when coarse (3-bit) quantization is applied the achievable capacity in ergodic channels was virtually indistinguishable from the case when full-CSI was available at the transmitter.

In Section 3.2.3 the analysis previously presented for ergodic channels was extended to the non-ergodic case. A brief derivation of the throughput based on distributed-OSTBCs with equal and unequal sub-channel gains was reviewed for comparative purposes. The section explicitly focused on the evaluation of QOSTBCs in non-ergodic channels. To aid in this undertaking closed-form expressions that approximate the throughput were derived. Whilst exact closed-form expressions for the outage probability of QOSTBCs prove to be mathemat-

ically intractable; a tight-approximation was derived for distributed-QOSTBCs operating in a range of scenarios without CSI (open-loop) at the transmitter and with equal and unequal sub-channel gains. The results presented clearly demonstrated that in the low-rate high reliability region QOSTBCs significantly outperform OSTBCs and make the requirement to switch between coding schemes redundant in order to minimize outage probability when increasing the data rate. Assuming the data-rate is fixed then QOSTBC still substantially reduces the outage probability over OSTBC counterparts therefore demonstrating the utility for deployment in robust cooperative wireless relay networks. In connection with the analysis undertaken for ergodic channels Toker's scheme is introduced for the non-ergodic case to orthogonalize the MIMO channel. A tight lower-bound is proposed for the outage-probability when applying Toker's scheme. The validity of this bound is demonstrated with numerical simulations and it provides a tight estimate even when coarse (3-bit) quantization is applied. Interestingly, all of the gains observed in the reduction of outage probability operating in the low-rate high reliability region are increased when the QOSTBC is orthogonalized using Toker's approach.

The theoretical advantages of implementing QOSTBCs in distributed-MIMO multi-stage relay networks are clearly illustrated in this chapter. The possibilities for increased coverage areas for a fixed power budget and throughput are one of a number of permutations that provide considerable performance improvements when deploying distributed-QOSTBCs. This then provides the motivation for the next chapter to reduce some of the assumptions regarding synchronization between participating nodes to developing novel asynchronous distributed space-time coding schemes that leverage the principles of QOSTBCs.

Chapter 4

Asynchronous Designs for Robust Flat-Fading Cooperative Relay Networks

4.1 Introduction

Space Time Block Codes (STBCs) from orthogonal designs [24] have been shown to be an effective technique for extracting spatial diversity for distributed cooperative systems [10]. In [10] Laneman et al. advocate the use of OSTBCs because full-diversity is guaranteed with a simple distributed network protocol in which relaying-Mobile Terminals (r-MTs) transmit their message using a spatial branch of the code matrix. In the event of node failure or observing deep-fading the transmitted waveforms remain orthogonal. In addition, orthogonal designs offer improved spectral efficiency over repetition-based cooperative diversity schemes [10]. Unfortunately, the set of complex valued space-time codes based upon orthogonal designs that achieve full rate, i.e. rate-one, transmission are limited to two transmit spatial branches using the well-known Alamouti-scheme [23]. Relaxing the orthogonality constraint has led to a set of codes generally referred to as QOSTBCs pioneered independently by Papadias [12] and Jafarkhani [11]; which offer similar characteristics whilst only deviating marginally in the implementation. These codes offered full-rate transmission whilst only guaranteeing a proportion of the diversity offered by the channel. Later works developed tech-

niques that enabled full-rate full-diversity QOSTBC and can be categorized into two groups; namely constellation rotation [47] and Closed-Loop Quasi-Orthogonal Space Time Block Code (CL-QOSTBC) [26].

Early studies of cooperative diversity enabled systems highlighted the significant synchronization challenges, such as timing and carrier synchronization, faced in implementing cooperation protocols [10]. In point-to-point systems where a base-station communicates directly with a MT such as in the Wireless Local-Area-Network (WLAN) standards [54], these issues are generally addressed through periodic transmission of known synchronization prefixes. However, distributed systems impose the additional challenges at the receiver of synchronizing with multiple transmitting terminals. In this chapter the issues of timing synchronization between all nodes participating in the relaying protocol are addressed.

Some initial studies focused on mitigating the issue of timing synchronization using equalizer and decoding strategies at the receiver. In [55] Wei et al. devised a novel MMSE receiver to combine the disparate inputs in the multiple relay channel with the broadcast signal from the source. This approach assumed the flat-fading relay channel takes on the characteristics of a frequency-selective channel through asynchronous re-transmission delays introduced through the relaying paths. Similar receiver compensated schemes were developed by Zheng et al. [56, 57] using both computationally feasible Parallel Interference Cancellation (PIC) and ML decoder techniques to remove ISI. The PIC scheme was extended to three and four relay terminals [58] to increase diversity gains from the cooperative channel; however, asynchronous delays in these schemes were limited to less than a symbol period. Alternative relay coding techniques in the presence of asynchronism include distributed-Space-Time Trellis Codes (STTCs) [59, 60, 61, 62] which are all limited to DF protocols at the relay nodes. In addition distributed-STTC can potentially impose much higher computational complexity at the receiver than distributed-STBC. Whilst [55] exploits the re-transmission delay encountered at each node to utilize decoder techniques designed primarily for frequency-selective channels; [63] effectively introduces multi-path in the flat-fading cooperative channel via the use of Cyclic Delay Diversity (CDD). This allows more flexibility than the underlying Alamouti OSTBC allows in the number of participating relays. Several papers have adapted a general class of Threaded Algebraic Space-Time (TAST) codes [64, 65]

for use in asynchronous wireless relay networks. In [66] Distributed Linear Convolutive Space-Time Codes (DLC-STCs) are introduced that are shown to be insensitive to timing errors and achieve full spatial diversity, even with sub-optimal ZF, MMSE and MMSE-Decision Feedback equalizer (DFE) receivers, from the cooperative relay channel under any delay profile. To combat the effects of asynchronism in the network many schemes [67, 68, 55] adopt OFDM transmission as a pre-coding technique to avoid ISI whist accepting a marginal loss in spectral efficiency as a result of the addition of a CP. Later [69, 70] aim to avoid the additional complexity of Inverse Fast Fourier Transform (IFFT) processing at the relay nodes by pre-coding the signal at the source node and adopting an AF protocol at the relays.

In this chapter novel QOSTBCs are introduced that build upon many of the ideas already developed in the literature to develop flexible asynchronous full-rate code designs that are deployable in both DF and AF protocols and offer both multi-carrier and single-carrier transmission. This chapter which is organized as follows: In Section 4.2, the network model is introduced along with system assumptions regarding the channel model and network protocol constraints. Two transmission methodologies are illustrated in the form of multi-carrier and single-carrier systems where the differences in source-Mobile Terminal (s-MT) processing are addressed. A novel distributed space-time network coding scheme derived from Jafarkhani's QOSTBCs [11] and based on AF network coding is presented which is shown to be independent of the transmission scheme implemented at the s-MT. Section 4.3 derives several receiver structures for decoding when multi-carrier transmission is adopted at the s-MT. Issues regarding computational complexity versus decoding performance are addressed in the derivation and verified through Monte-Carlo simulation studies. Later in Section 4.4, receiver structures implemented at the destination-Mobile Terminal (d-MT) when performing single-carrier transmission are investigated. The additional complexity of ISI observed in the time-domain is characterized to aid receiver design. Sub-optimal receivers based on ZF and MMSE techniques are shown to demonstrate comparable complexity and performance results to that of multi-carrier transmission.

4.2 Network Model

To illustrate the network model, a parallel relay channel configuration is adopted as shown in Figure 4.1. Transmission is initiated at the s-MT denoted by S then data are forwarded to a target d-MT denoted by D via a series of participating r-MTs denoted by R_j for $j \in \{1, \ldots, 4\}$. In this configuration it is assumed that there is no direct communication link between the s-MT and d-MT due to possible path-loss and shadowing effects. Instead the protocol is implemented in two stages; firstly the s-MT broadcasts coded symbols to cooperating r-MTs, the s-MT then terminates transmission and the r-MTs re-transmit the processed signals to the d-MT. The half-duplex operation of the r-MTs significantly reduces the design complexity at the cost of halving the maximum achievable data-rate. The complex channel gains between the s-MT and the jth r-MT referred to as R_j are denoted by $h_{s,j}$; subsequently adopting the same semantics the complex channel gains between the jth r-MT and the d-MT are denoted by $h_{d,j}$.

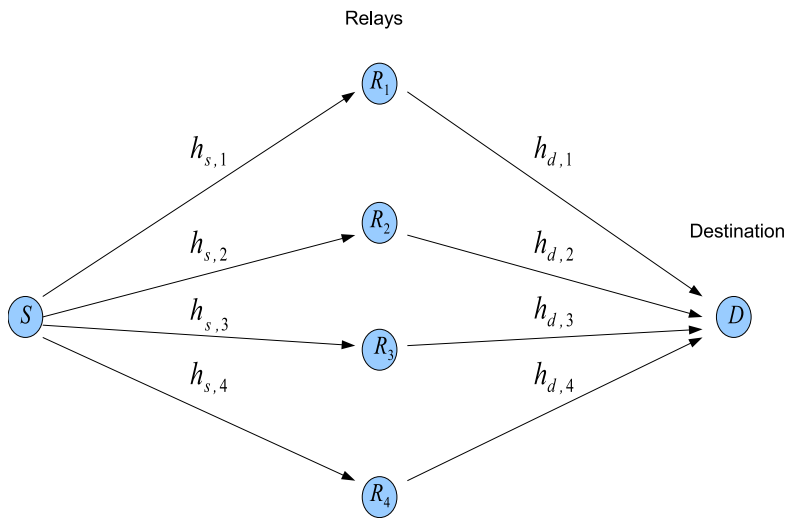

Figure 4.1: Two stage cooperative relay network architecture

Further insight into the network model is gained by formulating the problem using a simple signal flow diagram as illustrated in Figure 4.2. The input signal vector originating from the s-MT is denoted by $\mathbf{x}^{(i)}$ where the superscript indexes the ith frame in the time-domain. The final signal vector observed at the d-MT is denoted by $\mathbf{y}^{(i)}$. For the purpose of understanding the effects of asyn-

chronous re-transmission across the relay network it is assumed that each r-MT simply performs a form of AF relaying which assumes each r-MT transparently forwards the noisy copy of the s-MT signal $\mathbf{x}^{(i)}$ which has been perturbed by a flat-fading channel response. To facilitate the use of space-time coding techniques, all point-to-point channels in the network are assumed to be quasi-static for the length of the codeword. For analysis all complex channel gains are assumed to be independent flat Rayleigh fading and are modelled using ZMCSCG random variables with unity variance. At the first-stage of the relaying protocol a broadcast channel between an s-MT and particular r-MT is assumed thereby enabling the use of a vast array of literature on point-to-point synchronization where significant insight into these techniques can be found in [2]. Subsequently, during the second-stage, the problem of synchronizing the r-MTs with the d-MT so that copies of the source signal arrive synchronously is extremely challenging. Instead additional delay introduced across each relay branch due to varying propagation delays is modeled in the z-domain (or frequency-domain), where τ_j denotes a single *lumped* parameter denoting the fractional delay with respect to the symbol period. This representation overcomes the difficulties of representing a uniformly sampled band-limited (baseband) signal in the discrete time-domain when the delay observed is not an integer multiple of the sampling period and therefore representing a signal between two samples.

4.2.1 Source Node Processing

At the source node, complex modulated symbols are grouped into four blocks of length N, represented by the vector $\mathbf{s}^{(i)}$ where $i \in \{1, \ldots, 4\}$. Symbol mapping is used to later represent the proposed STBC in the original form [11],

$$\tilde{\mathbf{s}} = \begin{bmatrix} \mathbf{s}^{(1)} \\ -\mathbf{s}^{(2)*} \\ -\mathbf{s}^{(3)*} \\ \mathbf{s}^{(4)} \end{bmatrix} \tag{4.1}$$

Each block is assumed to be subject to a uniformly distributed channel delay with range $[0, \tau_{max})$ and upper bounded by τ_{max}. Without any design consideration Inter-Block-Interference (IBI) is possible between adjacent blocks at the

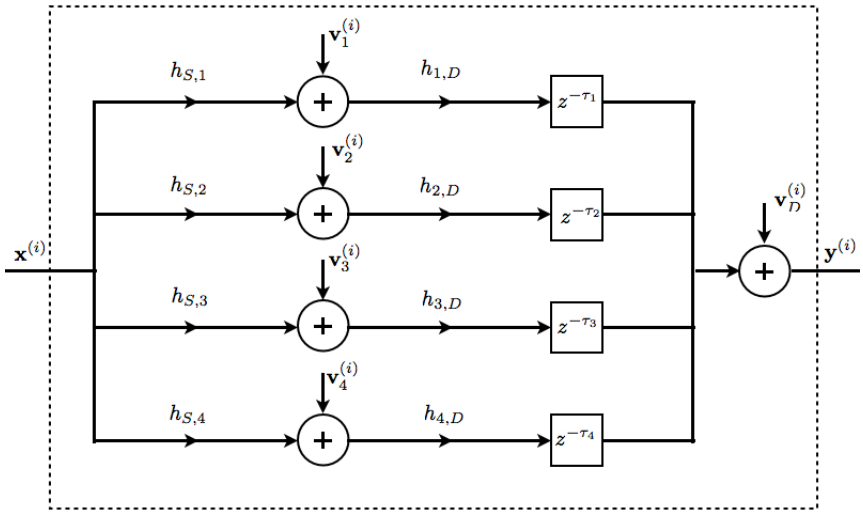

Figure 4.2: Network signal model with simple transparent relaying

destination as a result of individual relay nodes asynchronously re-transmitting according to the propagation delays encountered. To mitigate IBI a CP is inserted which is represented using the matrix operation,

$$\mathbf{T}_{cp} = \begin{bmatrix} \mathbf{0}_{N_p \times (N-N_p)} \mid \mathbf{I}_{N_p} \\ \mathbf{I}_N \end{bmatrix}_{J \times N} \tag{4.2}$$

of length $N_p \geq \tau_{max}$ at the source increasing the block length to $J = N + N_p$.

Adapting space-time coding schemes designed for frequency selective MIMO fading channels for asynchronous relay networks, two methodologies are proposed for processing at the s-MT:

Single-Carrier Source Processing: For single-carrier transmission the information bearing symbols are coded in the time-domain where transmitted blocks are denoted as,

$$\mathbf{x}^{(i)} = \sqrt{P_s}\, \mathbf{T}_{cp}\, \tilde{\mathbf{s}}^{(i)} \tag{4.3}$$

assuming P_s represents the source transmit power. Single-carrier transmission has the desired property that the transmitted signal, using judicious coding, has small fluctuations in the PAPR, which is a useful property for operating in the linear region of a power amplifier.

Multi-Carrier Source Processing: For multi-carrier transmission the information bearing symbols are assumed to be coded in the frequency-domain. Using the IDFT the symbols are then converted into time-domain samples,

$$\mathbf{t}_n^{(i)} := \frac{1}{\sqrt{N}} \sum_{k=0}^{N-1} \tilde{\mathbf{s}}_n^{(i)} e^{j\frac{2\pi}{N}kn}, \qquad 0 \leq n < N \tag{4.4}$$

where $\mathbf{t}_n^{(i)}$ denotes the nth time-domain sample of the ith frame. The s-MT transmitted frames using the multi-carrier methodology can then be neatly expressed in matrix notation as,

$$\mathbf{x}^{(i)} = \sqrt{P_s}\, \mathbf{T}_{cp}\, \mathbf{F}_N^H \tilde{\mathbf{s}}^{(i)} \tag{4.5}$$

where $\mathbf{F}_N$ denotes a unitary DFT matrix of dimension NxN. Without additional processing the signal transmitted by the s-MT can no longer be assumed to have the desired PAPR characteristics and instead the signal level is generally modeled according to a Gaussian distribution when N is large [71].

4.2.2 Relay Node Processing

Independent of the single-carrier or multi-carrier scheme executed at the s-MT the generic processing at the individual participating r-MTs is depicted in Figure 4.3. If the s-MT is transmitting in a particular time-slot then a r-MT assigned to the VAA receives a noisy copy of the broadcast signal from the source node perturbed by the source-relay flat-fading channel response $h_{s,j}$,

$$\mathbf{r}_j^{(i)} = H_{s,j}\, \mathbf{x}^{(i)} + \mathbf{v}_j^{(i)} \tag{4.6}$$

where $H_{s,j} = h_{s,j}\mathbf{I}_N$ is the diagonal channel matrix representing the quasi-static channel between the jth, $j \in \{1, \ldots, 4\}$, r-MT denoted by R_j and the s-MT. This

channel model is justified through the abundance of literature on synchronization of communication systems over a point-to-point wireless channel [2]; therefore ideal timing and carrier synchronization is assumed. For simplicity $\mathbf{v}_j^{(i)}$ denotes AWGN observed at the r-MT with zero mean and variance σ^2.

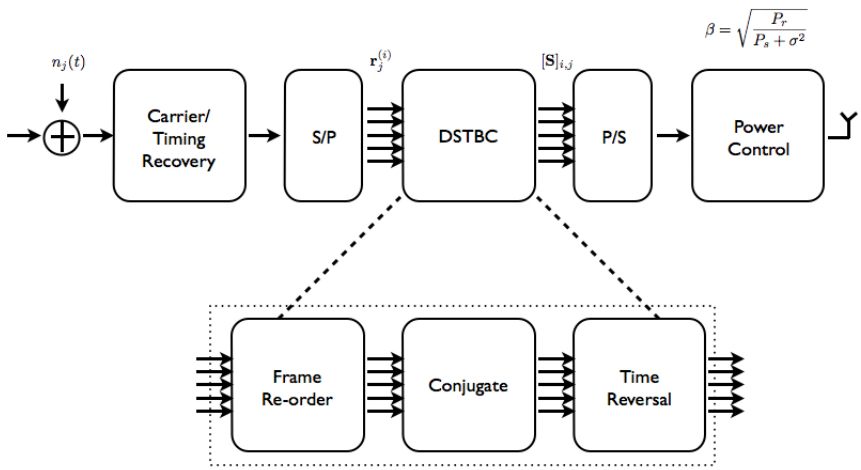

Figure 4.3: Relay Node Functional Blocks

To extract diversity from the relay channel a simple space-time block coding scheme utilizing an AF[1] protocol is deployed based on a novel generalized form of the Jafarkhani [11] QOSTBC,

$$S = \sqrt{\beta} \begin{bmatrix} \mathbf{r}_1^{(1)} & -\mathbf{r}_2^{(2)*} & -\mathbf{r}_3^{(3)*} & \mathbf{r}_4^{(4)} \\ \zeta(\mathbf{r}_1^{(2)}) & \zeta(\mathbf{r}_2^{(1)*}) & -\zeta(\mathbf{r}_3^{(4)*}) & -\zeta(\mathbf{r}_4^{(3)}) \\ \zeta(\mathbf{r}_1^{(3)}) & -\zeta(\mathbf{r}_2^{(4)*}) & \zeta(\mathbf{r}_3^{(1)*}) & -\zeta(\mathbf{r}_4^{(2)}) \\ \mathbf{r}_1^{(4)} & \mathbf{r}_2^{(3)*} & \mathbf{r}_3^{(2)*} & \mathbf{r}_4^{(1)} \end{bmatrix}_{4J \times 4} \tag{4.7}$$

where $\zeta(\cdot)$ performs time-reversal on all vector elements as illustrated with an arbitrary vector $\mathbf{a}$,

[1] A relaying method based on DF principles can be easily envisaged from the AF case.

$$\zeta(\mathbf{a}) = \begin{bmatrix} a(N + N_p - 1) \\ \vdots \\ a(0) \end{bmatrix}_{J \times 1} \tag{4.8}$$

Assuming the absence of CSI transmit power allocation for relaying is equally distributed over the relay nodes based on the expected signal power observed at the r-MT receiver,

$$\beta = \sqrt{\frac{P_r}{P_s + \sigma^2}} \tag{4.9}$$

where P_r is the allocated relay power. In accordance with Telatar's conjecture [15] power is equally distributed across the relaying terminals to minimize outage probability. In addition for the purpose of comparison the transmit power of each relay node is limited to $P_r = P_s/4$ ensuring each node in the network experiences an equivalent SNR, which is standard practice used in the evaluation of similar schemes [69, 72].

4.3 Multi-Carrier Receiver

4.3.1 Pre-processing

4.3.1.1 Delay Correction

As a precursor to linear combining, pre-processing in the form of CP removal and then re-alignment is required. Without loss of generality it shall be assumed that the spatial branch with the shortest propagation delay is observed through the relaying path associated with the r-MT denoted by R_1, as a basis for CP removal. Obtaining coarse synchronization with the relaying branch associated with the shortest propagation delay minimizes the CP length, as the CP length is only proportional to the delay spread, i.e. difference between the minimum and maximum propagation delay observed across the relaying branches as illustrated in Figure 4.4, in this implementation. Assuming the maximum delay spread is smaller than the redundancy in the form of a CP then the orthogonality between the OFDM symbols retransmitted via each r-MT is not violated. Furthermore, it is understood that CP insertion at the transmitter and removal at the receiver

converts a linear convolution into a circular convolution [73, Page 202] enabling channel matrix to be described using a circulant matrix which has the useful property of being reduced to a diagonal matrices through a DFT.

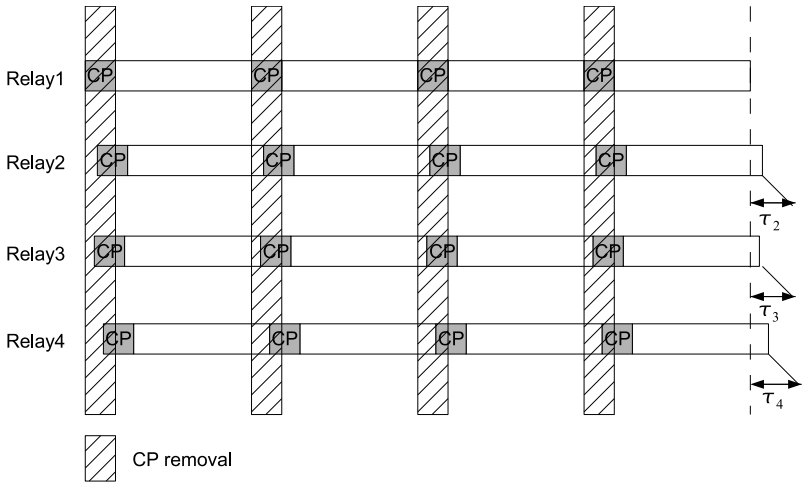

Figure 4.4: Representation of CP removal assuming synchronization with R_1

Recalling that a time-reversal operation (4.8) was implemented by all participating r-MTs on the 2nd and 3rd re-transmitted frames, a simple correction performed only on the 2nd and 3rd OFDM symbols at the d-MT is required to re-align the information symbols which is implemented in the form of a circular shift,

$$\zeta'(\mathbf{a}[n]) = \mathbf{a}[\langle n - (N_p + 1)\rangle_N] \tag{4.10}$$

where $\langle\cdot\rangle_N$ denotes a modulo-N operation. Overall processing at the r-MTs (4.8) and d-MT (4.10) is equivalent to an N-point DFT or IDFT transform applied twice, i.e. $\mathbf{P} = \mathbf{F}_N\ \mathbf{F}_N$, on the unordered OFDM symbols transmitted from the s-MT,

$$\mathbf{Pa} = [a[0], a[N-1], \ldots, a[1]]^T \tag{4.11}$$

The effective channel response via the r-MT denoted by R_j in the frequency-domain is encapsulated in the channel matrix H_j. The assumed flat-fading channel response over all the communication links in the channel introduces no variation in the absolute channel gains. Asynchronous delay in the time-domain does

however introduce a phase change in the frequency-domain as a function of the sub-carrier index k,

$$[H_j]_{k,k} := \begin{cases} h_{d,j} h_{s,j} e^{-j2\pi k \tau_j / N} & j \in \{1,4\} \\ h_{d,j} h_{s,j}^* e^{-j2\pi k \tau_j / N} & j \in \{2,3\} \end{cases} \tag{4.12}$$

This channel model approximates the linear phase rotations at discretely sampled frequency intervals arising due to the re-transmission delay τ_j associated with signals received via R_j. An equivalent input-output relationship, derived in Appendix 4.7 (Derivation I), for the collaborative network in the frequency-domain can now be represented in matrix notation which collaborates the processing described above,

$$\begin{bmatrix} \mathbf{y}^{(1)} \\ \mathbf{y}^{(2)*} \\ \mathbf{y}^{(3)*} \\ \mathbf{y}^{(4)} \end{bmatrix} = \sqrt{\beta} \begin{bmatrix} H_1 & H_2\mathbf{P} & H_3\mathbf{P} & H_4 \\ H_2^* & -H_1^*\mathbf{P} & H_4^*\mathbf{P} & -H_3^* \\ H_3^* & H_4^*\mathbf{P} & -H_1^*\mathbf{P} & -H_2^* \\ H_4 & -H_3\mathbf{P} & -H_2\mathbf{P} & H_1 \end{bmatrix} \begin{bmatrix} \mathbf{s}^{(1)} \\ \mathbf{s}^{(2)} \\ \mathbf{s}^{(3)} \\ \mathbf{s}^{(4)} \end{bmatrix} + \begin{bmatrix} \mathbf{w}^{(1)} \\ \mathbf{w}^{(2)*} \\ \mathbf{w}^{(3)*} \\ \mathbf{w}^{(4)} \end{bmatrix} \tag{4.13}$$

$$\mathbf{y} = \mathbf{H}\mathbf{s} + \mathbf{w} \tag{4.14}$$

where $\mathbf{y}^{(i)}$ and $\mathbf{w}^{(i)}$ denote the ith OFDM symbol received at the d-MT with the associated noise component respectively. The noise incident at the d-MT is composed of the forwarded noise observed at the r-MTs and is therefore conditioned on the MISO channel response between r-MTs and the d-MT as shown,

$$\mathbf{w}^{(i)} = \sum_{j=1}^{4} h_{d,j} \tilde{\mathbf{v}}_j^{(i)} + \mathbf{v}_d^{(i)} \tag{4.15}$$

which demonstrates the decomposition of the observed noise in the frequency-domain forwarded from the relays and denoted by $\tilde{\mathbf{v}}_j^{(i)}$ in addition to incident noise at the d-MT receiver alone denoted by $\mathbf{v}_d^{(i)}$. The new noise vector $\mathbf{w}$ in (4.15) remains uncorrelated with the statistics $N(\mathbf{0}, \mathbf{\Sigma_w})$ assuming,

$$\mathbf{\Sigma_w} := N_0 \mathbf{I}_{4N} \left(\beta^2 \sum_{j=1}^{4} |h_{d,j}|^2 + 1 \right) \tag{4.16}$$

which shows that the noise incident at the d-MT is conditioned on the individual channel gains between the r-MTs and the d-MT.

4.3.1.2 Linear Combining

Efficient linear combining in the frequency-domain is proved possible via exploiting the diagonal structure of H_j (4.12) using frequency-domain processing via the efficient FFT algorithm,

$$\begin{bmatrix} \mathbf{z}^{(1)} \\ \mathbf{z}^{(2)} \\ \mathbf{z}^{(3)} \\ \mathbf{z}^{(4)} \end{bmatrix} = \sqrt{\beta} \begin{bmatrix} H_1^H & H_2^T & H_3^T & H_4^H \\ \mathbf{P}H_2^H & -\mathbf{P}H_1^T & \mathbf{P}H_4^T & -\mathbf{P}H_3^H \\ \mathbf{P}H_3^H & \mathbf{P}H_4^T & -\mathbf{P}H_1^T & -\mathbf{P}H_2^H \\ H_4^H & -H_3^T & -H_2^T & H_1^H \end{bmatrix} \begin{bmatrix} \mathbf{y}^{(1)} \\ \mathbf{y}^{(2)*} \\ \mathbf{y}^{(3)*} \\ \mathbf{y}^{(4)} \end{bmatrix} \tag{4.17}$$

$$\mathbf{z} = \mathbf{H}^H \mathbf{y} \tag{4.18}$$

Relay reordering (4.8) and re-alignment at the destination (4.10) now enable the exploitation of the following properties for any arbitrary circulant matrix $\mathbf{X}$,

$$\mathbf{PXP} = \mathbf{X}^{\,T} \text{ and } \mathbf{PX}^*\mathbf{P} = \mathbf{X}^{\,H} \tag{4.19}$$

Adopting an overall input-output relationship it is relatively straightforward to incorporate the intermediate expressions (4.13)-(4.18) into a simple system model,

$$\mathbf{z} = \mathbf{As} + \mathbf{v} \tag{4.20}$$

where $\mathbf{v} = \mathbf{H}^H \mathbf{w}$ and,

$$\mathbf{A} = \beta \begin{bmatrix} \mathbf{\Gamma}_z & \mathbf{0} & \mathbf{0} & \mathbf{\Lambda}_z \\ \mathbf{0} & \mathbf{\Gamma}_z & -\mathbf{P}\mathbf{\Lambda}_z\mathbf{P} & \mathbf{0} \\ \mathbf{0} & -\mathbf{P}\mathbf{\Lambda}_z\mathbf{P} & \mathbf{\Gamma}_z & \mathbf{0} \\ \mathbf{\Lambda}_z & \mathbf{0} & \mathbf{0} & \mathbf{\Gamma}_z \end{bmatrix} \tag{4.21}$$

with diagonal sub-matrices composed as follows,

$$\mathbf{\Gamma}_z = \sum_{j=1}^{4} H_j^H H_j \tag{4.22}$$

$$\mathbf{\Lambda}_z = 2\Re\{H_1^H H_4 - H_2^T H_3^*\} \tag{4.23}$$

After matched filtering at the d-MT the new noise vector $\mathbf{v}$ becomes correlated with the statistics $N(0, \mathbf{\Sigma}_v)$, where

$$\mathbf{\Sigma}_v := \mathbf{\Sigma}_w^{\frac{1}{2}} \mathbf{A} \mathbf{\Sigma}_w^{\frac{1}{2}}. \tag{4.24}$$

However, the sparsity of the system matrix $\mathbf{A}$ decouples the information blocks $\{\mathbf{s}^{(1)}, \mathbf{s}^{(4)}\}$ and $\{\mathbf{s}^{(2)}, \mathbf{s}^{(3)}\}$,

$$\begin{bmatrix} \mathbf{z}^{(1)} \\ \mathbf{z}^{(4)} \end{bmatrix} = \beta \begin{bmatrix} \mathbf{\Gamma}_z & \mathbf{\Lambda}_z \\ \mathbf{\Lambda}_z & \mathbf{\Gamma}_z \end{bmatrix} \begin{bmatrix} \mathbf{s}^{(1)} \\ \mathbf{s}^{(4)} \end{bmatrix} + \begin{bmatrix} \mathbf{v}^{(1)} \\ \mathbf{v}^{(4)} \end{bmatrix} \tag{4.25}$$

$$\mathbf{z}_{14} = \mathbf{A}_{14} \mathbf{s}_{14} + \mathbf{v}_{14} \tag{4.26}$$

$$\begin{bmatrix} \mathbf{z}^{(2)} \\ \mathbf{z}^{(3)} \end{bmatrix} = \beta \begin{bmatrix} \mathbf{\Gamma}_z & -\mathbf{P}\mathbf{\Lambda}_z\mathbf{P} \\ -\mathbf{P}\mathbf{\Lambda}_z\mathbf{P} & \mathbf{\Gamma}_z \end{bmatrix} \begin{bmatrix} \mathbf{s}^{(2)} \\ \mathbf{s}^{(3)} \end{bmatrix} + \begin{bmatrix} \mathbf{v}^{(2)} \\ \mathbf{v}^{(3)} \end{bmatrix} \tag{4.27}$$

$$\mathbf{z}_{23} = \mathbf{A}_{23} \mathbf{s}_{23} + \mathbf{v}_{23} \tag{4.28}$$

simplifying the computational complexity of decoding the transmitted symbols at the d-MT. In the next section the decoupled structure of $\mathbf{A}$ is leveraged to propose low-complexity linear and non-linear decoders.

4.3.2 Multi-Carrier Decoding Strategies

4.3.2.1 Maximum-Likelihood Decoder

An ML decoder aims at solving an optimization problem by minimizing the metric M over all feasible transmitted symbol vectors $\mathbf{s}$ from a given symbol alphabet Ω,

$$\hat{\mathbf{s}} = \arg \min_{\hat{\mathbf{s}} \in \Omega^{4N}} \|\mathbf{y} - \mathbf{H}\hat{\mathbf{s}}\|_2^2 \tag{4.29}$$

where $\|\cdot\|_2$ denotes the Euclidean norm operator. The ZMCSCG characteristics of the noise component (4.16) negate the requirement for a pre-whitening transform to evaluate the decision metric. Leveraging the decoupling observed after matched filtering at the receiver yields an equivalent optimization problem under a pre-whitening transform (4.24) to (4.29) as shown in Appendix 4.7 (Derivation II),

$$\hat{\mathbf{s}} = \arg\min_{\hat{\mathbf{s}}\in\Omega^{4N}} \|\Sigma_v^{-1/2}(\mathbf{z}-\mathbf{A}\hat{\mathbf{s}})\|_2^2 \tag{4.30}$$

$$\equiv \arg\min_{\hat{\mathbf{s}}\in\Omega^{4N}} \frac{1}{a}\|\mathbf{y}-\mathbf{H}\hat{\mathbf{s}}\|_2^2. \tag{4.31}$$

where $a = N_0\left(\beta^2\sum_{j=1}^{4}|h_{d,j}|^2+1\right)$. To exploit the sparsity structure of $\mathbf{A}$ to reduce the ML computational complexity the objective function in (4.30) is expanded yielding,

$$\|\Sigma_v^{-1/2}(\mathbf{z}-\mathbf{A}\hat{\mathbf{s}})\|_2^2 = \mathbf{z}^H\Sigma_v^{-1}\mathbf{z} - \mathbf{z}^H\Sigma_v^{-1}\mathbf{A}\hat{\mathbf{s}} - \hat{\mathbf{s}}^H\mathbf{A}^H\Sigma_v^{-1}\mathbf{z} \tag{4.32}$$

$$+\hat{\mathbf{s}}^H\mathbf{A}^H\Sigma_v^{-1}\mathbf{A}\hat{\mathbf{s}} \tag{4.33}$$

$$= \mathbf{z}^H\Sigma_v^{-1}\mathbf{z} - \frac{1}{a}\mathbf{z}^H\hat{\mathbf{s}} - \frac{1}{a}\hat{\mathbf{s}}^H\mathbf{z} + \frac{1}{a}\hat{\mathbf{s}}^H\mathbf{A}\hat{\mathbf{s}} \tag{4.34}$$

using the substitution $\mathbf{\Sigma}_v = a\mathbf{A}$ and elementary manipulations. Clearly, the first term in (4.34) is independent of the decision vector $\hat{\mathbf{s}}$ and therefore doesn't affect the value of the objective function when evaluating prospective symbol estimates, reducing (4.30) to,

$$\hat{\mathbf{s}} = \arg\min_{\hat{\mathbf{s}}\in\Omega^{4N}} \hat{\mathbf{s}}^H\mathbf{A}\hat{\mathbf{s}} - \mathbf{z}^H\hat{\mathbf{s}} - \hat{\mathbf{s}}^H\mathbf{z} \tag{4.35}$$

assuming the objective function is scalar invariant. Further decomposition is possible when applying system decoupling similarly demonstrated in (4.25) and (4.27) to yield two reduced order optimization problems equivalent to (4.35),

$$\hat{\mathbf{s}}_{14} = \arg\min_{\hat{\mathbf{s}}_{14}\in\Omega^{2N}} \hat{\mathbf{s}}_{14}^H\mathbf{A}_{14}\hat{\mathbf{s}}_{14} - \mathbf{z}_{14}^H\hat{\mathbf{s}}_{14} - \hat{\mathbf{s}}_{14}^H\mathbf{z}_{14} \tag{4.36}$$

$$\hat{\mathbf{s}}_{23} = \arg\min_{\hat{\mathbf{s}}_{23}\in\Omega^{2N}} \hat{\mathbf{s}}_{23}^H\mathbf{A}_{23}\hat{\mathbf{s}}_{23} - \mathbf{z}_{23}^H\hat{\mathbf{s}}_{23} - \hat{\mathbf{s}}_{23}^H\mathbf{z}_{23} \tag{4.37}$$

Further decoupling of the optimization problem is possible by observing the structure of $\mathbf{A}$ to determine two optimization metrics that enable pairwise symbol estimation for each sub-carrier indexed by the variable k,

$$M_{14,k}\left(\hat{\mathbf{s}}_k^{(1)},\hat{\mathbf{s}}_k^{(4)}\right) = \left(\beta\sum_{j=1}^{4}|h_k^{(j)}|^2\right)\left(|\hat{\mathbf{s}}_k^{(1)}|^2+|\hat{\mathbf{s}}_k^{(4)}|^2\right)$$

$$+2Re\{\alpha_k\beta\hat{\mathbf{s}}_k^{(1)}\hat{\mathbf{s}}_k^{(4)*} - \mathbf{z}_k^{(1)*}\hat{\mathbf{s}}_k^{(1)} - \mathbf{z}_k^{(4)*}\hat{\mathbf{s}}_k^{(4)}\} \tag{4.38}$$

$$M_{23,k}\left(\hat{\mathbf{s}}_k^{(2)}, \hat{\mathbf{s}}_k^{(3)}\right) = \left(\beta \sum_{j=1}^{4} |h_k^{(j)}|^2\right)\left(|\hat{\mathbf{s}}_k^{(2)}|^2 + |\hat{\mathbf{s}}_k^{(3)}|^2\right)$$
$$+2Re\{-\tilde{\alpha}_k \beta \hat{\mathbf{s}}_k^{(2)} \hat{\mathbf{s}}_k^{(3)*} - \mathbf{z}_k^{(2)*} \hat{\mathbf{s}}_k^{(2)} - \mathbf{z}_k^{(3)*} \hat{\mathbf{s}}_k^{(3)}\} \quad (4.39)$$

where for simplicity $h_k^{(j)} := [H_j]_{k,k}$ according to (4.12), $\alpha = diag(\Lambda)$ and $\tilde{\alpha} = \mathbf{P}\alpha$.

Optimizing the ML estimator based on the structure of the coupling matrix $\mathbf{A}$ after matched filtering reduces the computational complexity to order $O(2N|\Omega|^2)$ through pairwise decoding, using $|\cdot|$ in this instance to define the cardinality of the symbol alphabet.

4.3.2.2 Zero-Forcing Decoder

ML decoders offer the best estimator at the expense of additional computation complexity. A simpler and more straightforward method for estimation is one that simply inverts the process that generates interference between the symbols to be estimated, this type of receiver technique is referred as *ZF*. Assuming matched filtering is performed then the output of the ZF operation can be expressed as,

$$\mathbf{z}_{zf} = \mathbf{A}^{\dagger}\mathbf{z} \quad (4.40)$$
$$= \mathbf{s} + \mathbf{A}^{\dagger}\mathbf{v} \quad (4.41)$$

where † denotes the pseudo-inverse operator. Clearly, (4.41) eliminates ISI at the cost of possible noise enhancement. The decoupling arising from matched filter allows for separate ZF-operations to be performed on (4.26) and (4.28) respectively,

$$\mathbf{z}_{14,zf} = \mathbf{A}_{14}^{\dagger}\mathbf{z}_{14} \quad (4.42)$$
$$\mathbf{z}_{23,zf} = \mathbf{A}_{23}^{\dagger}\mathbf{z}_{23} \quad (4.43)$$

In the case of non-singular $\mathbf{A}_{14}$ (4.25) and $\mathbf{A}_{23}$ (4.27), which occurs with a high degree of probability, the sparsity patterns of the matrices represented in the frequency-domain can be solved efficiently utilizing the factorization,

$$\mathbf{A}_{14} = \Pi \mathbf{D}_{14} \Pi^T \tag{4.44}$$

$$\mathbf{A}_{23} = \Pi \mathbf{D}_{23} \Pi^T \tag{4.45}$$

assuming Π is a $2N \times 2N$ permutation matrix with the associated block diagonal matrices $\mathbf{D}_{14} := blkdiag(\mathbf{A}_{14}^{(1)}, \mathbf{A}_{14}^{(2)}, \ldots, \mathbf{A}_{14}^{(N)})$ and $\mathbf{D}_{14} := blkdiag(\mathbf{A}_{23}^{(1)}, \mathbf{A}_{23}^{(2)}, \ldots, \mathbf{A}_{23}^{(N)})$ where,

$$\mathbf{A}_{14}^{(k)} = \begin{bmatrix} \gamma & \alpha_k \\ \alpha_k & \gamma \end{bmatrix} \tag{4.46}$$

$$\mathbf{A}_{23}^{(k)} = \begin{bmatrix} \gamma & -\tilde{\alpha}_k \\ -\tilde{\alpha}_k & \gamma \end{bmatrix} \tag{4.47}$$

using the notation $\gamma := \sum_{j=1}^{4} |\mathbf{h}_k^{(j)}|^2$. Leveraging the block diagonal structure enables the ZF filters for each sub-carrier k to be determined as the simple inversion of a 2×2 matrix yielding,

$$\begin{bmatrix} \hat{\mathbf{s}}_k^{(1)} \\ \hat{\mathbf{s}}_k^{(4)} \end{bmatrix} = \frac{1}{\beta\left(\gamma^2 - \alpha_k^2\right)} \begin{bmatrix} \gamma & -\alpha_k \\ -\alpha_k & \gamma \end{bmatrix} \begin{bmatrix} \mathbf{z}_k^{(1)} \\ \mathbf{z}_k^{(4)} \end{bmatrix} \tag{4.48}$$

$$\hat{\mathbf{s}}_{14}^k = \mathbf{A}_{14}^{(k)-1} \mathbf{z}_{14}^k \tag{4.49}$$

$$\begin{bmatrix} \hat{\mathbf{s}}_k^{(2)} \\ \hat{\mathbf{s}}_k^{(3)} \end{bmatrix} = \frac{1}{\beta\left(\gamma^2 - \tilde{\alpha}_k^2\right)} \begin{bmatrix} \gamma & \tilde{\alpha}_k \\ \tilde{\alpha}_k & \gamma \end{bmatrix} \begin{bmatrix} \mathbf{z}_k^{(2)} \\ \mathbf{z}_k^{(3)} \end{bmatrix} \tag{4.50}$$

$$\hat{\mathbf{s}}_{23}^k = \mathbf{A}_{23}^{(k)-1} \mathbf{z}_{23}^k \tag{4.51}$$

The resulting decoding complexity is therefore linear in frame length O(N) and the introduction of asynchronicity causes no additional computational complexity over a ZF decoder operating on a symbol-by-symbol implementation in the asynchronous case [48, Eq.3.45-3.46].

4.3.2.3 Minimum Mean Square Error Decoder

It is possible to derive an estimator that aims to minimize the MSE when incorporating the affects of the noise into the estimation process; this category of estimator is referred to as a MMSE estimator. Using the signal model described previously (4.19) it is possible to express the residual MSE after filtering the observation with a linear-MMSE filter $\mathbf{Q}$ as,

$$\begin{aligned} J &= E\left\{\|\mathbf{Qz}-\mathbf{s}\|_F^2\right\} && (4.52)\\ &= E\left\{\|\left(\mathbf{QA}-\mathbf{I}\right)\mathbf{s}-\mathbf{Qv}\|_F^2\right\} && (4.53)\\ &= E\left\{tr\left\{\left(\left(\mathbf{QA}-\mathbf{I}\right)\mathbf{s}-\mathbf{Qv}\right)\left(\left(\mathbf{QA}-\mathbf{I}\right)\mathbf{s}-\mathbf{Qv}\right)^H\right\}\right\} && (4.54)\\ &= tr\left\{\left(\mathbf{QA}-\mathbf{I}\right)\left(\mathbf{A}^H\mathbf{Q}^H-\mathbf{I}\right)\right\}+tr\left\{\mathbf{Q}\boldsymbol{\Sigma}_w\mathbf{A}\mathbf{Q}^H\right\} && (4.55)\end{aligned}$$

where $\|\cdot\|_F$ and $tr\{\cdot\}$ denote the Frobenius norm and trace operators respectively. The following a-priori statistical expectations,

$$\begin{aligned} E\{\mathbf{ss}^H\} &= \sigma_s^2\mathbf{I}_{4N} && (4.56)\\ E\{\mathbf{vv}^H\} &= \boldsymbol{\Sigma}_v=\boldsymbol{\Sigma}_w\mathbf{A} && (4.57)\\ E\{\mathbf{sv}^H\} &= \mathbf{0}_{4N} && (4.58)\end{aligned}$$

are used to determine the expression (4.55) from (4.54). Differentiating (4.55) with respect to the linear filter $\mathbf{Q}^H$ results in,

$$\frac{\partial J}{\partial \mathbf{Q}^H}=\sigma_s^2\ \left(\mathbf{QA}-\mathbf{I}\right)\mathbf{A}^H+\mathbf{Q}\boldsymbol{\Sigma}_w\mathbf{A} \qquad (4.59)$$

The filter resulting in the minimum MSE is then determined as,

$$\begin{aligned} \hat{\mathbf{Q}} &= \mathbf{A}^H\left(\mathbf{AA}^H+\frac{1}{\sigma_s^2}\Sigma_w\mathbf{A}\right)^{-1} && (4.60)\\ &= \left(\mathbf{A}+\frac{1}{\sigma_s^2}\Sigma_w\right)^{-1} && (4.61)\end{aligned}$$

Observing that (4.61) has the same structure as $\mathbf{A}$, equivalent factorization operations using permutation matrices can be repeated (but not shown here for

brevity) from the analysis in the ZF decoder to yield pairwise decoupled MMSE decoders as shown,

$$\begin{bmatrix} \hat{\mathbf{s}}_k^{(1)} \\ \hat{\mathbf{s}}_k^{(4)} \end{bmatrix} = \frac{1}{\beta\left(\left(\gamma + \frac{\sigma_w^2}{\beta\sigma_s^2}\right)^2 - \alpha_k^2\right)} \begin{bmatrix} \gamma + \frac{\sigma_w^2}{\beta\sigma_s^2} & -\alpha_k \\ -\alpha_k & \gamma + \frac{\sigma_w^2}{\beta\sigma_s^2} \end{bmatrix} \begin{bmatrix} \mathbf{z}_k^{(1)} \\ \mathbf{z}_k^{(4)} \end{bmatrix} \tag{4.62}$$

$$\hat{\mathbf{s}}_{14}^k = \mathbf{Q}_{14}^k \mathbf{z}_{14}^k \tag{4.63}$$

$$\begin{bmatrix} \hat{\mathbf{s}}_k^{(2)} \\ \hat{\mathbf{s}}_k^{(3)} \end{bmatrix} = \frac{1}{\beta\left(\left(\gamma + \frac{\sigma_w^2}{\beta\sigma_s^2}\right)^2 - \alpha_k^2\right)} \begin{bmatrix} \gamma + \frac{\sigma_w^2}{\beta\sigma_s^2} & \tilde{\alpha}_k \\ \tilde{\alpha}_k & \gamma + \frac{\sigma_w^2}{\beta\sigma_s^2} \end{bmatrix} \begin{bmatrix} \mathbf{z}_k^{(2)} \\ \mathbf{z}_k^{(3)} \end{bmatrix} \tag{4.64}$$

$$\hat{\mathbf{s}}_{23}^k = \mathbf{Q}_{23}^k \mathbf{z}_{23}^k \tag{4.65}$$

4.3.3 Simulation Results

For multi-carrirer QOSTBC enabled asynchronous designs various decoding strategies at the d-MT are examined to compare decoding performance against complexity. The simulation environment assumes the parameters; $N = 64$, $N_p = 15$, $\tau_{max} = 15$ and $\tau_i \sim U(0, \tau_{max}]$. The symbols are assumed to be QPSK. Decoding performance is evaluated against the normalized SNR, energy per bit to noise power spectral density ratio E_b/N_0, observed at the r-MTs. The channel observed in the second phase of transmission is assumed to be MISO.

Case Study 15: Figure 4.5 depicts BER versus E_b/N_0 [dB] for DF relaying using multi-carrier asynchronous Alamouti [69] and QOSTBC processing at the r-MTs. The DF protocol for Alamouti coded OFDM proposed in [67] assumes perfect decoding in the first-phase at all the r-MTs. To allow a comparison against proposed AF schemes which will be later presented; perfect decoding is not assumed. Instead a transport block (4.1) is defined as the number of information symbols broadcast from the s-MT to the participating r-MTs. If a single r-MT decodes the transport block without error[1] then it retransmits

[1]The r-MT may perform a simple Cyclic Redundancy Check (CRC) to determine decoding errors.

the ST-encoded data to the d-MT. In the event that errors are detected in the decoded transport block then it is discarded and the r-MT does not re-transmit any data in the second phase of the protocol [69]. The DF variant performs the same ST-processing as the AF with the exception that noise incident at the r-MT is not forwarded to the d-MT. It is worth noting the BER results are now a function of the transport block size and the probability of a transport block being discarded by a r-MT is proportional to N,

$$Pr_{tb}(R_i) = 1 - (1 - Pr_{bit}(R_i))^N \tag{4.66}$$

where $Pr_{tb}(R_i)$ and $Pr_{bit}(R_i)$ are the probabilities that a transport block and bit errors are observed at r-MT R_i.

In the very low-SNR range there is a high probability that the r-MTs will not decode a transport block without errors; therefore resulting in a high-probability of a transport block being discarded. To simplify the protocol in the simulation study it is assumed that d-MT decodes without knowledge of this event and therefore a near 50% BER is observed for all schemes. For a mid-to-high SNR range ($E_b/N_0 > 5$ dB) it is clearly demonstrated in Figure 4.5 that the QOSTBC more than compensates over the Alamouti scheme for the increased likelihood of transport block errors and resulting discards at the r-MT through diversity gain.

Focusing on the QOSTBC results, it is observed that at a low SNR little decoding advantage is achieved between the ZF and ML decoders. Without knowledge at the d-MT of decoding error state at individual r-MT then adopting an assumption that all mobiles retransmit clearly results in sub-optimal decoding at the d-MT. Under the DF protocol used here the marginal benefit of decoding complexity against BER performance is illustrated in the results.

Case Study 16: Depicted in Figure 4.6 are BER versus E_b/N_0 [dB] for AF relaying protocol using multi-carrier asynchronous Alamouti [69] and QOSTBC processing at the r-MTs. Again the results are generated with the same parameters adopted in the previous simulation study to enable direct comparison. In this case study an r-MT retransmits transparently and independently of the observed symbols therefore simplifying the processing at the r-MT since no additional decoding is required.

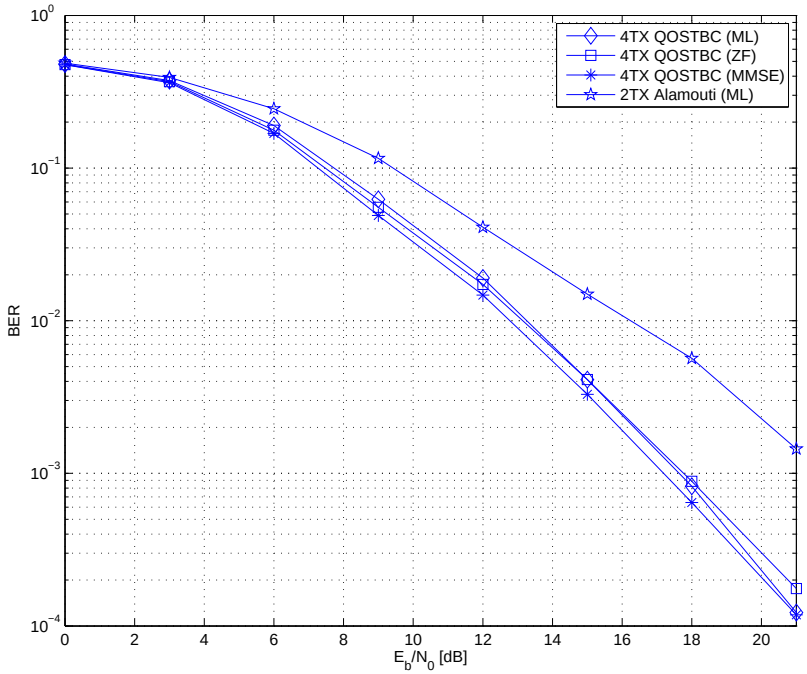

Figure 4.5: Evaluation of Robust DF Multi-Carrier Asynchronous Relay Schemes; BER versus E_b/N_0 [dB].

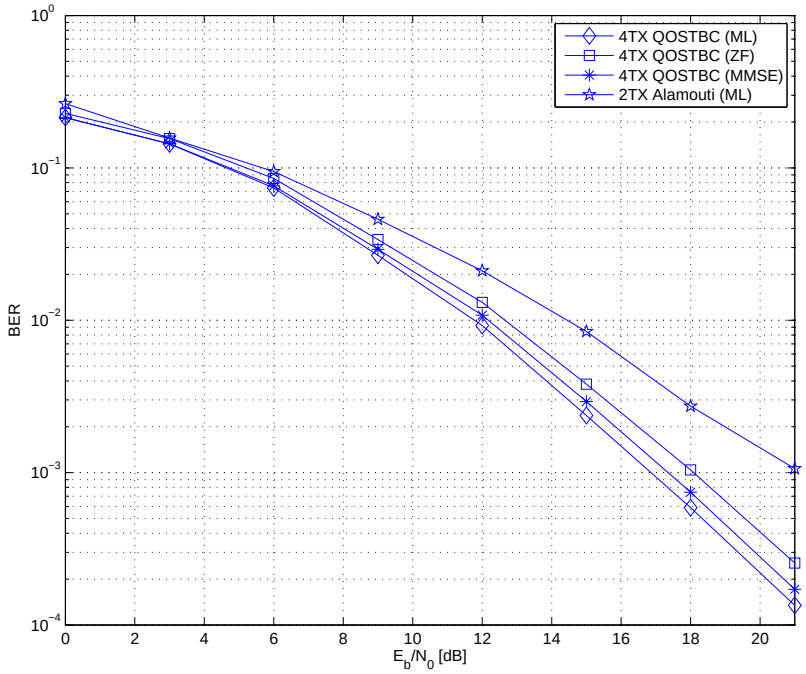

Figure 4.6: Evaluation of Robust AF Multi-Carrier Asynchronous Relay Schemes; BER versus E_b/N_0 [dB].

In Figure 4.6 it is observed that there is marginal gain in deploying the additional r-MTs in the low-SNR region ($E_b/N_0 < 5$ dB). In the higher-SNR region ($E_b/N_0 \geq 5$ dB), there is a distinct diversity gain in exploiting a higher-order VAA independent of the decoding technique used at the d-MT. Improved decoder performance in BER is possible at a higher SNR ($E_b/N_0 > 10$ dB) when performing the more computationally complex ML decoding. Interestingly, the MMSE decoder shadows the performance of the ML decoder whilst offering little additional complexity over the ZF decoder which discards noise statistics in deriving an estimate of the transmitted symbols. Interestingly, although when operating using an AF protocol additional noise is observed at the d-MT the decoding performance of the AF schemes compares favorably to the DF counterpart depicted in Figure 4.5 and only starts to introduce a higher BER at the end of the SNR range evaluated in the simulations.

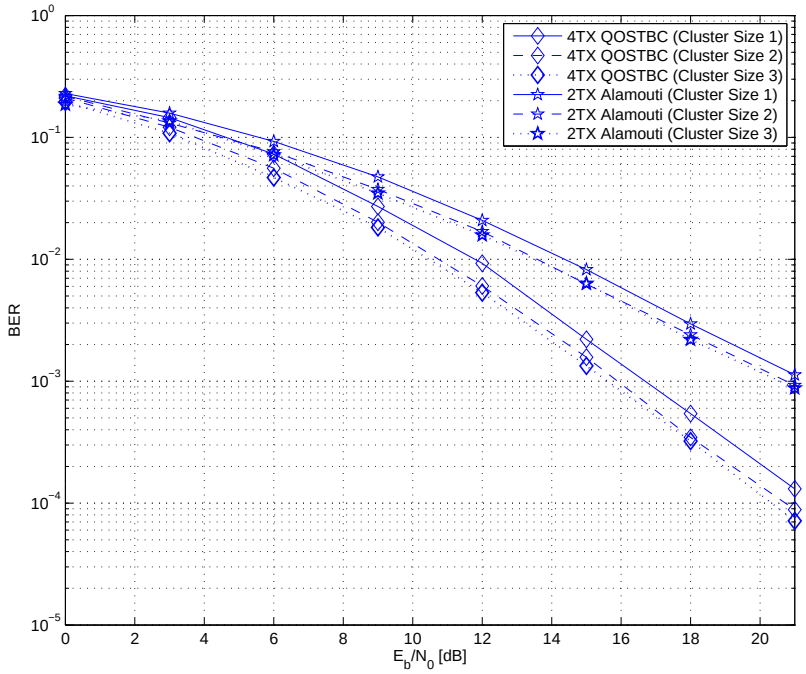

Figure 4.7: Evaluation of Robust AF Multi-Carrier Asynchronous Relay Schemes with Clustering; BER versus E_b/N_0

Case Study 17: Depicted in Figure 4.7 is the network performance evaluated using the BER metric versus E_b/N_0 [dB] for various cluster sizes assuming optimal-ML decoding at the d-MT. When implementing clustering it is assumed that several r-MTs spaced geographically close together form a cluster and execute the same spatial branch of the space-time code-book. Clearly, Figure 4.7 illustrates that increasing the cluster size improves BER performance for any given SNR. The available transmit power at the r-MTs is inversely proportional to the cluster size so that the total relaying power constraint P_s is still satisfied. One distinct advantage of adopting clustering is the reduction in the required transmit power for an individual r-MT, which is inversely proportional to the cluster size when compared with a scheme not adopting clustering.

4.3.4 Summary

When the condition $\tau_{max} \leq N_p$ and the CP is not violated the proposed asynchronous scheme achieves exactly the same decoding performance as the synchronous case. As demonstrated previously the computational complexity of the proposed ZF, MMSE and ML decoders is equivalent to a synchronous scheme where transmitter encoding is performed on a symbol-by-symbol basis instead of block-encoding advocated for asynchronous transmission. The disadvantage of the asynchronous schemes as compared to equivalent synchronous schemes is a degradation in bandwidth efficiency due to the additional redundancy of the CP.

4.4 Single-Carrier Receiver

4.4.1 Pre-processing and Interference Issues

Many of the initial pre-processing stages adopted for multi-carrier transmission are replicated at the receiver side in the single-carrier scheme to simplify equalization. These include CP removal in order to remove IBI and timing correction applied to the 2nd and 3rd received frames; these operations are documented in Section 4.3.1 and therefore will not be discussed in detail when reviewing the operations of the single-carrier receiver.

The proposed single-carrier receiver again leverages the DFT to express the input-output system using diagonal frequency-domain channel matrices defined in (4.12),

$$\begin{bmatrix} \mathbf{y}^{(1)} \\ \mathbf{y}^{(2)*} \\ \mathbf{y}^{(3)*} \\ \mathbf{y}^{(4)} \end{bmatrix} = \begin{bmatrix} \mathbf{F}_N^H H_1 \mathbf{F}_N & \mathbf{F}_N^H H_2 \mathbf{F}_N & \mathbf{F}_N^H H_3 \mathbf{F}_N & \mathbf{F}_N^H H_4 \mathbf{F}_N \\ \mathbf{F}_N H_2^* \mathbf{F}_N^H \mathbf{P} & -\mathbf{F}_N H_1^* \mathbf{F}_N^H \mathbf{P} & \mathbf{F}_N H_4^* \mathbf{F}_N^H \mathbf{P} & -\mathbf{F}_N H_3^* \mathbf{F}_N^H \mathbf{P} \\ \mathbf{F}_N H_3^* \mathbf{F}_N^H \mathbf{P} & \mathbf{F}_N H_4^* \mathbf{F}_N^H \mathbf{P} & -\mathbf{F}_N H_1^* \mathbf{F}_N^H \mathbf{P} & -\mathbf{F}_N H_2^* \mathbf{F}_N^H \mathbf{P} \\ \mathbf{F}_N^H H_4 \mathbf{F}_N & -\mathbf{F}_N^H H_3 \mathbf{F}_N & -\mathbf{F}_N^H H_2 \mathbf{F}_N & \mathbf{F}_N^H H_1 \mathbf{F}_N \end{bmatrix} \begin{bmatrix} \mathbf{s}^{(1)} \\ \mathbf{s}^{(2)} \\ \mathbf{s}^{(3)} \\ \mathbf{s}^{(4)} \end{bmatrix} + \begin{bmatrix} \mathbf{w}^{(1)} \\ \mathbf{w}^{(2)*} \\ \mathbf{w}^{(3)*} \\ \mathbf{w}^{(4)} \end{bmatrix} \tag{4.67}$$

Utilizing the properties of the permutation matrix $\mathbf{P}$ to manipulate (4.67) leads to,

$$\begin{bmatrix} \mathbf{y}^{(1)} \\ \mathbf{y}^{(2)*} \\ \mathbf{y}^{(3)*} \\ \mathbf{y}^{(4)} \end{bmatrix} = \begin{bmatrix} \mathbf{F}_N^H & & & \\ & \mathbf{F}_N & & \\ & & \mathbf{F}_N & \\ & & & \mathbf{F}_N^H \end{bmatrix} \begin{bmatrix} H_1 & H_2 & H_3 & H_4 \\ H_2^* & -H_1^* & H_4^* & -H_3^* \\ H_3^* & H_4^* & -H_1^* & -H_2^* \\ H_4 & -H_3 & -H_2 & H_1 \end{bmatrix} \begin{bmatrix} \mathbf{F}_N\mathbf{s}^{(1)} \\ \mathbf{F}_N\mathbf{s}^{(2)} \\ \mathbf{F}_N\mathbf{s}^{(3)} \\ \mathbf{F}_N\mathbf{s}^{(4)} \end{bmatrix} + \begin{bmatrix} \mathbf{w}^{(1)} \\ \mathbf{w}^{(2)*} \\ \mathbf{w}^{(3)*} \\ \mathbf{w}^{(4)} \end{bmatrix} \tag{4.68}$$

$$\mathbf{y} = \mathbf{H}\left(\mathbf{I}_4 \otimes \mathbf{F}_N\right)\mathbf{s} + \mathbf{w} \tag{4.69}$$

where $\otimes$ denotes the Kronecker product and again $\mathbf{y}^{(i)}$ and $\mathbf{w}^{(i)}$ denote the ith processed received frame at the d-MT with the associated noise component respectively which has identical statistical characteristics to that of the noise observed at the multi-carrier receiver (4.16).

4.4.1.1 Linear Combining

Again efficient linear combining via a matched filter is possible in the frequency-domain. This time the matched filter is constructed in matrix form as,

$$\mathbf{H}^H = \begin{bmatrix} H_1^H & H_2^T & H_3^T & H_4^H \\ H_2^H & -H_1^T & H_4^T & -H_3^H \\ H_3^H & H_4^T & -H_1^T & -H_2^H \\ H_4^H & -H_3^T & -H_2^T & H_1^H \end{bmatrix} \begin{bmatrix} \mathbf{F}_N^H & & & \\ & \mathbf{F}_N & & \\ & & \mathbf{F}_N & \\ & & & \mathbf{F}_N^H \end{bmatrix} \tag{4.70}$$

Multiplying (4.69) by the matched filtering matrix yields the decoupled form similar to the multi-carrier protocol,

$$\mathbf{z} = \tilde{\mathbf{A}}\left(\mathbf{I}_4 \otimes \mathbf{F}_N\right)\mathbf{s} + \mathbf{v} \tag{4.71}$$

where again $\mathbf{v} = \mathbf{H}^H\mathbf{w}$. However, unlike the multi-carrier scheme (4.21) the coupling matrix does not in the single-carrier implementation result in time-reversal on the off-diagonal,

$$\tilde{\mathbf{A}} = \beta \begin{bmatrix} \mathbf{\Gamma}_z & \mathbf{0} & \mathbf{0} & \mathbf{\Lambda}_z \\ \mathbf{0} & \mathbf{\Gamma}_z & -\mathbf{\Lambda}_z & \mathbf{0} \\ \mathbf{0} & -\mathbf{\Lambda}_z & \mathbf{\Gamma}_z & \mathbf{0} \\ \mathbf{\Lambda}_z & \mathbf{0} & \mathbf{0} & \mathbf{\Gamma}_z \end{bmatrix} \tag{4.72}$$

To simplify the process of equalization and detection the structure of $\tilde{\mathbf{A}}$ allows for an equivalent set of expressions which decouple the overall system into two equivalent subsystems as was previously elaborated in the discussion of the multi-carrier receiver and therefore will not be covered in any further detail here,

$$\begin{bmatrix} \mathbf{z}^{(1)} \\ \mathbf{z}^{(4)} \end{bmatrix} = \beta \begin{bmatrix} \mathbf{\Gamma}_z & \mathbf{\Lambda}_z \\ \mathbf{\Lambda}_z & \mathbf{\Gamma}_z \end{bmatrix} \begin{bmatrix} \mathbf{F}_N \mathbf{s}^{(1)} \\ \mathbf{F}_N \mathbf{s}^{(4)} \end{bmatrix} + \begin{bmatrix} \mathbf{v}^{(1)} \\ \mathbf{v}^{(4)} \end{bmatrix} \tag{4.73}$$

$$\mathbf{z}_{14} = \tilde{\mathbf{A}}_{14} \left(\mathbf{I}_2 \otimes \mathbf{F}_N \right) \mathbf{s}_{14} + \mathbf{v}_{14} \tag{4.74}$$

$$\begin{bmatrix} \mathbf{z}^{(2)} \\ \mathbf{z}^{(3)} \end{bmatrix} = \beta \begin{bmatrix} \mathbf{\Gamma}_z & -\mathbf{\Lambda}_z \\ -\mathbf{\Lambda}_z & \mathbf{\Gamma}_z \end{bmatrix} \begin{bmatrix} \mathbf{F}_N \mathbf{s}^{(2)} \\ \mathbf{F}_N \mathbf{s}^{(3)} \end{bmatrix} + \begin{bmatrix} \mathbf{v}^{(2)} \\ \mathbf{v}^{(3)} \end{bmatrix} \tag{4.75}$$

$$\mathbf{z}_{23} = \tilde{\mathbf{A}}_{23} \left(\mathbf{I}_2 \otimes \mathbf{F}_N \right) \mathbf{s}_{23} + \mathbf{v}_{23} \tag{4.76}$$

In the next section the structure of the system matrices in the frequency-domain is exploited to perform low-complexity equalization and pre-processing techniques.

4.4.1.2 ISI-Generating Mechanism

In the original network model the underlying sub-channels, denoted as the channels observed between participating nodes with the network, were classified as quasi-static flat-fading for the duration of the codeword transmission. Conspicuously, it can be observed that allowing for asynchronous retransmission at the relay nodes can introduce frequency selective characteristics which are observed at the destination node. Previously when designing the receiver for the multi-carrier scheme significant ISI, i.e. more than the pairwise interference observed in QOSTBCs, was avoided. The single-carrier scheme however suffers from significant ISI, it is therefore worth understanding the properties of the ISI generating mechanism before designing a receiver for its compensation.

A sub-carrier coupling matrix that exhibits fluctuations across the diagonal is known to be frequency selective and introduces ISI in the time-domain which complicates the symbol estimation task. Defining the N-point rectangular window

$$u_k := \begin{cases} 1 & 0 \leq n < N \\ 0 & else \end{cases} \tag{4.77}$$

it is possible to specify the ISI generating effects in matrix form (using doubly infinite sums unless otherwise stated),

$$
\begin{aligned}
[\mathbf{\Lambda}_t]_{m,n} &= [\mathbf{F}_N^H \mathbf{\Lambda} \mathbf{F}_N]_{m,n} && (4.78)\\
&= \frac{1}{N}\sum_{k,l} u_k u_l [\mathbf{\Lambda}]_{k,l} \times e^{j\frac{2\pi}{N}(mk-nl)} && (4.79)\\
&= \frac{1}{N}\sum_{k} u_k \alpha_k \times e^{j\frac{2\pi}{N}(m-n)k} && (4.80)\\
&= (S(\phi) * V(\phi))\,|_{\phi=-(m-n)} && (4.81)
\end{aligned}
$$

In (4.81), $S(\phi)$ denotes,

$$
\begin{aligned}
S(\phi) &:= \sum_{k=0}^{N-1} \alpha_k e^{-j\frac{2\pi k}{N}\phi} && (4.82)\\
&= 2\sum_{k=0}^{N-1} \Re\{h_{1,k}h_{4,k}^* - h_{2,k}h_{3,k}^*\} e^{-j\frac{2\pi k}{N}\phi} && (4.83)\\
&= 2\sum_{k=0}^{N-1} \rho\, cos\,(2\pi k\tau_{14} + \psi) - \kappa\, cos\,(2\pi k\tau_{23} + \varphi)\, e^{-j\frac{2\pi k}{N}\phi} && (4.84)
\end{aligned}
$$

where for simplicity the following notation is adopted,

$$
\begin{aligned}
\rho &:= |\mathbf{h}_1\mathbf{h}_4^*| && (4.85)\\
\kappa &:= |\mathbf{h}_2\mathbf{h}_3^*| && (4.86)\\
\tau_{14} &:= \tau_1 - \tau_4 && (4.87)\\
\tau_{23} &:= \tau_2 - \tau_3 && (4.88)\\
\psi &:= \theta_1 - \theta_4 && (4.89)\\
\varphi &:= \theta_2 - \theta_3 && (4.90)\\
& && (4.91)
\end{aligned}
$$

where the sub-carrier index for the channel notation in the definitions of ρ and κ have been discarded since the cooperative channel is assumed to be flat-fading. Additionally, $V(\phi)$ denotes the Dirichlet sinc function in the time-domain,

$$V(\phi) := \frac{1}{N}\sum_{k=0}^{N-1} e^{-j\frac{2\pi k}{N}\phi} \tag{4.92}$$

$$= \frac{1}{N}\frac{1-e^{-j2\pi\phi}}{1-e^{-j\frac{2\pi}{N}\phi}} \tag{4.93}$$

$$= \frac{sin(\pi\phi)}{Nsin(\pi\phi/N)}e^{-j\pi\phi(N-1)/N} \tag{4.94}$$

Equation (4.81) expresses the residual ISI generating mechanism where a visualization of the problem is illustrated in Figure 4.8 a). Essentially, the residual interference denoted by $\mathbf{\Lambda}$ generates a series of impulses $S(\phi)$ under a Discrete Time Fourier Transform (DTFT) with spacing a function of the relative delay between the spatial branches $\{1,4\}$, $\{2,3\}$. These impulses are then convolved with the Dirichlet sinc $V(\phi)$ and sampled on the regular grid $\{\phi : \phi = m-n, (m-n) \in Z\}$. With no asynchronous delay, i.e. $\tau_{14} = 0$ and $\tau_{23} = 0$, the nulls of $V(\phi) * S(\phi)$ fall on the sampling points of the regular grid, implying

$$\mathbf{\Lambda}_t = 2\Re\{h_1 h_4^* - h_2 h_3^*\}\mathbf{I}_N \tag{4.95}$$

However, in the asynchronous scenario the nulls of $V(\phi)*S(\phi)$ no longer fall on the grid therefore non-zero ISI is generated across the entire frame. This is illustrated when transforming the sub-system coupling matrix into the time-domain, e.g.

$$\tilde{\mathbf{A}}_{14,t} = \mathbf{F}_{2N}^H \mathbf{A}_{14}\mathbf{F}_{2N} \tag{4.96}$$

which is illustrated in Figure 4.8 a).

4.4.2 Sub-Optimal Equalizers

4.4.2.1 Zero-Forcing Decoder

The structure of the observed signal after pre-processing and matched filtering allows for very-low complexity equalization via the ZF-method. As with the multi-carrier system the aim of the ZF-equalizer is to remove ISI without any design consideration towards the possibility of noise enhancement that might degrade the overall SNR, i.e.

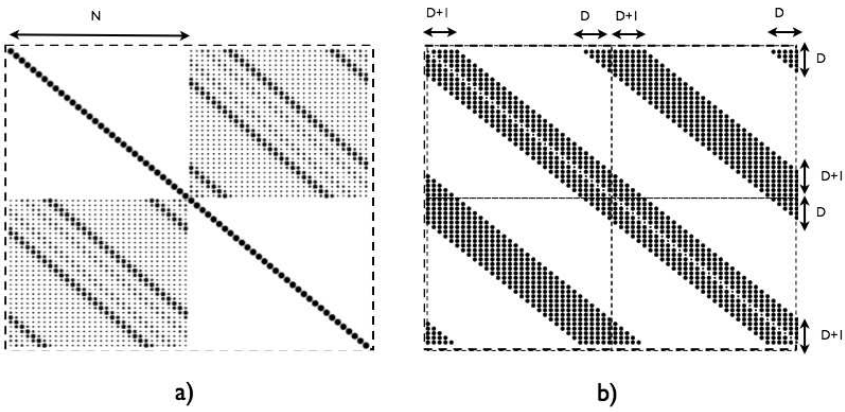

Figure 4.8: Single-carrier ISI representation: a) ISI illustration for subsystem coupling matrix, b) Masking matrix

$$\mathbf{z}_{zf} = \mathbf{Q}\mathbf{z} \tag{4.97}$$

$$= \mathbf{s} + \mathbf{Q}\mathbf{v} \tag{4.98}$$

It is observed (4.72) that after matched filtering IBI between $\mathbf{s}_{14}$ and $\mathbf{s}_{23}$ is cancelled,

$$\mathbf{z}_{14,zf} = \mathbf{Q}_{14}\mathbf{z}_{14} \tag{4.99}$$

$$\mathbf{z}_{23,zf} = \mathbf{Q}_{23}\mathbf{z}_{23} \tag{4.100}$$

Using block matrix inversion techniques it is possible to show that the ZF-filters can be expressed respectively as,

$$\mathbf{Q}_{14} = \frac{1}{\beta}\begin{bmatrix} \mathbf{F}_N^H & \\ & \mathbf{F}_N^H \end{bmatrix}\begin{bmatrix} \mathbf{S}^{-1} & -\mathbf{S}^{-1}\mathbf{\Lambda}_z\mathbf{\Gamma}_z^{-1} \\ -\mathbf{\Gamma}_z^{-1}\mathbf{\Lambda}_z\mathbf{S}^{-1} & \mathbf{S}^{-1} \end{bmatrix} \tag{4.101}$$

$$\mathbf{Q}_{23} = \frac{1}{\beta}\begin{bmatrix} \mathbf{F}_N^H & \\ & \mathbf{F}_N^H \end{bmatrix}\begin{bmatrix} \mathbf{S}^{-1} & \mathbf{S}^{-1}\mathbf{\Lambda}_z\mathbf{\Gamma}_z^{-1} \\ \mathbf{\Gamma}_z^{-1}\mathbf{\Lambda}_z\mathbf{S}^{-1} & \mathbf{S}^{-1} \end{bmatrix} \tag{4.102}$$

where $\mathbf{S} := \mathbf{\Gamma}_z - \mathbf{\Lambda}_z\mathbf{\Gamma}_z^{-1}\mathbf{\Lambda}_z$ defines the Schur complement. The noise covariance matrix at the output of the ZF-receiver is,

$$\begin{aligned} \mathbf{R}_{zf} &= \mathbf{Q}E\{\mathbf{v}\mathbf{v}^H\}\mathbf{Q}^H & (4.103)\\ &= \Sigma_w\tilde{\mathbf{F}}_{4N}^H\tilde{\mathbf{A}}^{-1}\tilde{\mathbf{F}}_{4N} & (4.104) \end{aligned}$$

Omitting the complexity of the linear pre-processing stages and observing that the matrix multiplication in the ZF-filters (4.101) and (4.102) involve diagonal matrix multiplication, the linear pre-processing required to equalize using a ZF-receiver equates to one N-point FFT and IFFT per frame amounting to $O(2log_2N)$ operations per information symbol.

4.4.2.2 Block Minimum Mean Square Error Decoder

Block MMSE equalization is also computationally inexpensive when performed in the frequency-domain.

$$\begin{aligned} J &= E\left\{\|\mathbf{Q}\mathbf{z} - \mathbf{s}\|_F^2\right\} \\ &= E\left\{\|\left(\mathbf{Q}\tilde{\mathbf{A}}\tilde{\mathbf{F}}_{4N} - \mathbf{I}\right)\mathbf{s} - \mathbf{Q}\mathbf{v}\|_F^2\right\} \\ &= E\left\{tr\left\{\left(\left(\mathbf{Q}\tilde{\mathbf{A}}\tilde{\mathbf{F}}_{4N} - \mathbf{I}\right)\mathbf{s} - \mathbf{Q}\mathbf{v}\right)\left(\left(\mathbf{Q}\tilde{\mathbf{A}}\tilde{\mathbf{F}}_{4N} - \mathbf{I}\right)\mathbf{s} - \mathbf{Q}\mathbf{v}\right)^H\right\}\right\} \\ &= tr\left\{\left(\mathbf{Q}\tilde{\mathbf{A}}\tilde{\mathbf{F}}_{4N} - \mathbf{I}\right)\left(\tilde{\mathbf{F}}_{4N}^H\tilde{\mathbf{A}}^H\mathbf{Q}^H - \mathbf{I}\right)\right\} + tr\left\{\mathbf{Q}\mathbf{\Sigma}_w\tilde{\mathbf{A}}\mathbf{Q}^H\right\} \qquad (4.105) \end{aligned}$$

Assuming that the a-priori statistical expectations used to derive the MMSE equalizer for the multi-carrier scheme (4.19) then the block MMSE equalizer is determined by differentiating (4.55) with respect to the linear filter $\mathbf{Q}^H$ results in,

$$\frac{\partial J}{\partial \mathbf{Q}^H} = \sigma_s^2\left(\mathbf{Q}\tilde{\mathbf{A}}\tilde{\mathbf{F}}_{4N} - \mathbf{I}\right)\tilde{\mathbf{F}}_{4N}^H\tilde{\mathbf{A}}^H + \mathbf{Q}\mathbf{\Sigma}_w\tilde{\mathbf{A}} \tag{4.106}$$

The filter resulting in the minimum MSE is then determined as,

$$\hat{\mathbf{Q}} = \tilde{\mathbf{F}}_{4N}^{H}\tilde{\mathbf{A}}^{H}\left(\tilde{\mathbf{A}}\tilde{\mathbf{A}}^{H} + \frac{1}{\sigma_s^2}\Sigma_w\tilde{\mathbf{A}}\right)^{-1} \tag{4.107}$$

$$= \tilde{\mathbf{F}}_{4N}^{H}\left(\tilde{\mathbf{A}} + \frac{1}{\sigma_s^2}\Sigma_w\right)^{-1} \tag{4.108}$$

It can be noted that the MMSE-equalizer expressed in (4.107) can be further simplified to operate on the decoupled symbol blocks yielding,

$$\mathbf{Q}_{14} = \frac{1}{\beta}\begin{bmatrix} \mathbf{F}_N^H & \\ & \mathbf{F}_N^H \end{bmatrix}\begin{bmatrix} \tilde{\mathbf{S}}^{-1} & -\tilde{\mathbf{S}}^{-1}\mathbf{\Lambda}_z\tilde{\mathbf{\Gamma}}_z^{-1} \\ -\tilde{\mathbf{\Gamma}}_z^{-1}\mathbf{\Lambda}_z\tilde{\mathbf{S}}^{-1} & \tilde{\mathbf{S}}^{-1} \end{bmatrix} \tag{4.109}$$

$$\mathbf{Q}_{23} = \frac{1}{\beta}\begin{bmatrix} \mathbf{F}_N^H & \\ & \mathbf{F}_N^H \end{bmatrix}\begin{bmatrix} \tilde{\mathbf{S}}^{-1} & \tilde{\mathbf{S}}^{-1}\mathbf{\Lambda}_z\tilde{\mathbf{\Gamma}}_z^{-1} \\ \tilde{\mathbf{\Gamma}}_z^{-1}\mathbf{\Lambda}_z\tilde{\mathbf{S}}^{-1} & \tilde{\mathbf{S}}^{-1} \end{bmatrix} \tag{4.110}$$

where $\tilde{\mathbf{\Gamma}} := \mathbf{\Gamma} + \frac{\sigma_w^2}{\sigma_s^2}\mathbf{I}_N$ and $\tilde{\mathbf{S}} := \tilde{\mathbf{\Gamma}}_z - \mathbf{\Lambda}_z\tilde{\mathbf{\Gamma}}_z^{-1}\mathbf{\Lambda}_z$. Assuming the noise statistics have been estimated there is minimal computational difference between the implementation of the MMSE and ZF equalizers.

4.4.3 Simulation Results

Case Study 18: Figure 4.9 depicts BER versus E_b/N_0 [dB] for DF relaying using single-carrier asynchronous Alamouti and QOSTBC processing at the r-MTs. The following simulation parameters, $N = 64$, $N_p = 15$, $\tau_{max} = 15$ and $\tau_i \sim U(0, \tau_{max}]$, are adopted to facilitate comparison with the previously proposed multi-carrier schemes illustrated earlier in the chapter. The symbols are assumed to be QPSK.

Interestingly, both the Alamouti-based multi-carrier scheme, Figure 4.5, and single-carrier scheme, Figure 4.9, demonstrate comparable results when ML-decoding is adopted at the d-MT. This is also equally demonstrated when implementing QOSTBC at the VAA in-conjunction with a ZF or MMSE processing at the d-MT. When operating under a DF protocol the only, marginal, between the multi-carrier and single-carrier enabled scheme is in the marginal difference of transferring the DFT processing from the s-MT to the d-MT to facilitate low-complexity combining and equalization. In addition the DF protocol when operating under a multi-carrier transmission scheme introduces the additional

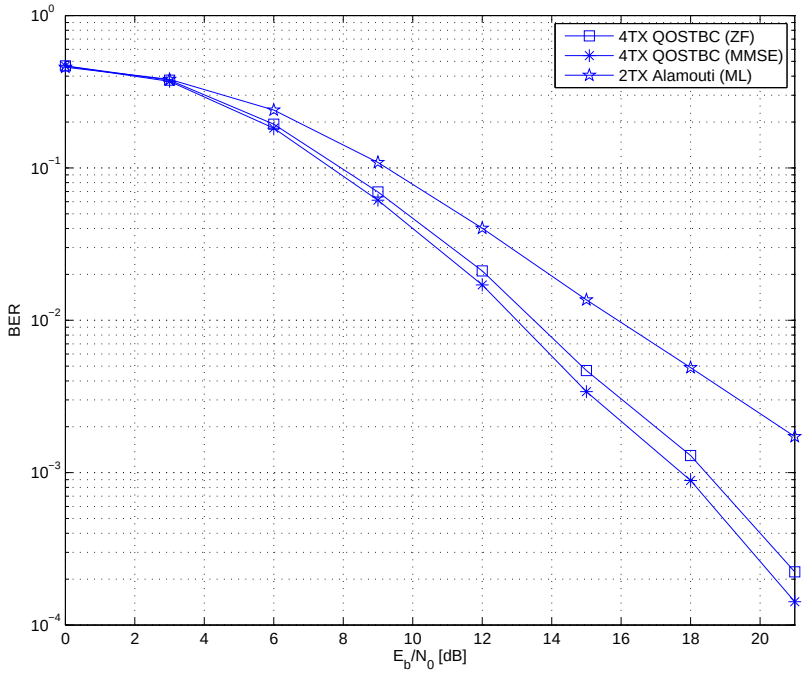

Figure 4.9: Comparison of performance of various sub-optimal decoder strategies for single-carrier asynchronous relay scheme; BER versus E_b/N_0

IDFT and DFT processing at the r-MTs to decode the received symbols from the s-MT before re-transmission; this additional processing at the r-MT is not required in single-carrier transmission.

Case Study 19: Figure 4.10 depicts BER versus E_b/N_0 [dB] for AF relaying using single-carrier asynchronous Alamouti and QOSTBC processing at the r-MTs. The simulation parameters used for the previous study are adopted in this simulation study.

Again both the multi-carrier, Figure 4.6, and single-carrier schemes, Figure 4.10, demonstrate results similar to those of comparable decoding strategies at the d-MT. Because the r-MTs adopt effectively transparent processing in the AF protocol there is no requirement to transform the received symbols into the frequency-domain for decoding purposes; therefore reducing the processing to a generic implementation at the r-MTs independent of the carrier transmssion used

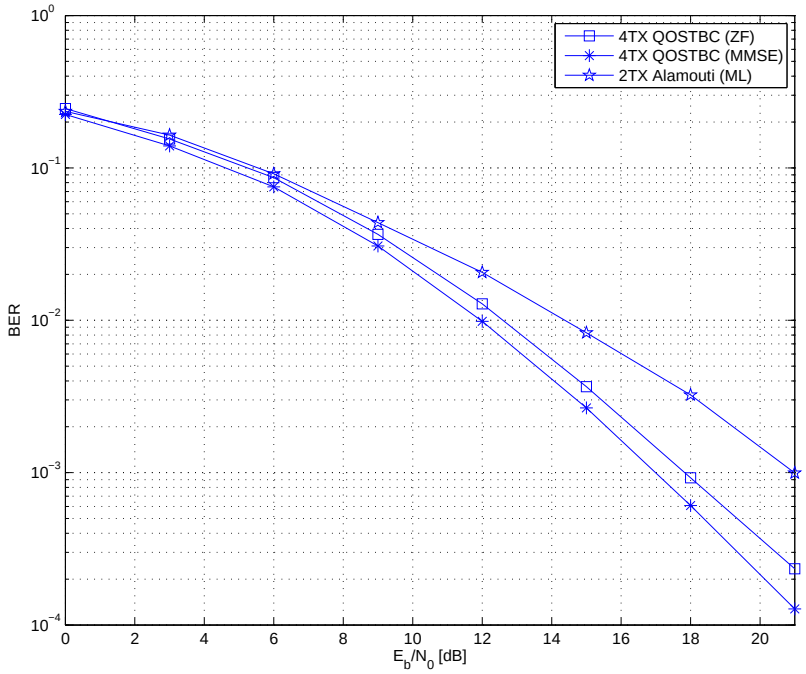

Figure 4.10: Comparison of performance of various sub-optimal decoder strategies for single-carrier asynchronous relay scheme; BER versus E_b/N_0

at the s-MT and d-MT.

Case Study 20: Depicted in Figure 4.11 is the network performance evaluated using the BER metric versus E_b/N_0 [dB] for various cluster sizes. The parameters adopted for previous simulation studies in the chapter remain constant and only specific changes for this study are highlighted. It is assumed for Alamouti-based ST coding that the d-MT performs ML decoding for the QOSTBC case MMSE decoding is assumed.

As with the AF protocol under multi-carrier transmission depicted in Figure 4.7; the multi-carrier transmission also advocates the use of clustering to reduce the effective noise variance forwarded from the r-MTs. As with multi-carrier transmission it is evident that the marginal benefits in increasing the cluster order is reduced. However for participating r-MTs the addition benefit in reduced transmit power for increasing the cluster order size provides an argument for

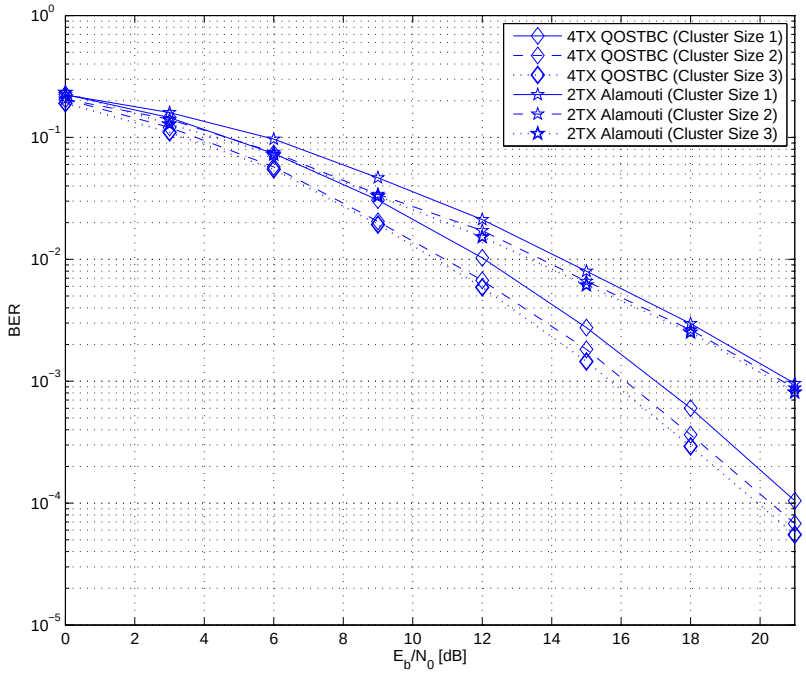

Figure 4.11: Comparison of performance of various sub-optimal decoder strategies for single-carrier asynchronous relay scheme; BER versus E_b/N_0

adopting high order clustering in cooperative relay networks.

4.5 Orthogonalization of Asynchronous Distributed-QOSTBC Designs

Assuming matched filtering is performed at the destination node for each of the $k = 1, \ldots, N$ sub-carriers, then because of the quasi-orthogonality of the coding scheme each symbol estimate is perturbed by ISI; as shown in the expression below [26],

$$\begin{bmatrix} \gamma_k & 0 & 0 & \alpha_k \\ 0 & \gamma_k & -\alpha_k & 0 \\ 0 & -\alpha_k & \gamma_k & 0 \\ \alpha_k & 0 & 0 & \gamma_k \end{bmatrix} \begin{bmatrix} \mathbf{s}_k^{(1)} \\ \mathbf{s}_k^{(2)} \\ \mathbf{s}_k^{(3)} \\ \mathbf{s}_k^{(4)} \end{bmatrix} \tag{4.111}$$

where $\gamma_k = \sum_{j=1}^{4} \|\mathrm{h}_{j,k}\|^2$ and $\alpha_k = 2Re\left\{\mathrm{h}_{1,k}\mathrm{h}_{4,k}^* - \mathrm{h}_{2,k}\mathrm{h}_{3,k}^*\right\}$. To cancel the α_k terms Toker et al. [26] proposed simple phase rotations, denoted by ϕ_k and θ_k, at the third and fourth transmit antennas, corresponding to relay nodes three and four in the scheme under consideration.

4.5.1 Frequency-Domain Orthogonalization

Although the original implementation of [26] was designed for a single-stage single-carrier implementation, this can be extended to the scheme under study by applying Toker's algorithm for each OFDM sub-carrier independently using the equivalent frequency-domain source to destination channel coefficients $h_{j,k}$. Applying the phase rotations at the appropriate nodes then enables the cross diagonal α_k terms to be canceled, i.e. $\alpha'_k = 0$,

$$\begin{aligned} \alpha'_k &= 2Re\{\mathrm{h}_{1,1}\mathrm{h}_{4,1}^* e^{j(\psi(k-1)+\theta_k)} \\ &\quad -\mathrm{h}_{2,1}\mathrm{h}_{3,1}^* e^{j(\omega(k-1)+\phi_k)}\} \end{aligned} \tag{4.112}$$

where

$$\psi = 2\pi(\tau_4 - \tau_1)/N \tag{4.113}$$

$$\omega = 2\pi(\tau_3 - \tau_2)/N \tag{4.114}$$

denote the incremental phase offset introduced between sub-carriers by the asynchronous delay spread between the fourth and first relay node and the delay spread between the second and third nodes respectively. However, this simple linear phase relationship across sub-carriers simplifies the calculation of the phase rotators ϕ_k and θ_k to,

$$\theta_k = \theta_1 - \psi(k-1) \tag{4.115}$$

$$\phi_k = \phi_1 - \omega(k-1) \tag{4.116}$$

therefore only requiring the computation of the phase offset variables for the first sub-carrier, i.e. θ_1 and ϕ_1, knowledge about the CSI for the first sub-carrier and the asynchronous offset delays τ_1, τ_2, τ_3 and τ_4. This then reduces the feedback requirements for the proposed scheme to the quantized parameters ϕ_1, θ_k, ω and ψ enabling the relay nodes to interpolate the necessary phase rotations over each individual sub-carrier.

Assuming ideal error free feedback between the destination and relay nodes three and four, the phase rotation can be implemented at each node using an all-pass Linear-Time-Invariant (LTI) filter calculated using the computationally efficient FFT/IFFT algorithm; this is illustrated in the following phase rotated frequency domain channels,

$$\begin{aligned} \mathrm{H}_3 &= FP_{\tau_3}H_{d,3}F^H\mathrm{D}(\phi)FH^*_{s,3}F^H & (4.117)\\ \mathrm{H}_4 &= FP_{\tau_4}H_{d,4}F^H\mathrm{D}(\theta)FH_{s,4}F^H & (4.118) \end{aligned}$$

Clearly, the processing suggested in (4.117) and (4.118) would require the signal observed at the r-MTs to be transformed into the frequency-domain by use of a DFT. Only then could a linear phase correction by applied to correct for the asynchronicity across the VAA. In the ensuing analysis in the next section time-domain Finite Impulse Response (FIR) and allpass filter designs will be applied to approximate the bandlimited correction of the fractional digital delay observed between relaying pairs.

4.5.2 Time-Domain Orthogonalization

In the preceeding analysis the distributed-QOSTBC was orthogonalized using a phase compensation in the frequency-domain (4.117)-(4.118) to correct for a delay spread due to the asynchronous retransmission of r-MTs. To mitigate the effects of asynchronous re-transmission delay spread has to be nullified for each transmitter pair,

$$(\tau_4 - \tau_1) = 0 \tag{4.119}$$

$$(\tau_3 - \tau_2) = 0 \tag{4.120}$$

In the case of limiting the processing to the 3rd and 4th r-MTs would require; delaying the re-transmitted signal in the event $\tau_4 < \tau_1$ and/or $\tau_3 < \tau_2$, or predictive filtering in the event $\tau_4 > \tau_1$ and/or $\tau_3 > \tau_2$. To limit the scope of the analysis to the former; processing to introduce a delay to satisfy the conditions (4.119) and (4.120) may be implemented across all participating r-MTs. One fundamental advantage of digital signal processing is in the event that the required delay is an integer multiple of the sampling interval then a constant delay is simply performed by storing samples in a memory buffer. When fractional delay of the sampling interval is required more sophisticated signal processing techniques are required. In the ensuing analysis both FIR and allpass filter design techniques are presented with an emphasis on efficient implementations that provide fast coefficient updating and provide accurate approximation of the continuous delay. To simplify the processing at the r-MTs, the designs are limited to an in-depth review of filter designs for Fractional Delay (FD) processing which are summarized in some detail in [74] and only the most pertinent designs are reviewed for application here.

4.5.2.1 Problem formulation and Ideal Solution

Assuming that a FD is required denoted by τ then the z-domain transfer function of the LTI operation is defined as,

$$H_{id}(z) = \frac{Y(z)}{X(z)} = z^{-\tau} \tag{4.121}$$

where $X(z)$, $Y(z)$ and $H_{id}(z)$ denote the z-domain transforms of the input, output and ideal filter response signals respectively. The frequency response of the filter is then given by substituting $z = e^{-j\omega}$,

$$H_{id}(e^{-j\omega}) = e^{-j\omega\tau} \tag{4.122}$$

The impulse response $h[n]$ of the ideal discrete-time linear-phase allpass filter with unitary magnitude and constant group delay τ is obtained via the Inverse Discrete Time Fourier Transform (IDTFT) [75],

$$h[n] = \frac{1}{2\pi}\int_{-\pi}^{\pi} H(e^{-j\omega})e^{j\omega n}d\omega, \qquad \forall n \tag{4.123}$$

Substituting (4.122) into (4.123) defines the ideal impulse response as [74],

$$h_{id}[n] = \frac{sin[\pi(n-\tau)]}{\pi(n-\tau)} = sinc(n-\tau), \qquad \forall n \tag{4.124}$$

It is well known that this infinite-length solution does not define a causal filter. Approximating the ideal fractional delay τ by an Nth-order FIR filter yields [75],

$$H(z) = \sum_{n=0}^{N} h[n]z^n \tag{4.125}$$

This introduces the problem of designing a filter $h[n]$ such that the frequency-domain error function [74],

$$E(e^{-j\omega}) = H(e^{-j\omega}) - H_{id}(e^{-j\omega}) \tag{4.126}$$

is minimized with respect to an arbitrary objective function $J\{E(e^{-j\omega})\}$.

4.5.2.2 Lagrange FIR Approach

Using a specific filter design method, based on Lagrange interpolation, the error function (4.129) can be made maximally flat at a specified frequency ω_0. The approximation is exact at this frequency therefore the derivatives of the frequency-domain error function when evaluated at ω_0 are set to zero [74],

$$\frac{d^m E(e^{-j\omega})}{d\omega^m}|_{\omega=\omega_0} = 0, \qquad m = 0, 1, \ldots, N \tag{4.127}$$

Differentiating then evaluating at $\omega_0 = 0$ produces a set of linear equations [74],

$$\sum_{n=0}^{N} n^m h[n] = \tau^m \tag{4.128}$$

This can also be expressed in matrix notation [74],

$$\mathbf{Vh} = \mathbf{d} \tag{4.129}$$

where $\mathbf{V}$ represents a Vandermonde matrix [76],

$$\begin{bmatrix} 1 & 1 & 1 & \cdots & 1 \\ 0 & 1 & 2 & & N \\ 0 & 1 & 2^2 & & N^2 \\ \vdots & & & \ddots & \vdots \\ 0 & 1 & 2^N & \cdots & N^N \end{bmatrix} \tag{4.130}$$

and $\mathbf{h} = [h[0], h[1], \ldots, h[N]]^T$ with $\mathbf{d} = [0, \tau^1, \ldots, \tau^N]^T$. Oetken [76] then presented the solution using the classical Lagrange interpolation formula expressing the solution,

$$h[n] = \prod_{k=0, k\neq n}^{N} \frac{\tau - k}{n - k} \qquad n = 0, 1, \ldots, N \tag{4.131}$$

The Lagrange filtering method for FD filtering has the following advantages [74]:

1. Easy closed-form explicit expressions for the coefficients enabling fast and simple updating at the r-MTs.
2. Minimal magnitude distortion at low frequencies which can be upper bounded to unity to maintain power constraints.
3. Selecting a symmetrical even-length filter which exhibits linear-phase.
4. Low order filters provide reasonable phase and magnitude response and are fast and simple to compute at the r-MTs.

Generally, recursive Infinite Impulse Response (IIR) filters satisfy the required frequency-domain specifications with lower order filters resulting in fewer multiplication operations than FIR counterparts. Therefore in the next section a suitable closed-form all-pass filter design will be reviewed that can be viewed as a recursive form of Lagrange interpolation.

4.5.2.3 Thiran IIR Approach

Similar to the FIR Lagrange interpolation filter previously proposed for FD processing at the r-MTs; Thiran [77] proposed a suitable all-pole lowpass closed-form filter design method demonstrating a maximally flat group delay response at zero

frequency. It is worth noting that in the all-pole Thiran design the FD parameter τ must be halved because of the property that the group delay of an all-pass filter is twice that of the equivalent all-pole filter [74].

Assuming the z-domain transfer function for an Nth-order allpass filter takes the form,

$$H(z) = \frac{z^{-N}D(z^{-1})}{D(z)} \tag{4.132}$$

$$= \frac{a_N + a_{N-1}z^{-1} + \ldots + a_1 z^{-(N-1)} + z^{-N}}{1 + a_1 z^{-1} + \ldots + a_{N-1}z^{-(N-1)} + a_N z^{-N}} \tag{4.133}$$

Thiran's solution for the all-pass filter coefficients approximating the delay τ is given by [77],

$$a_k = (-1)^k \begin{pmatrix} N \\ k \end{pmatrix} \prod_{n=0}^{N} \frac{\tau - N + n}{\tau - N + k + n} \tag{4.134}$$

where,

$$\begin{pmatrix} N \\ k \end{pmatrix} = \frac{N!}{k!(N-k)!} \tag{4.135}$$

is a binomial coefficient and $(\cdot)!$ denotes the factorial operand. The Thiran filtering method for FD filtering has the following advantages [74]:

1. Only known solution where coefficients are expressed in closed-form [74], which is similar to the Lagrange method enabling fast and simple updating at the r-MTs.

2. All-pass properties introduce zero magnitude distortion at all frequencies.

3. For large enough τ the all-pass IIR filter design is guaranteed to be stable [77].

4. Low-order filters provide reasonable phase and magnitude response and are fast and simple to compute at the r-MTs.

The application of Thiran filtering in addition to the Lagrangian method for FD processing is considered next in the following system level simulation studies.

4.5.3 Simulation Results

Case Study 21: Depicted in Figure 4.12 are BER versus E_b/N_0 [dB] for AF relaying protocol using multi-carrier asynchronous Alamouti [69] and QOSTBC processing at the r-MTs. In this simulation study; CSI and optimal-ML decoding is assumed at the d-MT. Again to enable comparisons between simulation results the following simulation parameters are adopted; $N = 64$, $N_p = 15$, $\tau_{max} = 15$ and $\tau_i \sim U(0, \tau_{max}]$. The symbols are assumed to be QPSK.

Figure 4.12 compares the novel full-rate QOSTBC scheme with the Alamouti-based OFDM implementation [69] and illustrates the performance improvements achieved using the feedback enabled phase rotation proposed by Toker [26] at the r-MTs. Firstly, in the absence of feedback, QOSTBC enabled ST-coding across the VAA demonstrates increased diversity gains and improved BER performance over the SNR range observed when compared with the Alamouti-based OFDM scheme. When infinite precision feedback is introduced, Figure 4.12 clearly demonstrates the increased diversity gain offered by orthogonalizing the channel. In the event that errors are introduced in the feedback channel, either through CSI estimation errors at the d-MT or time-variations in the channel, the QOSTBC enabled scheme adopts the open-loop BER characteristics therefore ensuring a robust transmission scheme in the event of feedback channel failure. In this simulation study it is assumed that the r-MT processing to perform channel orthogonalization is based on the frequency-domain orthogonalization described in Section 4.5.1.

Case Study 22: Depicted in Figure 4.13 are BER versus E_b/N_0 [dB] for AF relaying protocol using multi-carrier asynchronous QOSTBC processing at the r-MTs with optimal-ML implemented at the d-MT. Again to enable comparisons between simulation results the previous simulation parameters are adopted.

The previous simulation study assumed a feedback channel between the d-MT and r-MTs that supported infinite precision. For a realizable system some quantization of the phase rotation should be adopted to limit the bandwidth requirements of the feedback channel; therefore two simple strategies are adopted to obtain the results presented in Figure 4.13. The first strategy, termed Sub-Carrier Phase Quantization (SCPQ), quantizes the phase rotation variables $\phi_k, \theta_k \in \{0, \pm\frac{\pi}{2}, \pi\}$ by only feeding back two-bits per sub-carrier to r-MTs R_3 and R_4;

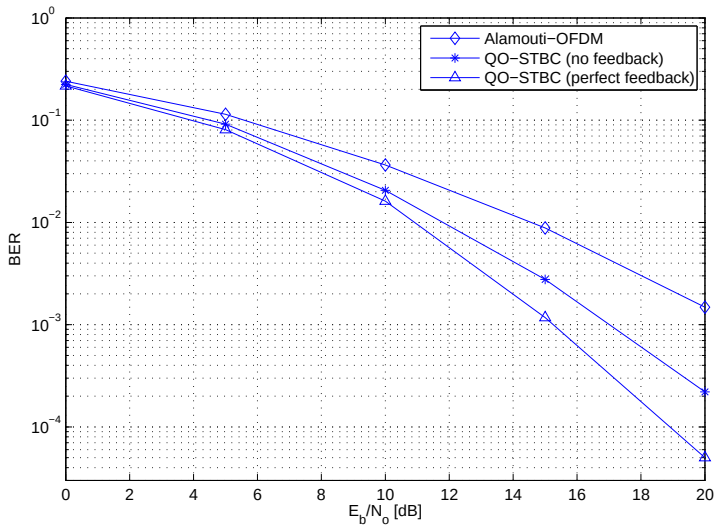

Figure 4.12: Comparison of BER performance for multi-carrier QOSTBC asynchronous relay scheme with ideal frequency-domain channel orthogonalization; BER versus E_b/N_0

therefore creating an overhead of 128 bits per feedback channel when $N = 64$. The second strategy, referred to on Figure 4.12 as Sub-Carrier Quantized Linear Phase Interpolation (SCQLPI), adopts the same encoding approach previously used for the first sub-carrier, $k = 1$. In addition a quantized linear phase offset; the linear relationship in (4.115,4.116), is encoded to the nearest half-sampled delay interval, i.e. $\{0, 1/2, \ldots, 15\}$ therefore providing a resolution to the nearest half-sampling interval. This SCQLPI scheme reduces the feedback overhead in the simulations to 12-bits, providing a feedback overhead saving in excess of 90%, assuming 4-bits account for the quantized phase rotation for the first sub-carrier [k=1] and the remaining 8-bits determine the delay offset correction between sub-carriers. As shown in Figure 4.13 SCQLPI performs favorably in contrast to SCPQ, and the feedback overhead is proportional to the maximum asynchronous delay between relay nodes in contrast to the SCPQ scheme which is proportional to the OFDM symbol length.

Case Study 23: Depicted in Figure 4.14 is the magnitude and phase response of Lagrange FD filter designs of order $\{1, 2, \ldots, 5\}$. The FD under which the

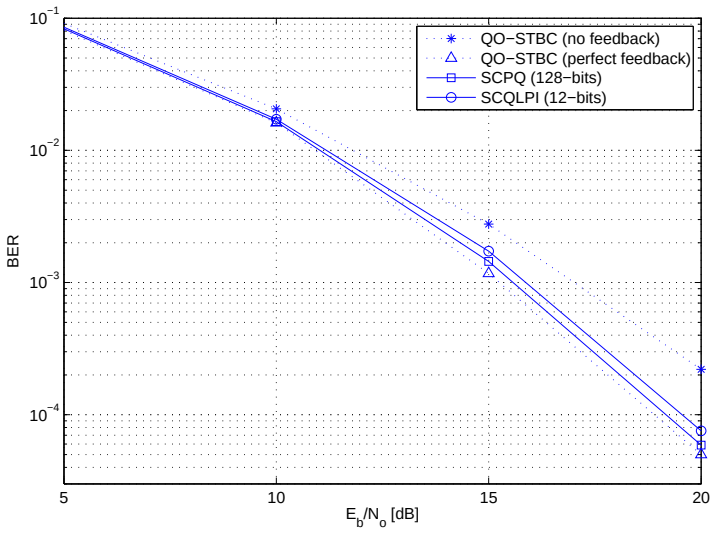

Figure 4.13: Comparison of BER performance for multi-carrier QOSTBC asynchronous relay scheme with quantized frequency-domain channel orthogonalization; BER versus E_b/N_0

filters are evaluated is assumed to be the worse-case approximation of half a sample delay $\tau = 0.5$ [74]. Only the fractional part of the delay is illustrated in the results, clearly the filter will introduce some delay proportional to the filter order which needs to be compensated for in the deployment for cooperative networks.

Interestingly, when $\tau = 0.5$ the coefficient symmetry of the even-length filters results in linear-phase across the normalized frequency[74]. However the magnitude response deteriorates at high-frequencies due to the zero at $\omega = \pi$ [74]. The tradeoff between odd and even filters will be evident in the simulation results presented next.

Case Study 24: Depicted in Figure 4.15 are BER versus E_b/N_0 [dB] for AF relaying protocol using various Lagrange FD designs assuming multi-carrier asynchronous QOSTBC processing at the r-MTs with optimal-ML implemented at the d-MT. Again to enable comparisons between simulation results the previous simulation parameters are adopted. It is assumed that the time-domain filtering is implemented at baud rate. Increasing the sampling-rate improves the approx-

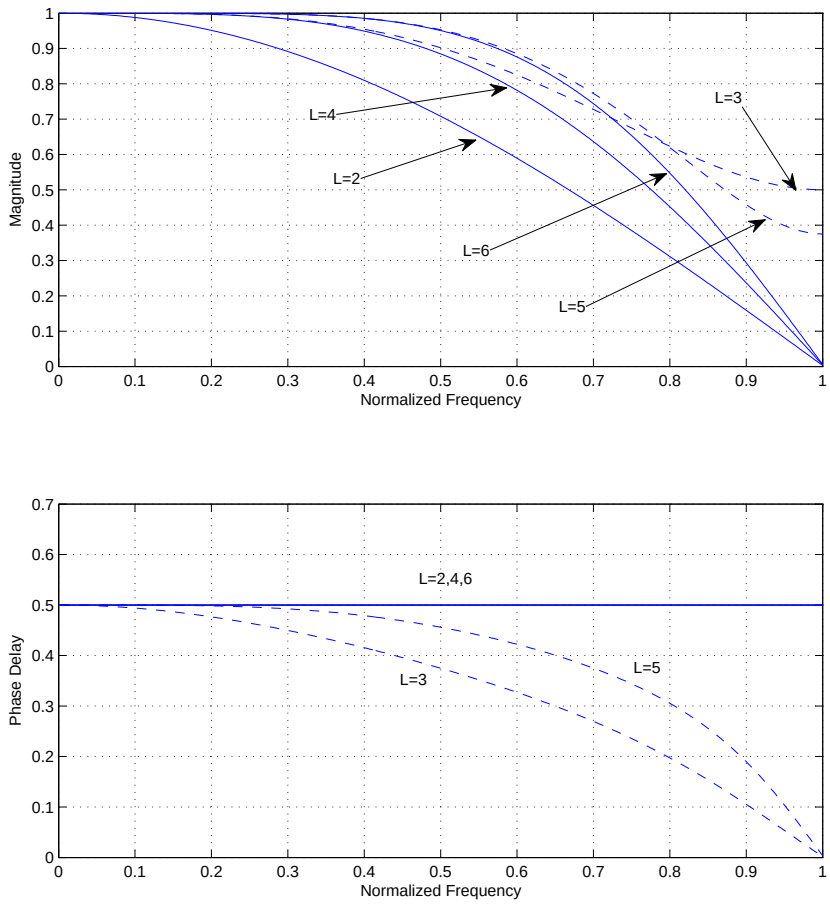

Figure 4.14: FIR Fractional Delay Filter Lagrange Interpolation Design; Magnitude & Phase Delay Response

imation bandwidth of the Lagrange FD filter designs, as illustrated in Figure 4.14.

Initially it is evident in Figure 4.15 that some of the Lagrange FD filter designs yield a worsening in BER performance than when operating in open-loop QOSTBC as is demonstrated in Figure 4.12. This can be explained by the loss in magnitude in the upper frequency range which is a characteristic of the Lagrange design as exhibited in Figure 4.14. Conspicuously, the only design to outperform open-loop QOSTBC was $L = 5$ and this is attributed to a trade-off in approxi-

mation performance both in magnitude and phase to the ideal solution (4.124). Increasing the filter order based on Lagrange designs improves the approximation to the ideal solution at high frequencies; however the approximation bandwidth increased very slowly as the filter order increases [74].

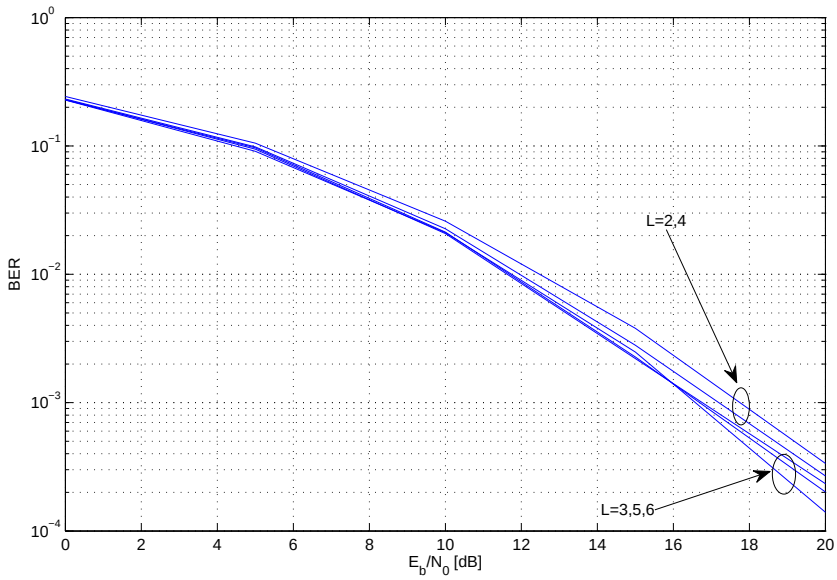

Figure 4.15: Comparison of BER performance for multi-carrier QOSTBC asynchronous relay scheme with Lagrange time-domain channel orthogonalization; BER versus E_b/N_0

Case Study 25: Depicted in Figure 4.16 are the magnitude and phase responses of Thiran FD filter designs of orders $\{1, 2, \ldots, 5\}$. The FD under which the filters are evaluated is assumed to be the same as that used to generate Lagrange results in Figure 4.14, i.e. half a sample delay $\tau = 0.5$.

Case Study 26: Depicted in Figure 4.17 are BER versus E_b/N_0 [dB] for AF relaying protocol using various Thiran FD designs assuming multi-carrier asynchronous QOSTBC processing at the r-MTs with optimal-ML implemented at the d-MT. Again to enable comparisons between simulation results the previous simulation parameters are adopted. It is assumed that the time-domain filtering is implemented at the baud rate. As with the Lagrange designs, increasing

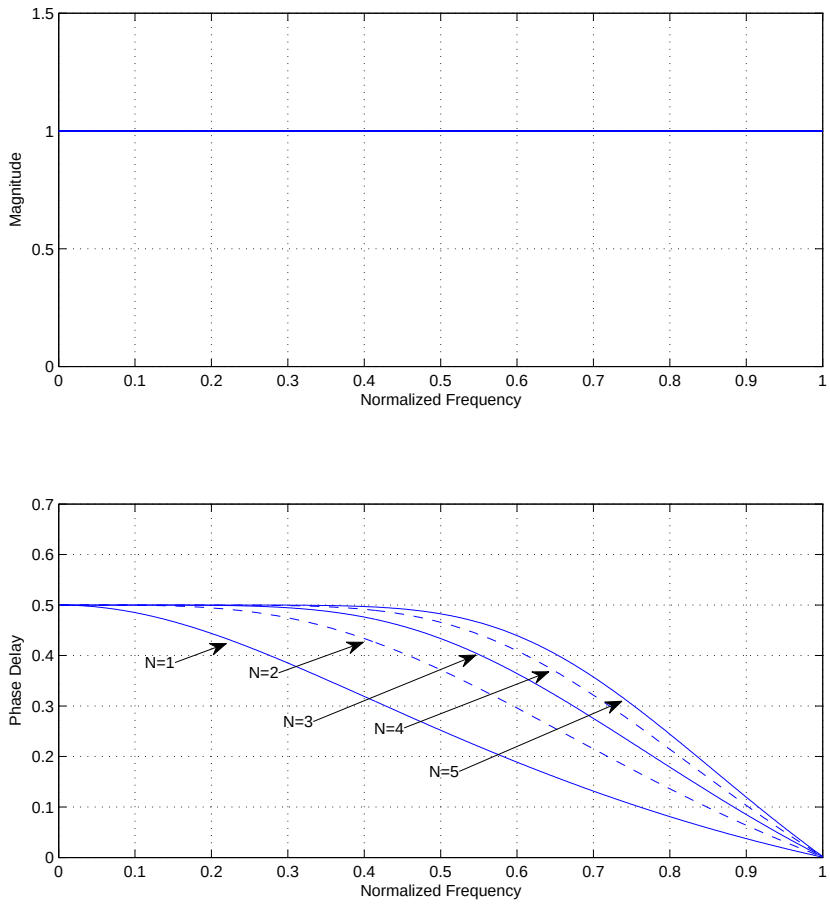

Figure 4.16: IIR Fractional Delay Filter Thiran Closed-Form Design; Magnitude & Phase Delay Response

the sampling-rate improves the approximation bandwidth of the Thiran FD filter designs, as illustrated in Figure 4.16.

In contrast to Lagrange FD filter designs, Figure 4.17 demonstrates significant improvement in BER performance for the Thiran implementation. This can be attributed to the all-pass magnitude response of the filter and the robustness of the feedback scheme advocated by Toker [48] to phase errors. Clearly very simple first and second order designs yield improvements over the open-loop implementation.

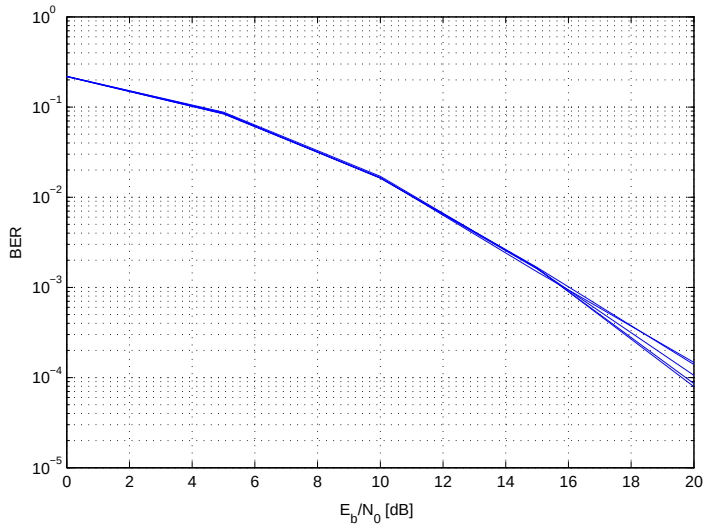

Figure 4.17: Comparison of BER performance for multi-carrier QOSTBC asynchronous relay scheme with Thiran time-domain channel orthogonalization; BER versus E_b/N_0

4.6 Conclusions

This chapter introduced novel asynchronous designs for robust flat-fading cooperative relay networks. Based on the fundamental analysis of the previous chapter; QOSTBCs were shown to demonstrate significant capacity and throughput enhancements over more traditional orthogonal-designs. Specifically, the significant gains offered in non-ergodic channels demonstrated the robustness of QOSTBC to outage. This provided the motivation to focus on overcoming one of the fundamental challenges to realizable distributed-ST enabled cooperative networks; namely, timing synchronization between all the participating nodes in the protocol. This chapter introduced novel asynchronous designs that leverage the diversity gains offered by QOSTBC as well as exploiting transmission schemes already adapted for frequency-selective channels to the pertinent problem of timing-synchronization. The specific details of the material covered in the chapter can be summarized as follows.

After a brief introduction, Section 4.2 introduces a simplified network model based on a single s-MT communicating with a d-MT via a set of r-MTs form-

ing a VAA. It is assumed that the nodes cooperate according to a half-duplex protocol to simplify the requirements for each r-MT. The problem of asnychronization between the r-MTs which observe a different round-trip-delay is illustrated through a network signal model that gives valuable insight into the design of asynchronous designs for cooperative relay networks. The processing at the s-MT to mitigate delay observed at the d-MT is described for both multi-carrier and single-carrier transmission. Finally, the VAA generic processing for the novel cooperative QOSTBC scheme is derived for the versatile AF relaying where it can easily be adapted for DF. The proposed processing at the r-MTs proves to be independent of both single- and multi-carrier transmission.

In Section 4.3 the specific processing required to facilitate decoding at the d-MT is detailed. The intricacies of delay correction, CP removal and combining at the receiver are discussed specifically for the proposed asynchronous multi-carrier QOSTBC scheme. After the symbols are initially pre-processed several computationally feasible decoding strategies are presented: namely, ZF, MMSE and ML. Although the processing to mitigate the effects of asynchronous re-transmssion at the r-MTs is block-based it is proven to be comparable to the more traditional QOSTBC schemes deployed in traditional synchronous co-located systems. Simulation results based on both DF and AF relaying verify the utility of the proposed scheme.

In Section 4.4 the strategies used at the d-MT to decode a QOSTBC base on single-carrier transmission are explored. Differences in the required pre-processing are discussed with the main deviation resulting from the transferal of the IDFT from the s-MT to the d-MT to still enabling efficient linear combing to be performed in the frequency-domain. Uniquely to QOSTBC using the proposed asynchronous scheme, which is not observed for OSTBC, the effect of round-trip-delays at the r-MTs introduces ISI within a transmission frame. This phenomenon is not observed in the multi-carrier scheme since decoding can be performed solely in the frequency-domain. Specifically, for the single-carrier scheme block-based ZF and MMSE equalizers are derived to mitigate these effects. Simulation results based on both DF and AF relaying verify that even in the presence of ISI the single-carrier scheme produces comparable BER performance to the multi-carrier scheme under ZF and MMSE.

In Section 4.5 the idea of orthogonalizing the quasi-orthogonal channel using

techniques derived by Toker [26] is revisited for adaptation to asynchronous cooperative relay networks. Initially a very simple implementation is presented that orthogonalizes the channel by correcting for the delay introduced by performing a simple phase rotation at the r-MTs in the frequency-domain. Later two time-domain techniques are presented in the form of FD filters that compensate for delays introduced at the r-MTs. The requirement for an adaptive FD filter in arbitrary network deployments and low-mobility situations is catered for by using closed-form FD filtering designs that closely approximate optimal solutions when implemented close to the baud rate of the system. Various simulation studies based on both DF and AF relaying verify the BER performance gains offer through quantized feedback and simple processing at the r-MTs.

This chapter presented novel QOSTBC schemes that overcome some of the pertinent challenges facing the deployment of robust cooperative relay networks. In the next chapter the coding schemes developed here are extended to the more challenging channels experienced under high-data rates.

4.7 Appendix

Derivation I. It is proven here that,

$$\begin{bmatrix} \mathbf{y}^{(1)} \\ \mathbf{y}^{(2)*} \\ \mathbf{y}^{(3)*} \\ \mathbf{y}^{(4)} \end{bmatrix} = \begin{bmatrix} H_1 & H_2\mathbf{P} & H_3\mathbf{P} & H_4 \\ H_2^* & -H_1^*\mathbf{P} & H_4^*\mathbf{P} & -H_3^* \\ H_3^* & H_4^*\mathbf{P} & -H_1^*\mathbf{P} & -H_2^* \\ H_4 & -H_3\mathbf{P} & -H_2\mathbf{P} & H_1 \end{bmatrix} \begin{bmatrix} \mathbf{s}^{(1)} \\ \mathbf{s}^{(2)} \\ \mathbf{s}^{(3)} \\ \mathbf{s}^{(4)} \end{bmatrix} + \begin{bmatrix} \mathbf{w}^{(1)} \\ \mathbf{w}^{(2)*} \\ \mathbf{w}^{(3)*} \\ \mathbf{w}^{(4)} \end{bmatrix} \tag{4.136}$$

To simplify the ensuing expressions the noise terms are omitted for brevity. Using the previously stated expressions for the source (5.163), relay received (4.6) and relay transmitted (4.7) signals it is possible to show the equivalent expressions for each frame received at the destination following initial pre-processing to be,

$$\mathbf{y}^{(1)} = h_1\mathbf{\Phi}_1\mathbf{F}_N\mathbf{F}_N^H\tilde{\mathbf{s}}^{(1)} - h_2\mathbf{\Phi}_2\mathbf{F}_N\mathbf{F}_N\tilde{\mathbf{s}}^{(2)*} - h_3\mathbf{\Phi}_3\mathbf{F}_N\mathbf{F}_N\tilde{\mathbf{s}}^{(3)*} + h_4\mathbf{\Phi}_4\mathbf{F}_N\mathbf{F}_N^H\tilde{\mathbf{s}}^{(4)} \tag{4.137}$$

$$\mathbf{y}^{(2)} = h_2\mathbf{\Phi}_2\mathbf{F}_N\mathbf{P}\mathbf{F}_N\tilde{\mathbf{s}}^{(1)*}+h_1\mathbf{\Phi}_1\mathbf{F}_N\mathbf{P}\mathbf{F}_N^H\tilde{\mathbf{s}}^{(2)}-h_4\mathbf{\Phi}_4\mathbf{F}_N\mathbf{P}\mathbf{F}_N^H\tilde{\mathbf{s}}^{(3)}-h_3\mathbf{\Phi}_3\mathbf{F}_N\mathbf{P}\mathbf{F}_N\tilde{\mathbf{s}}^{(4)*} \tag{4.138}$$

$$\mathbf{y}^{(3)} = h_3\mathbf{\Phi}_3\mathbf{F}_N\mathbf{P}\mathbf{F}_N\tilde{\mathbf{s}}^{(1)*}-h_4\mathbf{\Phi}_4\mathbf{F}_N\mathbf{P}\mathbf{F}_N^H\tilde{\mathbf{s}}^{(2)}+h_1\mathbf{\Phi}_1\mathbf{F}_N\mathbf{P}\mathbf{F}_N^H\tilde{\mathbf{s}}^{(3)}-h_2\mathbf{\Phi}_2\mathbf{F}_N\mathbf{P}\mathbf{F}_N\tilde{\mathbf{s}}^{(4)*} \tag{4.139}$$

$$\mathbf{y}^{(4)} = h_4\mathbf{\Phi}_4\mathbf{F}_N\mathbf{F}_N^H\tilde{\mathbf{s}}^{(1)} + h_3\mathbf{\Phi}_3\mathbf{F}_N\mathbf{F}_N\tilde{\mathbf{s}}^{(2)*} + h_2\mathbf{\Phi}_2\mathbf{F}_N\mathbf{F}_N\tilde{\mathbf{s}}^{(3)*} + h_1\mathbf{\Phi}_1\mathbf{F}_N\mathbf{F}_N^H\tilde{\mathbf{s}}^{(4)} \tag{4.140}$$

where the asynchronous delay is characterized in the matrix with diagonal elements $[\mathbf{\Phi}_j]_{k,k} := e^{-j2\pi k\tau_j/N}$ and following notation is used to simplify the expressions,

$$h_1 = h_{d,1}h_{s,1} \tag{4.141}$$
$$h_2 = h_{d,2}h_{s,2}^* \tag{4.142}$$
$$h_3 = h_{d,3}h_{s,3}^* \tag{4.143}$$
$$h_4 = h_{d,4}h_{s,4} \tag{4.144}$$

Substituting the symbol remapping for the original symbols (4.1) and observing the frequency-domain channel matrices (4.12) it is possible to express (4.137)-(4.140) as,

$$\mathbf{y}^{(1)} = \mathbf{H}_1\mathbf{s}^{(1)} + \mathbf{H}_2\mathbf{P}\mathbf{s}^{(2)} + \mathbf{H}_3\mathbf{P}\mathbf{s}^{(3)} + \mathbf{H}_4\mathbf{s}^{(4)} \tag{4.145}$$

$$\mathbf{y}^{(2)} = \mathbf{H}_2\mathbf{s}^{(1)*} - \mathbf{H}_1\mathbf{P}\mathbf{s}^{(2)*} + \mathbf{H}_4\mathbf{P}\mathbf{s}^{(3)*} - \mathbf{H}_3\mathbf{s}^{(4)*} \tag{4.146}$$

$$\mathbf{y}^{(3)} = \mathbf{H}_3\mathbf{s}^{(1)*} + \mathbf{H}_4\mathbf{P}\mathbf{s}^{(2)*} - \mathbf{H}_1\mathbf{P}\mathbf{s}^{(3)*} - \mathbf{H}_2\mathbf{s}^{(4)*} \tag{4.147}$$

$$\mathbf{y}^{(4)} = \mathbf{H}_4\mathbf{s}^{(1)} - \mathbf{H}_3\mathbf{P}\mathbf{s}^{(2)} - \mathbf{H}_2\mathbf{P}\mathbf{s}^{(3)} + \mathbf{H}_1\mathbf{s}^{(4)} \tag{4.148}$$

Finally to express the equivalent input-output matrix form as shown in (4.136) the observations $\mathbf{y}^{(2)}$ and $\mathbf{y}^{(3)}$ are conjugated.

Derivation II It is proven here that,

$$\|\mathbf{y} - \mathbf{H}\hat{\mathbf{s}}\|_2^2 \equiv a\|\Sigma_v^{-1/2}\left(\mathbf{z} - \mathbf{A}\hat{\mathbf{s}}\right)\|_2^2 \tag{4.149}$$

where $a = N_0\left(\beta^2 \sum_{j=1}^{4} |h_{d,j}|^2 + 1\right)$. Expanding the term on the left of (4.149) results in,

$$\begin{aligned}
\|\mathbf{y} - \mathbf{H}\hat{\mathbf{s}}\|_2^2 &= \|\mathbf{H}\left(\mathbf{s} - \hat{\mathbf{s}}\right) + \mathbf{w}\|_2^2 \\
&= \left(\mathbf{s} - \hat{\mathbf{s}}\right)^H \mathbf{A}\left(\mathbf{s} - \hat{\mathbf{s}}\right) + \left(\mathbf{s} - \hat{\mathbf{s}}\right)^H \mathbf{H}^H\mathbf{w} + \mathbf{w}^H\mathbf{H}\left(\mathbf{s} - \hat{\mathbf{s}}\right) + \mathbf{w}^H\mathbf{w}.
\end{aligned}$$

where in the second line the substitution $\mathbf{A} = \mathbf{H}^H\mathbf{H}$. In addition the expansion of the right term results in,

$$\begin{aligned}
\|\mathbf{\Sigma}_v^{-1/2}\left(\mathbf{z} - \mathbf{A}\hat{\mathbf{s}}\right)\|_2^2 &= \|\mathbf{\Sigma}_v^{-1/2}\left(\mathbf{A}\left(\mathbf{s} - \hat{\mathbf{s}}\right) + \mathbf{v}\right)\|_2^2 \\
&= \left(\mathbf{s} - \hat{\mathbf{s}}\right)^H \mathbf{A}^H\mathbf{\Sigma}_v^{-1}\mathbf{A}\left(\mathbf{s} - \hat{\mathbf{s}}\right) \\
&\qquad + \left(\mathbf{s} - \hat{\mathbf{s}}\right)^H \mathbf{A}^H\mathbf{\Sigma}_v^{-1}\mathbf{v} + \mathbf{v}^H\mathbf{\Sigma}_v^{-1}\mathbf{A}\left(\mathbf{s} - \hat{\mathbf{s}}\right) + \mathbf{v}^H\mathbf{\Sigma}_v^{-1}\mathbf{v} \\
&= \left(\mathbf{s} - \hat{\mathbf{s}}\right)^H \mathbf{A}\mathbf{\Sigma}_w^{-1}\left(\mathbf{s} - \hat{\mathbf{s}}\right) \\
&\qquad + \left(\mathbf{s} - \hat{\mathbf{s}}\right)^H \mathbf{\Sigma}_w^{-1}\mathbf{H}^H\mathbf{w} + \mathbf{w}^H\mathbf{H}\mathbf{\Sigma}_w^{-1}\left(\mathbf{s} - \hat{\mathbf{s}}\right) + \mathbf{w}^H\mathbf{\Sigma}_w^{-1}\mathbf{w} \\
&= \frac{1}{a}\|\mathbf{y} - \mathbf{H}\hat{\mathbf{s}}\|_2^2
\end{aligned}$$

where the second line expands the Euclidean norm, the third line uses the substitutions $\mathbf{\Sigma}_v = \mathbf{\Sigma}_w\mathbf{A}$ and $\mathbf{v} = \mathbf{H}^H\mathbf{w}$ with simple mathematical manipulations. Finally it is noted that $\mathbf{\Sigma}_w$ (4.16) is simply a scalar multiplied identity matrix allow the last line of the expression to be reduced accordingly.

Chapter 5

Asynchronous Broadband Designs for Cooperative Relay Networks

5.1 Introduction

A key requirement for future wireless networks will be the support of high-data rate transfers whilst maintaining minimum Quality-of-Service (QoS) requirements for the next generation of applications. Recent research into cooperative relay networks has demonstrated comparable diversity gains to MIMO systems with local antenna arrays using the concept of cooperative diversity over a distributed network of participating relay nodes. The spatial diversity offered by separate single-antenna nodes cooperating to form a virtual antenna array can mitigate some of the practical performance limitations of a local antenna array; such as correlation which can reduce the achievable capacity and diversity gains offered by the MIMO channel. Cooperative communication however poses addition challenges, specifically in the synchronization between participating nodes both in time and frequency. In Chapter 4, asynchronous cooperative schemes were developed based on QOSTBCs to extract spatial diversity from the relay channel. In this chapter those ideas are progressed for use in broadband networks.

For high-rate broadband wireless communication, channels can exhibit frequency selectivity when the symbol period approximates the delay spread of the

channel which can cause ISI [40]. Initially some asynchronous relaying schemes [78, 79] tailored the simple but effective AF relaying methodology derived from Alamouti coding [23] for use in flat-fading channels [69] to relay channels experiencing frequency-selectivity. Although these schemes promised the simple AF relay processing based on both single- and multi-carrier transmission; only spatial diversity was extracted from the channel. Limiting the relaying protocol to DF, asynchronous distributed-STTCs [80, 81] were adapted to exploit both the spatial and multi-path diversity offered by the frequency-selective relay channel. Although the STTC were optimized to offer full-diversity and maximum coding gain; in some applications the deployment maybe constrained by the decoding complexity. Reduced complexity ST-coded transmission schemes offering both multi-path and spatial diversity were presented in [82, 83]; however both offer reductions in the transmission rate. Full-rate distributive-Space-Frequency (SF) codes achieving full spatial and multi-path diversity for asynchronous cooperative communications are presented in [84, 85, 86]. However, the schemes are limited to DF processing only.

This chapter presents a novel distributed application of a STF coding scheme for asynchronous multi-relay networks using OFDM transmission over frequency-selective Rayleigh fading channels. The scheme is based on distributed inner and outer coders that are shown to achieve the maximum diversity and coding gains with low-complexity decoding. The chapter is organized as follows: In Section 5.2, the network model introduced in Chapter 4 for the development of robust asynchronous designs for flat-fading cooperative relay networks is extended for broadband networks that demonstrate additional frequency-selective fading. The model allows for the flexibility of distributed wireless relay networks that may observe different channel orders, path-loss and correlation statistics when transmitted via different r-MTs.

Section 5.3 introduces the notation used to analyze and develop distributed-STF codes for use in cooperative relay networks under DF and AF relying protocols. In this section the main design criterion is formally stated. This will provide the necessary framework upon which the ensuing code designs are evaluated.

Section 5.4 formulates distributed-STF based on QOSTBC as the ST-component coding. This section builds upon the advantages of QOSTBCs for use in broadband enabled networks adopting a DF protocol at the r-MTs. Initially, the dis-

tributed MIMO channel observed by the r-MTs and d-MT in the second phase of the protocol is analyzed using a PEP to determine the diversity and coding gains that can be exploited independent of the particular coding scheme implemented at the VAA. The outcome of this analysis can then be used to design efficient coding schemes to achieve the design criteria previously stated. The design of the proposed coding scheme is detailed extensively in Section 5.4.2 where design considerations such as: optimal sub-carrier grouping, ST-component coding, constellation pre-coding and power allocation are discussed in some detail to meet the objectives specified in the design criteria. Simulation studies are used to verify the utility of the proposed coding scheme in a multitude of networking scenarios.

Section 5.5 builds upon many of the insights already gained from the analysis for deployment in DF relaying networks for use with AF protocols. However, significant differences between the protocols make a re-examination of the achievable diversity and coding in Section 5.5 essential to devising coding strategies both at the s-MT and across the VAA to extract both spatial in the form of cooperative diversity as well as the available multi-path diversity. The complexity of analysis under AF relaying results in deriving the achievable diversity and coding gains offered by the AF under specific conditions and limiting assumptions. The results however lead to robust designs specifically tailored to the AF that meet the initial design criteria. Simulation studies as well as verifying the analysis and proposed coding scheme give valuable insight to coding designs which are intractable through analytical techniques.

5.2 Broadband Network Model

In this section the parallel relay channel architecture first introduced in Chapter 4 and illustrated in Figure 4.1 is extended for use in broadband wireless relay networks. Data are transmitted from the s-MT again denoted as S to the d-MT denoted as D via participating r-MTs operating under two relaying methodologies, namely: Decode-and-Forward (DF) and Amplify-and-Forward (AF) respectively. Both protocols adopt the same scheduling strategy proposed by Nebar et al. [87, 88]. Specifically in the first phase the s-MT broadcasts to N_t participating r-MTs denoted by R_j. It is assumed that no direct communication between the

s-MT and d-MT is observed in this phase enabling the d-MT to perform other unrelated processing. In the second phase the r-MTs forward a processed version of the s-MT signal to the d-MT. When the r-MTs operate using the DF protocol the assumption that all participating r-MT have correctly decoded the information symbols in the first phase of the protocol proposed by Li et al. [89] is adopted. This assumption may be validated assuming that there exists a large number of available r-MTs in which only a subset of these relays decode the transmitted data from the first phase without error; these r-MTs may then participate in the second phase of the protocol. In the case where the AF protocol is adopted the r-MTs forward a processed noisy version of the original s-MT signal. It is worth noting that under the proposed two phase scheme the half-duplex operation of the participating r-MTs simplifies the RF transceiver specification at the cost of halving the achievable data rate.

For high-rate transmission all sub-channels observed by the r-MTs and d-MT in the network model are assumed to be frequency-selective with the associated CIR,

$$h_{\mu\nu}(\tau) = \sum_{l=0}^{L_{\mu\nu}} \alpha_{\mu\nu}\delta(\tau - \tau_{\mu\nu}(l)) \tag{5.1}$$

where $\delta(\cdot)$ denotes the Dirac delta function and $L_{\mu\nu}$ denotes the variable channel order for transmit antenna $\mu \in \{S, R_1, \ldots, R_{N_r}\}$ to receive antenna $\nu \in \{D_1, \ldots, D_{N_r}, R_1, \ldots, R_{N_r}\}$. The complex amplitude and l^{th} multi-path for the channel denoted $\{\mu\nu\}$ is given by the ZMCSCG random variable $\alpha_{\mu\nu}$ and delay $\tau_{\mu\nu}(l)$ respectively. In digital systems at the receiver the channel is only observed at discrete instances in time denoted by the sampling period T_s; therefore $\tau_{\mu\nu}(l)$ is assumed to be an integer multiple of T_s. This facilitates using a discrete-time base-band equivalent impulse response vector,

$$\mathbf{h}_{\mu\nu} := [\alpha_{\mu\nu}[0], \ldots, \alpha_{\mu\nu}[L_{\mu\nu}]]^T \in \mathbb{C}^{(L_{\mu\nu}+1)\times 1} \tag{5.2}$$

as the channel description. The channel between the VAA and a specified d-MT receiver element ν can be described as,

$$\mathbf{h}_{\nu} := [\mathbf{h}^T_{R_1\nu}, \ldots, \mathbf{h}^T_{R_{N_t}\nu}]^T \in \mathbb{C}^{(L_\nu)\times 1} \tag{5.3}$$

with an associated full-rank covariance matrix,

$$E\{\mathbf{h}_\nu \mathbf{h}_\nu^H\} = \mathbf{R}_\nu \tag{5.4}$$

assuming $\mathbf{h}_\nu$ is a zero-mean random vector. Therefore, $\mathbf{R}_\nu$ allows for correlated wireless channel taps, with various power profiles that enable the normalizing of channels power in the presence of varying channel orders. The model assumes $\mathbf{h}_\nu$ for different ν are statistically independent.

The flexibility in this cooperative channel model allows the differences from conventional MIMO systems to be expressed. Specifically, sub-channel characteristics in distributed systems may encounter variable channel lengths and power delay profiles due to the different scattering environments. The differences usually are not so pronounced in conventional MIMO systems where the antennas are co-located and channel lengths and power delay profiles are generally assumed to be the same.

5.3 Problem formulation & Design Criteria

To analyze the code design the following notation to describe the codeword is adopted. Individual transmitted symbol $x_i^\mu(p)$ which are defined as the ith OFDM symbol transmitted from the μth node on subcarrier p. The symbols $\{x_i^\mu(p), i = 1, \ldots, N_x, \mu = S, R_1, \ldots, R_{N_t}, p = 0, \ldots, N_c - 1\}$ are transmitted in parallel on the N_c subcarriers from the s-MT or one of N_t participating r-MTs for N_x OFDM symbol durations. The variables i, μ and p index the time, space and frequency dimensions of the transmitted codeword.

5.3.1 Generic Cooperative Processing - Source Node

Consider the first stage of the protocol where the source node groups N_I information symbols $\mathbf{s} := [s_0, \ldots, s_{N_I-1}]^T \in \mathbb{C}^{N_I \times 1}$. The formulation of the codeword at the s-MT can be described as a one-to-one mapping Ψ_S,

$$\Psi_S : \mathbf{s} \rightarrow \mathbf{X}^S \tag{5.5}$$

Without loss of generality the codeword $\mathbf{X}^S$ can be thought to span space-time-frequency with dimensions $1 \times N_{x_s} \times N_c$ where the mapping results in the following

N_{x_s} OFDM symbols $i \in \{1, \ldots, N_{x_s}\}$ denoted by $x_i^S(p) \in \mathbb{C}$. The frequency-domain symbol $\mathbf{x}_i^S := [x_i^S(0), \ldots, x_i^S(N_c - 1)]^T \in \mathbb{C}^{N_c \times 1}$ is then mapped into the time domain symbols $\mathbf{t}_i^S \in \mathbb{C}^{J \times 1}$ according to,

$$\mathbf{t}_i^S = \mathbf{T}_{cp} \mathbf{F}_N^H \mathbf{x}_i^S \tag{5.6}$$

where $J = N_c + N_p$ and $\mathbf{T}_{cp}$ introduces a CP of length N_p and was defined for use in the previous chapter in expression (4.2). Assuming all participating r-MTs synchronize perfectly in time with the s-MT; orthogonality between OFDM symbols is preserved if the CP length contraint $N_p \geq \max\{L_{SR_j} + 1\}$ is satisfied. The ith received OFDM symbol at r-MT R_j is denoted,

$$\mathbf{r}_i^{R_j} = \sqrt{\bar{\gamma}_{SR_j}} \tilde{\mathsf{H}}_{SR_j} \mathbf{s}_i^S + \mathbf{v}_i^{R_j} \tag{5.7}$$

where $\bar{\gamma}_{\mu\nu}$ generically denotes the average received signal power which incorporates slow-fading processes as a result of path-loss and shadowing effects associated with the sub-channel pair $\{\mu\nu\}$, $\tilde{\mathsf{H}}_{SR_j}$ is a $J \times J$ Toeplitz matrix denoted by the first column

$$[\tilde{\mathbf{h}}_{SR_j}^T, \mathbf{0}_{1 \times (J - L_{SR_j} - 1)}]^T \in \mathbb{C}^{J \times 1} \tag{5.8}$$

where $\tilde{\mathbf{h}}_{SR_j}^T := \mathbf{h}_{SR_j}^T / \sqrt{\bar{\gamma}_{SR_j}}$ and $\mathbf{v}_i^{R_j}$ is AWGN with variance $N_0/2$ per dimension incident at the r-MT R_j.

5.3.2 Generic Cooperative Processing - Virtual Antenna Array

The VAA comprising of distributed r-MTs then independently performs a one-to-one mapping Ψ_{R_j} of the received signal $\mathbf{r}^{R_j} := [\mathbf{r}_0^{R_j}, \ldots, \mathbf{r}_{N_{x_s}}^{R_j}]^T$ onto a corresponding codeword $\mathbf{X}^{R_j}$,

$$\Psi_{R_j} : \mathbf{r}^{R_j} \rightarrow \mathbf{X}^{R_j} \tag{5.9}$$

$\mathbf{X}^{R_j}$ spans space-time-frequency with dimensions $N_t \times N_x \times N_c$ where the mapping results in the following N_x OFDM symbols $i \in \{1, \ldots, N_x\}$ denoted by $x_i^{R_j}(p) \in \mathbb{C}$. Similar to the processing implemented at the s-MT the frequency-domain

symbols $\mathbf{x}_i^{R_j} := [x_i^{R_j}(0), \ldots, x_i^{R_j}(N_c - 1)]^T \in \mathbb{C}^{N_c \times 1}$ are then mapped into the time-domain symbols $\mathbf{t}_i^S \in \mathbb{C}^{J \times 1}$ according to,

$$\mathbf{t}_i^{R_j} = \mathbf{T}_{cp}\mathbf{F}_N^H \mathbf{x}_i^{R_j} \tag{5.10}$$

To maintain orthogonality between OFDM symbols at the d-MT the r-MT must generate a CP sufficient to encapsulate the delay spread as a function of the channel order and the maximum delay-spread amongst relay retransmission expressed as $N_p \geq \max\{L_{\mu\nu} + \lceil \tau_{max}/T_s \rceil\}, \forall \mu, \nu$; where τ_{max} denotes the maximum delay-spread.

After initial pre-processing is performed at the d-MT, involving CP removal and DFT, an equivalent input-output network signal model can be expressed in the frequency-domain as,

$$y_i^{\nu}(p) = \sum_{\mu \in \{R_1, \ldots, R_{N_t}\}} \sqrt{\bar{\gamma}_{\mu\nu}} \tilde{H}_{\mu\nu}(p) x_i^{R_j}(p) + w_i^{\nu}(p) \tag{5.11}$$

where $\mathbf{y}_i(p) := [y_i^{D_1}(p), \ldots, y_i^{D_{N_r}}(p)]^T$ denotes the received signal at the d-MT adopting the same STF indexing and $\mathbf{w}_i(p) := [w_i^{D_1}(p), \ldots, w_i^{D_{N_r}}(p)]^T$ is AWGN with variance $N_0/2$ observed at the d-MT. The channel matrix denoted by $H_{\mu\nu}(p)$ is the frequency-response at the pth sub-carrier of the sub-channel associated with the transmit-receiver pair $\{\mu, \nu\}$ evaluated using the generalized expression,

$$H_{\mu\nu}(p) = \sum_{l=0}^{L_{\mu\nu}} \alpha_{\mu\nu}[l] e^{-j(2\pi l p)/N}. \tag{5.12}$$

with the normalized channel defined as $\tilde{H}_{\mu\nu}(p) := H_{\mu\nu}(p)/\sqrt{\bar{\gamma}_{\mu\nu}}$. For the purposes of design simplicity it is also possible to re-formulate the signal model (5.11) as a series of layered ST systems organized in block matrix form,

$$\mathbf{X} := [\mathbf{X}(0)\ \mathbf{X}(1)\ \ldots\ \mathbf{X}(N_c - 1)] \in \mathbb{C}^{N_t \times N_c N_x} \tag{5.13}$$

where each sub-matrix is equivalent to coding over a virtual flat-fading channel corresponding to the MIMO channel response at subcarrier p,

$$\mathbf{X}(p) := \begin{bmatrix} x_0^{R_1}(p) & \cdots & x_{N_x-1}^{R_1}(p) \\ \vdots & & \vdots \\ x_0^{R_{N_t}}(p) & \cdots & x_{N_x-1}^{R_{N_t}}(p) \end{bmatrix} \in \mathbb{C}^{N_t \times N_x} \tag{5.14}$$

Using the ST codeword definition (5.14) allows for a series of N_c equivalent ST systems with the following input-output system,

$$\mathbf{Y}(p) = \left(\mathbf{E}_{RD} \odot \tilde{\mathbf{H}}_{RD}(p)\right) \mathbf{X}(p) + \mathbf{W}(p) \tag{5.15}$$

where $\odot$ defines element wise multiplication and the following definitions are adopted,

$$\mathbf{Y}(p) := [\mathbf{y}_1(p) \cdots \mathbf{y}_{N_x}(p)] \in \mathbb{C}^{N_r \times N_x} \tag{5.16}$$

$$\mathbf{E}_{RD} := \begin{bmatrix} \sqrt{\bar{\gamma}_{R_1 D_1}} & \cdots & \sqrt{\bar{\gamma}_{R_{N_t} D_1}} \\ \vdots & & \vdots \\ \sqrt{\bar{\gamma}_{R_1 D_{N_r}}} & \cdots & \sqrt{\bar{\gamma}_{R_{N_t} D_{N_r}}} \end{bmatrix} \in \mathbb{C}^{N_r \times N_t} \tag{5.17}$$

$$\tilde{\mathbf{H}}_{RD}(p) := \begin{bmatrix} \tilde{H}_{R_1 D_1} & \cdots & \tilde{H}_{R_{N_t} D_1} \\ \vdots & & \vdots \\ \tilde{H}_{R_1 D_{N_r}} & \cdots & \tilde{H}_{R_{N_t} D_{N_r}} \end{bmatrix} \in \mathbb{C}^{N_r \times N_t} \tag{5.18}$$

$$\mathbf{W}(p) := [\mathbf{w}_1(p) \cdots \mathbf{w}_{N_x}(p)] \in \mathbb{C}^{N_r \times N_x} \tag{5.19}$$

Leveraging the properties of OFDM transmission to orthogonalize the waveforms of the STF encoded signal model (5.15) can now be viewed as N_c parallel ST transmissions $\mathbf{X}(p)$ over various subcarriers. Clearly, the problem formulation is the design of Ψ_S and Ψ_{R_j} to satisfy the desired design criterion which is specified in detail in the ensuing section.

5.3.3 Codeword Design Criteria

To facilitate the codeword design to be implemented distributively across the cooperative wireless relay network there must be a design criterion to be satisfied. The criterion for the analysis of achievable diversity, design constraints and objectives is formally stated as follows:

1. Maximum likelihood (ML) detection is performed with perfect channel-state-information (CSI) of all links in the cooperative network available at the destination node.

2. The proposed scheme shall operate in the high SNR range; therefore the main design objective is to maximize available diversity gain.

3. In addition to maximizing diversity gain any proposed scheme shall aim to maximize coding gain.

5.4 Decode-and-Forward Cooperative Space-Time Frequency Coding

The problem of designing Ψ_S and Ψ_{R_j} to satisfy certain design criteria is simplified when adopting a DF relaying protocol under the assumption that participating relay nodes decode the symbols broadcast from the s-MT without error. In the following analysis and code construction only the design of Ψ_{R_j} is considered.

5.4.1 Diversity and Coding Gain Analysis

5.4.1.1 Pairwise Probability Analysis

Considering the assumptions 1-3 made in Section 5.3.3 a bounded analysis of the PEP is performed to optimize performance for STF codes in asynchronous cooperative networks. Although exact error probability analysis may well be tractable a more insightful design metric is achieved by adopting a PEP analysis which determines the probability that the receiver decides erroneously, in a ML sense, in favor of $\mathbf{X}'$ over the transmitted $\mathbf{X}$. The choice of analysis technique is justified through assumption 2 and facilitates the well known rank and determinant criterion first proposed by Tarokh et al. [25] for the design of ST codes. According to (5.15) the ML decision metric is evaluated under the expression,

$$\hat{\mathbf{X}} = \arg\min_{\mathbf{X}\in A_s} \sum_{p=0}^{N_c-1} \|\mathbf{Y}(p) - \left(\mathbf{E}_{RD} \odot \tilde{\mathbf{H}}_{RD}(p)\right) \mathbf{X}(p)\|_F^2 \tag{5.20}$$

where the search is performed over the symbol alphabet A_s. Conditioned on the known channel realizations $\tilde{\mathbf{H}}_{RD}(p)$ at the specific subcarrier p the PEP can be expressed as [40, Page 40],

$$P(\mathbf{X} \rightarrow \mathbf{X}'|\mathbf{E}_{RD}, \tilde{\mathbf{H}}_{RD}(0), \ldots, \tilde{\mathbf{H}}_{RD}(N_c - 1)) = Q\left(\sqrt{\frac{d^2(\mathbf{X}, \mathbf{X}')}{2N_0}}\right) \tag{5.21}$$

where $Q(\cdot)$ is defined as $Q(x) := \int_x^\infty \frac{1}{\sqrt{2\pi}} e^{-t^2/2} dt$ and,

$$d^2(\mathbf{X}, \mathbf{X}') = \sum_{p=0}^{N_c-1} \| \left(\mathbf{E}_{RD} \odot \tilde{\mathbf{H}}_{RD}(p)\right) \boldsymbol{\Delta}(p)\|^2 \tag{5.22}$$

where $\boldsymbol{\Delta}(p) := \mathbf{X}(p) - \mathbf{X}'(p)$. It is then possible to upper bound the PEP in (5.21) using the Chernoff bound $Q(x) \leq e^{-x^2/2}$ [2],

$$P(\mathbf{X} \rightarrow \mathbf{X}'|\mathbf{E}_{RD}, \tilde{\mathbf{H}}_{RD}(0), \ldots, \tilde{\mathbf{H}}_{RD}(N_c - 1)) \leq \exp\left[-\frac{d^2(\mathbf{X}, \mathbf{X}')}{4N_0}\right] \tag{5.23}$$

Defining $\omega_{L_{\mu\nu}}(p) := [1, \exp(-j2\pi p/N_c), \ldots, \exp(-j2\pi p L_{\mu\nu}/N_c)]^T \in \mathbb{C}^{(L_{\mu\nu}+1)\times 1}$ enables (5.12) to be expressed in the vector notation,

$$H_{\mu\nu}(p) = \mathbf{h}_{\mu\nu}^T \omega_{L_{\mu\nu}}(p) \tag{5.24}$$

Note for the analysis for the DF protocol it is assumed that $\mathbf{E}_{RD}$ is encapsulated by the correlation matrix, $\mathbf{R}_\nu$. In addition it is noted that $\mathbf{R}_\nu$ is positive-definite Hermitian symmetric allowing the decomposition $\mathbf{R}_\nu = \mathbf{B}_\nu \mathbf{B}_\nu^H$ where $\mathbf{B}_\nu \in \mathbb{C}^{L_\nu \times L_\nu}$ is the square root of $\mathbf{R}_\nu$ with full-rank and

$$L_\nu := \sum_{\mu \in \{R_1, \ldots, R_{N_t}\}} (L_{\mu\nu} + 1)\,. \tag{5.25}$$

The whitened channel vector can now be defined as,

$$\bar{\mathbf{h}}_\nu = \mathbf{B}_\nu^{-1} \mathbf{h}_\nu \tag{5.26}$$

Substituting (5.24) into (5.22), and allowing for some elementary mathematics [90], enables $d^2(\mathbf{X}, \mathbf{X}')$ to be re-written as,

$$d^2(\mathbf{X},\mathbf{X}') = \sum_{\nu\in\{D_1,\ldots,D_{N_r}\}} \mathbf{h}_\nu^T \Lambda_\nu \mathbf{h}_\nu^* \tag{5.27}$$

$$= \sum_{\nu\in\{D_1,\ldots,D_{N_r}\}} \bar{\mathbf{h}}_\nu^T \bar{\Lambda}_\nu \bar{\mathbf{h}}_\nu^* \tag{5.28}$$

where,

$$\bar{\Lambda}_\nu := \mathbf{B}_\nu^T \Lambda_\nu \mathbf{B}_\nu^* \in \mathbb{C}^{L_\nu\times L_\nu} \tag{5.29}$$

$$\Lambda_\nu := \sum_{p=0}^{N_c-1} \Omega_\nu(p)\Delta(p)\Delta(p)^H\Omega_\nu(p)^H \in \mathbb{C}^{L_\nu\times L_\nu} \tag{5.30}$$

$$\Omega_\nu(p) := \begin{bmatrix} \omega_{L_{1\nu}}(p) & & & \\ & \omega_{L_{2\nu}}(p) & & \\ & & \ddots & \\ & & & \omega_{L_{N_t\nu}}(p) \end{bmatrix} \in \mathbb{C}^{L_\nu\times N_t} \tag{5.31}$$

To satisfy the design criteria set out in Section 5.3.3 of maximum diversity and coding gain without channel knowledge at the transmitter the expected PEP is evaluated over all channel realizations. Using the results by Turin to derive the characteristic function for Hermitian quadratic forms in complex variables [51] the channel averaged PEP can be expressed as,

$$P(\mathbf{X}\to\mathbf{X}') \le \prod_{\nu\in\{D_1,\ldots,D_{N_r}\}} \left|\mathbf{I} + \frac{1}{4N_0}\bar{\Lambda}_\nu\right|^{-1} \tag{5.32}$$

where $|\cdot|$ denotes the determinant. Then based on eigen-analysis and standard derivations (5.32) can be re-written as,

$$P(\mathbf{X}\to\mathbf{X}') \le \prod_{\nu\in\{D_1,\ldots,D_{N_r}\}} \prod_{i=1}^{r(\bar{\Lambda}_\nu)} \frac{1}{1+\frac{1}{4N_0}\lambda_{\nu,i}} \tag{5.33}$$

where the operator $r(\bar{\Lambda}_\nu)$ denotes the rank of Λ_ν and $\lambda_{\nu,i}$ for $i = 1,\ldots,r(\bar{\Lambda}_\nu)$ represent the non-zero eigenvalues of $\bar{\Lambda}_\nu$. In the high-SNR regime the diversity and coding gains can be explicitly illustrated using the template,

$$P(\mathbf{X} \rightarrow \mathbf{X}') \leq \frac{1}{(G_{\nu,c})} \left(\frac{1}{4N_0} \right)^{-G_{\nu,d}} \tag{5.34}$$

where by definition the coding and diversity gain are represented by $G_{\nu,c}$ and $G_{\nu,d}$ respectively [25],

$$\begin{aligned} G_{\nu,c} &= \prod_{\nu \in \{D_1,\ldots,D_{N_r}\}} \prod_{i=1}^{r(\bar{\Lambda}_\nu)} \lambda_{\nu,i} && (5.35) \\ &= \prod_{\nu \in \{D_1,\ldots,D_{N_r}\}} \det(\bar{\Lambda}_\nu) && (5.36) \end{aligned}$$

$$\begin{aligned} G_{\nu,d} &= \sum_{\nu \in \{D_1,\ldots,D_{N_r}\}} r(\bar{\Lambda}_\nu) && (5.37) \\ &\leq \sum_{\mu \in \{R_1,\ldots,R_{N_t}\}} \sum_{\nu \in \{D_1,\ldots,D_{N_r}\}} (L_{\mu\nu} + 1) && (5.38) \end{aligned}$$

Recalling (5.32) it is clear to see that the derived coding metrics (5.35) and (5.37) are dependent upon on a particular error event $\{\mathbf{X} \rightarrow \mathbf{X}'\}$. Therefore the minimum achievable diversity $G'_{\nu,d}$ gain is determined via a search over all codeword pairs [40],

$$G'_{\nu,d} = \arg \min_{\mathbf{X} \neq \mathbf{X}' \in A_x} G_{\nu,d} \tag{5.39}$$

In accordance with the specified design criteria highlighted in Section 5.3.3 a subset of codewords can then be identified based on the rank criteria to narrow the search for codewords that offer the minimum overall coding $G'_{\nu,c}$ gain [40],

$$G'_{\nu,c} = \arg \min_{\mathbf{X} \neq \mathbf{X}' \in A_x, G'_{\nu,d} = G_{\nu,d}} G_{\nu,c} \tag{5.40}$$

With both important design metrics now derived it is possible to specify a STF code that provides optimum error performance in a cooperative wireless network where only partial-CSI is known at the receiver.

Observing (5.29) it is easy to see that the rank is bounded by the dimensionality of $\bar{\Lambda}_\nu$ and shows the maximum diversity offered by the channel to be

$G'^{\,max}_{\nu,d} = \sum_{\mu=1}^{N_t} (L_{\mu\nu} + 1)$ (5.38), i.e. the sum of all the channel orders from the μth transmitting antennas to the νth receive antenna.

Furthermore, as stated in [90] if $\mathbf{B}_\nu$ is assumed to have full-rank then maximum diversity gain is only achieved if Λ_ν (5.30) is also full-rank. Clearly just coding over one sub-carrier, i.e. reproducing the same codeword over each subcarrier, effectively ST coding would limit the rank of Λ_ν to a maximum N_t as shown by the maximum achievable rank of each summand $\Omega(p)\Delta(p)\Delta(p)^H\Omega(p)^H \in \mathbb{C}^{N_t \times N_t}$ in (5.30). Assuming only ST coding techniques are utilized the number of independent columns or rows is limited to N_t, therefore only extracting spatial diversity.

To extract the full multi-path diversity available from the channel coding should be applied across multiple subcarriers as suggested in [91, 92]. In traditional co-located MIMO systems where the channel order between the transmitter and receiver antenna can be assumed constant, independent of the transmitter-receiver pair. Therefore the number of sub-carriers required to achieve the full diversity gain is exactly proportional to the channel order. Alternatively, the distributed case where it is assumed differing channel orders between transmitting and receiving antenna are observed (5.12); therefore the number of subcarriers required for coding is related instead to the maximum channel order. To achieve the design criteria of maximizing the diversity gain in a distributed system the following constraint has to be satisfied $N_c \geq \max\{L_{\mu\nu} + 1\}, \forall L_{\mu\nu}$; whilst for the DF protocol restricting to the channels observed in the second phase of the protocol $\mu \in \{R_1, \ldots R_{N_t}\}$.

It is possible to meet the rank criterion set out here by forming a space-frequency code, i.e. coding over a single OFDM frame $N_x = 1$ as suggested in [89], because the time dimension is not utilized limiting the maximum achievable rank of the summand $\Omega(p)\Delta(p)\Delta(p)^H\Omega(p)^H$ (5.30) to rank-1 coding across $N_c \geq N_t \max\{L_{\mu\nu} + 1\}$ would be required.

The proceeding PEP analysis grants valuable insight into the coding design for asynchronous cooperative relay networks which shall be leveraged for the proposed DF coding scheme presented in the next section.

5.4.1.2 Designs Based on Sub-Carrier Grouping

Sub-carrier grouping has been proposed to solve an array of problems ranging from multi-user interference elimination [34] to tackling the problem of PAPR fluctuations [93]. More relevant use of sub-carrier grouping is demonstrated in design of Grouped-STF (GSTF) proposed by Liu et. al. [90] which demonstrated simplification in the code design and reduces computational complexity in the decoding process at the receiver.

The design of GSTF codes is well documented in [90] so only a brief summary of the outcome is discussed here where the results have been adapted for the distributed case. Next the criteria for sub-channel grouping is derived which will enable the design of smaller GSTF codewords $\mathbf{X}_g$, $g = \{0, \ldots, N_g - 1\}$ where N_g defines the number of groups, with dimension much smaller than $\mathbf{X} \in \mathbb{C}^{N_t \times N_c N_x}$. To reduce the number of subcarriers needed per grouping it is necessary to code over multiple OFDM symbols in the time-domain, i.e. $N_x \geq N_t$, so that the full-rank can be extracted from each summand $\Omega(p)\Delta(p)\Delta(p)^H\Omega(p)^H$ in (5.30) [90]. Firstly, it was demonstrated in the preceding PEP analysis in Section 5.4.1 that to extract the maximum diversity available, coding over a minimum $L_g \geq \max\{L_{\mu,\nu} + 1\}$ subcarriers is necessary. To begin the following notation is introduced:

$$\bar{\Lambda}_{\nu,g} := \mathbf{B}_\nu^T \Lambda_{\nu,g} \mathbf{B}_\nu^* \in \mathbb{C}^{L_\nu \times L_\nu} \tag{5.41}$$

$$\Lambda_{\nu,g} := \sum_{l=0}^{L_g-1} \Omega_{\nu,g}(l)\Delta_g(l)\Delta_g(l)^H\Omega_{\nu,g}(l)^H \in \mathbb{C}^{L_\nu \times L_\nu} \tag{5.42}$$

$$\Omega_{\nu,g}(l) := \Omega_\nu(\mathbb{S}_g(l)) \in C^{L_\nu \times N_t} \tag{5.43}$$

$$\mathbf{\Delta}_g(p) := \mathbf{X}_g(p) - \mathbf{X}'_g(p) \in \mathbb{C}^{N_t \times N_x} \tag{5.44}$$

where $\mathbb{S}_g \subset \{0, \ldots, N_c - 1\}$ denotes the set of sub-carrier indices with cardinality $|\mathbb{S}_g| = L_g$ utilized in the gth GSTF codeword. To simplify the codeword design the sub-carrier sets are assumed to be orthogonal, i.e. $\mathbb{S}_g \cup \mathbb{S}_{g'} \in \emptyset$. It is clear that the dimensionality of (5.42) still enables full-diversity assuming $\Lambda_{\nu,g}$ is full-rank,

$$G_{g,\nu,d} = G_{\nu,d} \tag{5.45}$$
$$= r(\bar{\Lambda}_{\nu,g}) \tag{5.46}$$

In addition it is worth noting that the diversity gain of the proposed GSTF coding scheme does not depend upon the selection of L_g subcarriers that constitute the group.

Optimal sub-carrier grouping Again reiterating the design objective as one of obtaining maximal available diversity gain whilst maximizing coding gain. Firstly, reformulating the composite matrices of (5.30),

$$\Delta'_\mu := \begin{bmatrix} \Delta^1_\mu(0) & \cdots & \Delta^{N_x}_\mu(0) \\ \vdots & & \vdots \\ \Delta^1_\mu(N_c-1) & \cdots & \Delta^{N_x}_\mu(N_c-1) \end{bmatrix} \in \mathbb{C}^{N_c \times N_x} \tag{5.47}$$

$$\mathbf{\Delta}' := \begin{bmatrix} \Delta'_{R_1} & & \\ & \ddots & \\ & & \Delta'_{R_{N_t}} \end{bmatrix} \in \mathbb{C}^{(N_c N_t)\times(N_t N_x)} \tag{5.48}$$

$$\mathbf{\Omega}'_\nu := \begin{bmatrix} \mathbf{\Omega}'_{R_1\nu} & & \\ & \ddots & \\ & & \mathbf{\Omega}'_{R_{N_t}\nu} \end{bmatrix} \in \mathbb{C}^{L_\nu \times N_c N_t} \tag{5.49}$$

$$\mathbf{\Omega}'_{\mu\nu} := \left[\omega_{L_{\mu\nu}}(0), \ldots, \omega_{L_{\mu\nu}}(N_c-1)\right] \in \mathbb{C}^{(L_{\mu\nu}+1)\times N_c} \tag{5.50}$$

illustrates the dependance on the selection of sub-carriers in addition to giving insight into the optimal sub-channel grouping to maximize coding gain. At this stage it is worth remarking that after reformulation the relationship between the code construction and spatial-frequency dimensions is decoupled whilst retaining the equivalence to (5.30) as shown $\mathbf{\Lambda}_\nu = \mathbf{\Omega}'_\nu \mathbf{\Delta}' \mathbf{\Delta}'^H \mathbf{\Omega}'^H_\nu$. This reformulation will later be used in the PEP analysis under AF protocols discussed later in the chapter.

To facilitate an optimal sub-carrier grouping strategy the analysis (5.47)-(5.50) can be modified for use under GSTF coding,

$$\Lambda_{\nu,g} := \mathbf{\Omega}'_{\nu,g}\mathbf{\Delta}'_g\mathbf{\Delta}'^H_g\mathbf{\Omega}'^H_{\nu,g} \tag{5.51}$$

$$\Delta'_{\mu,g} := \begin{bmatrix} \Delta^1_\mu(\mathbb{S}_g(0)) & \cdots & \Delta^{N_x}_\mu(\mathbb{S}_g(0)) \\ \vdots & & \vdots \\ \Delta^1_\mu(\mathbb{S}_g(L_g-1)) & \cdots & \Delta^{N_x}_\mu(\mathbb{S}_g(L_g-1)) \end{bmatrix} \in \mathbb{C}^{L_g\times N_x} \tag{5.52}$$

$$\mathbf{\Delta}'_g := \begin{bmatrix} \Delta'_{1,g} & & \\ & \ddots & \\ & & \Delta'_{N_t,g} \end{bmatrix} \in \mathbb{C}^{L_gN_t\times N_tN_x} \tag{5.53}$$

$$\mathbf{\Omega}'_{\nu,g} := \begin{bmatrix} \mathbf{\Omega}'_{R_1\nu,g} & & \\ & \ddots & \\ & & \mathbf{\Omega}'_{R_{N_t}\nu,g} \end{bmatrix} \in \mathbb{C}^{L_\nu\times L_gN_t} \tag{5.54}$$

$$\mathbf{\Omega}'_{\mu\nu,g} := \left[\omega_{L_{\mu\nu}}(\mathbb{S}_g(0)),\ldots,\omega_{L_{\mu\nu}}(\mathbb{S}_g(L_g-1))\right] \in \mathbb{C}^{(L_{\mu\nu}+1)\times N_g} \tag{5.55}$$

Briefly considering the scenario of co-located antenna elements, under the common assumption $L_{\mu\nu} = L$, (5.54) reduces to a block diagonal matrix with common sub-matrices (5.55). Using the property for determinants of square matrices, $|\mathbf{AB}| = |\mathbf{A}||\mathbf{B}|$, implies that optimization the sub-carrier grouping in this framework is independent of the coding and therefore coding gain is increased when both determinants $|\mathbf{\Omega}'_\nu|$ and $|\mathbf{\Delta}'|$ are increased [90]. Now using the Leibniz formula and induction it is possible to express the relationship between the determinants,

$$|\mathbf{\Omega}'_{\nu,g}| = |\mathbf{\Omega}'_{\mu\nu,g}|^{N_t} \tag{5.56}$$

This implies that optimal sub-channel grouping can be achieved simply through the careful selection of sub-carriers to maximize $|\mathbf{\Omega}'_{\mu\nu,g}|$. To provide an achievable upper bound we adopt $|\mathbf{\Omega}'_{\mu\nu,g}|^2 = |\mathbf{\Omega}'_{\mu\nu,g}\mathbf{\Omega}'^H_{\mu\nu,g}|$, therefore because $\mathbf{V}_L\mathbf{V}_L^H$ is positive definite the inequality $|A| \leq \prod_{i=1}^N a_{ii}$ can be used where a_{ii} is the ith diagonal entry of the $N\times N$ positive definite matrix A. Clearly, the determinant is maximized by selecting L_g orthogonal subcarriers forming an orthogonal basis, this is achieved using $\mathbb{S}(l) := N_gl + g$ where $N_g = N_c/L$, $N_g \in \mathbb{Z}$ [90].

In the case of cooperative communications the target is to maximize $|\mathbf{\Lambda}_{\nu,g}|$ by judicious selection of sub-carriers for optimal grouping. Clearly, decoupling of the composite matrices to enable independent design of the difference (5.53) and sub-carrier grouping (5.54) matrices is not feasible in the scenario when (5.54) is non-square. Although the development of an optimal sub-carrier grouping strategy for cooperative communications is still an open research topic; a simple strategy is adopted that selects sub-carriers according to the spacing $N_g = N_c/L^{max}$ where $L^{max} := \max\{L_{\mu,\nu} + 1\}$. This selection is justified through the analysis in Section 2.3.2 when attempting to minimize the correlation between sub-carriers formulating a codeword group.

5.4.1.3 Deployment Guidelines

The following guidelines give a technical summary and guidance of the code design under DF protocols based on the knowledge gained under PEP analysis. They prove a useful framework for general code design in cooperative relay networks.

1. Coding over a single-subcarrier, effectively ST-coding, limits the achievable rank of the codeword; therefore only spatial (cooperative) diversity gains can be realized in multi-path channels.

2. To extract full-diversity from the frequency-selective cooperative relay channel under DF protocols, STF-coding is required over at least as many sub-carriers as the maximum channel order observed in the second phase of the protocol, i.e. requiring $N_c \geq \max_{\mu\nu}\{L_{\mu\nu} + 1\}$.

3. Under SF-coding where the codeword is constrained to the space-frequency dimensions, $N_x = 1$, it is required that coding be extended by a factor equalling the number of transmit antennas over that needed for STF-coding, i.e. $N_c \geq N_t \max_{\mu\nu}\{L_{\mu\nu} + 1\}$.

5.4.2 Distributed Quasi-Orthogonal Space-Time-Frequency Design

The objectives stated in Section 5.3.3 specifically guide the distributed-STF code design to maximise the coding gain whilst achieving maximal diversity gains.

The encoding architecture follows the two-stage inner- and outer-coding methodology and notation used by Giannakis et al. [90] as a basis for the following implementation.

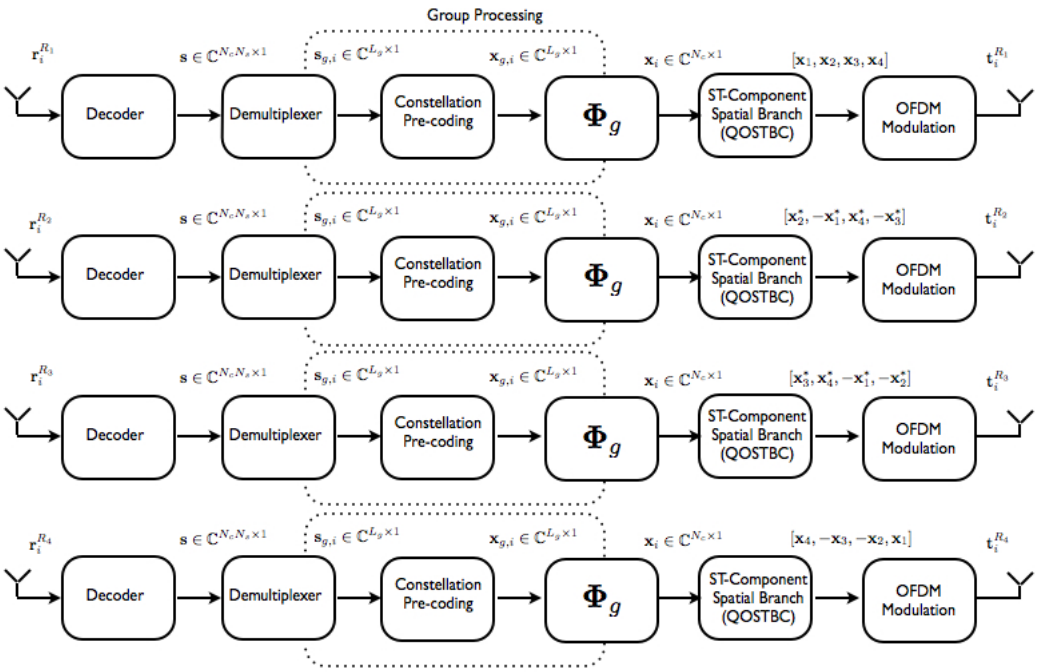

Figure 5.1: Distributed-QOSTBC STF-Coded VAA Encoding chain

The encoding chain at the r-MTs when operating using the DF is illustrated in Figure 5.1. Recall from (5.7) that individual r-MT participating in the VAA receive the broadcast symbols $\{\mathbf{r}_i^{R_j} \in \mathbb{C}^{J\times 1}, i = 1, \ldots, N_{x_s}, j = 1, \ldots, N_t\}$ from the s-MT. It is assumed that the r-MT individually detect the transmitted symbols stream $\mathbf{s} \in \mathbb{C}^{N_c N_{x_S} \times 1}$ without error, where $N_c N_{x_S} = N_I$ defines the number of information symbols to be transmitted from s-MT to d-MT. The symbol stream is then demultiplexed into the group symbol $\mathbf{s}_g$ into $\{\mathbf{s}_{g,i} \in \mathbb{C}^{Lg\times 1}, i = 1, \ldots, N_x\}$ where $\mathbf{s}_g := [\mathbf{s}_{g,1}^T, \ldots, \mathbf{s}_{g,N_x}^T]^T$ and $N_x = N_{x_s}$. Using constellation pre-coding to encode the information symbols over multiple sub-carriers harnesses the available multipath diversity offered by the cooperative channel. This is achieved using a square pre-coder $\mathbf{\Theta}_{LCF} \in \mathbb{C}^{L_g \times L_g}$, discussed in section 2.4.3.3, to obtain

$\mathbf{x}_{g,i} := \mathbf{\Theta}_{LCF}\mathbf{s}_{g,i}$. Assuming $\mathbf{e}(g,l) := [\mathbf{I}_{N_c}]_{N_g l+g} \in \mathbb{C}^{N_c\times 1}$ as the $(N_g l + g + 1)^{st}$ column of the $N_c \times N_c$ identity matrix $\mathbf{I}_{N_c}$. Then $\mathbf{\Phi}_g \in \mathbb{Z}^{N_c\times L_g}$ can be expressed as [90],

$$\mathbf{\Phi}_g := [e(g,0), e(g,1), \ldots, e(g, L_g - 1)] \tag{5.57}$$

This enables the grouped constellation pre-coded symbols to be mapped onto the full N_c subcarriers,

$$\mathbf{x}_i := \sum_{g=0}^{N_g-1} \mathbf{\Phi}_g \mathbf{x}_{g,i} \in \mathbb{C}^{N_c\times 1} \tag{5.58}$$

ST-component coding in the form of distributed-QOSTBC is then performed to extract cooperative diversity from the distributed relay channel. The justification for the design of the ST-component and constellation pre-coder are discussed in the next section.

5.4.2.1 Quasi-Orthogonal Space-Time Component Coding

In the design of a distributed-STF code utilising four transmit antennas it is proposed that the ST component coding adopts the CL-QOSTBC to orthogonalize the code. In the ensuing analysis, the ST-component code is designed firstly without knowledge of the constellation pre-coder, therefore knowledge regarding subcarrier grouping is irrelevant in the ensuing discussion and will be re-introduced in the next section. To simplify the analysis it is assumed $\mathbf{E}_{RD} = \mathbf{I}_{L_\nu}$ which enables (5.22) to be expressed as,

$$d^2(\mathbf{X}, \mathbf{X}') = \sum_{p=0}^{N_c-1} \|\tilde{\mathbf{H}}_{RD}(p)\mathbf{\Delta}(p)\|_F^2 \tag{5.59}$$

Assuming QOSTBC is used as the ST-component code then $\mathbf{\Delta}(p)$ can be defined as,

$$\mathbf{\Delta}(p) := \begin{bmatrix} \delta_1^{R_1}(p) & \left(\delta_2^{R_2}(p)\right)^* & \left(\delta_3^{R_3}(p)\right)^* & \delta_4^{R_4}(p) \\ \delta_2^{R_1}(p) & -\left(\delta_1^{R_2}(p)\right)^* & \left(\delta_4^{R_3}(p)\right)^* & -\delta_3^{R_4}(p) \\ \delta_3^{R_1}(p) & \left(\delta_4^{R_2}(p)\right)^* & -\left(\delta_1^{R_3}(p)\right)^* & -\delta_2^{R_4}(p) \\ \delta_4^{R_1}(p) & -\left(\delta_3^{R_2}(p)\right)^* & -\left(\delta_2^{R_3}(p)\right)^* & \delta_1^{R_4}(p) \end{bmatrix}^T \in \mathbb{C}^{N_t\times N_s} \tag{5.60}$$

where $\delta_i^{R_j}(p) := x_i^{R_j}(p) - \left(x_i^{R_j}(p)\right)'$. For all practical purposes it can be assumed $\delta_i(p) = \delta_i^{\mu}(p), \forall \mu \in \{R_1, \ldots, R_4\}$. However, (5.60) gives valuable insight as to how the code will be implemented across a VAA. It is possible to deconstruct (5.59) into receiver dependent terms,

$$d^2(\mathbf{X}, \mathbf{X}') = \sum_{\forall \nu} \sum_{p=0}^{N_c-1} \|\mathbf{h}_\nu(p)\mathbf{\Delta}(p)\|_2^2 \tag{5.61}$$

where $\mathbf{h}_\nu(p)$ is defined at the νth row of $\tilde{\mathbf{H}}_{RD}(p)$. Toker demonstrated in [48] that it is possible to orthogonalize the quasi-orthogonal MIMO channel using phase rotation of the transmitted signal implemented at the r-MTs designated as R_3 and R_4. This operation is expressed by inserting a phase rotation matrix $\mathbf{\Theta}_\nu(p)$ into (5.61),

$$d^2(\mathbf{X}, \mathbf{X}') = \sum_{\forall \nu} \sum_{p=0}^{N_c-1} \|\mathbf{h}_\nu(p)\mathbf{\Theta}_\nu(p)\mathbf{\Delta}(p)\|_2^2 \tag{5.62}$$

where $\mathbf{\Theta}_\nu(p) := diag\{1, 1, e^{j\theta_\nu(p)}, e^{j\theta_\nu(p)}\}$. Adopting the notation used for the STF code construction to index the space-frequency-domain channel coefficients $\mathbf{h}_\nu^\mu(p) \in \mathbb{C}$ then $\mathbf{h}_\nu(p) := [\mathbf{h}_\nu^{R_1}(p), \ldots, \mathbf{h}_\nu^{R_4}(p)]$. It is then possible to reformulate (5.62) by adopting an effective channel representation[1] here since OFDM enables the code to be represented as a layered ST system,

$$d^2(\mathbf{X}, \mathbf{X}') = \sum_{\forall \nu} \sum_{p=0}^{N_c-1} \|\delta(p)^T \mathbf{H}_{\nu,eff}(p)\|_2^2 \tag{5.63}$$

where $\delta(p) := [\delta_1(p), \ldots, \delta_4(p)]^T \in \mathbb{C}^{N_t \times 1}$ and $\mathbf{H}_{\nu,eff}(p)$ is defined according to,

$$\mathbf{H}_{\nu,eff}(p) := \begin{bmatrix} h_\nu^{R_1}(p) & -\left(h_\nu^{R_2}(p)\right)^* & -\left(\tilde{h}_\nu^{R_3}(p)\right)^* & \tilde{h}_\nu^{R_4}(p) \\ h_\nu^{R_2}(p) & \left(h_\nu^{R_1}(p)\right)^* & -\left(\tilde{h}_\nu^{R_4}(p)\right)^* & -\tilde{h}_\nu^{R_3}(p) \\ \tilde{h}_\nu^{R_3}(p) & -\left(\tilde{h}_\nu^{R_4}(p)\right)^* & \left(h_\nu^{R_1}(p)\right)^* & -h_\nu^{R_2}(p) \\ \tilde{h}_\nu^{R_4}(p) & \left(\tilde{h}_\nu^{R_3}(p)\right)^* & \left(h_\nu^{R_2}(p)\right)^* & h_\nu^{R_1}(p) \end{bmatrix}^T \in \mathbb{C}^{N_t \times N_x} \tag{5.64}$$

[1]Demonstrated in Section 2.4.3.2 for flat-fading channels

Note that the $\mathbf{\Theta}_\nu(p)$ has been encapsulated into (5.64) using the definitions $\tilde{h}_\nu^{R_3}(p) := h_\nu^{R_3}(p)e^{j\theta_\nu(p)}$ and $\tilde{h}_\nu^{R_4}(p) := h_\nu^{R_4}(p)e^{j\theta_\nu(p)}$. Recalling from Section 2.4.3.2 that a characteristic of QOSTBC when represented in effective channel form $\mathbf{H}_{\nu,eff}(p)$ is shown as,

$$\mathbf{H}_{\nu,eff}(p)\mathbf{H}_{\nu,eff}^H(p) := \begin{bmatrix} \gamma_\nu(p) & & & \alpha_\nu(p) \\ & \gamma_\nu(p) & -\alpha_\nu(p) & \\ & -\alpha_\nu(p) & \gamma_\nu(p) & \\ \alpha_\nu(p) & & & \gamma_\nu(p) \end{bmatrix}^T \in \mathbb{C}^{N_t \times N_t} \tag{5.65}$$

where,

$$\gamma_\nu(p) := \sum_{\mu \in \{R_1,\ldots,R_4\}} |h_\nu^\mu(p)|^2 \tag{5.66}$$

$$\begin{aligned} \alpha_\nu(p) &:= 2\Re\left\{h_\nu^{R_1}(p)\left(\tilde{h}_\nu^{R_4}(p)\right)^* - h_\nu^{R_2}(p)\left(\tilde{h}_\nu^{R_3}(p)\right)^*\right\} && (5.67) \\ &= 2\Re\left\{h_\nu^{R_1}(p)\left(h_\nu^{R_4}(p)e^{j\theta_\nu(p)}\right)^* - h_\nu^{R_2}(p)\left(h_\nu^{R_3}(p)e^{j\theta_\nu(p)}\right)^*\right\} && (5.68) \end{aligned}$$

Toker demonstrated [48] that it is possible to calculate $\theta_\nu(p)$ to cancel the interference terms $\alpha_\nu(p)$ (5.67) by equating,

$$\Re\left\{h_\nu^{R_1}(p)\left(h_\nu^{R_4}(p)e^{j\theta_\nu(p)}\right)^*\right\} = \Re\left\{h_\nu^{R_2}(p)\left(h_\nu^{R_3}(p)e^{j\theta_\nu(p)}\right)^*\right\} \tag{5.69}$$

Interestingly, Toker also made the observation [48, Eq. 3.75] that it is possible to cancel the interference terms by solving the following expression with a common phasor $\theta(p)$ represented by,

$$\mathbf{\Theta}(p) := diag\{1, 1, e^{j\theta(p)}, e^{j\theta(p)}\} \tag{5.70}$$

at the transmitter that is not tailored for the MISO channel to individual d-MT receiver antenna ν,

$$\Re\left\{\sum_{\forall\nu} h_\nu^{R_1}(p)\left(h_\nu^{R_4}(p)e^{j\theta(p)}\right)^*\right\} = \Re\left\{\sum_{\forall\nu} h_\nu^{R_2}(p)\left(h_\nu^{R_3}(p)e^{j\theta(p)}\right)^*\right\} \tag{5.71}$$

Adopting $\hat{\theta}(p)$ as the solution to (5.71) allows (5.63) to be expressed as,

$$d^2(\mathbf{X}, \mathbf{X}')|_{\theta(p)=\hat{\theta}(p)} = \sum_{\forall \nu} \sum_{p=0}^{N_c-1} \|\delta(p)^T \mathbf{H}_{\nu,eff}(p)\|_2^2 \tag{5.72}$$

$$= \sum_{p=0}^{N_c-1} \gamma(p) \sum_{i=1}^{N_x} |\delta_i(p)|^2 \tag{5.73}$$

where,

$$\gamma(p) := \sum_{\forall \nu} \gamma_\nu(p) \tag{5.74}$$

assuming the interference terms $\alpha_\nu(p)$ are cancelled from (5.65) when $\hat{\theta}(p)$ is adopted. The difference equation (5.73), as alluded to in [90], leads to the design criteria and code construction of the outer- constellation pre-coder used to extract multi-path diversity from the cooperative relay channel.

5.4.2.2 Constellation Precoding

The detailed construction of the constellation pre-coder shall not be pursued here as this has been eloquently demonstrated in [39] [1]. However the design criteria are briefly reviewed for completeness from the originally proposed STF coding [90].

Deconstructing the linear pre-coder into a series of row vectors, $\mathbf{\Theta}_{LCF} := [\theta_0, \ldots, \theta_{L_g-1}]^T$,

$$\mathbf{x}_{g,i} = \theta_l^T \mathbf{s}_{g,i} \tag{5.75}$$

where $\theta_l^T \in \mathbb{C}^{1\times L_g}$ is the lth row of $\mathbf{\Theta}_{LCF}$. Using (5.75) to rewrite (5.73) expresses the difference matrix using the pre-coder notation with respect to a specific group as,

$$d^2(\mathbf{X}_g, \mathbf{X}'_g) = \sum_{l=0}^{L_g-1} \gamma(\mathbb{S}_g(l)) \sum_{i=1}^{N_x} |\theta_l^T(\mathbf{s}_{g,i} - \mathbf{s}'_{g,i})|^2 \tag{5.76}$$

[1] Some of the background material can be found in Section 2.4.3.3.

which facilitates the design of a pre-coder that maximizes diversity and coding gains. An intuitive design metric using the arithmetic-geometric mean inequality yields a lower bound of (5.76) by,

$$d^2(\mathbf{X}_g, \mathbf{X}'_g) \geq \sum_{l=0}^{L_g-1} \gamma(\mathbb{S}_g(l)) N_x \prod_{i=1}^{N_x} |\theta_l^T(\mathbf{s}_{g,i} - \mathbf{s}'_{g,i})|^{\frac{2}{N_x}} \tag{5.77}$$

$$\geq L_g N_x^{L_g} \prod_{l=0}^{L_g-1} \gamma(\mathbb{S}_g(l)) \prod_{i=1}^{N_x} |\theta_l^T(\mathbf{s}_{g,i} - \mathbf{s}'_{g,i})|^{\frac{2}{N_x L_g}} \tag{5.78}$$

The inequality is satisfied when $|\theta_p^T(\mathbf{s}_{g,i} - \mathbf{s}'_{g,i})|^2 = |\theta_p^T(\mathbf{s}_{g,i'} - \mathbf{s}'_{g,i'})|^2, \forall i \neq i'$ and $\gamma(\mathbb{S}_g(l)) = \gamma(\mathbb{S}_g(l')), \forall l \neq l'$. Clearly, in the presence of AWGN the Symbol Error Rate (SER) performance of the proposed code is dominated by the distance metric $d^2(\mathbf{X}, \mathbf{X}')$ pertaining to codewords with the minimum Euclidean spacing. The optimal STF codeword is the solution of a max-min problem over all possible $\mathbf{s}_{g,i} \neq \mathbf{s}'_{g,i'}$; therefore the design problem reduced to maximizing the lower bound (5.77). The problem of designing $\mathbf{\Theta}_{LCF}$ to maximize,

$$\min_{\forall \mathbf{s}_{g,i} \neq \mathbf{s}_{g,i'}} \prod_{i=1}^{N_x} |\theta_p^T(\mathbf{s}_{g,i} - \mathbf{s}'_{g,i})|^{\frac{2}{N_x}} \tag{5.79}$$

has been considered in [94], [95] and [39] to construct constellation pre-coders for flat-fading channels. The construction of such codes are detailed in Section 2.4.3.3 and will therefore not be discussed further here. Interestingly these codes can only be considered optimal assuming $\gamma(\mathbb{S}_g(l)) = \gamma(\mathbb{S}_g(l')), \forall l \neq l'$; however simulation studies demonstrate the error-rate performance of utilizing this coding strategy in cooperative networks.

5.4.2.3 Decoding QOSTBC Enabled STF Codes

As with most communication decoding chains the encoding process is reversed by applying the inverse in reverse order. Without loss of generality it is assumed for the following decoder description is only applied to the group defined by the index $g \in \{1, \ldots, N_g\}$. It is trivial to extrapolate to the other group since apart from de-mapping the symbols by reversing $\mathbf{\Phi}_g$ all other processing steps are common amongst the various code groups.

The processing steps for decoding the distrubted-QOSTBC enabled STF code can be categorized as,

1. De-mapping onto grouped STF codewords: De-map the group-STF coded symbols from the received OFDM symbol.
2. ST-component decoding: Perform linear combining via matched filtering with the effective QOSTBC MIMO channel to decouple the subsystems.
3. Pre-whitening: For each sub-system perform a pre-whitening of the noise after combining.
4. Sphere-Decoding:Recover the original symbols transmitted by the s-MT using ML decoding (or the near-optimal sphere decoding algorithm).

The previous steps are now discussed in some detail.

De-mapping onto grouped STF codewords At the d-MT the STF encoded received signal (5.11) can be expressed in vector notation $\mathbf{y}_i^\nu := [y_i^\nu(0), \ldots, y_i^\nu(N_c - 1)]^T \in \mathbb{C}^{N_c \times 1}$ for the ith received OFDM symbol. It is then possible to define the observe symbols for a particular codeword group using the following de-mapping,

$$\mathbf{y}_{g,i}^\nu = \mathbf{\Phi}_g^T \mathbf{y}_i^\nu \in \mathbb{C}^{L_g \times 1} \tag{5.80}$$

where $\mathbf{y}_{g,i}^\nu := [y_{g,i}^\nu(0), \ldots, y_{g,i}^\nu(L_g - 1)]^T \in \mathbb{C}^{L_g \times 1}$. The ST-component decoding may now be performed on the de-mapped symbols.

ST-component decoding The de-mapped symbols are now decoupled into two effective sub-systems using a linear combining approach based on matched filtering. The ST-component decoding is implemented in the space-time dimension therefore the following notation is adopted $\mathbf{y}_g^\nu(l) := [y_{g,1}^\nu(l), \ldots, y_{g,N_x}^\nu(l)]^T \in \mathbb{C}^{N_x \times 1}$. For $l \in \{0, \ldots, L_g - 1\}$ and $\nu \in \{D_1, \ldots, D_{N_r}\}$ the following linear combining is applied,

$$\mathbf{z}_g^\nu(l) = \mathbf{H}_{\nu,eff}^H(\mathbb{S}_g(l))\tilde{\mathbf{y}}_g^\nu(l) \in \mathbb{C}^{N_x \times 1} \tag{5.81}$$

where the observations from the 2nd and 3rd time-slots are conjugated

$$\tilde{\mathbf{y}}_g^{\nu}(l) := [y_{g,1}^{\nu}(l), \left(y_{g,2}^{\nu}(l)\right)^*, \left(y_{g,3}^{\nu}(l)\right)^*, y_{g,4}^{\nu}(l)]^T \tag{5.82}$$

and using (5.64) with the specific sub-carrier indexing $\mathbb{S}_g(l) := N_g l + g$. The filtered observations $\mathbf{z}_g^{\nu}(l)$ can now be combined using an MRC over all receive antenna,

$$\mathbf{z}_g(l) := \sum_{\forall \nu} \mathbf{z}_g^{\nu}(l) \in \mathbb{C}^{N_x \times 1} \tag{5.83}$$

Assuming that the post constellation pre-coded symbols (5.75) can be defined in vector notation as $\mathbf{x}_g(l) := [x_{g,1}(l), \ldots, x_{g,N_x}(l)]^T \in \mathbb{C}^{N_x \times 1}$ then substituting (5.81) into (5.83) results in the ST-component decoded representation,

$$\mathbf{z}_g(l) = \sum_{\forall \nu} \mathbf{H}_{\nu,eff}^H(\mathbb{S}_g(l))\tilde{\mathbf{y}}_g^{\nu}(l) \tag{5.84}$$

$$= \sum_{\forall \nu} \mathbf{A}_{g,\nu}(l)\mathbf{x}_g(l) + \tilde{\mathbf{w}}_g^{\nu}(l) \tag{5.85}$$

where $\mathbf{A}_{g,\nu}(l) := \mathbf{H}_{\nu,eff}^H(\mathbb{S}_g(l))\mathbf{H}_{\nu,eff}(\mathbb{S}_g(l))$ according to (5.65) can be deconstructed as,

$$\mathbf{A}_{g,\nu}(l) := \begin{bmatrix} \gamma_\nu(\mathbb{S}_g(l)) & & & \alpha_\nu(\mathbb{S}_g(l)) \\ & \gamma_\nu(\mathbb{S}_g(l)) & -\alpha_\nu(\mathbb{S}_g(l)) & \\ & -\alpha_\nu(\mathbb{S}_g(l)) & \gamma_\nu(\mathbb{S}_g(l)) & \\ \alpha_\nu(\mathbb{S}_g(l)) & & & \gamma_\nu(\mathbb{S}_g(l)) \end{bmatrix} \in \mathbb{C}^{N_t \times N_t} \tag{5.86}$$

with effective noise component $\tilde{\mathbf{w}}_g^{\nu}(l) := \mathbf{H}_{g,\nu,eff}^H(l)\mathbf{w}_g^{\nu}(l)$ represented as $\mathbf{w}_g^{\nu}(l) := [\mathbf{w}_1^{\nu}(\mathbb{S}_g(l)), \ldots, \mathbf{w}_{N_x}^{\nu}(\mathbb{S}_g(l))] \in \mathbb{C}^{N_x \times 1}$ according to the generic signal model (5.11). Of relevance particularly when adopting QOSTBC as the ST-component code is the characteristic that (5.86) also represents the noise covariance matrix [48],

$$E\{\tilde{\mathbf{w}}_g^{\nu}(l)(\tilde{\mathbf{w}}_g^{\nu}(l))^H\} = N_0\mathbf{A}_{g,\nu}(l) \in \mathbb{C}^{N_x \times N_x} \tag{5.87}$$

This statistic is important in pre-whitening of (5.84) required prior to ML-decoding using the Sphere-Decoding algorithm. Importantly, in simplifying the ML-search performed by the sphere-decoder (5.84) can be decomposed into two independent sets determined by the sparsity pattern of (5.86),

$$\begin{bmatrix} z_{g,1}(l) \\ z_{g,4}(l) \end{bmatrix} = \begin{bmatrix} \gamma(\mathbb{S}_g(l)) & \alpha(\mathbb{S}_g(l)) \\ \alpha(\mathbb{S}_g(l)) & \gamma(\mathbb{S}_g(l)) \end{bmatrix} \begin{bmatrix} x_{g,1}(l) \\ x_{g,4}(l) \end{bmatrix} + \begin{bmatrix} \tilde{w}_{g,1}(l) \\ \tilde{w}_{g,4}(l) \end{bmatrix} \tag{5.88}$$

$$\mathbf{z}_{g,14}(l) = \mathbf{A}_{g,14}(l)\mathbf{x}_{g,14}(l) + \tilde{\mathbf{w}}_{g,14}(l) \tag{5.89}$$

and,

$$\begin{bmatrix} z_{g,2}(l) \\ z_{g,3}(l) \end{bmatrix} = \begin{bmatrix} \gamma(\mathbb{S}_g(l)) & -\alpha(\mathbb{S}_g(l)) \\ -\alpha(\mathbb{S}_g(l)) & \gamma(\mathbb{S}_g(l)) \end{bmatrix} \begin{bmatrix} x_{g,2}(l) \\ x_{g,3}(l) \end{bmatrix} + \begin{bmatrix} \tilde{w}_{g,2}(l) \\ \tilde{w}_{g,3}(l) \end{bmatrix} \tag{5.90}$$

$$\mathbf{z}_{g,23}(l) = \mathbf{A}_{g,23}(l)\mathbf{x}_{g,23}(l) + \tilde{\mathbf{w}}_{g,23}(l) \tag{5.91}$$

The noise pre-whitening shall be performed independently on the symbol sets dictated above.

Noise pre-whitening As detailed in [48] the ST-component decoding at this stage has separated the grouped-STF codeword into two distinct set denoted by (5.89) and (5.91). The covariance matrices for $\tilde{\mathbf{w}}_{g,14}(l)$ and $\tilde{\mathbf{w}}_{g,23}(l)$ are,

$$\Sigma_{g,14}(l) := N_0\mathbf{A}_{g,14}(l) \in \mathbb{C}^{N_x/2\times N_x/2} \tag{5.92}$$

and,

$$\Sigma_{g,23}(l) := N_0\mathbf{A}_{g,23}(l) \in \mathbb{C}^{N_x/2\times N_x/2} \tag{5.93}$$

The whitened matched filter processed versions of (5.89) and (5.91) are expressed as,

$$\tilde{\mathbf{z}}_{g,14}(l) = \Sigma_{g,14}^{-\frac{1}{2}}(l)\mathbf{z}_{g,14}(l) \tag{5.94}$$

and,

$$\tilde{\mathbf{z}}_{g,23}(l) = \Sigma_{g,23}^{-\frac{1}{2}}(l)\mathbf{z}_{g,23}(l) \tag{5.95}$$

where the effective noise component now follow distribution $\mathcal{N}_{\mathbb{C}}(0, \mathbf{I}_{N_x/2})$.

ML-decoding After the previous processing stages are completed there still exists some coupling within the temporal dimension, exemplified in (5.89)-(5.91), as a characteristic of QOSTBC which is not evident in orthogonal designs originally investigated for STF coding [90]. Where QOSTBC has been traditionally adopted for flat-fading channels this required an ML-search over pairwise symbols [11]. For simplicity the ensuing analysis will only describe the ML-search over the decoupled set denoted by the temporal dimension $i \in \{1, 4\}$. The analysis is easily generalized to the independent ML-search over the decoupled set denoted by the temporal dimension $i \in \{2, 3\}$ in addition to independent ML-searches for each grouped-STF codeword required to detect all the symbols transmitted from the s-MT.

With regard to the encoding process and decoding steps previously described; the ML-search is performed to satisfy the decoding metric,

$$\hat{\mathbf{s}}_{g,14} = \arg \min_{\hat{\mathbf{s}}_{g,14} \in \mathbb{S}^{2L_g \times 1}} \|\tilde{\mathbf{z}}_{g,14} - \tilde{\mathbf{H}}_{g,14}\hat{\mathbf{s}}_{g,14}\|_2^2 \tag{5.96}$$

where the observation $\tilde{\mathbf{z}}_{g,14} := [\mathbf{z}_{g,14}^T(0), \ldots, \mathbf{z}_{g,14}^T(L_g - 1)]^T \in \mathbb{C}^{2L_g \times 1}$ is defined from (5.94) and $\tilde{\mathbf{H}}_{g,14} := \tilde{\mathbf{A}}_{g,14}\mathbf{\Phi}_{QOSTBC}\tilde{\mathbf{\Theta}}_{LCF}$ which can be decomposed with the following definitions,

$$\tilde{\mathbf{A}}_{g,14} = \begin{bmatrix} \mathbf{A}_{g,14}(0) & & & \\ & \mathbf{A}_{g,14}(1) & & \\ & & \ddots & \\ & & & \mathbf{A}_{g,14}(L_g - 1) \end{bmatrix} \tag{5.97}$$

$$\mathbf{\Phi}_{QOSTBC} = \begin{bmatrix} 1 & & & & & 0 & & & \\ & 0 & & & & & 1 & & \\ & & 1 & & & & & 0 & \\ & & & \ddots & & & & & \ddots \\ & & & & 0 & & & & 1 \end{bmatrix} \tag{5.98}$$

$$\tilde{\mathbf{\Theta}}_{LCF} = \begin{bmatrix} \mathbf{\Theta}_{LCF} & \\ & \mathbf{\Theta}_{LCF} \end{bmatrix} \tag{5.99}$$

With the effective-MIMO channel established then ML or near-ML decoding algorithms can be employed, including: Lattice Reduction Algorithm (LRA) [96],

Probabilistic Data Association Algorithm (PDA) [97] and relaxed convex optimization approaches based on Semi-Definite Programming (SDP) [98]. However, the numerical simulations are based on adopting a SDA [40] because it is capable of returning the exact-ML solution and has a useful trade-off in error performance against complexity [40].

5.4.3 Numerical Simulations

Case Study 27: Figure 5.2 depicts the SER against SNR [dB] for a set of distributed-GSTF codes. The GSTF consists of an inner and outer code. The inner code is formulated using a set of OSTBCs and QOSTBC to extract the spatial diversity available from the channel, the outer code is based on LCFC designs. The case study focuses on a network configuration where the s-MT and d-MT operate a single antenna; the virtual antenna array operating under a DF protocol comprises of a variable number of r-MTs depending on the ST-coding component employed. For simplicity it is assumed that all participating r-MTs decode the data without error. In this configuration the channel order observed between each r-MT and the d-MT is the same length: this is characteristic of channels observed when the transmit antenna array is co-located. The number of sub-carriers is set to $N_c = 64$ for all schemes.The simulations assume $L = 1$ for all multi-ray sub-channels and this is adopted for all schemes. In additional all multi-rays are assumed to be uncorrelated with a flat Power Delay Profile (PDP).

Depicted are the following cases: (1) 2TX-Alamouti, (2) 4TX-OSTBC (Half-Rate), (3)4TX-QOSTBC (Open-Loop) , (4) 4TX-QOSTBC (Closed-Loop, full CSI). To facilitate a comparison of the coding schemes; QPSK modulation is assumed with the exception of the half-rate OSTBC where 16-QAM modulation is employed to compensate for the reduced rate. It can be observed that in the SNR range simulated the higher order modulation scheme adopted for half-rate OSTBC significantly impacts the SER performance throughout the SNR region illustrated. However, the extra diversity gain offered by employing four transmit antennas as opposed to two with the Alamouti variant steepens the gradient over Alamouti as expected in the high-SNR region ($\geq$ 10 dB). Clearly, when QOSTBC is adopted the diversity gain achieved is greater than an Alamouti based scheme because of the additional transmit antenna, and therefore spatial

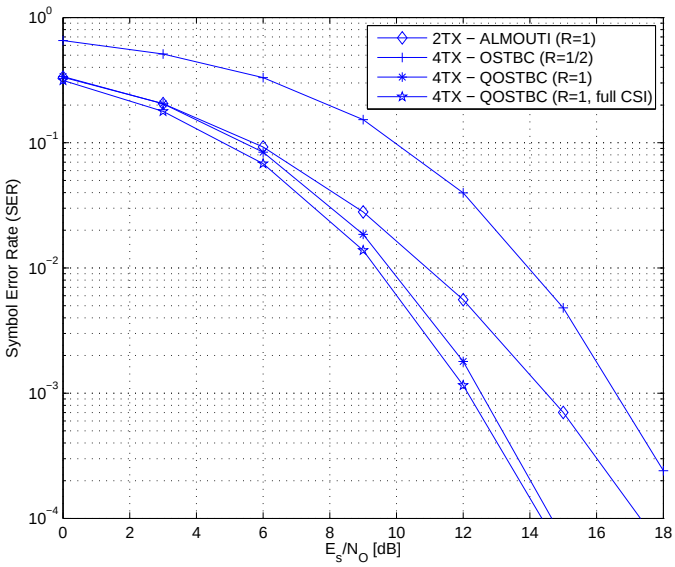

Figure 5.2: Symbol Error Rate vs SNR for distributed-GSTF codes based on various OSTBCs & QOSTBCs Space-Time component codes under DF relaying

degrees of freedom, available. Interestingly, it can be observed that when LCFC pre-coding is employed the open-loop QOSTBC based implementation achieves the full-diversity offered by the distributed MISO channel; as is demonstrated by comparing the gradient with the QOSTBC scheme which leverages CSI according to Toker [26] (full CSI). The additional design effort, facilitated by PEP analysis, to maximize the coding is evident in the outperformance of the QOSTBC schemes when feedback based on CSI at the d-MT is utilized.

Case Study 28: Figure 5.3 depicts the SER against SNR [dB] for a set of distributed-GSTF codes with varying degrees of feedback between the r-MTs and d-MT. Illustrated are the following cases: (1) 4TX-QOSTBC (Open-Loop), (2) 4TX-QOSTBC (Closed-Loop, partial CSI), (3) 4TX-QOSTBC (Closed-Loop, full CSI).This case study adopts the same network architecture previously used with the emphasis on observing the SER vs SNR when the feedback is quantized. Using Toker's scheme [26] to orthogonalize the MIMO channel, it is infeasible to feedback the precise value of the phase angle in the range $[\pi/2, \pi/2)$ with, for example, fixed or floating point resolution requires very large feedback overhead.

Therefore, the phase angles should be quantized before feedback. To simplify the quantization strategy the simulation is based in that proposed by Lambotharan et al. for broadband access networks [99], which is summarized briefly.

Firstly, a group is composed of K number of consecutive subcarriers and one quantized phase angle is proposed to feedback for each group. instead of feeding back the phase angle for each subcarrier. The phase angle required for each group is determined based on the majority of phase angles within that group. Suppose K feedback bits are available per subcarrier. Defining a set of quantized phase angles as,

$$\Omega = \{\pm\frac{\pi}{2^{K+1}}(2n-1), n = 1, 2, \ldots, 2^{K-1}\} \tag{5.100}$$

The quantized phase angle feedback can be determined as,

$$\theta_k = \arg\min_{\hat{\theta}_k} \Re\{\left(\mathbf{h}_{1,k}\mathbf{h}_{4,k}^* - \mathbf{h}_{2,k}\mathbf{h}_{3,k}^*\right) e^{-j\hat{\theta}_k}\} \tag{5.101}$$

Within a group a the required phase rotations θ_k are calculated per subcarrier. Then a simple voting methodology is applied where the phase angle to be applied across the group is the majority winner.

In Figure 5.3 both sub-carrier grouping and quantization of the phase rotators is applied. It is assumed that the 64 subcarriers used in the simulation study are sub-divided into groups consisting of eight sub-carriers for illustrative purposes. The phase rotation applied for each group is determined from one-bit. Figure 5.4, exemplifies the phase selections against the idea case assuming no-limitations on the feedback channel. The results demonstrate that only a coarse selection is made with significant deviation from the idea phase rotations calculated per sub-carrier at the transmit-side. The robustness of the scheme to these errors is attested to in Figure 5.3; where little deviation is observed comparing the case under quantization (partial CSI) and the idea case where no quantization or grouping is implemented (full CSI). When referring to partial CSI in the remaining simulations studies in this chapter, it is assumed that the quantization and grouping parameters remain the same as those used in this study for the purposes of comparison.

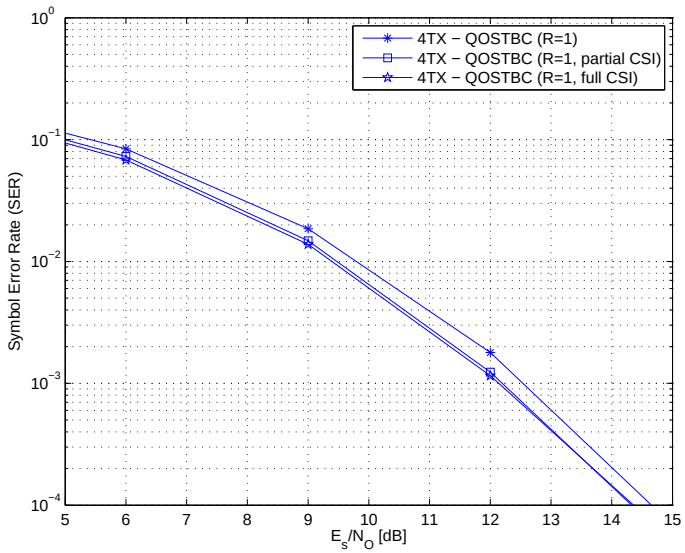

Figure 5.3: Symbol Error Rate vs SNR for distributed-GSTF codes based on QOSTBCs Space-Time component codes with partial CSI

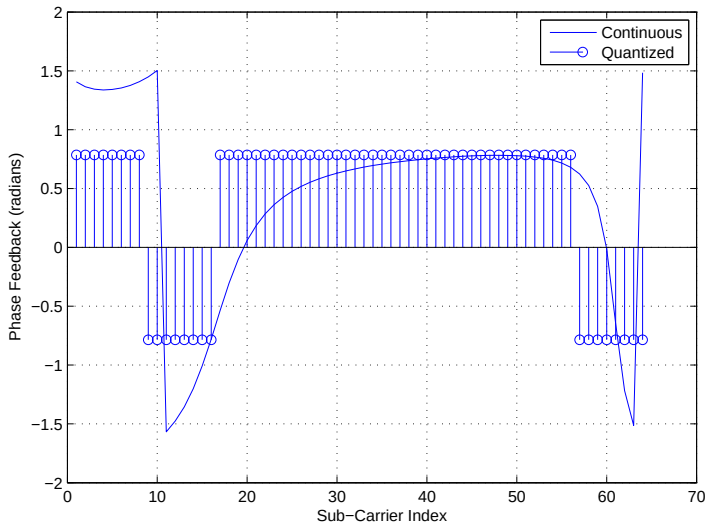

Figure 5.4: Phase Angle Feedback vs Sub-carrier Index for distributed-GSTF codes based on QOSTBCs Space-Time component codes

Case Study 29: Figure 5.5 depicts the SER against SNR [dB] for a set of distributed-GSTF codes with the additional aspect of channel correlation in the spatial dimension. Highlighted are the following distributed-STF coding schemes with various different ST component coding: (1) 2TX-Alamouti, (2) 4TX-OSTBC (Half-Rate), (3)4TX-QOSTBC (Open-Loop), (4) 4TX-QOSTBC (Closed-Loop, full CSI). Note that QOSTBC with quantized feedback has been included in the study and adopts that same quantization parameterization used previously. Again for comparison the network and coding parameters remain constant from previous studies: $N_c = 64$, $L = 1$. To illustrate the error performance of the different diversity schemes under channel correlation; the correlation coefficients used in the Long Term Evolution (LTE) standards are assumed [100, pg. 493] and generate the following correlation matrices

$$\begin{bmatrix} 1 & \alpha \\ \alpha^* & 1 \end{bmatrix} \tag{5.102}$$

$$\begin{bmatrix} 1 & \alpha^{\frac{1}{9}} & \alpha^{\frac{4}{9}} & \alpha \\ \alpha^{\frac{1}{9}*} & 1 & \alpha^{\frac{1}{9}} & \alpha^{\frac{4}{9}} \\ \alpha^{\frac{4}{9}*} & \alpha^{\frac{1}{9}*} & 1 & \alpha^{\frac{1}{9}} \\ \alpha^* & \alpha^{\frac{4}{9}*} & \alpha^{\frac{1}{9}*} & 1 \end{bmatrix} \tag{5.103}$$

for two and four transmit antennas respectively assuming a correlation coefficient of α. The top plot in Figure 5.5 illustrates coding performance with a correlation coeffficient $\alpha = 0.3$ whilst the bottom plot is generated under $\alpha = 0.9$.

Introducing correlation at the transmit side, normally associated with the r-MTs being spaced no more than a few wavelengths apart, degrades the achievable spatial diversity gain offered by the channel. Clearly, Figure 5.5 demonstrates this when comparing the degraded SER performance of any depicted scheme with increasing channel correlation. Interestingly in this particular the Alamouti scheme demonstrates robustness to correlation; however this manifests as the results of the correlation model adopted in the correlation matrix which assumes closer spacing of antenna elements when the order is increased. The main observation from this study demonstrates the attractiveness of increasing the number of transmit antennas in a distributed system that suffers less from the effects of correlation over more conventional co-located counterparts. Finally, Figure 5.5 shows clearly that the additional coding gain offered by using a Toker based

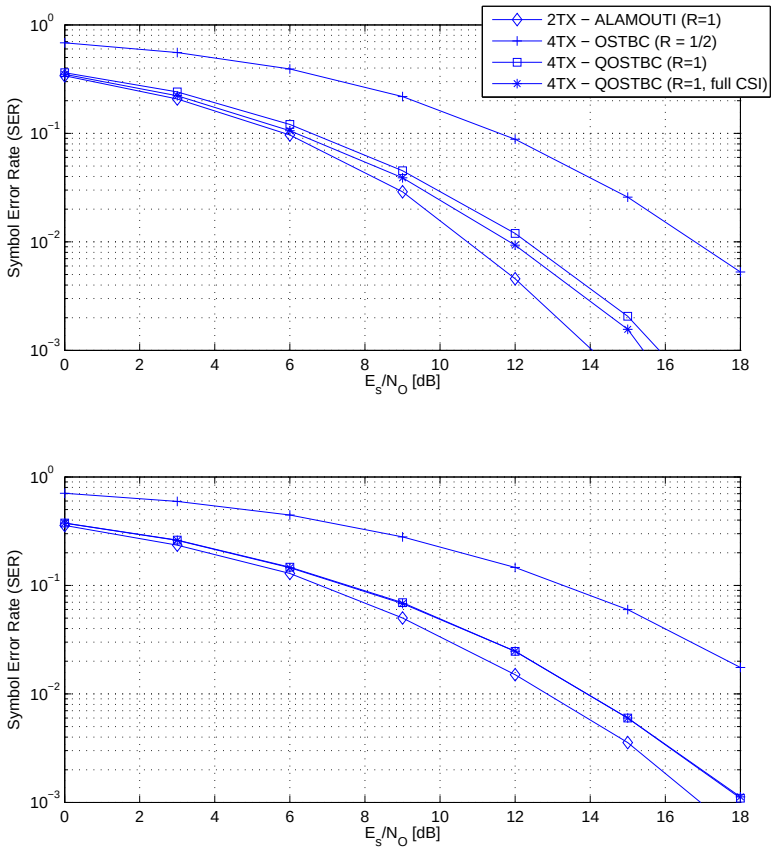

Figure 5.5: Symbol Error Rate vs SNR for distributed-GSTF codes based on QOSTBCs Space-Time component codes with in the presence of channel correlation

CL-QOSTBC reduces over the open-loop QOSTBC scheme with increasing correlation and therefore demonstrates the employability in distributed relay networks.

Case Study 30: Depicted in Figure 5.6 is the SER versus the normalized power of the first link $\bar{\gamma}_1$ over various distributed schemes at SNR of 10dB. Again for comparison the network and coding parameters remain constant from previous studies: $N_c = 64$, $L = 1$. The simulation study replicates Figure 3.15 in Chapter 3 that demonstrated the robustness of various coding schemes to distributed shadowing and path-loss effects. The channel powers of the remaining sub-channel

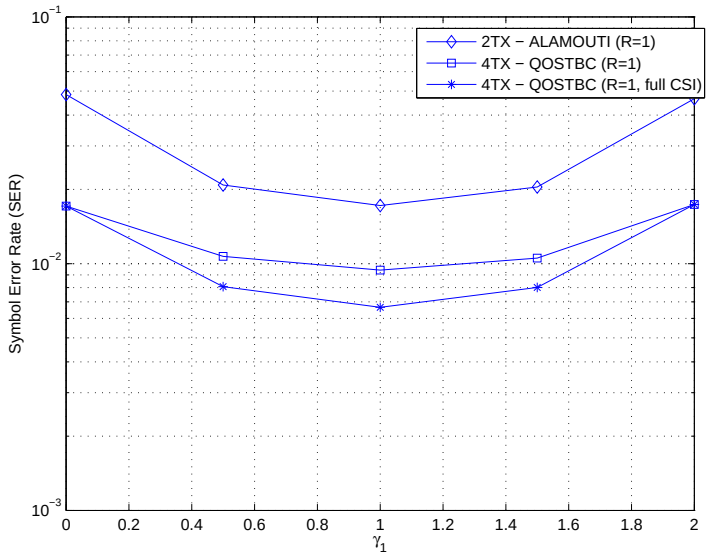

Figure 5.6: Symbol Error Rate vs SNR for distributed-GSTF codes based on QOSTBCs Space-Time component codes with sub-channel gain imbalances

vary inversely to the first link, reproducing a scenario where one sub-channel experiences severe shadowing. Therefore to maintain equivalence amongst schemes the constraint $\sum_{i=1}^{N_t} \bar{\gamma}_i = N_t$; which translates for the Alamouti code to $\bar{\gamma}_2 = 2 - \bar{\gamma}_1$ and the remaining four transmit antennas are satisfied by $\bar{\gamma}_4 = \bar{\gamma}_1$ and $\bar{\gamma}_3 = \bar{\gamma}_2$. Clearly, Figure 5.6 demonstrates the robust SER performance of both Alamouti and QOSTBCs. Specifically the Alamouti code only varied in the SER probability by 0.04 whilst QOSTBCs varied by 0.01. As was the case in non-ergodic channels, Figure 3.15, it is worth noting that the performance benefits of using Toker's scheme in the distributed scenario are marginalized compared to the open-loop equivalent scheme when the sub-channels experience more than marginal imbalancing.

Case Study 31: Depicted in Figure 5.7 is the SER versus SNR assuming open-loop QOSTBC is adopted for the ST-component coding. In this simulation study it is assumed that maximum channel order corresponds to $L = 1$. Here the robustness of the proposed distributed-STF code is examined in situations where the channel orders vary. Specifically the familiar *Co-located* case assumes all

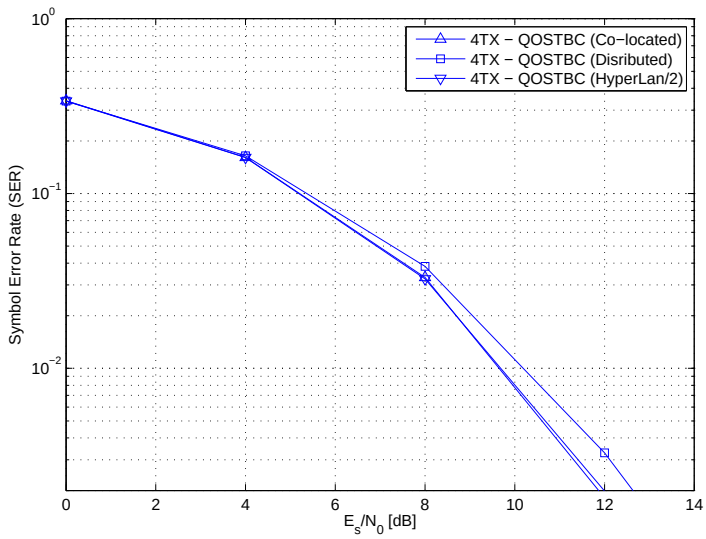

Figure 5.7: Symbol Error Rate vs SNR for distributed-GSTF codes based on open-loop QOSTBCs Space-Time component codes with various sub-channel orders

the sub-channels are of length $L = 1$ as demonstrated in previous studies and provides a benchmark for comparison.

The *Distributed* case is examined assuming $L = 1$ from relay nodes $\{R_1, R_2\}$ and $L = 0$ from relay nodes $\{R_3, R_4\}$. Clearly, there is a loss in diversity gain over the co-located case resulting from the loss of diversity offered from the sub-channels associated with R_3 and R_4. This case is of interest in cooperative deployments and demonstrates the effectiveness of pre-coding to extract the available multi-path diversity offered by some sub-channels.

The *HiperLan/2* case is examined assuming $L = 7$ on all sub-channels. In this simulations study the HiperLan/2 channel model is used to define the channel lengths; although associated doppler, correlation and power profiles are not adopted to simplify the anaysis. Interestingly, without coding over additional sub-carriers and only designing the constellation pre-coder based on the assumption $L = 1$ does not extract the additional diversity offered by the channel. However, this study demonstrated the robustness of the code when inaccuracies are introduced in identifying the channel order.

5.5 Amplify-and-Forward Cooperative Space-Time Frequency Coding

The problem of designing Ψ_S and Ψ_{R_j} to satisfy the design criterion is not as straightforward when adopting an AF relaying protocol as was the case under the DF protocol since participating relay nodes do not decode the symbols broadcast from the s-MT. Therefore the following analysis and code construction considers both the design of Ψ_S and Ψ_{R_j}.

5.5.1 Diversity and Coding Gain Analysis

5.5.1.1 Analysis Under Limited Fading Conditions

To determine the relevant performance metrics of the code design under the AF protocol it is assumed that the MIMO channel observed between the participating r-MTs and d-MT is static under the assumption $\mathbf{h}_{R_\mu D_\nu}[0] = \bar{\gamma}_{R_\mu D_\nu}$. This assumption removes the conditionality of the statistics of the noise forwarded from the r-MT on the statistics of a fading channel and greatly simplifies the PEP analysis in AF relay networks. This assumption is justified under an operating scenario assuming the d-MT has LoS with all r-MTs. It is worth noting that for the contrary DF relaying the processing at the r-MTs adopted in the ensuing analysis does not remove the frequency-selective channel perturbations observed in the first phase of the protocol. To gain insight into the design of Ψ_S and Ψ_{R_j} it is assumed that the channel observed in the first phase of the protocol perturbs the codeword transmitted by the r-MTs; the generic signal model (5.15) can then be modified to include these assumptions,

$$\mathbf{Y}(p) = \mathbf{E}_{RD}\left(\mathbf{H}_{SR}(p)\mathbf{X}(p) + \mathbf{V}(p)\right) + \mathbf{W}(p) \tag{5.104}$$

where,

$$\mathbf{H}_{SR}(p) := \begin{bmatrix} H_{SR_1}(p) & & \\ & \ddots & \\ & & H_{SR_{N_t}}(p) \end{bmatrix} \in \mathbb{C}^{N_t \times N_t} \tag{5.105}$$

$$\mathbf{V}(p) := \begin{bmatrix} v_1^{R_1}(p) & \cdots & v_{N_x}^{R_1}(p) \\ \vdots & & \vdots \\ v_1^{R_{N_t}}(p) & \cdots & v_{N_x}^{R_{N_t}}(p) \end{bmatrix} \in \mathbb{C}^{N_t \times N_x} \tag{5.106}$$

To simplify the model the total noise observed at the d-MT is denoted $\mathbf{U}(p) \in \mathbb{C}^{N_r \times N_x}$ and defined as $\mathbf{U}(p) := \mathbf{E}_{RD}\mathbf{V}(p) + \mathbf{W}(p)$ which is characterised as i.i.d. ZMCSCG with variance[1],

$$E\left\{u_i^{\nu}(p)u_i^{\nu *}(p)\right\} = N_0 \left(1 + \sum_{\mu \in \{R_1,\ldots,R_{N_t}\}} \frac{\bar{\gamma}_{\mu\nu}}{\bar{\gamma}_{S\mu} + N_0}\right) \tag{5.107}$$

Without loss of generality the noise $u_i^{\nu}(p)$ can be normalized to the power spectral density N_0 using the factor,

$$\beta_{\nu\mu} = \sqrt{1/\left(1 + \sum_{\mu \in \{R_1,\ldots,R_{N_t}\}} \frac{\bar{\gamma}_{\mu\nu}}{\bar{\gamma}_{S\mu} + N_0}\right)} \tag{5.108}$$

A signal model equivalent to (5.104) can now be expressed,

$$\tilde{\mathbf{Y}}(p) = \tilde{\mathbf{E}}\tilde{\mathbf{H}}_{SR}(p)\mathbf{X}(p) + \tilde{\mathbf{U}}(p) \tag{5.109}$$

where $\tilde{\mathbf{U}}(p)$ denotes the normalized ZMCSCG noise term with variance $N_0/2$ per dimension, $\tilde{\mathbf{Y}}_{\nu\mu}(p) := \beta_{\nu\mu}\mathbf{Y}_{\nu\mu}(p)$ and,

$$\tilde{\mathbf{E}} := \begin{bmatrix} \tilde{E}_{D_1R_1} & \cdots & \tilde{E}_{D_1R_{N_t}} \\ \vdots & & \vdots \\ \tilde{E}_{D_{N_r}R_1} & \cdots & \tilde{E}_{D_{N_r}R_{N_t}} \end{bmatrix} \in \mathbb{R}^{N_r \times N_t} \tag{5.110}$$

$$\tilde{E}_{\nu\mu} := \sqrt{\frac{\bar{\gamma}_{S\mu}\bar{\gamma}_{\mu\nu}}{\left(1 + \sum_{\mu' \in \{R_1,\ldots,R_{N_t}\}} \frac{\bar{\gamma}_{\mu'\nu}}{\bar{\gamma}_{S\mu'} + N_0}\right)}} \in \mathbb{R} \tag{5.111}$$

[1]It is assumed that the received signal power is normalized at the r-MT $\frac{1}{\bar{\gamma}_{S\mu}+N_0}$ as previously adopted

$$\tilde{\mathbf{H}}_{SR}(p) := \begin{bmatrix} \frac{1}{\sqrt{\bar{\gamma}_{SR_1}}} H_{SR_1}(p) & & \\ & \ddots & \\ & & \frac{1}{\sqrt{\bar{\gamma}_{SR_{N_t}}}} H_{SR_{N_t}}(p) \end{bmatrix} \in \mathbb{C}^{N_t \times N_t} \tag{5.112}$$

It is worth remarking that the signal models defined in (5.104) and (5.109) share an equivalent SNR so decoding performance is unaffected. However, (5.109) now enables the use of the powerful PEP analysis exploited for the DF protocol in Section 5.4.1 to aid AF codeword design. For the purposes of brevity in the ensuing PEP analysis of the AF scheme only the stages for the PEP analysis for the DF scheme that are specifically relevant will be highlighted.

To determine the transmitted codeword the ML-decoder is required to evaluate,

$$\hat{\mathbf{X}} = \arg\min_{\mathbf{X} \in A_s} \sum_{p=0}^{N_c-1} \|\mathbf{Y}(p) - \tilde{\mathbf{E}}\tilde{\mathbf{H}}_{SR}(p)\mathbf{X}(p)\|_F^2 \tag{5.113}$$

The difference operator is now given by,

$$d^2(\mathbf{X}, \mathbf{X}') = \sum_{p=0}^{N_c-1} \|\tilde{\mathbf{E}}\tilde{\mathbf{H}}_{SR}(p)\mathbf{\Delta}(p)\|^2 \tag{5.114}$$

To facilitate the evaluation of the PEP the SIMO channel vector is defined as $\mathbf{h}_S \in \mathbb{C}^{L\times 1}$ and constructed according to,

$$\mathbf{h}_S := [h_{SR_1}(0), \ldots, h_{SR_1}(L_{SR_1}), \ldots, h_{SR_{N_t}}(0), \ldots, h_{SR_{N_t}}(L_{SR_{N_t}})]^T \mathbb{C}^{L\times 1} \tag{5.115}$$

Therefore the whitened channel vector is defined as $\bar{\mathbf{h}}_S = \mathbf{B}_S^{-1}\mathbf{h}_S$ assuming the following covariance matrix $E\{\mathbf{h}_S\mathbf{h}_S^H\} = \mathbf{B}_S\mathbf{B}_S^H$ of the zero mean channel vector of length $L := \sum_{\mu\in\{R_1,\ldots,R_{N_t}\}}(L_{S\mu}+1)$. As was the case under the DF protocol, the different equation (5.114) can be re-written to expose the relationship to the time-domain channel as,

$$d^2(\mathbf{X}, \mathbf{X}') = \mathbf{h}_S^T \mathbf{\Lambda} \mathbf{h}_S^* = \bar{\mathbf{h}}_S^T \bar{\mathbf{\Lambda}} \bar{\mathbf{h}}_S^* \tag{5.116}$$

where,

$$\bar{\mathbf{\Lambda}} := \mathbf{B}^T \mathbf{\Lambda} \mathbf{B}^* \in \mathbb{C}^{L \times L} \tag{5.117}$$

$$\mathbf{\Lambda} := \sum_{p=0}^{N_c-1} \Omega(p)\Delta(p)\Delta(p)^H \Omega(p)^H \in \mathbb{C}^{L \times L} \tag{5.118}$$

$$\Omega(p) := \begin{bmatrix} \omega_{L_{SR_1}}(p) & & & \\ & \omega_{L_{SR_2}}(p) & & \\ & & \ddots & \\ & & & \omega_{L_{SR_{N_t}}}(p) \end{bmatrix} \in \mathbb{C}^{L \times N_t} \tag{5.119}$$

Following the same procedure used for the DF protocol in Section 5.4.1 and evaluating the expected PEP over all possible channel realisation yields,

$$P\left(\mathbf{X} \to \mathbf{X}'\right) \leq \left| \mathbf{I} + \frac{1}{4N_0} \bar{\mathbf{\Lambda}} \right|^{-1} \tag{5.120}$$

$$= \prod_{i=1}^{r(\bar{\mathbf{\Lambda}})} \frac{1}{1 + \frac{1}{4N_0}\lambda_i} \tag{5.121}$$

where λ_i denotes the ith eigenvalue of $\bar{\mathbf{\Lambda}}$. This analysis demonstrates that the diversity gain offered by this network scenario is limited by the dimensionality of $\bar{\mathbf{\Lambda}}$ which is upper bounded by the sum of the channel orders between s-MT and r-MTs, i.e. $r(\bar{\mathbf{\Lambda}}) \leq \sum_{\mu \in \{R_1, \ldots, R_{N_t}\}} (L_{S\mu} + 1)$.

As demonstrated in (5.120), increasing the order of receive antenna at the d-MT has no effect on the diversity gain due to the LoS condition between the r-MTs and d-MT. To fully appreciate the dependance of the array size at the d-MT on the achievable coding gain the channels are assumed briefly to be uncorrelated,

$$\mathbf{B} := \begin{bmatrix} \sqrt{\tilde{\gamma}}_{R_1} \mathbf{I}_{L_{SR_1}} & & & \\ & \sqrt{\tilde{\gamma}}_{R_2} \mathbf{I}_{L_{SR_2}} & & \\ & & \ddots & \\ & & & \sqrt{\tilde{\gamma}}_{R_{N_t}} \mathbf{I}_{L_{SR_{N_t}}} \end{bmatrix} \in \mathbb{C}^{L \times L} \tag{5.122}$$

where,

$$\tilde{\gamma}_\mu := \sum_{\nu \in \{D_1,\ldots,D_{N_r}\}} \frac{\bar{\gamma}_{S\mu}\bar{\gamma}_{\mu\nu}}{\left(1 + \sum_{\mu' \in \{R_1,\ldots,R_{N_t}\}} \frac{\bar{\gamma}_{\mu'\nu}}{\bar{\gamma}_{S\mu'}+N_0}\right)} \tag{5.123}$$

Further insight is gained from reformulating (5.116)-(5.119) by adopting the coding matrix structures (5.47)-(5.50) presented in Section 5.4.1.2; focuses the PEP analysis on the diversity and coding gain available via a relaying path and are repeated here for clarity,

$$\Delta'_\mu := \begin{bmatrix} \Delta^1_\mu(0) & \cdots & \Delta^{N_x}_\mu(0) \\ \vdots & & \vdots \\ \Delta^1_\mu(N_c-1) & \cdots & \Delta^{N_x}_\mu(N_c-1) \end{bmatrix} \in \mathbb{C}^{N_c \times N_x} \tag{5.124}$$

$$\mathbf{\Delta}' := \begin{bmatrix} \Delta'_{R_1} & & \\ & \ddots & \\ & & \Delta'_{R_{N_t}} \end{bmatrix} \in \mathbb{C}^{(N_c N_t)\times(N_t N_x)} \tag{5.125}$$

$$\mathbf{\Omega}' := \begin{bmatrix} \mathbf{\Omega}'_{SR_1} & & \\ & \ddots & \\ & & \mathbf{\Omega}'_{SR_{N_t}} \end{bmatrix} \in \mathbb{C}^{L \times N_c N_t} \tag{5.126}$$

where $\mathbf{\Omega}'_{SR_1}$ is defined previously (5.50). Since the reformulation still evaluates (5.118) to $\mathbf{\Lambda} = \mathbf{\Omega}'\mathbf{\Delta}'\mathbf{\Delta}'^H\mathbf{\Omega}'^H$, (5.116) can now be defined as,

$$d^2(\mathbf{X},\mathbf{X}') = \sum_{\mu \in \{R_1,\ldots,R_{N_t}\}} \tilde{\gamma}_\mu \mathbf{h}^T_{S\mu}\mathbf{\Lambda}'_\mu \mathbf{h}^*_{S\mu} \tag{5.127}$$

and $\mathbf{\Lambda}'_\mu$ selects the spatial coding difference matrix associated with the r-MT R_j. The expected PEP focusing on the spatial dimension is given by,

$$P(\mathbf{X} \to \mathbf{X}') \leq \prod_{\mu \in \{R_1,\ldots,R_{N_t}\}} \left| \mathbf{I} + \frac{\tilde{\gamma}_j}{4N_0}\mathbf{\Lambda}'_\mu \right|^{-1} \tag{5.128}$$

$$= \prod_{\mu \in \{R_1,\ldots,R_{N_t}\}} \prod_{i=1}^{r(\mathbf{\Lambda}'_\mu)} \frac{1}{1 + \frac{\tilde{\gamma}_\mu}{4N_0}\lambda'_{\mu,i}} \tag{5.129}$$

Assuming that the rank criterion is satisfied $r(\mathbf{\Lambda}'_\mu) \geq (L_{S\mu}+1)$, the diversity gain offered by the MISO fading-channel between the s-MT and VAA in the first phase of the protocol can be realized,

$$P(\mathbf{X} \rightarrow \mathbf{X}') \leq \prod_{\mu \in \{R_1,\ldots,R_{N_t}\}} \prod_{i=1}^{L_{S\mu}+1} \frac{1}{1 + \frac{\tilde{\gamma}_\mu}{4N_0}\lambda'_{\mu,i}} \tag{5.130}$$

In the high-SNR regime $\tilde{\gamma}_j/N_0 \rightarrow \infty$ this can be approximated further,

$$P(\mathbf{X} \rightarrow \mathbf{X}') \leq \prod_{\mu \in \{R_1,\ldots,R_{N_t}\}} \left(\frac{\tilde{\gamma}_\mu}{4N_0}\right)^{L_{S\mu}+1} \prod_{i=1}^{L_{S\mu}+1} \frac{1}{\lambda'_{\mu,i}} \tag{5.131}$$

Noticably, in the high-SNR regime and under the assumption that the path-loss in the first phase is significantly less than that encountered in the second phase of the relaying protocol, i.e. $E_{S\mu} >> E_{\mu\nu}, \forall \mu\nu$, (5.123) tends to,

$$\lim_{N_0 \rightarrow 0} \tilde{\gamma}_\mu = E_{S\mu} \sum_{\nu \in \{D_1,\ldots,D_{N_r}\}} E_{\mu\nu} \tag{5.132}$$

where the definition (5.111) is used. Interestingly (5.132) encapsulates the effects of *array gain* at the d-MT and substituting (5.132) into (5.131) clearly shows that the *array gain* offered by multiple antenna at the d-MT is leveraged by the diversity gain in the channels observed between the s-MT and relaying VAA.

5.5.1.2 Analysis Under Full Fading Conditions

The LoS constraint used to simplify the PEP analysis in the previous section is relaxed to allow the general case where all the underlying sub-channels observe frequency-selective fading. To introduce the problem the generic ST representation (5.15) is extended to derive the signal model under these new AF conditions,

$$\mathbf{Y}(p) = \mathbf{H}_{RD}(p)\left(\mathbf{H}_{SR}(p)\mathbf{X}(p) + \mathbf{V}(p)\right) + \mathbf{W}(p) \tag{5.133}$$

Again to facilitate PEP analysis the effective noise term $\mathbf{U}(p)$ is redefined as $\mathbf{U}(p) := \mathbf{H}_{RD}(p)\mathbf{V}(p) + \mathbf{W}(p)$ with zero mean and variance per element,

$$E\left\{u_n^\nu(p)u_n^{\nu*}(p)|\mathbf{H}_{RD}(p)\right\} = N_0\left(1 + \sum_{\mu \in \{R_1,\ldots,R_{N_t}\}} \frac{\bar{\gamma}_{\mu\nu}}{\bar{\gamma}_{S\mu} + N_0}|\tilde{H}_{\mu\nu}(p)|^2\right) \tag{5.134}$$

clearly demonstrating the conditionality on the frequency-selective MIMO channel in the second protocol phase, where the path-loss effects are isolated from the fast-fading component of the channel matrix using $\tilde{H}_{\mu\nu}(p) := \frac{1}{\sqrt{\bar{\gamma}_{\mu\nu}}} H_{\mu\nu}(p)$.

As with the limiting fading case (5.109), performing a whitening transform on (5.133) which has no effect on the SNR observed. Modifying (5.133) by performing an element-wise multiplication of each row, defined by ν, of the observation matrix by a noise scaling factor, $\tilde{\mathbf{Y}}_\nu(p) := \beta_\nu \mathbf{Y}_\nu(p)$, where the scaling is associated with the received noise according to,

$$\beta_\nu = \sqrt{\frac{1}{1 + \sum_{\mu \in \{R_1, \ldots, R_{N_t}\}} \frac{\bar{\gamma}_{\mu\nu}}{\bar{\gamma}_{S\mu} + N_0} |\tilde{H}_{\mu\nu}(p)|^2}} \tag{5.135}$$

In the full fading case yields a more concise representation signal representation,

$$\mathbf{Y}(p) = \Big(\mathbf{E}(p) \odot \tilde{\mathbf{H}}_{SD}(p)\Big) \mathbf{X}(p) + \tilde{\mathbf{U}}(p) \tag{5.136}$$

where,

$$\mathbf{E}(p) := \begin{bmatrix} E_{D_1 R_1}(p) & \cdots & E_{D_1 R_{N_t}}(p) \\ \vdots & & \vdots \\ E_{D_{N_r} R_1}(p) & \cdots & E_{D_{N_r} R_{N_t}}(p) \end{bmatrix} \in \mathbb{C}^{N_r \times N_t} \tag{5.137}$$

and $\tilde{\mathbf{H}}_{SD}(p)$ is defined as the normalized end-to-end effective MIMO channel observed between the s-MT and d-MT defined as,

$$\tilde{\mathbf{H}}_{SD}(p) := \begin{bmatrix} \tilde{H}_{R_1 D_1}(p) \tilde{H}_{SR_1}(p) & \cdots & \tilde{H}_{R_{N_t} D_1}(p) \tilde{H}_{SR_{N_t}}(p) \\ \vdots & & \vdots \\ \tilde{H}_{R_1 D_{N_r}}(p) \tilde{H}_{SR_1}(p) & \cdots & \tilde{H}_{R_{N_t} D_{N_r}}(p) \tilde{H}_{SR_{N_t}}(p) \end{bmatrix} \in \mathbb{C}^{N_r \times N_t} \tag{5.138}$$

evaluated at sub-carrier p. The full derivation of $E_{\nu\mu}(p)$ is presented in Appendix 5.7 (Derivation I), and can be summarized as,

$$E_{\nu\mu}(p) = \sqrt{\frac{(\bar{\gamma}_{S\mu}/N_0)\, \bar{\gamma}_{\mu\nu} \prod_{\mu' \in \{R_1, \ldots, R_{N_t}\}, \mu' \neq \mu} \left(1 + \frac{\bar{\gamma}_{S\mu'}}{N_0}\right)}{\prod_{\mu' \in \{R_1, \ldots, R_{N_t}\}} \left(1 + \frac{\bar{\gamma}_{S\mu'}}{N_0}\right) + \sum_{\forall R_j} \frac{\bar{\gamma}_{R_j \nu}}{N_0} |H_{R_j \nu}(p)|^2 \prod_{\forall \mu' \neq R_j} \left(1 + \frac{\bar{\gamma}_{S\mu'}}{N_0}\right)}} \tag{5.139}$$

The effective noise $\tilde{\mathbf{U}}(p) \in \mathbb{C}^{N_r \times N_x}$ observed at the d-MT is now i.i.d. with variance $N_0/2$ per dimension allowing the Chernoff bound to be applied for the calculation of the PEP. For the evaluation of the PEP the following codeword distance metric is applicable for the case where all sub-channels experience frequency-selective fading,

$$d^2(\mathbf{X}, \mathbf{X}') = \sum_{p=0}^{N_c-1} \| \left(\mathbf{E}(p) \odot \tilde{\mathbf{H}}_{SD}(p) \right) \mathbf{\Delta}(p) \|_F^2 \tag{5.140}$$

At this stage it is worth making several observations before embarking on the channel avaeraged PEP analysis:

1. The normalization factor (5.139) is conditioned on the instantaneous channel realizations.

2. The effective MIMO STF channel of the network is formulated as a product in frequency-domain of the channel coefficients observed at the first and second phase (5.138).

Specifically referring to the design criteria specified in Section 5.3.3; the main objective is to maximize diversity gain which is advantageous in the high-SNR regime. Therefore because $H_{R_j\nu}(p)$ is present in (5.139) the channel averaged PEP analysis is intractable [101]; only the asymptotic case assuming $N_0 \to 0$ and perfect power control $\bar{\gamma}_{S\mu} >> \bar{\gamma}_{\mu\nu}$ assuming $\mu \in \{R_1, \ldots, R_{N_t}\}, \nu \in \{D_1, \ldots, D_{N_r}\}$ is derived. Under the perfect power control conditions[1] (5.139) reduces to,

$$\lim_{N_0 \to 0} \mathbf{E}_{\nu\mu}(p)|_{\bar{\gamma}_{S\mu} >> \bar{\gamma}_{\mu\nu}} = \sqrt{\bar{\gamma}_{\mu\nu}} \tag{5.141}$$

Therefore (5.140) can now be expressed with emphasis on contribution from each relaying branch as,

$$d^2(\mathbf{X}, \mathbf{X}') = \sum_{p=0}^{N_c-1} \| \left(\mathbf{E}(p) \odot \tilde{\mathbf{H}}_{SD}(p) \right) \mathbf{\Delta}(p) \|_F^2 \tag{5.142}$$

$$\approx \sum_{\nu \in \{D_1, \ldots, D_{N_r}\}} \sum_{\mu \in \{R_1, \ldots, R_{N_t}\}} \bar{\gamma}_{\mu\nu} \| \tilde{\mathbf{H}}'_{\mu\nu} \tilde{\mathbf{H}}'_{S\mu} \mathbf{\Delta}'_{\mu} \|_F^2 \tag{5.143}$$

[1]Feasible if participating r-MTs are located much closer to the s-MT than the d-MT to mitigate path-loss effects.

where,

$$\tilde{\mathbf{H}}'_{\mu\nu} := diag\left(\tilde{H}_{\mu\nu}(0), \ldots, \tilde{H}_{\mu\nu}(N_c - 1)\right) \tag{5.144}$$

and,

$$\tilde{\mathbf{H}}'_{S\mu} := diag\left(\tilde{H}_{S\mu}(0), \ldots, \tilde{H}_{S\mu}(N_c - 1)\right) \tag{5.145}$$

symbolize the normalized frequency-domain diagonal channel matrices associated with the relaying path denoted by $\mu\nu$. Each relaying path can now be decoupled for the purpose of PEP analysis as shown in the Chernoff bound,

$$P(\mathbf{X} \to \mathbf{X}') \leq \prod_{\nu \in \{D_1, \ldots, D_{N_r x}\}} \prod_{\mu \in \{R_1, \ldots, R_{N_t}\}} \exp\left[-\frac{\bar{\gamma}_{\mu\nu} \|\tilde{\mathbf{H}}'_{\mu\nu} \tilde{\mathbf{H}}'_{S\mu} \mathbf{\Delta}'_{\mu}\|_F^2}{4N_0}\right] \tag{5.146}$$

Each spatial relaying branch can now be evaluated independently under PEP analysis to extract the distributed code design specifications. Without loss of generality it is assumed $L_{\mu\nu} > L_{S\mu}$ to derive the channel averaged PEP[1]. The channel averaged PEP can be determined via the solution $\forall \mu, \nu$ to the expectation,

$$E\left\{\exp\left[-\frac{\bar{\gamma}_{\mu\nu} \|\tilde{\mathbf{H}}'_{\mu\nu} \tilde{\mathbf{H}}'_{S\mu} \mathbf{\Delta}'_{\mu}\|_F^2}{4N_0}\right]\right\} \tag{5.147}$$

Assuming that the channels in the respective relaying stages are independent and uncorrelated; [101] demonstrated that the following decoupling can be safely applied in the high-SNR regime to evaluate (5.147),

$$E\left\{\exp\left[-\frac{\bar{\gamma}_{\mu\nu} \|\tilde{\mathbf{H}}'_{\mu\nu} \tilde{\mathbf{H}}'_{S\mu} \mathbf{\Delta}'_{\mu}\|_F^2}{4N_0}\right]\right\} \approx E\left\{\exp\left[-\frac{\bar{\gamma}_{\mu\nu}\left(\|\mathbf{h}_{\mu\nu}\|_2^2 \|\tilde{\mathbf{H}}'_{S\mu} \mathbf{\Delta}'_{\mu}\|_F^2\right)}{4N_0}\right]\right\} \tag{5.148}$$

Expanding the Frobenius norm in (5.148),

$$\begin{aligned} \|\tilde{\mathbf{H}}'_{S\mu} \mathbf{\Delta}'_{\mu}\|_F^2 &= \|\mathbf{F}_{N_c}^H \mathsf{H}_{S\mu} \mathbf{F}_{N_c} \mathbf{\Delta}'_{\mu}\|_F^2 && (5.149) \\ &= \mathbf{h}_{S\mu}^T \mathbf{\Omega}'_{S\mu} \mathbf{\Delta}'_{\mu} \left(\mathbf{\Delta}'_{\mu}\right)^H \mathbf{\Omega}'^H_{S\mu} \mathbf{h}^*_{S\mu} && (5.150) \end{aligned}$$

[1]The analysis can be simply repeated by exchanging variables for the case $L_{S\mu} > L_{\mu\nu}$

exposes the underlying channel vector $\mathbf{h}_{S\mu}$. Then without loss of generality it is further defined that $\bar{\mathbf{h}}_{S\mu} := \mathbf{U}_\mu \mathbf{B}_{S\mu}^{-1} \mathbf{h}_{S\mu}$, where $\mathbf{B}_{S\mu}$ is the channel whitening matrix and $\mathbf{U}_\mu$ defines the eigenvector matrix of $\mathbf{\Omega}'_{S\mu} \mathbf{\Delta}'_\mu \left(\mathbf{\Delta}'_\mu\right)^H \mathbf{\Omega}'^H_{S\mu}$ with the associated eienvectors $\Lambda_\mu = diag\left(\lambda_{\mu,0}, \ldots, \lambda_{\mu,L_{S\mu}}\right)$. This enables (5.148) to be redefined as,

$$E\left\{\exp\left[-\frac{\bar{\gamma}_{\mu\nu}\left(\|\mathbf{h}_{\mu\nu}\|_2^2 \|\Lambda_\mu^{1/2} \bar{\mathbf{h}}_{S\mu}\|_2^2\right)}{4N_0}\right]\right\} \tag{5.151}$$

Defining the random variables $Z_{\mu\nu} := X_{\mu\nu} Y_{S\mu}$ according to $X_{\mu\nu} := \sum_{l=0}^{L_{\mu\nu}} |\mathbf{h}_{\mu\nu}(l)|^2$, $Y_{S\mu} := \sum_{l=0}^{L_{S\mu}} |\bar{\mathbf{h}}_{S\mu}(l)|^2 \lambda_{\mu,l}$ the Chernoff bound on the error probability can be defined as,

$$P(\mathbf{X} \to \mathbf{X}') \leq \prod_{\nu \in \{D_1,\ldots,D_{N_r x}\}} \prod_{\mu \in \{R_1,\ldots,R_{N_t}\}} E\left\{\exp\left[-\frac{\bar{\gamma}_{\mu\nu} Z_{\mu\nu}}{4N_0}\right]\right\} \tag{5.152}$$

$$= \prod_{\nu \in \{D_1,\ldots,D_{N_r x}\}} \prod_{\mu \in \{R_1,\ldots,R_{N_t}\}} \phi_{Z_{\mu\nu}}(\omega)\big|_{j\omega = -\frac{\bar{\gamma}_{\mu\nu}}{4N_0}} \tag{5.153}$$

where $\phi_{Z_{\mu\nu}}$ is the characteristic function of $Z_{\mu\nu}$. Fortunately $\phi_{Z_{\mu\nu}}$ has been evaluated in the high-SNR regime in [101] by the analysis of Mheidat et al. and is included with the corresponding notation in Appendix 5.7 (Derivation II) for completeness. In the High-SNR regime the channel averaged PEP (5.152) can now be expressed generically as,

$$P(\mathbf{X} \to \mathbf{X}') \leq \prod_{\nu \in \{D_1,\ldots,D_{N_r x}\}} \prod_{\mu \in \{R_1,\ldots,R_{N_t}\}} K_{\mu\nu} \left(\frac{\bar{\gamma}_{\mu\nu}}{4N_0}\right)^{-(L_{\mu\nu}^{min}+1)} \prod_{l=0}^{L_{\mu\nu}^{min}} \left(\lambda_\mu(l)\right)^{-1} \tag{5.154}$$

where,

$$K_{\mu\nu} = (L_{\mu\nu}^{max} + 1)^{(L_{\mu\nu}^{min}+1)} \frac{\Gamma(|L_{\mu\nu} - L_{S\mu}| + 1)}{\Gamma(L_{\mu\nu}^{max} + 1)} \tag{5.155}$$

assuming $L_{\mu\nu}^{max} := \max\{L_{S\mu}, L_{\mu\nu}\}$ and $L_{\mu\nu}^{min} := \min\{L_{S\mu}, L_{\mu\nu}\}$ denote the first and second relaying stage maximum and minimum channel orders respectively. For the purposes of analyzing the PEP for coding design parameters (5.154) can

be formulated in terms of coding $G_{\mu\nu,c}$ and diversity gain $G_{\mu\nu,d}$, as was the case with the DF protocol (5.34) and repeated here for convenience,

$$P(\mathbf{X} \rightarrow \mathbf{X}') \leq \frac{1}{(G_{\nu,c})} \left(\frac{1}{4N_0}\right)^{-G_{\nu,d}} \tag{5.156}$$

The fundamental difference between coding for the DF and AF protocols is clearly highlighted in the design metrics,

$$G_{\mu\nu,c} = \prod_{\nu\in\{D_1,\ldots,D_{N_r x}\}} \prod_{\mu\in\{R_1,\ldots,R_{N_t}\}} \det(\mathbf{\Lambda}_\mu) \tag{5.157}$$

$$G_{\mu\nu,d} = \sum_{\nu\in\{D_1,\ldots,D_{N_r}\}} r(\mathbf{\Lambda}_\mu) \tag{5.158}$$

$$\leq \sum_{\mu\in\{R_1,\ldots,R_{N_t}\}} \sum_{\nu\in\{D_1,\ldots,D_{N_r}\}} \left(L_{\mu\nu}^{min} + 1\right) \tag{5.159}$$

The preceding analysis has illustrated some valuable insights into code design for cooperative relay networks operating under a AF protocol these are briefly summarized in the next section.

5.5.1.3 Deployment Guidelines

The following guidelines give a technical summary and guidance of the code design under AF protocols based on the knowledge gained under PEP analysis. Only specific points relating to AF protocols are reviewed here.

1. As with DF coding over a single-subcarrier, effectively ST-coding, limits the achievable rank of the codeword; therefore only spatial (cooperative) diversity gains can be realized in multi-path channels.

2. To extract full-diversity from the frequency-selective cooperative relay channel under AF protocols, STF-coding is required over at least as many subcarriers as the maximum of the minimum sub-channel orders observed over the first and second phase of the protocol, i.e. requiring $N_c \geq \max_{\mu\nu}\{L_{\mu\nu}^{min} + 1\}$.

3. Under SF-coding where the codeword is constrained to the space-frequency dimensions, $N_x = 1$, it is required that coding be extended by a factor equalling the number of transmit antennas over that needed for STF-coding, i.e. $N_c \geq N_t \max_{\mu\nu}\{L_{\mu\nu}^{min} + 1\}$.

4. When LoS is observed in the second relaying phase and the channel is assumed to be Gaussian between the VAA and d-MT, only the channels observed in the first phase offer diversity gains. However, adopting multiple antennas at the d-MT was shown to provide array gains.

5.5.2 Multi-Stage Distributed Quasi-Orthogonal Space-Time-Frequency Code Design

The encoding architecture adopted for use in the DF protocol under the assumption of perfect decoding at the r-MT can now be tailored specifically for an AF enabled scheme. Specifically the two-stage inner- and outer-coding methodology used by Giannakis et al. [90] for co-located systems can now be applied distributively across the various phases of the protocol; extracting diversity where it is offered by the cooperative relaying channel. The details of the distributed encoding process are presented in the following sections.

5.5.2.1 Source Node Processing

In the description of the encoding process for the DF protocol detailed in Section 5.4.2; no encoding was performed at the s-MT. In the description that follows the encoder Ψ_s specified in Section 5.3 is described.

At the s-MT the symbol stream is then demultiplexed into the group symbol $\mathbf{s}_g$ into $\{\mathbf{s}_{g,i} \in \mathbb{C}^{(Lg+1)\times 1}, i = 0, \ldots, N_{x_s} - 1\}$ where $\mathbf{s}_g := [\mathbf{s}_{g,0}^T, \ldots, \mathbf{s}_{g,N_{x_s}-1}^T]^T$ and is consistent with the processing performed across the VAA for use in the DF protocol described in Section 5.4.2. In the AF protocol constellation pre-coding to extract the available multi-path diversity from the cooperative relay channel is performed solely at the s-MT. This is again achieved using a square pre-coder $\mathbf{\Theta}_{LCF} \in \mathbb{C}^{(L_g+1)\times(L_g+1)}$, discussed in Section 2.4.3.3, to obtain $\mathbf{x}_{g,i} := \mathbf{\Theta}_{LCF}\mathbf{s}_{g,i}$. As was exposed in Section 5.4.2 the grouped constellation pre-coded symbols to be mapped onto the full N_c subcarriers,

$$\mathbf{x}_i := \sum_{g=0}^{N_g-1} \mathbf{\Phi}_g \mathbf{x}_{g,i} \in \mathbb{C}^{N_c \times 1} \tag{5.160}$$

At the source node, the following symbol mapping specific for QOSTBC at the r-MTs facilitates correct decoding at the d-MT as shown in appendix 5.7 (Derivation III),

$$\tilde{\mathbf{x}} = \begin{bmatrix} \mathbf{x}_1 \\ -\mathbf{x}_2^* \\ -\mathbf{x}_3^* \\ \mathbf{x}_4 \end{bmatrix} \tag{5.161}$$

where $\mathbf{P}$ is specified in (4.11) and is adopted for use in frequency-selective channels. To mitigate IBI a CP is inserted using (4.2), where it is assumed that the CP length is $N_p \geq \tau_{max} + L_{max} + 1$ according to,

$$L_{max} = \max\{L_{\mu\nu}^{max}\} \tag{5.162}$$

The s-MT transmitted frames using OFDM can then be neatly expressed in matrix notation as,

$$\mathbf{t}_i = \mathbf{T}_{cp}\, \mathbf{F}_N^H \tilde{\mathbf{x}}_i \tag{5.163}$$

The following description will demonstrate how the encoding at the r-MTs will complement the constellation pre-coding to extract cooperative diversity in the presence of four participating r-MTs.

5.5.2.2 Relay Node Processing

Independent of the pre-coding scheme executed at the s-MT the generic processing at individual participating r-MTs is fundamentally the same as previously illustrated in Figure 4.3 with specific processing for frequency-selective channels between the s-MT and r-MTs,

$$S = \beta^R \begin{bmatrix} \mathbf{r}_1^{R_1} & \zeta(\mathbf{r}_2^{R_2*}) & \zeta(\mathbf{r}_3^{R_3*}) & \mathbf{r}_4^{R_4} \\ \mathbf{r}_2^{R_1} & -\zeta(\mathbf{r}_1^{R_2*}) & \zeta(\mathbf{r}_4^{R_3*}) & -\mathbf{r}_3^{R_4} \\ \mathbf{r}_3^{R_1} & \zeta(\mathbf{r}_4^{R_2*}) & -\zeta(\mathbf{r}_1^{R_3*}) & -\mathbf{r}_2^{R_4} \\ \mathbf{r}_4^{R_1} & -\zeta(\mathbf{r}_3^{R_2*}) & -\zeta(\mathbf{r}_2^{R_3*}) & \mathbf{r}_1^{R_4} \end{bmatrix}_{4J \times 4} \tag{5.164}$$

where the received signal power at the r-MT is normalized according to,

$$\beta_{i\mu}^R := \sqrt{\frac{1}{\bar{\gamma}_{S\mu} + N_0}} \tag{5.165}$$

It is worth noting that the time-reversal processing denoted by $\zeta(\cdot)$ (4.8) are now applied at individual r-MTs instead of specific time-slots as was the case with flat-fading schemes (4.7).

5.5.2.3 Destination Node Processing

To preserve brevity, only the subtle differences in the decoding between the AF and DF protocols shall be examined in this section. It is worth reviewing the processing steps required to perform decoding at the d-MT:

1. De-mapping onto grouped STF codewords: De-map the group-STF coded symbols from the received OFDM symbol.
2. ST-component decoding: Perform linear combining via matched filtering with the effective QOSTBC MIMO channel to decouple the subsystems.
3. Pre-whitening: For each sub-system perform a pre-whitening of the noise after combining.
4. Sphere-Decoding:Recover the original symbols transmitted by the s-MT using ML decoding (or the near-optimal sphere decoding algorithm).

At the d-MT the received signal under the AF protocol is derived in Appendix 5.7 (Derivation III). as,

$$\begin{bmatrix} \mathbf{y}_1^{\nu} \\ \mathbf{y}_2^{\nu*} \\ \mathbf{y}_3^{\nu*} \\ \mathbf{y}_4^{\nu} \end{bmatrix} = \begin{bmatrix} \mathbf{H}_1 & \mathbf{H}_2 & \mathbf{H}_3 & \mathbf{H}_4 \\ -\mathbf{H}_2^* & \mathbf{H}_1^* & -\mathbf{H}_4^* & \mathbf{H}_3^* \\ -\mathbf{H}_3^* & -\mathbf{H}_4^* & \mathbf{H}_1^* & \mathbf{H}_2^* \\ \mathbf{H}_4 & -\mathbf{H}_3 & -\mathbf{H}_2 & \mathbf{H}_1 \end{bmatrix} \begin{bmatrix} \mathbf{x}_1 \\ \mathbf{x}_2 \\ \mathbf{x}_3 \\ \mathbf{x}_4 \end{bmatrix} + \begin{bmatrix} \mathbf{u}_1^{\nu} \\ \mathbf{u}_2^{\nu*} \\ \mathbf{u}_3^{\nu*} \\ \mathbf{u}_4^{\nu} \end{bmatrix} \tag{5.166}$$

where the effective frequency-domain diagonal channel matrices for a given relaying path are expressed as,

$$\mathbf{H}_{R_1\nu} = \mathbf{\Phi}_{\tau_1}\mathbf{F}\mathsf{H}_{R_1\nu}\mathbf{F}^H\mathbf{F}\mathsf{H}_{SR_1}\mathbf{F}^H \tag{5.167}$$

$$\mathbf{H}_{R_2\nu} = \mathbf{\Phi}_{\tau_2}\mathbf{F}\mathsf{H}_{R_2\nu}\mathbf{F}^H\mathbf{F}\mathbf{P}\mathsf{H}^*_{SR_2}\mathbf{F} \tag{5.168}$$

$$\mathbf{H}_{R_3\nu} = \mathbf{\Phi}_{\tau_3}\mathbf{F}\mathsf{H}_{R_3\nu}\mathbf{F}^H\mathbf{F}\mathbf{P}\mathsf{H}^*_{SR_3}\mathbf{F} \tag{5.169}$$

$$\mathbf{H}_{R_4\nu} = \mathbf{\Phi}_{\tau_4}\mathbf{F}\mathsf{H}_{R_4\nu}\mathbf{F}^H\mathbf{F}\mathsf{H}_{SR_4}\mathbf{F}^H \tag{5.170}$$

assuming $\mathbf{F}$ denotes an N_c-point unitary DFT matrix and the time-domain channel matrix $\mathsf{H}_{\mu\nu}$ is a circulant matrix. This model allows the flexibility to analyze the LoS case by substituting the channel gain $\bar{\gamma}_{R_j\nu}$ for $\mathsf{H}_{R_j\nu}$. However, the case where full fading is observed over all the sub-channels is analyzed further since LoS can without difficulty be determined from the ensuing derivation.

Decoding under the DF protocol involved a transform to reverse the noise correlation introduced by the combining resulting for ST-component decoding. In the receiver under AF relaying the forwarded noise from the r-MTs observed at the d-MT is colored by the frequency-selective channel $\mathbf{H}_{R_j\nu}$; as observed under the PEP analysis (5.134). Pre-whitening the observed signal

$$\tilde{\mathbf{y}}_i^\nu(p) := \beta_\nu(p)\mathbf{y}_i^\nu(p)$$

using (5.135), then allows the same decoding methodology used under the DF protocol to be applied for AF relaying taking into account the AF channel.

5.5.3 Numerical Simulations

The GSTF consists of an inner and outer code; the inner code is formulated using a set OSTBCs and QOSTBC to extract the spatial diversity available from the channel, the outer code is based on LCFC designs. The code implementation is distributed according to the code design outlined in section 5.5.2, where the LCFC component is implemented at the s-MT and the ST-component is executed in a distributed fashion across the r-MTs. To simplify the analysis the case study focuses on a network configuration where the s-MT and d-MT operate a single antenna; the virtual antenna array operating under a AF protocol comprises of a variable number of r-MTs depending on the ST-coding component employed.

Case Study 32: Depicted in Figure 5.8 is the SER versus SNR assuming OSTBC and QOSTBC is adopted for the ST-component coding under the AF relay protocol. This simulation study enables the verification of the PEP analysis in Section 5.5.1.1 conducted under the following network scenario. It is assumed that the sub-channel order for the phase of the protocol are $L_{S\mu} = 1$ and follow a Rayleigh distribution. In the second phase it is assumed that the r-MT observe a strong LoS with the destination node so a static channel is adopted $\mathbf{h}_{\mu\nu} = \bar{\gamma}_{\mu\nu} = 1$. The simulation were run under with $N_c = 64$ subcarriers.

Applying the correct constellation pre-coding, as stated in the deployment guidelines under AF protocols, enables the multi-path gain available from the first phase of the protocol to be harnessed. Alamouti ST-component coding shown in Figure 5.8 clearly demonstrates that both multi-path and spatial diversity is extracted from the frequency-selective channel observed in the first phase of the protocol. The additional degrees for freedom offered by the higher-order VAA under QOSTBC component coding demonstrate additional diversity gain advantage over the full-rate OSTBC despite using the same constellation pre-coding. Comparing with the DF protocol illustrated in Figure 5.2 it is clear that the additional noise forwarded from the r-MTs degrades the SER performance for a given SNR.

Case Study 33: Figure 5.9 extends the previous simulation study to the case where AF relay protocol is adopted under full frequency-selective fading conditions observed over all the sub-channels and protocol phases, i.e. $L_{\mu\nu} = 1, \mu \in \{S, R_1, \ldots, R_{N_t}\}, \forall\nu$. Again the sub-channels coefficients follow the Rayleigh-fading distribution and $N_c = 64$ sub-carriers are used.

Verifying the PEP analysis performed Section 5.5.1.2; Figure 5.9 illustrates that under the AF protocol the multi-path diversity gains offered by the sub-channels in the second phase of the protocol cannot be harvested. This is clearly observed when comparing the gradients for specific ST-component codes with that demonstrated in Figure 5.8 under the LoS assumption. Additionally there is a performance degradation in SER for a given SNR introduced because of the fading process of the channels compared with the Gaussian equivalent model assumed in the previous simulation study.

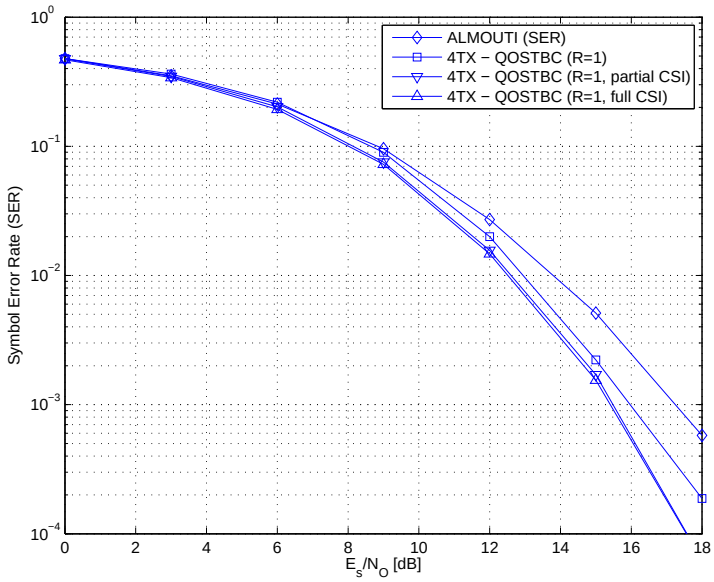

Figure 5.8: Symbol Error Rate vs SNR for distributed-GSTF codes based on various OSTBCs & QOSTBCs Space-Time component codes under AF relaying with LoS in second phase

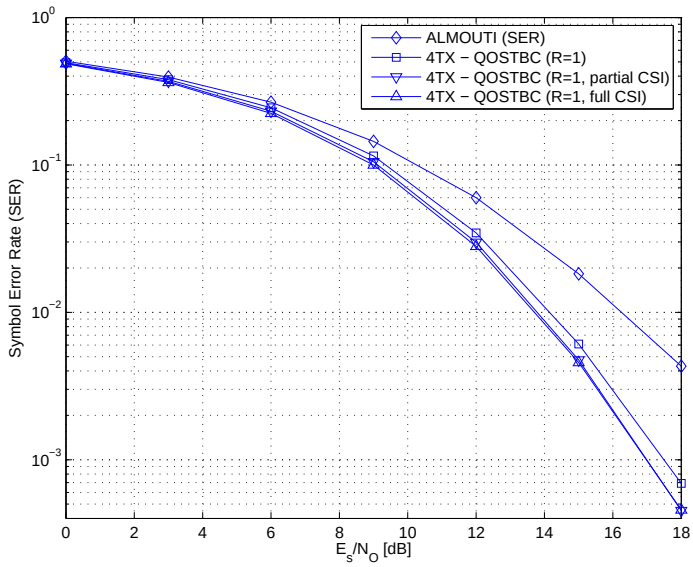

Figure 5.9: Symbol Error Rate vs SNR for distributed-GSTF codes based on various OSTBCs & QOSTBCs Space-Time component codes under AF relaying with full fading

Case Study 34: Depicted in Figure 5.10 are simulation studies when the effective sub-channel gains are asymmetric between the first and second stage of the relaying protocol. In this simulation study it is assumed that all the sub-channels are frequency-selective of order $L_{\mu\nu} = 1$ and are Rayleigh-distributed. The other simulation parameters are retained from the previous studies.

In the top plot of Figure 5.10 it is assumed that the sub-channel gains are asymmetric between the first and second relaying stage according to $\bar{\gamma}_{S\mu} = \frac{1}{5}$ and $\bar{\gamma}_{\mu\nu} = 5$. This ensures the effective path via a r-MT to a specific antenna element on the d-MT is comparable to previous simulation studies, i.e. $\bar{\gamma}_{S\mu}\bar{\gamma}_{\mu\nu} = 1$. The bottom plot shows the reciprocal scenario with the relatively larger channel gains observed in the first stage of the protocol; $\bar{\gamma}_{S\mu} = 5$ and $\bar{\gamma}_{\mu\nu} = \frac{1}{5}$. The relative noise powers applied at the r-MTs and d-MT are not varied with between simulation studies and were applied assuming $\bar{\gamma}_{\mu\nu} = 1$.

Interestingly, in the top plot when the first stage has substantially lower sub-channel gains than that observed in the second stage, the noise incident at the individual r-MT contributes to a higher noise power at the d-MT resulting in a

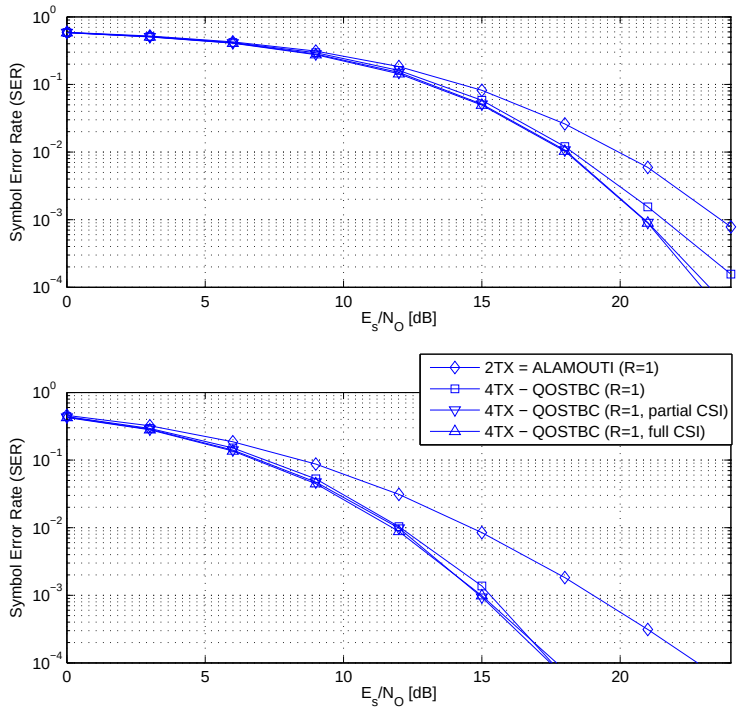

Figure 5.10: Symbol Error Rate vs SNR for distributed-GSTF codes based on various OSTBCs & QOSTBCs Space-Time component codes under AF relaying with full fading with asymmetric relay-stage sub-channel gains

degradation of SER for a given SNR when compared to the lower plot. In the lower plot the effective SNR observed at the r-MTs is higher due to the larger sub-channel gains observed; therefore after normalization at the r-MT to meet a transmit power constraint the contribution of the relayed noise is less. However, in the high-SNR asymptotic region the diversity gains offered by the channels are realized in both network scenarios.

Case Study 35: Depicted in Figure 5.11 are simulation studies when the effective sub-channel orders observed by nodes participating in first and second phase of the relaying protocol are asymmetric. It is assumed that equal sub-channel gains between the first and second phases are restored to isolate the variable of interest. All further simulation parameters are adopted from previous simulation

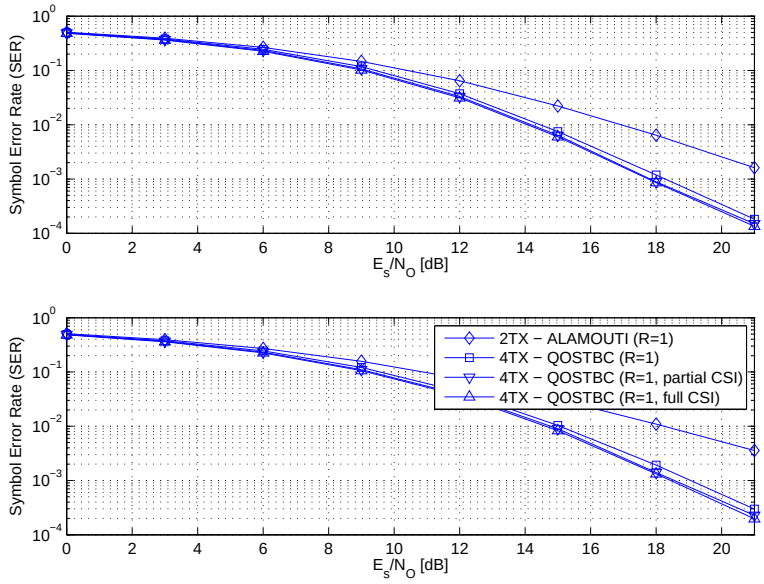

Figure 5.11: Symbol Error Rate vs SNR for distributed-GSTF codes based on various OSTBCs & QOSTBCs Space-Time component codes under AF relaying with full fading with asymmetric relay-stage sub-channel orders

studies to again enable direct comparisons to be made.

In the top plot of Figure 5.11 it is assumed that the channel orders in the first phase of the protocol are frequency-selective $L_{S\mu} = 1$, whilst the second phase experiences flat-fading channels. The reverse channel orders are applied to the lower plot.

As predicted in the PEP analysis under AF protocols in Section 5.5.1.2, the achievable diversity gain available from the channel is limited by the minimum channel order observed between two nodes on a relaying path. In Figure 5.11 it is demonstrated that applying higher-order channels in the first phase of the protocol improves error rate performance marginally.

5.6 Conclusions

This chapter extended the novel asynchronous cooperative schemes based on distributed-QOSTBC developed in the previous chapter for use in broadband

applications. As a foundation STF codes were adapted for use in a cooperative wireless networks to extract both cooperative- (spatial) and multi-path diversity offered by the relay channel. The specific details of the material covered in the chapter can be summarized as follows.

Adopting the same network architecture as the previous chapter; frequency-selective sub-channels observed between the participating mobile terminals are introduced. The cooperative channel deviates from the co-located case by allowing variable channel lengths and delay profiles specifically tailored to individual sub-channels. The generic processing and signal notations are defined in Section 5.2. The problem formulation with specific design criteria is stated for the code construction which aims to maximize coding gain whilst achieving the maximal diversity gain offered by the relay channel.

Section 5.4 specifically analyses distributed-STF coding techniques to be applied in networks using DF relaying protocol. This assumes that the r-MTs decode the data broadcast from the s-MT without errors. With the design criteria specifically stated in Section 5.3.3; PEP analysis is performed to determine the diversity and coding gains available under the DF protocol. It is observed that in order to extract all the diversity from the cooperative channel constellation precoding over a group of sub-carriers is required where the group size is defined by the maximum sub-channel length observed. The design of the distributed-STF is then presented with detailed guidelines on the ST-component code and constellation pre-coder design.The design of the quasi-orthogonal ST-component coding under ideal phase rotations is used to justify the use of existing constellation precoding techniques, namely Linear Complex Field Code (LCFC). The decoding stages at the d-MT are then fully documented including; ST-component decoding, whitening transform, ML-decoding. Numerical simulations using Monte-Carlo techniques then verify the utility of the design under; co-located, distributed and correlated channel conditions. The simulations also demonstrate the robustness of the proposed scheme with feedback and under quantization of the feedback channel.

In Section 5.5 the AF protocol is assumed. Under this assumption the frequency-selective channel perturbations observed in the first phase of the protocol must be taken into account when designing cooperative schemes that perform with an element of transparent relaying. To optimize the coding scheme a PEP was

performed firstly under the condition that no fading was observed in the second phase of the protocol; LoS was assumed between the r-MTs and d-MT. This simplified the analysis by removing the conditionality of the noise forward from the relays on the channel fading process. The results yielded similar findings to that of DF with modified noise statistics to include the noise observed at the r-MTs. In the second stage of analysis fading was introduced on all sub-channels under specific power control constraints. Specifically it was assumed that averaged received SNR observed at the r-MT would be significantly higher than that observed at the d-MT. This could be observed in scenarios where the VAA composing of r-MTs is closer in proximity to the s-MT than the d-MT; therefore observing significantly less path-loss. This yielded interesting design requirements for constellation pre-coding. Finally, the section closes with the detailed design of an asynchronous distributed-STF coding scheme where the two-stage encoding of the data is performed both at the s-MT and r-MT to meet the design criteria. Again numerical simulation studies verify the utility of the proposed scheme using the AF protocol under different network scenarios.

5.7 Appendix

5.7.1 Derivation I

It is proven here that,

$$[\mathbf{E}(p)]_{\nu\mu} = \sqrt{\frac{(\bar{\gamma}_{S\mu}/N_0)\,\bar{\gamma}_{\mu\nu}\prod_{\mu'\in\{R_1,\ldots,R_{N_t}\},\mu'\neq\mu}\left(1+\frac{\bar{\gamma}_{S\mu'}}{N_0}\right)}{\prod_{\mu'\in\{R_1,\ldots,R_{N_t}\}}\left(1+\frac{\bar{\gamma}_{S\mu'}}{N_0}\right)+\sum_{\forall R_j}\frac{\bar{\gamma}_{R_j\nu}}{N_0}H_{R_j\nu}(p)\prod_{\forall\mu'\neq R_j}\left(1+\frac{\bar{\gamma}_{S\mu'}}{N_0}\right)}} \tag{5.171}$$

Considering the average receive power at a given r-MT μ is denoted by $\bar{\gamma}_{S\mu}$. After processing the received signal under the AF protocol the normalized power is denoted,

$$\frac{\bar{\gamma}_{S\mu}}{\bar{\gamma}_{S\mu}+N_0}. \tag{5.172}$$

The averaged signal power received originonating from the μth r-MT obseved at the νth antenna of the d-MT is then represented as,

$$\frac{\bar{\gamma}_{S\mu}\bar{\gamma}_{\mu\nu}}{\bar{\gamma}_{S\mu}+N_0}. \tag{5.173}$$

Scaling the received power to whiten and normalize the noise observed at the d-MT using $\beta^2_{\mu\nu}$ (5.135) results in,

$$\frac{\bar{\gamma}_{S\mu}\bar{\gamma}_{\mu\nu}}{(\bar{\gamma}_{S\mu}+N_0)\left(1+\sum_{\mu'\in\{R_1,\ldots,R_{N_t}\}}\frac{\bar{\gamma}_{\mu'\nu}}{\bar{\gamma}_{S\mu'}+N_0}|H_{\mu'\nu}(p)|^2\right)} \tag{5.174}$$

which enables the scaling term $[\mathbf{E}(p)]_{\nu\mu}$ corresponding to the realying path $\{\mu\nu\}$ to be re-written as,

$$[\mathbf{E}(p)]_{\nu\mu}=\sqrt{\frac{\bar{\gamma}_{S\mu}\bar{\gamma}_{\mu\nu}}{(\bar{\gamma}_{S\mu}+N_0)\left(1+\sum_{\mu'\in\{R_1,\ldots,R_{N_t}\}}\frac{\bar{\gamma}_{\mu'\nu}}{\bar{\gamma}_{S\mu'}+N_0}|H_{\mu'\nu}(p)|^2\right)}} \tag{5.175}$$

Multiplying the numerator and denominator of (5.175) by $\sqrt{\prod_{\mu'\in\{R_1,\ldots,R_{N_t}\}}(\bar{\gamma}_{S\mu'}+N_0)}$ yields,

$$[\mathbf{E}(p)]_{\nu\mu}=\sqrt{\frac{\bar{\gamma}_{S\mu}\bar{\gamma}_{\mu\nu}\prod_{\mu'\in\{R_1,\ldots,R_{N_t}\},\mu'\neq\mu}(\bar{\gamma}_{S\mu'}+N_0)}{\prod_{\mu'\in\{R_1,\ldots,R_{N_t}\}}(\bar{\gamma}_{S\mu'}+N_0)+\sum_{\forall R_j}\bar{\gamma}_{R_j\nu}|H_{R_j\nu}(p)|^2\prod_{\forall\mu'\neq R_j}(\bar{\gamma}_{S\mu'}+N_0)}} \tag{5.176}$$

Finally, multiplying the numerator and denominator of (5.176) by $N_0^{-N_t}$ concludes the proof.

5.7.2 Derivation II

The following analysis has been adapted from [101, Appendix II] and assumes $L_{\mu\nu} > L_{S\mu}$; where it has been extended by the author for the case $L_{S\mu} = L_{\mu\nu}$. According to [102] $\phi_{Z_{\mu\nu}}$ can be evaluated as,

$$\phi_{Z_{\mu\nu}}(\omega)=\int_0^\infty f_{X_{\mu\nu}}(x_{\mu\nu})\phi_{Y_{S\mu}}(\omega y_{S\mu})dx_{\mu\nu} \tag{5.177}$$

where $f_{X_{\mu\nu}}(x_{\mu\nu})$ is the pdf of $X_{\mu\nu}$ denoted by,

$$f_{X_{\mu\nu}}(x_{\mu\nu}):=\frac{(L_{\mu\nu}+1)^{L_{\mu\nu}+1}}{\Gamma(L_{\mu\nu}+1)}x_{\mu\nu}^{(L_{\mu\nu})}e^{-x_{\mu\nu}(L_{\mu\nu}+1)} \tag{5.178}$$

and $\phi_{Y_{S\mu}}(\omega y_{S\mu})$ is the characteristic function of $Y_{S\mu}$ evaluated as,

$$\phi_{Y_{S\mu}}|_{j\omega=-\frac{\bar{\gamma}_{\mu\nu}}{4N_0}} = \prod_{l=0}^{L_{S\mu}} \left(1 + \frac{\bar{\gamma}_{\mu\nu}}{4N_0}\lambda_\mu(l)\right)^{-1} \tag{5.179}$$

Substituting (5.178) and (5.179) into (5.177); (5.177) can then be expressed as the solution to the integral,

$$\begin{aligned} \phi_{Z_{\mu\nu}}|_{j\omega=-\frac{\bar{\gamma}_{\mu\nu}}{4N_0}} &= \frac{(L_{\mu\nu}+1)^{L_{\mu\nu}+1}}{\Gamma(L_{\mu\nu}+1)}\left(\frac{\bar{\gamma}_{\mu\nu}}{4N_0}\right)^{-(L_{S\mu}+1)} \\ &\times \prod_{l_{S\mu}=0}^{L_{S\mu}} (\lambda_\mu(l_{S\mu}))^{-1} \int_0^\infty \frac{x_{\mu\nu}^{L_{\mu\nu}} e^{-x_{\mu\nu}(L_{\mu\nu}+1)}}{\prod_{l_{S\mu}=0}^{L_{S\mu}}\left(\frac{1}{\lambda_\mu(l_{S\mu})\frac{\bar{\gamma}_{\mu\nu}}{4N_0}} + x_{\mu\nu}\right)} dx_{\mu\nu} \end{aligned} \tag{5.180}$$

Assuming high SNR, $\bar{\gamma}_{\mu\nu} >> 4N_0$, the following approximation can be made,

$$\begin{aligned} \phi_{Z_{\mu\nu}}|_{j\omega=-\frac{\bar{\gamma}_{\mu\nu}}{4N_0}} &= \frac{(L_{\mu\nu}+1)^{L_{\mu\nu}+1}}{\Gamma(L_{\mu\nu}+1)}\left(\frac{\bar{\gamma}_{\mu\nu}}{4N_0}\right)^{-(L_{S\mu}+1)} \\ &\times \prod_{l_{S\mu}=0}^{L_{S\mu}} (\lambda_\mu(l_{S\mu}))^{-1} \int_0^\infty x_{\mu\nu}^{L_{\mu\nu}-L_{S\mu}} e^{-x_{\mu\nu}(L_{\mu\nu}+1)} dx_{\mu\nu} \end{aligned} \tag{5.181}$$

It is well known that the integral in (5.181) can be solved iteratively using integration by parts to yield,

$$\phi_{Z_{\mu\nu}}|_{j\omega=-\frac{\bar{\gamma}_{\mu\nu}}{4N_0}} = (L_{\mu\nu}+1)^{L_{S\mu}+1}\frac{\Gamma(L_{\mu\nu}-L_{S\mu}+1)}{\Gamma(L_{\mu\nu}+1)}\left(\frac{\bar{\gamma}_{\mu\nu}}{4N_0}\right)^{-(L_{S\mu}+1)} \prod_{l_{S\mu}=0}^{L_{S\mu}} (\lambda_\mu(l_{S\mu}))^{-1} \tag{5.182}$$

Interestingly, if $L_{\mu\nu} = L_{S\mu}$ then (5.181) resolves to,

$$\phi_{Z_{\mu\nu}}|_{j\omega=-\frac{\bar{\gamma}_{\mu\nu}}{4N_0}} = \frac{(L_{\mu\nu}+1)^{L_{\mu\nu}}}{\Gamma(L_{\mu\nu}+1)}\left(\frac{\bar{\gamma}_{\mu\nu}}{4N_0}\right)^{-(L_{S\mu}+1)} \prod_{l_{S\mu}=0}^{L_{S\mu}} (\lambda_\mu(l_{S\mu}))^{-1} \tag{5.183}$$

5.7.3 Derivation III

It is proven here for the AF protocol that after initial pre-processing at the d-MT the received signal at the νth antenna in the frequency-domain can be expressed as,

$$\begin{bmatrix} \mathbf{y}_1^{\nu} \\ \mathbf{y}_2^{\nu *} \\ \mathbf{y}_3^{\nu *} \\ \mathbf{y}_4^{\nu} \end{bmatrix} = \begin{bmatrix} \mathbf{H}_1 & \mathbf{H}_2 & \mathbf{H}_3 & \mathbf{H}_4 \\ -\mathbf{H}_2^* & \mathbf{H}_1^* & -\mathbf{H}_4^* & \mathbf{H}_3^* \\ -\mathbf{H}_3^* & -\mathbf{H}_4^* & \mathbf{H}_1^* & \mathbf{H}_2^* \\ \mathbf{H}_4 & -\mathbf{H}_3 & -\mathbf{H}_2 & \mathbf{H}_1 \end{bmatrix} \begin{bmatrix} \mathbf{x}_1 \\ \mathbf{x}_2 \\ \mathbf{x}_3 \\ \mathbf{x}_4 \end{bmatrix} + \begin{bmatrix} \mathbf{u}_1^{\nu} \\ \mathbf{u}_2^{\nu *} \\ \mathbf{u}_3^{\nu *} \\ \mathbf{u}_4^{\nu} \end{bmatrix} \tag{5.184}$$

To define the matrix representation above the following effective channel matrices in the frequency-domain are defined,

$$\mathbf{H}_{R_1\nu} = \mathbf{\Phi}_{\tau_1}\mathbf{F}\mathsf{H}_{R_1\nu}\mathbf{F}^H\mathbf{F}\mathsf{H}_{SR_1}\mathbf{F}^H \tag{5.185}$$

$$\mathbf{H}_{R_2\nu} = \mathbf{\Phi}_{\tau_2}\mathbf{F}\mathsf{H}_{R_2\nu}\mathbf{F}^H\mathbf{F}\mathbf{P}\mathsf{H}_{SR_2}^*\mathbf{F} \tag{5.186}$$

$$\mathbf{H}_{R_3\nu} = \mathbf{\Phi}_{\tau_3}\mathbf{F}\mathsf{H}_{R_3\nu}\mathbf{F}^H\mathbf{F}\mathbf{P}\mathsf{H}_{SR_3}^*\mathbf{F} \tag{5.187}$$

$$\mathbf{H}_{R_4\nu} = \mathbf{\Phi}_{\tau_4}\mathbf{F}\mathsf{H}_{R_4\nu}\mathbf{F}^H\mathbf{F}\mathsf{H}_{SR_4}\mathbf{F}^H \tag{5.188}$$

where $\mathbf{F}$ denotes an N_c-point unitary DFT matrix and the time-domain channel matrix $\mathsf{H}_{\mu\nu}$ is a circulant matrix where the first row is defined as,

$$[\alpha_{\mu\nu}[0], 0, \ldots, 0, \alpha_{\mu\nu}[L_{\mu\nu}], \ldots, \alpha_{\mu\nu}[2]] \in \mathbb{C}^{1\times N_c}.$$

It is worth noting that the conjugation performed in the time-domain on R_2 and R_3, which is evident in (5.186)-(5.187), requires correction in the form of a time-reversal $\mathbf{P}$ on R_2 and R_3 as demonstrated in (5.186)-(5.187). The equivalent channel matrices (5.185)-(5.188) now retain a diagonal structure and do not permutate the transmitted symbols in the frequency-domain. The asynchronicity of the scheme introduces a phase rotation proportional to the round-trip delay observed; $[\mathbf{\Phi}_{\tau_j}]_{k,k} := e^{-j2\pi k\tau_j/N_c}$. To simplify the ensuing expressions the noise terms are omitted for brevity. The equivalent expressions for each frame received at the d-MT following initial pre-processing are,

$$\mathbf{y}_1^{\nu} = \mathbf{H}_{R_1\nu}\tilde{\mathbf{x}}_1 + \mathbf{H}_{R_2\nu}\tilde{\mathbf{x}}_2^* + \mathbf{H}_{R_3\nu}\tilde{\mathbf{x}}_3^* + \mathbf{H}_{R_4\nu}\tilde{\mathbf{x}}_4 \tag{5.189}$$

$$\mathbf{y}_2^\nu = \mathbf{H}_{R_1\nu}\tilde{\mathbf{x}}_2 - \mathbf{H}_{R_2\nu}\tilde{\mathbf{x}}_1^* + \mathbf{H}_{R_3\nu}\tilde{\mathbf{x}}_4^* - \mathbf{H}_{R_4\nu}\tilde{\mathbf{x}}_3 \tag{5.190}$$

$$\mathbf{y}_3^\nu = \mathbf{H}_{R_1\nu}\tilde{\mathbf{x}}_3 + \mathbf{H}_{R_2\nu}\tilde{\mathbf{x}}_4^* - \mathbf{H}_{R_3\nu}\tilde{\mathbf{x}}_1^* - \mathbf{H}_{R_4\nu}\tilde{\mathbf{x}}_2 \tag{5.191}$$

$$\mathbf{y}_4^\nu = \mathbf{H}_{R_1\nu}\tilde{\mathbf{x}}_4 - \mathbf{H}_{R_2\nu}\tilde{\mathbf{x}}_3^* - \mathbf{H}_{R_3\nu}\tilde{\mathbf{x}}_2^* + \mathbf{H}_{R_4\nu}\tilde{\mathbf{x}}_1 \tag{5.192}$$

Conjugating $\mathbf{y}_2^\nu$ and $\mathbf{y}_3^\nu$ in addition to substituting $\mathbf{x}$ (5.161) for $\tilde{\mathbf{x}}$ completes the proof.

Chapter 6

Concluding Remarks

6.1 Conclusion

This thesis explores the concept of distributed-QOSTBCs implemented across VAAs to exploit additional spatial diversity gains offered by a wireless relay network. Whilst the analysis and characterization of OSTBCs has been extensively studied for use in cooperative relay networks, the investigation has not been exhaustively undertaken for QOSTBCs. This thesis has attempted to answer some of the question with regard to theoretical performance and implementation specific questions for QOSTBCs.

An understanding of the Shannon capacity offered over a relaying-stage adopting STBC enabled a framework under which to assess the performance of distributed-QOSTBCs deployed in a VAA. Chapter 3 addressed this question directly by observing various ST-coding schemes under ergodic and non-ergodic channel conditions. The chosen theoretical performance metric for each channel classification is well known to be the Shannon capacity for ergodic channels and outage-probability for a given communications rate.

Chapter 3 presented novel closed-form expressions for the MIMO capacity of flat-fading Rayleigh distributed cooperative channels under the constraint of distributed-QOSTBC. The novel expressions allowed for full effects of distributed encoding where sub-channel gains may fluctuate due to the observation of different shadowing and path-loss characteristics which affect the channel gains. This enabled comparisons to be made against OSTBC counterparts which inherently

orthogonalize the MIMO channel and simplify the analysis into a set of parallel SISO channels with modified channel statistics. Alternatively QOSTBC decouple the MIMO channel, reducing the computational complexity of the detection problem. Adopting phase rotations on a subset of the r-MTs, based on channel observations at the d-MT, was demonstrated to orthogonalize fully the MIMO channel allowing the analytical techniques used for OSTBC to be applied to QOSTBCs. Relaxing the feedback channel requirements and introducing quantization, inevitably introduced errors in the applied phase rotations. For the first time closed-form expressions were derived to evaluate the effects of quantization on the degradation of the achievable channel capacity.

Following on in a similar manner, Chapter 3 extended the analysis of QOSTBC for the case of non-ergodic channels. Whilst exact closed-form expression of the outage-probability for a given SNR and communications rate proved elusive: tight approximations verified using numerical simulations were derived using the Mellin transform for flat-fading Rayleigh cooperative channels. Although QOSTBCs matched or exceeded the capacity of comparable OSTBCs under ergodic channels the performance gains were far superior in non-ergodic channels. In the case where perfect phase rotations could be applied to orthogonalize the channel under QOSTBC exact outage-probability expressions were presented.

The analysis in Chapter 3 demonstrated the applicability of distributed-QOSTBCs in a range of channel classifications. This provided the motivation to develop practical implementations for deployment in VAAs, in particular addressing synchronization between the relaying nodes. Chapter 4 addressed specifically timing synchronization in a relay network architecture comprising of an s-MT, d-MT and r-MTs under flat-fading Rayleigh channels. It was assumed since there is no direct communication between the s-MT and d-MT that transmission via a distributed r-MT incurs some round-trip delay. Without judicious design of the cooperative scheme ISI at the d-MT is unavoidable since synchronous re-transmission is not assumed. To compensate a block coding scheme was adopted with pre-coding implemented at the s-MT. Redundancy, in the form of a CP, introduced only a marginal loss in the code-rate proportional to the re-transmssion delay-spread. To provide greater flexibility in deployment asynchronous distributed-QOSTBC schemes were developed that utilize both single- and multi-carrier transmission. Specifically, the single-carrier scheme offered an important characteristic that

minimizes PAPR therefore simplifying the RF specification of the r-MTs. Both single- and multi-carrier clock based transmission demonstrated decoding complexity comparable to synchronous symbol based implementations. As was the case with the characterization of the cooperative quasi-orthogonal channel in Chapter 3; feedback was introduced to orthogonalize the channel. Several time- and frequency-domain processing techniques to apply the required phase rotation at the r-MT were illustrated.

With the demand for ever higher data-rates and QoS requirements the asynchronous QOSTBC enabled multi-carrier scheme introduced in Chapter 4 were modified for use in frequency-selective channels. Although the spatial-diversity offered by the cooperative channel in flat-fading conditions is well understood the additional degrees of freedom offered by the cooperative frequency-selective channel made further analysis an imperative precondition to the code design. Initially, specific design criteria were formally stated to ensure the code designs achieve maximal coding and diversity gains. With this in mind a PEP analysis was performed under the assumption of DF and AF protocols. Under DF the assumption was made that the r-MT detect the data broadcast by the s-MT without error. This isolated the analysis of the code design to the distributed processing implemented across the VAA. To further the investigation of the applicability of QOSTBCs in robust broadband networks; STF coding pioneered by Giannakis et al. was modified for use in a distributed network. Although much of the processing at the r-MTs for extracting spatial-diversity is common for use in DF and AF protocols, the constellation pre-coder was specifically tailored. In DF the constellation pre-coder distributively implemented at the r-MTs in conjunction with the ST-component code. PEP analysis specifically illustrated that this approach may not necessarily achieve maximum coding diversity requiring the constellation pre-coder to be implemented at the s-MT. This approach resulted in a full-distributed asynchronous cooperative-STF coding scheme that leverages QOSTBC as the ST-component code. Numerical analysis demonstrated the utility of QOSTBC enabled cooperative-STF coding as a robust solution when limited feedback is available.

6.2 Further Research

This thesis has made some early contributions to the development of robust low-complexity coding schemes that meet some of the requirements for future cooperative wireless relay networks. Inevitably more work is needed to fully realize the potential of cooperative diversity. Based upon the findings in this thesis some of the many questions that remain unanswered are discussed briefly in the following paragraphs of this section in an attempt to stimulate the ideas of future researchers.

Quasi-Orthogonal MIMO Channel Characterization: When characterizing the distributed-Quasi-Orthogonal MIMO channel it was assumed that sub-channels may experience different shadowing and path-loss effects. To evaluate various ST-coding schemes it was assumed that all paths originating from a transmitting antenna to a receiver are relatively equal and can be modeled using the Rayleigh-fading distribution [14]. However, in some environments a direct LoS is present in the mobile radio channel and is usually approximated with Rician-fading model. Generally, the Rician fading model is not frequently adopted by researchers due to the mathematical difficulties associated with its pdf [5]. However, the Rician-distribution can be well approximated with a Nakagami-distribution [103]. In [5] Dohler extended the characterization of O-MIMO channels in cooperative relay networks under a Rayleigh-fading distribution to deployments experiencing Nakagami fading. It is proposed that the framework developed in Chapter 3 for both ergodic and non-ergodic scenarios could be extended to include characterization of Quasi-Orthogonal MIMO Channels observing LoS.

QOSTBC Under Flat-Fading Channels: In this thesis both single- and multi-carrier transmission schemes were developed for cooperative relay networks deployed in flat-fading channels under both DF and AF protocols. In Chapter 4 an array of equalization and decoding strategies under the classifications ZF, MMSE and ML were presented for use under DF protocols. Under AF protocols it was demonstrated that ZF and MMSE techniques offered comparable complexity and decoding performance to that of their DF counterparts. However, the ISI generating mechanism, examined in Section 4.4.1.2, introduces

significant interference under certain delay spreads. In [104] some progress was made in devising frequency-domain pre-processing techniques which made use of insights used in simplifying the iterative-MMSE equalizers for doubly-selective channels by Schniter [105]. Devising a low-complex near-ML solution to decoding distributed-QOSTBCs under AF protocols would be advantageous.

QOSTBC Enabled Distributed-Space-Time-Frequency Coding: Chapter 5 introduced a distributed-STF code design using a ST-component code based on QOSTBCs. This novel versatile code design for use in asynchronous broadband networks was adapted for use under both AF and DF enabled networks. The various PDP that are encountered in cooperative relay networks, where the various relaying-paths via r-MTs exhibit path-loss and shadowing effects, requires resource allocations to optimize the end-to-end throughput and capacity of the relay channel VAA. Whilst Dohler VAA introduced a methodology based on closed-form approximations of the capacity and throughput under OSTBC: it would be beneficial to extend this work to encompass frequency-selective cooperative channels experiencing different channel orders between participating nodes.

Extended-OSTBCs: Extended-OSTBCs (EOSTBCs) have proven potential to outperform OSTBCs and QOSTBCs through the use of array gain enabled via a feedback channel [106]. The application of EOSTBCs to cooperative networks using multi-carrier transmission under AF protocols has already been demonstrated in [107] and builds upon the work undertaken in the same network configuration for QOSTBCs [108]. Therefore, a fruitful research opportunity exists in extending the research framework adopted for this thesis in examining QOSTBCs for use in cooperative relay networks to EOSTBC deployments.

References

[1] M.Conti and S.Giordano, "Multihop Ad Hoc Networking: The Theory," *IEEE Communications Magazine*, vol. 45, pp. 78–86, Apr. 2007. 1

[2] J.G.Proakis, *Digital Communications*. McGraw-Hill, fourth ed., 2001. 2, 25, 43, 99, 102, 154

[3] A.Sendonaris, E.Erkip, and B.Aazhang, "User cooperation diversity part I: System description," *IEEE Trans. on Communications*, vol. 51, no. 11, pp. 1927–1938, 2003. 2, 4

[4] A.Sendonaris, E.Erkip, and B.Aazhang, "User cooperation diversity part II: Implementation aspects and performance analysis," *IEEE Trans. Comms*, vol. 51, no. 11, pp. 1939–1948, 2003. 2, 4

[5] M.Dohler, *Virtual Antenna Arrays*. PhD thesis, University of London, Nov. 2003. 2, 4, 16, 52, 53, 55, 56, 68, 71, 76, 77, 209

[6] A.Paulraj, R.Nabar, and D.Gore, *Introduction to Space-Time Wireless Communications*. Cambridge University Press, 2003. 3, 18, 19, 23, 25, 27, 30, 31, 42, 50, 53

[7] V.Stankovic, A.Host-Madsen, and Z.Xiong, "Cooperative diversity for wireless ad-hoc networks," *IEEE Signal Processing Magazine*, vol. 23, pp. 37–49, Sep. 2006. 3

[8] N.Laneman, *Cooperative Diversity in Wireless Networks: Algorithms and Architectures*. PhD thesis, MIT, Sep. 2002. 4

[9] J.N.Laneman, D.N.C.Tse, and G.W.Wornell, "Cooperative diversity in wireless networks: Efficient protocols and outage behaviour," *IEEE Trans. on Information Theory*, vol. 50, pp. 3062–3080, Dec. 2004. 4

[10] J.N.Laneman and G.W.Wornell, "Distributed space-time-coded protocols for exploiting cooperative diversity in wireless networks," *IEEE Trans. on Information Theory*, vol. 49, pp. 2415 – 2425, Oct. 2003. 4, 48, 49, 95, 96

[11] H.Jafarkhani, "A quasi-orthogonal space-time block code," *IEEE Trans. on Communications*, vol. 49, pp. 1–4, Jan. 2001. 4, 33, 48, 58, 95, 97, 99, 102, 171

[12] C.B.Papadias and G.J.Foschini, "Capacity-approaching space-time codes for systems employing four transmitter antennas," *IEEE Trans. on Information Theory.*, vol. 49, pp. 726–732, Mar. 2003. 4, 33, 48, 95

[13] C. Shannon, "A mathematical theory of communication," *Bell Syst. Tech. Journal*, vol. 27, pp. 374–423, Jul. 1948. 5, 9, 17, 46, 54

[14] S.Haykin and M.Moher, *Modern Wireless Communications.* Prentice Hall, 2005. 10, 18, 20, 21, 22, 47, 50, 209

[15] I.E.Telatar, "Capacity of multi-antenna Gaussian channels," *European Trans. on Telecommunications*, vol. 10, pp. 585–595, Nov. 1999. 12, 13, 14, 15, 17, 18, 47, 52, 84, 103

[16] F.Nesser and J.Massey, "Proper complex random processes with applications to information theory," *IEEE Trans. on Information Theory*, vol. 39, pp. 1293–1302, Jul. 1993. 12

[17] T.M.Cover and J.A.Thomas, *Elements Of Information Theory.* John Wiley & Sons,Inc, 1991. 14

[18] C.Chuah, J.Khan, and D.Tse, "Capacity of multi-antenna array systems in indoor wireless environment," in *Proc. of the IEEE Globecom*, no. 4, 1998. 14

[19] C.Chuah, D.Tse, J.Kahn, and R.Valenzuela, "Capacity scaling in mimo wireless systems under correlated fading," *IEEE Transactions on Information Theory*, vol. 48, pp. 637–650, Mar. 2002. 14

[20] S. Boyd and L. Vandenberghe, *Convex Optimization*. Cambridge University Press, 2004. 14

[21] A. Edelman, *Eigenvalues and Condition Numbers of Random Matrices*. PhD thesis, Department of Mathematics, MIT, Cambridge, MA, 1989. 15

[22] T.Lo, "Maximal ratio transmission," *IEEE Trans. on Communications*, vol. 47, no. 10, pp. 1458–1461, Oct 1999. 27, 47

[23] S.M.Alamouti, "A simple transmit diversity technique for wireless communications," *IEEE Journal on Selected Areas in Communications*, vol. 16, pp. 1451–1458, Oct. 1998. 29, 32, 47, 95, 146

[24] V.Tarokh, H.Jafarkhani, and A.R.Calderbank, "Space-time block codes from orthogonal designs," *IEEE Trans. on Information Theory*, vol. 45, pp. 1456–1467, July 1999. 31, 47, 49, 51, 95

[25] V.Tarokh, N.Seshadri, and A.R.Calderbank, "Space-time codes for high data rate wireless communication: Performance criterion and code construction," *IEEE Trans. on Information Theory*, vol. 44, pp. 744–765, Mar. 1998. 31, 47, 153, 156

[26] C.Toker, S.Lambotharan, and J.A.Chambers, "Closed-loop quasi-orthogonal STBCs and their performance in multipath fading environment and when combined with turbo codes," *IEEE Trans. on Wireless Communications*, vol. 3, pp. 1890–1896, Nov. 2004. 35, 37, 48, 63, 90, 96, 127, 128, 134, 142, 173

[27] J.Boutros, E.Viterbo, C.Rastello, and J.C.Belfiore, "Good lattice constellations for both Rayleigh fading and Gaussian channel," *IEEE Trans. on Information Theory*, vol. 42, pp. 502–518, Mar. 1996. 37

[28] X.Giraud and J.C.Belfiore, "Constellations matched to the rayleigh fading channel," *IEEE Trans. on Information Theory*, vol. 42, pp. 106–115, Jan. 1996. 37

[29] X.Giraud, E.Boutillon, and J.C.Belfiore, "Algebraic tool to build modulation schemes for fading channel," *IEEE Trans. on Information Theory*, vol. 43, pp. 938–952, May. 1997. 37

[30] C.Lamy and J.Boutros, "On random rotations diversity and minimum MSE decoding of lattices," *IEEE Trans. on Information Theory*, vol. 46, pp. 1584–1589, Jul. 2000. 37

[31] G.B.Giannakis, Z.Wang, A.Scaglione, and S.Barbarossa, "Generalized multicarrier transceivers for blind CDMA irrespective of multipath," *IEEE Trans. on Communications*, vol. 48, pp. 2064–2076, Dec. 2000. 37

[32] Z.Liu and G.B.Giannakis, "Space-time block coded multiple access through frequency-selective fading channels," *IEEE Trans. on Communications*, vol. 49, pp. 1033–1044, Jun. 2001. 37

[33] A.Scaglione, G.B.Giannakis, and S.Barbarossa, "Redundant filterbank precoders and equalizers. part I: Unification and optimal designs," *IEEE Trans. on Signal Processing*, vol. 47, pp. 1988–2006, Jul. 1999. 37

[34] Z.Wang and G.B.Giannakis, "Wireless multicarrier communications: Where Fourier meets Shannon," *IEEE Signal Processing Magazine*, vol. 17, pp. 29–48, May 2000. 37, 42, 158

[35] Z.Wang and G.B.Giannakis, "Complex field coding for OFDM over fading channels," *IEEE Trans. on Information Theory.*, vol. 49, pp. 707–720, Mar. 2003. 37

[36] Z.Lui, Y.Xin, and G.B.Giannakis, "Linear constellation precoding for OFDM with maximum multipath and coding gains," *IEEE Trans. on Communications*, vol. 51, pp. 416–427, Mar. 2003. 37

[37] X.Ma and G.B.Giannakis, "Maximum-diversity transmission over doubly-selective wireless channels," *IEEE Trans. on Information Theory*, vol. 49, pp. 1832–1840, Jul. 2003. 37

[38] M.O.Damen, K.Abed-Meraim, and J.C.Belfiore, "Diagonal algebraic space-time block codes," *IEEE Trans. on Information Theory*, vol. 48, pp. 628–636, Mar. 2002. 37

[39] Y.Xin, Z.Wang, and G.B.Giannakis, "Space-time diversity systems based on linear constellation precoding," *IEEE Trans. on Wireless Communications*, vol. 2, pp. 294–309, Mar. 2003. 37, 39, 40, 41, 166, 167

[40] G.B.Giannakis, Z.Lui, X.MA, and S.Zhou, *Space-Time Coding For Broadband Wireless Communications*. John Wiley & Sons, Inc, 2007. 38, 39, 41, 146, 154, 156, 172

[41] G.H.Golub and C.F.van-Loan, *Matrix Computations*. John Hopkins University Press, 1996. 39

[42] R. W. Lucky, "Generalized automatic equalization for communication channels," *Proceedings of IEEE*, vol. 54, pp. 439–440, Mar. 1966. 42

[43] S. Alexander, *Adaptive Signal Processing: Theory and Applications*. Springer-Verlag, 1986. 44

[44] C. Berrou, A. Glavieux, and P. Thitimajshima, "Near Shannon limit error-correcting coding and decoding: Turbo Codes," in *Proc. IEEE Inter. Communication Conf.*, pp. 1064–1070, 1993. 47

[45] G. Foschini, "Layered space-time architecture for wireless communications in a fading environment when using multiple antennas," *Bell Labs Tech. J.*, pp. 41–59, 1996. 47

[46] G. Foschini and M. Gans, "On limits of wireless communications in a fading environment when using multiple antennas," *Wireless Personal Communications*, vol. 6, pp. 311–335, March 1998. 47

[47] N.Sharma and C.B.Papadias, "Improved quasi-orthogonal codes through constellation rotation," *IEEE Trans. on Communications*, vol. 51, pp. 332–335, Mar. 2003. 48, 88, 96

[48] C.Toker, *Signal Processing Algorithms and Architectures for Communication Transceivers*. PhD thesis, University of London, Dec 2002. 52, 110, 139, 164, 165, 169, 170

[49] I. Gradshteyn and I. Ryshik, *Table of Integrals, Series, and Products*. Academia Press, fifth ed., 1994. 54, 60, 79, 80, 82

[50] J.F.Hayes, "The Viterbi algorithm applied to digital data transmission," *IEEE Communications Magazine*, vol. 13, pp. 15–20, Feb. 1975. 58

[51] G. Turin, "The characteristic function of hermitian quadratic forms in complex normal variables," *Biometrika*, vol. 47, pp. 199–201, 1960. 60, 155

[52] A.Sezgin and T.J.Oechtering, "Complete Characterization of the Equivalent MIMO Channel for Quasi-Orthogonal Space-Time Codes," *IEEE Trans. on Information Theory*, vol. 54, pp. 3315–3327, Jul. 2008. 77, 78, 83

[53] W. T. Wells, R. L. Anderson, and J. W. Cell, "The distribution of the product of two central or non-central chi-square variates," *The Annals of Mathematical Statistics*, vol. 33, pp. 1016–1020, Sep. 1962. 78, 79

[54] V.Hayes, *Information TechnologyTelecommunications and Information Exchange Between SystemsLocal and Metropolitan Area Networks Specific Requirements. Part 11: Wireless LAN Medium Access Con- trol (MAC) and Physical Layer (PHY) Specifications.* IEEE Std 802.11-1997, 1997. 96

[55] S.Wei, D.L.Goeckel, and M.C.Valenti, "Asynchronous cooperative diversity," *IEEE Trans. on Wireless Communications*, vol. 5, pp. 1547–1557, Jun. 2006. 96, 97

[56] F.-C. Zheng, A. Burr, and S. Olafsson, "PIC based detection for distributed space-time block coding under imperfect synchronisation," in *Proc. European Wireless*, 2007. 96

[57] F.-C. Zheng, A. Burr, and S. Olafsson, "Distributed space-time block coding with incremental relay: Performance improvement under imperfect synchronisation," in *Proc. 16th Mobile and Wireless Communications Summit*, 2007. 96

[58] F.-C. Zheng, A. Burr, and S. Olafsson, "Distributed space-time block coding for 3 and 4 relay nodes: Imperfect synchronisation and a solution," in *Proc. IEEE 18th International Symposium on Personal, Indoor and Mobile Radio Communications*, 2007. 96

[59] Y.Li and X.G.Xia, "Full diversity distributed space-time trellis codes for asynchronous cooperative communications," in *Proc. International Symposium Information Theory*, 2005. 96

[60] Y.Li and X.G.Xia, "A family of distributed space-time trellis codes with asynchronous cooperative diversity," *IEEE Trans. on Communications*, vol. 55, pp. 790 – 800, Apr. 2007. 96

[61] Y.Shang and X.G.Xia, "Shift-full-rank matrices and applications in space-time trellis codes for relay networks with asynchronous cooperative diversity," *IEEE Trans. on Information Theory*, vol. 52, pp. 1353–1367, Jul. 2006. 96

[62] Y.Shang and X.G.Xia, "Space-time trellis codes with asynchronous full diversity up to fractional symbol delays," *IEEE Trans. on Wireless Communications*, vol. 7, pp. 2473–2479, Jul. 2008. 96

[63] D.Wang and S.Fu, "Asynchronous cooperative communications with stbc coded single carrier block transmission," in *Proc. of Global Telecommun. Conf.*, 2007. 96

[64] M.O.Damen and A.R.Hammons, "Delay-tolerant space-time block codes for asynchronous cooperative relaying," in *Proc. 2nd International Symposium on Wireless Pervasive Computing*, 2007. 96

[65] M.O.Damen and A.R.Hammons, "Delay-tolerant distributed-TAST codes for cooperative diversity," *IEEE Trans. on Information Theory*, vol. 53, pp. 3755–3773, Oct. 2007. 96

[66] X. Guo and X.-G.Xia, "Distributed linear convolutive space-time codes for asynchronous cooperative communication networks," *IEEE Trans. Wireless Communications*, vol. 7, pp. 1857–1861, May 2008. 97

[67] Y.Mei, Y.Hua, A.Swami, and B.Daneshrad, "Combating synchronization errors in cooperative relays," in *Proc. IEEE International Conference on Acoustics, Speech, and Signal Processing*, 2005. 97, 112

[68] X. Li, "Space-time coded multi-transmission among distributed transmitters without perfect synchronization," *IEEE Signal Processing Letters*, vol. 11, pp. 948–951, Dec. 2004. 97

[69] Z.Li and X.-G.Xia, "A simple Alamouti space-time transmission scheme for asynchronous cooperative systems," *IEEE Signal Processing Letters*, vol. 14, pp. 804–807, Nov. 2007. 97, 103, 112, 113, 134, 146

[70] X.Guo and X.-G.Xia, "A distributed space-time coding in asynchronous wireless relay networks," *IEEE Trans. on Wireless Communications*, vol. 7, pp. 1812–1816, May. 2008. 97

[71] T.Jiang and Y.Wu, "An overview: Peak-to-average power ratio reduction techniques for OFDM signals," *IEEE Trans. on Broadcasting*, vol. 54, pp. 257–268, Jun. 2008. 101

[72] Y. Jing and B. Hassibi, "Distributed space-time coding in wireless relay networks," *IEEE Trans. on Wireless Communications*, vol. 5, pp. 3524–3536, Dec. 2006. 103

[73] G.H.Golub and C. Loan, *Matrix Computations.* Johns Hopkins University Press, 3rd ed., 1996. 104

[74] T.I.Laakso, V.Valimaki, M.Karjalainen, and U.K.Laine, "Splitting the unit delay," *IEEE Signal Processing Magazine*, vol. 13, pp. 30–60, Jan 1996. 130, 131, 132, 133, 136, 138

[75] T. W. Parks and C. S. Burrus, *Digital Filter Design.* John Wiley & Sons, 1987. 130, 131

[76] G. Oetken, "A new approach for the design of digital interpolating filters," *IEEE Trans. on Acoustics, Speech and Signal Processing*, vol. 27, pp. 637–643, Dec. 1979. 131, 132

[77] J. Thiran, "Recursive digital filters with maximally flat goup delay," *IEEE Trans. Circuit Theory*, vol. 18, pp. 659–664, Nov. 1971. 132, 133

[78] K.Yan, D. K, Q.YunZhou, W.YingGuan, and L.HaiTao, "A simple single-carrier space-time transmission scheme for asynchronous cooperative communications over frequency-selective channels," in *Proc. IEEE 10th Intern. Conf. on Advanced Communication Technology*, 2008. 146

[79] K.Yan, D. K, Q.YunZhou, W.YingGuan, and L.HaiTao, "A simple Alamouti space-time transmission scheme for asynchronous cooperative communications over frequency-selective channels," in *Proc. IEEE 10th Intern. Conf. on Advanced Communication Technology*, 2008. 146

[80] Z.Zhong, S.Zhu, and A.Nallanathan, "A novel distributed space-time trellis code for asynchronous cooperative communications under frequency-selective channels," in *Proc. of IEEE Globecom*, 2008. 146

[81] Z.Zhimeng, Z.Shihua, and A.Nallanathan, "Distributed space-time trellis code for asynchronous cooperative communications under frequency-selective channels," *IEEE Trans. Wireless Communications*, vol. 8, pp. 796–805, Feb. 2009. 146

[82] X.Li, "Spacetime coded multi-transmission among distributed transmitters without perfect synchronization," *IEEE Signal Processing Letters*, vol. 11, pp. 948–951, Dec. 2004. 146

[83] Z.Li, X.-G.Xia, and M.H.Lee, "A simple orthogonal space-time coding scheme for asynchronous cooperative systems for frequency selective fading channels," *IEEE Trans. Communications*, vol. 58, pp. 2219–2224, Aug. 2010. 146

[84] Y.Li, W.Zhang, and X.-G.Xia, "Distributive high-rate space-frequency codes achieving full cooperative and multipath diversities for asynchronous cooperative communications," in *Proc. of the IEEE Globecom*, 2006. 146

[85] Y.Li, W.Zhang, and X.-G.Xia, "Distributive high-rate full-diversity space-frequency codes for asynchronous cooperative communications," in *Proc. of IEEE Intern. Symposium on Information Theory*, 2006. 146

[86] Z.Zhong, S.Zhu, G.Lv, and T.Liu, "Distributed space-time coded transmission achieving full cooperative and multipath diversities for asynchronous

cooperative communications," in *Proc. IEEE Vehicular Technology Conf.*, 2008. 146

[87] R. U. Nabar, H. Boelcskei, and F. W. Kneubhueler, "Fading relay channels: performance limits and space-time signal design," *IEEE Journal Selected Areas in Communications*, vol. 22, pp. 1099–1109, Aug 2004. 147

[88] R. U. Nabar and H. Bolcskei, "Space-time signal design for fading relay channels," in *Proc. of IEEE Globecom*, Dec. 2003. 147

[89] Y.Li, W.Zhang, and X.-G.Xia, "Distributive high-rate spacefrequency codes achieving full cooperative and multipath diversities for asynchronous cooperative communications," *IEEE Trans. on Vehicular Technology*, vol. 58, pp. 207–217, Jan. 2009. 148, 157

[90] Z.Liu, Y.Xin, and G.B.Giannakis, "Space-time-frequency coded OFDM over frequency-selective fading channels," *IEEE Trans. on Signal Processing*, vol. 50, pp. 2465–2476, Oct. 2002. 154, 157, 158, 160, 162, 163, 166, 171, 191

[91] H.Bolcskei and A.J.PaulRaj, "Space-frequency coded broadband OFDM systems," in *Proc. of Wireless Commun. Networking Conf.*, Sep. 2000. 157

[92] B.Lu and X.Wang, "Space-time code design in OFDM systems," in *Proc. of Global Telecommun. Conf.*, Nov. 2000. 157

[93] D.L.Goeckel, "Coded modulation with nonstandard signal sets for wireless ofdm systems," in *Proc. Intern. Conf. on Communications*, Jun. 1999. 158

[94] J. Boutros and E. Viterbo, "Signal space diversity: A power- and banwidth-efficient diversity technique for the rayleigh fading channel," *IEEE Trans. on Information Theory*, vol. 44, pp. 1453–1467, Jul. 1998. 167

[95] X. Giraud, E. Boutillon, and J. C. Belfiore, "Algebraic tools to build modulation schemes for fading channels," *IEEE Trans. on Information Theory*, vol. 43, pp. 938–952, May. 1997. 167

[96] D.Wubben, R.Bohnkeand, V.Kuhn, and K.-D.Kammeyer, "Near-maximum-likelihood detection of MIMO systems using MMSE-based lattice reduction," in *Proc. IEEE Inter. Communication Conf.*, 2004. 171

[97] D.Pham, K.R.Pattipati, P.K.Willett, and J.Luo, "An improved complex sphere decoder for V-BLAST systems," *IEEE Signal Processing Letters*, vol. 11, pp. 748–751, Sep. 2004. 172

[98] B.Steingrimsson, Z.-Q.Luo, and K.M.Wong, "Soft quasi-maximum-likelihood detection for multiple-antenna wireless channels," *IEEE Trans. on Signal Processing*, vol. 51, pp. 2710–2719, Nov. 2003. 172

[99] S.Lambotharan and C.Toker, "Closed-loop space time block coding techniques for OFDM based broadband wireless access systems," *IEEE Trans. on Consumer Electronics*, vol. 51, pp. 765–769, Aug. 2005. 174

[100] I.Toufik, M.Baker, and S.Sesia, *LTE: The UMTS Long Term Evolution: from Theory to Practice.* Wiley-Blackwell, 2009. 176

[101] H.Mheidat, M.Uysal, and N.Al-Dhahir, "Equalization techniques for distributed space-time block codes with amplify-and-forward relaying," *IEEE Trans. on Signal Processing*, vol. 55, pp. 1839–1852, May. 2007. 187, 188, 189, 202

[102] A.Stuart and K.Ord, *Kendall's Advanced Theory of Statistics.* 5th ed., 1987. 202

[103] M.K.Simon and M-S.Alouini, *Digital Communication over Fading Channels.* John Wiley & Sons,Inc, 2000. 209

[104] M.Hayes, J.A.Chambers, and M.D.Macleod, "A single-carrier quasi-orthogonal transmission scheme for asynchronous cooperative relay networks," in *Proc. of 17th European Signal Processing Conf.*, Aug. 2009. 210

[105] P.Schniter, "Low-complexity equalization of OFDM in doubly selective channels," *IEEE Trans. on Signal Processing*, vol. 52, pp. 1002–1011, Apr. 2004. 210

[106] M.N.Eltayeb, S.Lambotharan, and J.A.Chambers, "A phase feedback based extended space-time block code for enhancement of diversity," in *Proc. of 65th IEEE Vehicular Technology Conf.*, Apr. 2007. 210

[107] F.T.Alotaibi and J.A.Chambers, "Extended orthogonal space time block codes in wireless relay networks," in *Proc. of IEEE 15th Workshop on Statistical Signal Processing*, Apr. 2009. 210

[108] M.Hayes, J.A.Chambers, and M.D.Macleod, "A simple quasi-orthogonal space-time scheme for use in asynchronous virtual antenna array enabled cooperative networks," in *Proc. of 16th European Signal Processing Conf.*, Aug. 2008. 210